

École doctorale n° 432 : Science des Métiers de l'ingénieur

Doctorat ParisTech

T H È S E

pour obtenir le grade de docteur délivré par

l'École Nationale Supérieure d'Arts et Métiers

Spécialité " Génie Electrique "

présentée et soutenue publiquement par

Mario BERMÚDEZ GUZMÁN

le 21 Décembre 2018

**Novel Control Techniques in Multiphase Drives:
Direct Control Methods (DTC and MPC) Under Limit Situations**

Directeur de thèse : **Xavier KESTELYN**

Codirecteur de cotutelle de la thèse : **Federico José BARRERO GARCÍA**

Jury

Mme. Betty LEMAIRE-SEMAIL, Professeur des universités, L2EP, Université Lille1

M. Radu BOJOI, Full Professor, PEIC, Politecnico di Torino

M. Humberto HENAO, Professeur des universités, LTI, Université de Picardie Jules Verne

Mme. Inmaculada PLAZA GARCÍA, Associate Professor, EDUQTECH, Universidad de Zaragoza

M. Xavier KESTELYN, Professeur des universités, L2EP, Arts et Métiers – Campus de Lille

M. Federico José BARRERO GARCÍA, Full Professor, ACE-TI, Universidad de Sevilla

M. Mario Javier DURÁN MARTÍNEZ, Full Professor, ACE-TI, Universidad de Málaga

Président

Rapporteur

Rapporteur

Examineur

Examineur

Examineur

Invité

**T
H
È
S
E**

Table of Contents

Table of Contents	I
Nomenclature	V
List of Figures	XI
List of Tables	XVII
1 Introduction	1
1.1 Scientific context.....	1
1.2 Objectives.....	2
1.3 Position of the Doctoral Thesis	2
1.4 Document organization	4
1.5 List of publications derived from this work	4
2 State of the Art of Multiphase Drives	7
2.1 Historical review of multiphase drives.....	7
2.2 Modeling of the multiphase drive	9
2.2.1 Multiphase machines with one frequency-domain subspace: distributed winding induction machine case	9
2.2.2 Five-phase distributed winding induction machine: a case study	24
2.2.3 Extension to multiphase machines with two frequency-domain subspaces: a second case example using the five-phase concentrated winding induction machine.....	26
2.2.4 Multiphase machines with two frequency-domain subspaces: a third case example using the five-phase permanent magnet synchronous machine.....	29
2.2.5 Modeling of the multiphase power converter.....	32
2.3 State of the art in the multiphase drives control field.....	38
2.3.1 Field Oriented Control.....	38
2.3.2 Direct Torque Control	41
2.3.3 Model-based Predictive Control.....	48
2.4 Performance limits	52
2.4.1 Tolerance to open-phase faults.....	53
2.4.2 Electrical limits in the control strategy.....	57

2.5	Review on graphical formalisms for control	59
2.6	Chapter conclusions	63
3	Controller with one Frequency-Domain Subspace: The DTC Case	65
3.1	Modeling of an open-phase fault situation	66
3.2	DTC scheme in open-phase fault operation	67
3.3	Simulations of the open-phase fault operation using DTC	70
3.4	Experimental validation in a real test rig.....	74
3.5	A comparative analysis using conventional RFOC methods	80
3.5.1	RFOC techniques in open-phase fault operation.....	81
3.5.2	Simulation results	83
3.5.3	Experimental assessment.....	86
3.6	Chapter conclusions	92
4	Controller with two Independent Frequency-Domain Subspaces: The MPC Case	95
4.1	Electrical constraints for the optimal control strategy.....	96
4.2	Definition of an optimal controller using MPC techniques	97
4.3	Validation of the two-stage MPC method.....	101
4.3.1	Case example #1: five-phase PMSM drive	101
4.3.2	Case example #2: five-phase concentrated winding IM drive	111
4.4	Chapter conclusions	118
5	Conclusions and Future Research	119
5.1	Conclusions	119
5.2	Future research	120
6	Résumé étendu en français	123
6.1	Contexte scientifique.....	123
6.2	Objectifs	124
6.3	Positionnement de la thèse	125
6.4	Organisation du document.....	126
6.5	Etat de l’art des entraînements polyphasés.....	127
6.6	Contrôleur avec un unique sous-espace à contrôler dans le domaine fréquentiel : cas de la DTC	128
6.7	Contrôleur avec deux sous-espaces indépendants à contrôler dans le domaine fréquentiel : cas de la MPC	130
6.8	Conclusions	131
7	Resumen extenso en español	133
7.1	Contexto científico	133
7.2	Objetivos	134

7.3	Posicionamiento de la Tesis Doctoral	135
7.4	Organización del documento.....	136
7.5	Estado del arte de los accionamientos multifásicos	137
7.6	Controlador con un único subespacio a controlar en el dominio de frecuencia: caso del DTC	138
7.7	Controlador con dos subespacios independientes a controlar en el dominio de frecuencia: caso del MPC.....	139
7.8	Conclusiones	141
Bibliography		i
Appendices		xv
A Discrete-Time State-Space Models		xvii
A.1	Five-phase induction machine with distributed windings	xvii
A.2	Five-phase induction machine with concentrated windings.....	xx
A.3	Five-phase permanent magnet synchronous machine	xxv
B Flux and Torque Estimators for DTC		xxix
B.1	Healthy operation	xxix
B.2	Post-fault operation	xxx
C Electrical and Mechanical Parameters		xxxii
C.1	Five-phase IM drive with distributed windings	xxxii
C.2	Five-phase PMSM drive.....	xxxii
C.3	Five-phase IM drive with concentrated windings	xxxii

Nomenclature

Abbreviations and acronyms

AC	Alternating Current
ACE-TI	Cybernetics Applications of Electronics for Information Technology
CBPWM	Carrier Based Pulse Width Modulation
CCS-MPC	Continuous-Control-Set Model-based Predictive Control
CPU	Central Processing Unit
CW-IM	Concentrated Winding Induction Machine
DC	Direct Current
DRFOC	Direct Rotor Flux Oriented Control
DSP	Digital Signal Processor
DTC	Direct Torque Control
DW-IM	Distributed Winding Induction Machine
EMF	Electromotive Force
EMR	Energetic Macroscopic Representation
FCS-MPC	Finite-Control-Set Model-based Predictive Control
FOC	Field Oriented Control
FPGA	Field-Programable Gate Array
GPIO	General Purpose Input/Output
GVF	Generalized Vectorial Formalism
HDL	Hardware Description Language
HM	Homopolar Machine
IGBT	Insulated-Gate Bipolar Transistor
IM	Induction Machine
IRFOC	Indirect Rotor Flux Oriented Control
L2EP	Laboratoire d'Electrotechnique et d'Electronique de Puissance de Lille
MCL	Minimum Copper Loss
MM	Main Machine
MMF	Magnetomotive Force
MPC	Model-based Predictive Control
MT	Maximum Torque
PC	Personal Computer
PCC	Predictive Current Control
PI	Proportional Integral

PMSM	Permanent Magnet Synchronous Machine
PR	Proportional Resonant
PWM	Pulse Width Modulation
RFOC	Rotor Field Oriented Control
RMS	Root Mean Square
SM	Secondary Machine
ST-DTC	Switching Tables Direct Torque Control
SVM-DTC	Space Vector Modulated Direct Torque Control
SVPWM	Space Vector Pulse Width Modulation
US	University of Seville
VHDL	VHSIC Hardware Description Language
VHSIC	Very High Speed Integrated Circuits
VSD	Vector Space Decomposition
VSI	Voltage Source Inverter

Variables, parameters, matrices and vectors

$[A]$	Input matrix for the discrete-time state-space model
$[B]$	State matrix for the discrete-time state-space model
$[B_c]$	Constant elements of matrix $[B]$
B_m	Friction coefficient of the rotor-load bearings
$[B_{\omega_a}]$	Elements of matrix $[B]$ that depend on the instantaneous values of ω_a
$[B_{\omega_r}]$	Elements of matrix $[B]$ that depend on the instantaneous values of ω_r
$[C], [d], [E]$	Matrices for the constraints in the optimization problem expressed in the quadratic programming form
$[C_5]$	5-phase Clarke transformation matrix
$[C_n]$	n -phase Clarke transformation matrix
$[C_{n-m}]$	Reduced-order Clarke transformation matrix
$[C_{POST}]$	Clarke transformation matrix in post-fault situation
$[D]$	Constant matrix for the discrete-time state-space model
dT	Output of the torque hysteresis comparator
$d\lambda$	Output of the flux hysteresis comparator
$d\omega$	Output of the speed hysteresis comparator
$d-q$	Subspace in the rotating reference frame
e	Feedforward term for the FOC scheme
F	Objective function for the optimization problem
F_{QP}	Objective function for the optimization problem expressed in the quadratic programming form
f	Frequency
f_1	Frequency of the fundamental component
H	Air-gap magnetic field

$[H]$	Quadratic part of the objective function for the optimization problem expressed in the quadratic programming form
$[h]$	Linear part of the objective function for the optimization problem expressed in the quadratic programming form
$[I]$	Identity matrix for the discrete-time state-space model
i	Current
$[I_5]$	Identity matrix of order 5
$[i_{abcde}]$	Stator phase currents vector
$[i_{bcde}]$	Stator phase currents vector in post-fault situation
I_{max}	Maximum peak value between all phase currents
$I_{M,max}$	Maximum magnetizing current value
$[I_n]$	Identity matrix of order n
$[i_r]$	Rotor currents vector (referred to the stator)
$[i'_r]$	Rotor currents vector (real rotor components)
I_{RMS}	Maximum RMS phase current value established by the copper losses
$[i_s]$	Stator currents vector
$I_{sd,rated}$	Rated magnetizing current value
I_{sn}	Nominal stator current value
I_{VSI}	Maximum peak phase current value imposed by the VSI
J	Cost function for MPC
J_0	Initial value of J
J_m	Rotational inertia of the machine
k	Time instant (present)
$k + 1$	Time instant (future)
K_i	Integral parameter for PI and PR controllers
K_p	Proportional parameter for PI and PR controllers
K_{v1}, K_{v2}	Dwell time ratios that define the virtual voltage vector
k_w	Transformation ratio in the stator-rotor coupling, $k_w = N_s/N_r$
L_{lr}	Rotor leakage inductance
L_{ls}	Stator leakage inductance
L_m	Mutual inductance in the stationary/rotating reference frame, $L_m = (n/2) \cdot M$
L_r	Rotor inductance, $L_r = L_{lr} + L_m$
$[L_{rr}]$	Matrix including the self- and mutual inductances of the rotor phases
$[L_{rs}(\theta)]$	Matrix including the mutual inductances in the coupling rotor-stator
L_s	Stator inductance, $L_s = L_{ls} + L_m$
$[L_{sr}(\theta)]$	Matrix including the mutual inductances in the coupling stator-rotor
$[L_{ss}]$	Matrix including the self- and mutual inductances of the stator phases
M	Mutual inductance
$[M]$	Null space of $[C]$
m	Number of phases in open-circuit
$[M_{rr}(\vartheta)]$	Matrix that defines the mutual inductances in $[L_{rr}]$
$[M_{sr}(\theta)]$	Matrix that defines the mutual inductances in $[L_{rs}(\theta)]$ and $[L_{sr}(\theta)]$

$[M_{ss}(\vartheta)]$	Matrix that defines the mutual inductances in $[L_{ss}]$
n	Arbitrary number of phases
N_p	Prediction horizon
N_r	Rotor windings turns
N_s	Stator windings turns
p	Pairs of poles
$[P_{r5}]$	5-phase rotation matrix for rotor variables (from stationary to rotating reference frames)
$[P_{rn}]$	n -phase rotation matrix for rotor variables (from stationary to rotating reference frames)
$[P_{s5}]$	5-phase rotation matrix for stator variables (from stationary to rotating reference frames)
$[P_{sn}]$	n -phase rotation matrix for stator variables (from stationary to rotating reference frames)
QET	Torque quadratic error, $QET = (T_{em}^* - T_{em})^2$
QI	Quadratic stator current, $QI = i_{sd1}^2 + i_{sq1}^2 + i_{sd3}^2 + i_{sq3}^2$
R_r	Rotor resistance (referred to the stator), $R_r = k_w^2 \cdot R'_r$
$[R_r]$	Matrix of rotor resistances
R'_r	Rotor resistance (real value)
R_s	Stator resistance
$[R_s]$	Matrix of stator resistances
S	State of each VSI leg (1 or 0)
$[S]$	Switching state vector, $[S] = [S_a S_b S_c S_d S_e]^T$
$[S_0]$	Zero switching state vector, $[S_0] = [0 0 0 0 0]^T$
$[S_n]$	One of the available switching state vectors
$[S_{opt}]$	Optimum switching state vector
$sync$	Synchronization signal in OPAL-RT
t	Time
$[T_5]$	5-phase extended Park matrix (from phase to rotating reference frames)
T_{em}	Electromagnetic torque
T_L	Load torque
T_n	Nominal torque
$[T_r(\theta)]$	Rotation matrix for rotor variables (from rotor to stationary reference frames)
T_s	Sampling time
$[U]$	Input vector for the discrete-time state-space model
u	Phase-to-phase voltage
v	Voltage
$[v_{abcde}]$	Stator phase voltages vector
$[v_{bcde}]$	Stator phase voltages vector in post-fault situation
v_{cm}	Common-mode voltage
V_{dc}	DC-link voltage
v_{Long}	Long voltage vector

V_{max}	Maximum peak value between all phase-to-phase voltages
v_{Medium}	Medium voltage vector
v_N	Voltage between the negative DC-link bus and the common point of the star connection in the VSI
$[v_r]$	Rotor voltages vector (referred to the stator)
$[v'_r]$	Rotor voltages vector (real rotor components)
$[v_s]$	Stator voltages vector
v_{Short}	Short voltage vector
VV_i	Virtual voltage vector
VV_{Li}	Long virtual voltage vector
VV_{Si}	Short virtual voltage vector
W_{co}	Magnetic coenergy
$[X]$	State variables vector for the discrete-time state-space model
$[x]$	Dual optimization variable for the quadratic programming problem
$[x_{opt}]$	Optimal solution of the dual optimization variable in the quadratic programming problem
$x-y$	Secondary orthogonal subspace in the stationary reference frame
z	Homopolar component axis
$[z]$	Primal optimization variable for the quadratic programming problem
$\alpha-\beta$	Main orthogonal subspace in the stationary reference frame
$\alpha'-\beta'$	Rotor reference frame
$[\Gamma], [\Psi], [\Phi]$	Discretized matrices for the discrete-time state-space model
γ	Load angle (i.e. between stator and rotor flux vectors)
δ	Slip coordinate (i.e. between rotating and rotor reference frames)
Δ_k	Angle that defines matrix $[\Delta(\theta)]$
ΔT_{em}	Torque hysteresis band
ε	Speed-normalized back EMF
η	Ratio between the weighting factors, $\eta = \kappa_T/\kappa_i$
θ	Coordinate of the rotor with respect to the stationary reference frame
θ_a	Coordinate of the rotating reference frame with respect to the stationary one
ϑ	Electrical displacement between stator windings
κ_i	Weighting factor related to the minimization of the copper losses
κ_T	Weighting factor related to the reference torque tracking
λ	Flux
λ_m	Amplitude of the flux linkage due to the permanent magnets in PMSM
$[\lambda_m]$	Flux linkage matrix due to the permanent magnets in PMSM
$[\lambda_r]$	Rotor fluxes vector (referred to the stator)
$[\lambda'_r]$	Rotor fluxes vector (real rotor components)
$[\lambda_s]$	Stator fluxes vector
μ	Electrical variable (voltage, current or flux)
$[\mu_r]$	Rotor electrical variables vector (voltage, current or flux)
$[\mu_s]$	Stator electrical variables vector (voltage, current or flux)

σ, τ_s	Constants for the discrete-time state-space model
τ_r	Rotor time constant, $\tau_r = L_r/R_r$
τ_s	Stator time constant, $\tau_s = L_s/R_s$
φ	Angle considered in the expression of $I_{M,max}$
ω_a	Rotating reference frame speed
ω_m	Mechanical speed of the rotor shaft
ω_{mth}	Low-speed threshold for the DTC controller
ω_r	Rotor electrical speed (i.e. rotor reference frame speed)
ω_{sl}	Slip speed

Subscripts

1	Related to the fundamental component
3	Related to the third harmonic component
$a...e$	Related to the phases 'a' ... 'e' of the 5-phase machine
d	Related to the d -axis of the rotating reference frame
max	Maximum value of a variable
q	Related to the q -axis of the rotating reference frame
r	Related to the rotor
s	Related to the stator
x	Related to the x -axis of the stationary reference frame
y	Related to the y -axis of the stationary reference frame
z	Related to the homopolar component
α	Related to the α -axis of the stationary reference frame
β	Related to the β -axis of the stationary reference frame

Superscripts

k	Present value of a variable (time instant k)
$k+1$	Future value of a variable (time instant $k + 1$)
T	Transposition operation
*	Reference variable
\wedge	Estimated variable

List of Figures

Figure 1.1. Prototype of the electric vehicle that belongs to ACE-TI.....	3
Figure 2.1. Schematic of the symmetrical n -phase induction machine.....	10
Figure 2.2. Reference frames of stator (α - β) and rotor (α' - β') variables.....	17
Figure 2.3. Rotating reference frame (d - q).....	21
Figure 2.4. Schematic diagram of the n -leg two-level VSI.....	33
Figure 2.5. Five-leg two-level VSI with star-connected load.....	36
Figure 2.6. Five-leg two-level VSI load configuration scheme.....	36
Figure 2.7. Mapping of the phase voltages of the five-leg VSI into the α - β (left plot) and x - y (right plot) planes.....	37
Figure 2.8. IRFOC control scheme applied to a five-phase IM with distributed windings.....	40
Figure 2.9. Impact of a voltage vector on both the stator flux and the load angle. (a) Phasor diagram of the real model of the machine. (b) Estimated phasor diagram for the application of DTC.....	43
Figure 2.10. Diagram of the flux vectors together with the spatial voltage vectors available for the control.....	44
Figure 2.11. VV_{L1} projections in the (a) α - β and (b) x - y planes.....	45
Figure 2.12. Virtual voltage vectors in the α - β plane.....	45
Figure 2.13. DTC scheme applied to a five-phase IM with distributed windings.....	47
Figure 2.14. Model-based Predictive Control methods.....	48
Figure 2.15. FCS-MPC control scheme.....	50
Figure 2.16. Flow diagram of the FCS-MPC method.....	51
Figure 2.17. FCS-MPC prediction horizon principle.....	52
Figure 2.18. Schematic of different types of faults in a five-phase drive.....	54
Figure 2.19. Inversion-based control principle.....	59
Figure 2.20. EMR pictograms.....	60

Figure 2.21. EMR for a five-phase PMSM.61

Figure 2.22. Practical control scheme for a five-phase PMSM.....63

Figure 3.1. Schematic diagram of the five-phase IM drive.66

Figure 3.2. Available voltage vectors in the $\alpha\text{-}\beta$ (left plot) and $x\text{-}y$ (right plot) planes in open-phase fault operation.....68

Figure 3.3. Virtual voltage vectors (VV_i) in the $\alpha\text{-}\beta$ subspace during open-phase fault operation.69

Figure 3.4. DTC scheme regulating five-phase IM drives in open-phase fault situation. The ‘^’ and ‘*’ symbols identify the estimated and reference variables, respectively.....70

Figure 3.5. Simulation of the steady-state operation in post-fault mode of a 5-phase DW-IM drive. The reference speed is settled at 500 rpm. (a) Speed response. (b) Zoomed-in stator phase currents. (c) Zoom-in of the estimated and obtained stator flux waveforms. (d) Current trajectories in the $\alpha\text{-}\beta$ and $x\text{-}y$ planes.71

Figure 3.6. Simulation reversal test during the post-fault operation of a 5-phase DW-IM drive. A change in the reference speed from 500 to -500 rpm is applied. (a) Speed response. (b) Stator phase current and (c) stator flux waveforms in the $\alpha\text{-}\beta$ plane during the zero-speed crossing operating point.....72

Figure 3.7. Simulation of the transition from pre- to post-fault operation of a 5-phase DW-IM drive. The fault appearance is at $t = 0.2$ s. (a) Speed response. Zoomed-in (b) phase, (c) $\alpha\text{-}\beta$ and (d) $x\text{-}y$ currents before ($t < 0.2$ s) and after ($t > 0.2$ s) the fault occurrence.73

Figure 3.8. Graphical scheme of the experimental test rig based on a symmetrical five-phase distributed winding IM drive.74

Figure 3.9. Experimental test of the speed step response for a 5-phase DW-IM drive. The reference speed is changed from 0 to 500 rpm at $t = 0.1$ s, while no load torque condition is assumed. (a) Speed response. (b) Estimated electrical torque. (c) Estimated stator flux in the $\alpha\text{-}\beta$ plane.75

Figure 3.10. Experimental speed reversal test for a 5-phase DW-IM drive. The reference speed is changed from 500 to -500 rpm at 0.2 s. (a) Speed and (b) torque reference tracking. (c) Stator currents in the $\alpha\text{-}\beta$ plane at the zero-speed crossing point.76

Figure 3.11. Experimental load torque rejection test for a 5-phase DW-IM drive. A change from 0 to 50% of the nominal load torque is applied at $t = 1.1$ s. (a) Speed response. (b) Estimated electrical torque behavior. Stator current performance in $\alpha\text{-}\beta$ and $x\text{-}y$ planes in steady state with (c) null and (d) 50% of the nominal torque, respectively.77

Figure 3.12. Experimental test of the transition from pre- to post-fault operation of a 5-phase DW-IM drive considering instantaneous control reconfiguration when the fault appears at $t = 0.2$ s. A reference speed of 500 rpm is assumed with an applied load torque of (a) 28%, (b) 50% and (c) 70% of the nominal one. The speed and estimated torque response is depicted in left and right plots, respectively.78

Figure 3.13. Healthy stator phase currents from the current probes when the open-phase fault appears in a 5-phase DW-IM drive and instantaneous control reconfiguration is used.

The applied reference speed is 500 rpm and the demanded load torque is about 50% of the nominal one.	79
Figure 3.14. Experimental test of the low-speed operation of the 5-phase DW-IM drive. The reference speed is set to 50 rpm, while load torques of (a) 28% and (b) 50% of the nominal one are applied. The speed response and the estimated electrical torque are depicted in left and right plots, respectively. The fault is forced at $t = 0.2$ s.....	80
Figure 3.15. RFOC scheme based on PR (upper plot) and PCC (bottom plot) controllers.....	82
Figure 3.16. Simulation performance comparison of the steady-state operation of a 5-phase DW-IM drive, with a reference speed of 500 rpm and a load torque of about 25% of the nominal one. Stator phase currents (left-hand side plots) and evolution in the α - β (middle plots) and x - y (right-hand side plots) planes, implementing (a) PR, (b) PCC and (c) DTC controllers, respectively.....	83
Figure 3.17. Simulation performance comparison of the steady-state operation of a 5-phase DW-IM drive, with a reference speed of 500 rpm and a load torque of about 50% of the nominal one. Stator phase currents (left-hand side plots) and evolution in the α - β (middle plots) and x - y (right-hand side plots) planes, implementing (a) PR, (b) PCC and (c) DTC controllers, respectively.....	84
Figure 3.18. Simulation performance comparison when the reference speed is changed in a 5-phase DW-IM drive using a load torque of about 25% of the nominal one. (a) Speed response. (b) Zoom-in of the speed tracking.	85
Figure 3.19. Simulation performance comparison of the speed response if a reversal test from 500 to -500 rpm is carried out in a 5-phase DW-IM drive.....	85
Figure 3.20. Simulation performance comparison of the generated electrical torque in a 5-phase DW-IM drive when the load torque is changed from 0% to 25% of the nominal one. The reference speed is maintained at 500 rpm during the test.	86
Figure 3.21. Experimental performance comparison of the steady-state faulty operation of a 5-phase DW-IM drive. The reference speed is set to 500 rpm and a load torque of 28% of the nominal one is required. Stator phase currents obtained from the current probes and stator phase currents in α - β and x - y planes (left and right plots, respectively), while (a) PR, (b) PCC and (c) DTC controllers are used.	87
Figure 3.22. Experimental performance comparison of the steady-state faulty operation of a 5-phase DW-IM drive. The reference speed is set to 500 rpm and a load torque of 56% of the nominal one is required. Stator phase currents obtained from the current probes and stator phase currents in α - β and x - y planes (left and right plots, respectively), while (a) PR, (b) PCC and (c) DTC controllers are used.	88
Figure 3.23. Experimental comparison of the dynamic performance of a 5-phase DW-IM drive in faulty operation. The reference speed is changed from 500 to -500 rpm at $t = 0.2$ s, while no electrical load torque is demanded. Speed response and stator current waveforms in the α - β plane at the zero-speed crossing point (left and right plots, respectively), when (a) PR, (b) PCC and (c) DTC controllers are used.	89
Figure 3.24. Experimental performance comparison of the pre- to post-fault transition under realistic conditions (a delay of 40 ms in the fault detection is assumed) in a 5-phase DW-IM	

drive. A load torque of about 50% of the nominal one and a reference speed of 500 rpm are used. Speed response and zoom-in of the generated electrical torque at the fault occurrence instant (left and right plots, respectively), when (a) PR, (b) PCC and (c) DTC techniques are considered.90

Figure 3.25. Experimental performance comparison of the pre- to post-fault transition at low-speed operation of a 5-phase DW-IM drive, where a delay of 40 ms in the fault detection process is assumed. A load torque of about 50% of the nominal one and a reference speed of 50 rpm are used. Speed response and generated electrical torque (left and right plots, respectively), when considering (a) PR, (b) PCC and (c) DTC techniques.91

Figure 4.1. Scheme of the proposed optimal controller.97

Figure 4.2. First MPC stage to implement the proposed technique: optimization process for the reference current generation.99

Figure 4.3. Second MPC stage to implement the proposed technique: FCS-MPC inner current controller.100

Figure 4.4. Block diagram of the second control stage based on the FCS-MPC method.101

Figure 4.5. Description of the proposed technique in a real-time system based on OPAL-RT technologies for the case example #1.102

Figure 4.6. General architecture of the five-phase PMSM real-time model simulator in FPGA.103

Figure 4.7. Computation timeline of the simulation model in the real-time system.104

Figure 4.8. Extended Park matrix generator in the real-time system.105

Figure 4.9. Evaluation of the dimensionless QI and QET terms using different η values when the PMSM is driven at a particular operating point (50 rad/s and 10 N-m).106

Figure 4.10. Real-time simulation for the steady-state analysis of the 5-phase PMSM drive, including a speed ramp test where the speed is varied in the machine from 0 rad/s to 240 rad/s and the reference torque is higher than the maximum value. (a) Obtained electrical torque versus speed characteristic of the system. (b) Evolution of dq_1 and dq_3 stator current values.107

Figure 4.11. Real-time simulation of the steady-state operation of the 5-phase PMSM drive in cases 1 and 2: operation without considering voltage or current limits (left plots) and considering the current limit (right plots). (a) Stator phase current. (b) Filtered phase-to-phase stator voltages.109

Figure 4.12. Real-time simulation of the steady-state operation of the 5-phase PMSM drive in cases 3 and 4: operation considering a voltage limit (left plots) and taking into account current and voltage limits (right plots). (a) Stator phase current. (b) Filtered phase-to-phase stator voltages.109

Figure 4.13. Real-time simulation of the dynamic response of the 5-phase PMSM drive using the proposed technique under current and voltage limits. The reference torque is changed from 0 to 20 N-m (at $t = 0.01$ s approximately), while the machine operates at 150

rad/s (above the base speed). (a) Torque response. (b) Evolution in dq_1 and dq_3 stator currents.	110
Figure 4.14. Evaluation of the dimensionless QI and QET terms using different η values when the 5-phase CW-IM is driven at a particular operating point (20 rad/s and 6 N-m).	111
Figure 4.15. Experimental test for the steady-state analysis of the proposed controller using a 5-phase CW-IM drive. (a) Maximum obtained electrical torque versus speed. (b) Maximum phase-to-phase stator voltage and phase stator current (normalized to their limit values, V_{dc} and I_{VSI} , respectively). (c) Stator currents in d_1 - and d_3 -axes. (d) Stator currents in q_1 - and q_3 -axes.	113
Figure 4.16. Maximum electrical torque in the experimental system based on the 5-phase CW-IM drive with and without the injection of third harmonic stator current components.	113
Figure 4.17. Experimental test of the 5-phase CW-IM drive when the maximum load torque is applied at a reference speed of 20 rad/s. (a) Measured mechanical speed versus the applied reference. (b) Obtained electrical torque. (c) Stator currents in d_1 - and d_3 -axes. (d) Stator currents in q_1 - and q_3 -axes. (e) Stator phase current 'a'. (f) Time-domain performance and frequency spectrum of phase-to-phase voltage u_{ac}	114
Figure 4.18. Experimental test of the 5-phase CW-IM drive when the maximum load torque is applied at a reference speed of 60 rad/s. (a) Measured mechanical speed versus the applied reference. (b) Obtained electrical torque. (c) Stator currents in d_1 - and d_3 -axes. (d) Stator currents in q_1 - and q_3 -axes. (e) Stator phase current 'a'. (f) Time-domain performance and frequency spectrum of phase-to-phase voltage u_{ac}	115
Figure 4.19. Experimental test of the dynamic response of the 5-phase CW-IM drive for a reference speed of 20 rad/s and a load torque step from 6.4 N-m to 8.13 N-m. (a) Measured mechanical speed versus the applied reference. (b) Obtained electrical torque. (c) Stator currents in d_1 - and d_3 -axes. (d) Stator currents in q_1 - and q_3 -axes. (e) Stator phase current 'a'. (f) System evolution in the maximum torque-speed curve.	116
Figure 4.20. Experimental test of the dynamic response of the 5-phase CW-IM drive for a speed step from 40 to 60 rad/s and a load torque equal to 6.4 N-m (the maximum available at 60 rad/s). (a) Measured mechanical speed versus the applied reference. (b) Obtained electrical torque. (c) Stator currents in d_1 - and d_3 -axes. (d) Stator currents in q_1 - and q_3 -axes. (e) Stator phase current 'a'. (f) System evolution in the maximum torque-speed curve.	117
Figure 6.1. Prototipo del vehículo eléctrico perteneciente a ACE-TI.	126
Figura 7.1. Prototipo del vehículo eléctrico perteneciente a ACE-TI.	135

List of Tables

Table 2.1. Look-up table for the DTC controller	47
Table 3.1. Dwell times during the open-phase fault operation.....	69
Table 3.2. Look-up table for the DTC controller in post-fault situation.	69
Table 3.3. Proportional and integral parameters of PI and PR controllers.	86
Table 3.4. Qualitative comparison between RFOC and DTC methods in open-phase fault operation.	92
Table 4.1. A representative set of obtained QI and QET curves in terms of their crossing points at different working conditions for case example #1.....	106
Table 4.2. Analyzed steady-state reference points in Figs. 4.11 and 4.12.	108
Table 4.3. A representative set of obtained QI and QET curves in terms of their crossing points at different working conditions for case example #2.....	112
Table 5.1. Summary of the internationalization derived from this Doctoral Thesis	120
Tableau 6.1. Résumé de l'internationalisation résultant de cette thèse	132
Tabla 7.1. Sumario de la internacionalización derivada de esta Tesis Doctoral	142
Table C.1. Electrical and mechanical parameters of the five-phase DW-IM drive.....	xxxi
Table C.2. Parameters of the five-phase PMSM drive and considered limits.....	xxxi
Table C.3. Parameters of the five-phase CW-IM drive and considered limits.....	xxxii

Chapter 1

Introduction

1.1 Scientific context

The use of electrical drives in embedded systems instead of conventional engines has grown in recent times. This is the case of electric vehicles propulsion and railway traction, all-electric ships, more-electric aircraft, and renewable energies. The specific constraints imposed to the volume of such systems and the constant necessity for higher power ratings lead to optimize the utilization of all components of the electric power train. Therefore, the rated functioning zones are shifted towards their limits, appearing in the system fault situations or nonlinear behaviors such as voltage and current limitations or magnetic saturation. As an example, the use of electrical drives for the propulsion of electrical vehicles requires to control the drive in the whole speed range, including the flux-weakening region where voltage limits are reached.

Compared to classical three-phase drives, multiphase ones reduce the electrical stresses on machine and power electronic components, since they can manage more power with lower torque pulsation and lower current harmonic content, and have inherent fault-tolerance capabilities. Such advantages make them an ideal candidate for applications where limits can be reached and reliability is of special interest for economical and safety reasons. Recent research works on multiphase drives aim to exploit their special characteristics and present them to the industry as an alternative to the three-phase ones, where the higher number of phases results in higher control and design degrees of freedom that can improve the overall reliability and performance of the system.

Consequently, control techniques have been proposed in recent times for multiphase drives, which usually are an extension of the conventional three-phase control structures, aiming for the high speed/torque performance of the drive. Nevertheless, there still exists a lack of research with regard of limit situations that can occur in the machine. If the system works below its limits, it is possible to decompose the system into several subspaces that are independently controlled ('average control'). However, in the case of a system working close to its limits, it is no more possible and a direct control of the whole system is necessary. The main difficulty comes from the way to formalize the problem in order to be able to take into account the constraints along with respecting the given objectives.

In this context, different 'direct control' techniques are proposed in this Doctoral Thesis work to overcome these situations, being Direct Torque Control and Model-based Predictive Control the representatives of this type of techniques.

1.2 Objectives

The general objective of this Doctoral Thesis work is the development of direct control techniques to optimally control multiphase machines, studying the tolerance of the drive to different operating conditions, such as electrical limits (voltage, current and magnetization level limits) or fault tolerance (open-phase fault situation). The meaning of ‘direct control’ techniques is related to those whose control strategy is made without the intervention of a Pulse Width Modulation (PWM) stage or other form of modulation, providing control commands that are directly applied to the power converter. The direct control strategies that will be analyzed in this Thesis are the most used ones in literature, i.e. Direct Torque Control (DTC) and Model-based Predictive Control (MPC). For this purpose, the study will be focused on multiphase drives controlled using different frequency-domain control subspaces. On the one hand, five-phase induction machines with distributed windings, controlled using only one frequency-domain subspace (flux and torque in the α - β plane). On the other hand, five-phase permanent magnet synchronous machines and five-phase induction machines with concentrated windings, which have two controlled subspaces (flux and torque in the α_1 - β_1 and α_3 - β_3 planes). The general objective can be divided more specifically in the following tasks:

- Research on multiphase machines, their advantages/disadvantages over the three-phase ones and their industrial applications, with regard to identify the systems limitations and constraints. Likewise, analysis of the state-of art of direct control strategies (DTC and MPC, as main representatives) to be applied in the multiphase drives control.
- Study and analysis of conventional three-phase DTC strategies and their extension to the fault tolerance case in multiphase drives, focusing on a five-phase drive with one frequency-domain subspace. For this purpose, it is necessary the implementation of new look-up tables for the control variables, with the aim of taking into account in the control strategy the encountered constraints when an open-phase fault occurs in the machine.
- Comparison of the fault-tolerant capability of DTC with other control techniques, to conclude the strengths and weaknesses of the analyzed methods facing the open-phase fault operation.
- Development of an optimal current controller using MPC techniques that allows the optimal utilization of the system’s torque capability under voltage, current and magnetic limitations. The interest of the proposed controller will be verified using five-phase machines with two frequency-domain subspaces.

1.3 Position of the Doctoral Thesis

The Doctoral Thesis work is based on an international joint supervision agreement between the École Nationale Supérieure d’Arts et Métiers (Arts et Métiers from now on) – Campus de Lille, France, and the University of Seville (US), Spain. The supervisors in each institution are Prof. Xavier Kestelyn and Prof. Federico José Barrero García, respectively, who are internationally recognized in the field of multiphase drives and have many years of experience on the topic.

Therefore, making the Doctoral Thesis under their co-supervision is a great opportunity to work at the best level on this field.

At Arts et Métiers, the work takes place at the Laboratoire d'Electrotechnique et d'Electronique de Puissance de Lille (L2EP) within the Control team, being Prof. Kestelyn one of its members. This team is focused on the development of modeling and control formalisms dedicated to energy conversion systems. The Energetic Macroscopic Representation (EMR) and the Generalized Vectorial Formalism (GVF) are multi-physic formalisms that allow to handle a wide field of applications, focusing currently on electrical devices, multiphase drives, piezo-electric actuators and electrical vehicles. The Control team also leads the MEGEVH network (Energetic Management and Modeling of Hybrid Vehicles), which aims to foster collaboration between academic and industrial partners on the subject of modeling and power management of hybrid vehicles.

On the other hand, Prof. Barrero has led the research group Cybernetics Applications of Electronics for Information Technology (ACE-TI) at US. The research fields of this group are, among others, electric vehicles, smart cities or wireless sensor networks. Nowadays, ACE-TI is focused on adapting a test rig for multiphase drives, which belongs to the research group, for its application in the modeling, development and management of the energy in electrical vehicles. A picture of the prototype of the electric vehicle is presented in Fig. 1.1.



Figure 1.1. Prototype of the electric vehicle that belongs to ACE-TI.

This Doctoral Thesis work is focused on what can be defined as basic research. Accordingly, different direct control methods are analyzed to establish a presented and well-defined regulation technique in multiphase drives, where electrical/magnetic limits and critical operating conditions can be managed. However, the work needs a later stage of application-oriented research, which would involve the integration of the used electromagnetic drives and control techniques for their analysis in low- and medium-power electrical systems for industry applications.

Previous Doctoral Thesis works in both institutions are related to the use of multiphase drives and constitute the background of this work. On the part of L2EP, the Doctoral Theses of Xavier Kestelyn and Paul Sandulescu must be emphasized [1–3], which were centered on the modeling

of the machine and its control. Additionally, the studies of Bassel Aslan, Hussein Zahr and Tiago José Dos Santos Moraes [4–6] were focused on the design of different types of multiphase machines for industrial applications. It has to be noted also the works of Li Lu [7], related to the flux-weakening operation in multiphase machines, and Ousmane Fall [8], regarding the inclusion of limits in system. Furthermore, the Doctoral Theses of Raúl Igmarr Gregor Recalde, José Agustín Riveros Insfrán, Hugo Mauricio Guzmán Jiménez and Ignacio González Prieto, on the topic of the development of control strategies for multiphase drives under healthy [9, 10] and open-phase fault operation [11, 12] represent the precedent works from ACE-TI.

1.4 Document organization

This document is organized in the following way. **Chapter 1** introduces the scientific context and the objectives of the present Thesis, showing the position and the background in relation with the two institutions where the work is conducted. A summary of the journal papers and conference works behind this doctoral research work is presented at the end of the chapter. **Chapter 2** describes the state of the art related to the control of multiphase electrical drives. The most recent researches in the scientific literature are commented in order to emphasize the interest of this Thesis. **Chapter 3** is focused on the study of the open-phase fault operation using DTC in multiphase machines with one frequency-domain subspace. An experimental assessment is also carried out comparing the performances of different control strategies, when facing the fault situation. In **Chapter 4**, on the other hand, the case of machines with two frequency-domain subspaces is analyzed. In this case, the DTC strategy seems insufficient to address the situation, since it only allows the control of two degrees of freedom in the system. Therefore, a novel MPC technique is presented to generate online optimal current references taking into account programmed electrical and magnetic constraints, while regulating the currents of the system in order to track the optimal references. The conclusions and the proposition of future work are gathered in **Chapter 5**. Finally, in **Chapters 6 and 7**, a comprehensive summary of the Thesis in French and Spanish, respectively, is detailed to comply with the international joint supervision agreement that supports this work.

1.5 List of publications derived from this work

The publications resulting from this Doctoral Thesis work are listed down below. The main contributions presented in this manuscript are based on the journal papers *Journal I* to *Journal IV*, as well as on the conference papers *Conference I* to *Conference III*.

- **Journal I:** “Open-Phase Fault-Tolerant Direct Torque Control Technique for Five-Phase Induction Motor Drives”. **M. Bermúdez**, I. González-Prieto, F. Barrero, H. Guzmán, M.J. Durán, X. Kestelyn. IEEE Transactions on Industrial Electronics, February 2017.
- **Journal II:** “An Experimental Assessment of Open-Phase Fault-Tolerant Virtual-Vector-Based Direct Torque Control in Five-Phase Induction Motor Drives”. **M. Bermúdez**, I. González-Prieto, F. Barrero, H. Guzmán, X. Kestelyn, M.J. Durán. IEEE Transactions on Power Electronics, March 2018.

- **Journal III:** “Model predictive optimal control considering current and voltage limitations: real-time validation using OPAL-RT technologies and five-phase permanent magnet synchronous machines”. **M. Bermúdez**, O. Gomozov, X. Kestelyn, F. Barrero, N.K. Nguyen, E. Semail. *Mathematics and Computers in Simulation*, July 2018.
- **Journal IV:** “Predictive controller considering electrical constraints: a case example for five-phase induction machines”. **M. Bermúdez**, C. Martín, F. Barrero, X. Kestelyn. *IET Electric Power Applications*, October 2018. UNDER REVIEW.
- **Conference I:** “Open-phase fault operation of 5-phase induction motor drives using DTC techniques”. **M. Bermúdez**, I. González-Prieto, F. Barrero, M.J. Durán, X. Kestelyn. *IECON 2015 - 41st Annual Conference of the IEEE Industrial Electronics Society*, Yokohama, Japan, November 2015.
- **Conference II:** “Comparative study of DTC and RFOC methods for the open-phase fault operation of a 5-phase induction motor drive”. **M. Bermúdez**, H. Guzmán, I. González-Prieto, F. Barrero, M.J. Durán, X. Kestelyn. *IECON 2015 - 41st Annual Conference of the IEEE Industrial Electronics Society*, Yokohama, Japan, November 2015.
- **Conference III:** “Real-time validation of a cascaded model predictive control technique for a five-phase permanent magnet synchronous machine under current and voltage limits”. **M. Bermúdez**, O. Gomozov, X. Kestelyn, N.K. Nguyen, E. Semail, F. Barrero. *ELECTRIMACS 2017*, Toulouse, France, July 2017.

There are other publications related to this work in which the PhD student has collaborated and are listed hereunder. These research results are not directly embedded in this Thesis, although they helped in the development of the whole work.

- **Journal V:** “Optimal Fault-tolerant Control of Six-phase Induction Motor Drives with Parallel Converters”. M.J. Durán, I. González-Prieto, **M. Bermúdez**, F. Barrero, H. Guzmán, M.R. Arahal. *IEEE Transactions on Industrial Electronics*, January 2016.
- **Journal VI:** “Fault-tolerant Operation of Six-phase Energy Conversion Systems with Parallel Machine-Side Converters”. I. González-Prieto, M.J. Durán, H.S. Che, E. Levi, **M. Bermúdez**, F. Barrero. *IEEE Transactions on Power Electronics*, April 2016.
- **Journal VII:** “Impact of Postfault Flux Adaptation on Six-Phase Induction Motor Drives with Parallel Converters”. I. González-Prieto, M.J. Durán, F. Barrero, **M. Bermúdez**, H. Guzmán. *IEEE Transactions on Power Electronics*, January 2017.
- **Journal VIII:** “A Unified Analysis of the Fault Tolerance Capability in Six-phase Induction Motor Drive”. W.N.W.A. Munim, M.J. Durán, H.S. Che, **M. Bermúdez**, I. González-Prieto, N.A. Rahim. *IEEE Transactions on Power Electronics*, October 2017.
- **Journal IX:** “Sensitivity of predictive controllers to parameter variation in five-phase induction motor drives”. C. Martín, **M. Bermúdez**, F. Barrero, M.R. Arahal, X. Kestelyn, M.J. Durán. *Control Engineering Practice*, November 2017.
- **Journal X:** “Vectores Virtuales de Tensión en Control Directo de Par para una Máquina de Inducción de Seis Fases”. P. García, I. González-Prieto, M.J. Durán, **M. Bermúdez**, F. Barrero. *Revista Iberoamericana de Automática e Informática Industrial (RIAI)*, June 2018.
- **Journal XI:** “Tolerancia al Fallo en Control Directo de Par con Vectores Virtuales de Tensión”. I. González-Prieto, P. García, M.J. Durán, **M. Bermúdez**, F. Barrero. *Revista Iberoamericana de Automática e Informática Industrial (RIAI)*, July 2018.

- **Journal XII:** “A Universal Model Predictive Control for Normal and Faulty Operation of Six-Phase Induction Machines”. I. González-Prieto, M.J. Durán, **M. Bermúdez**, F. Barrero, C. Martín. IEEE Transactions on Power Electronics, September 2018. UNDER REVIEW.
- **Conference IV:** “A scientific approach in wind energy courses for electrical engineers”. M.J. Duran, F. Barrero, I. González-Prieto, H. Guzmán, A. Pozo, **M. Bermúdez**, C. Martín. Technologies Applied to Electronics Teaching (TAEE), Seville, Spain, June 2016.
- **Conference V:** “Application of Modern Microprocessor in Power Conversion Systems: A Practical Approach for Multiphase Drives”. C. Martín, **M. Bermúdez**, F. Barrero, H. Guzmán. 12th International Scientific Conference on Electrical, Computer, Electronics and Engineering, Dubai, United Arab Emirates, September 2016.

Chapter 2

State of the Art of Multiphase Drives

The literature explored in this chapter is focused to describe the state of the art related to the control of multiphase electrical drives. For such purpose, the most recent research works in the area are analyzed to generate a theoretical framework that allows a better understanding of the work presented in this Thesis. More specifically, **Section 2.1** introduces the fundamentals and origins of multiphase electrical drives. **Section 2.2** presents the mathematical model for various types of multiphase machines and for the power converter. Subsequently, **Section 2.3** analyzes different techniques proposed for the control of multiphase drives. With the aim of emphasizing the interest of this Thesis, **Section 2.4** examines different limit situations that can be considered in the study of multiphase drives. A brief review regarding the graphical formalisms for control is also presented in **Section 2.5**. This chapter ends with the most relevant conclusions in **Section 2.6**.

2.1 Historical review of multiphase drives

The term ‘multiphase drives’ refers to energy conversion systems that use electrical machines with stator windings with more than three phases. Despite the fact that the study of multiphase drives goes back to the end of the 60’s [13], the interest in their technological development has only recently been shown, and at a more scientific than industrial level. At that time, the main problem with the three-phase motors fed by the existing electronic switching devices was the torque fluctuation on the machine shaft, at a frequency six times higher than the fundamental frequency of the inverter. The increase in the number of phases was proposed in [13] as a solution to this problem, reporting torque ripples three times smaller in five-phase machines than the one obtained with its three-phase equivalent, although with an increase in the third harmonic. This proposal was postponed due to the PWM techniques developed for three-phase drives, which mitigated the fluctuation that occurred in the torque of the machine and thus achieved the correct performance of the system.

Since then, the interest and study of multiphase machines had limited attention due to the increment in the number of variables to be controlled and their greater complexity. It was not until the beginning of this last century that multiphase machine became one of the main focuses of the scientific community, after the development achieved in several technologies, like high power and high switching frequency semiconductor devices, and powerful microelectronic control units (digital signal processors and field-programmable gate arrays) [14]. These developments together

with the increasing computational power have led the exploitation of new and more sophisticated control techniques. Consequently, recent research works propose multiphase drives for high performance industrial applications, such as wind energy generation, electric propulsion of ships (all-electric ships), traction (covering both hybrid and electric vehicles and locomotives), and the concept of more-electric aircraft, which seeks the replacement of traditional auxiliary mechanical, pneumatic and hydraulic systems in aircrafts by electrical, electromechanical or electrohydraulic systems [14–16]. For example, a recent overview states that multiphase machines can be a favored choice for general aerospace applications [17], and an actual work details a nine-phase permanent magnet traction motor used in ultrahigh-speed elevators [18]. Likewise, another work proposes the use of a six-phase permanent magnet machine for the application of oil pumping to increase its fault tolerance and reduce the retention of the system operation [19]. In such applications, the use of multiphase drives is more appropriate than three-phase ones, since they present the following advantages [14,15,20,21]:

- The stator excitation in a multiphase machine produces a field with lower harmonic content and higher efficiency than those achieved in a three-phase machine.
- Lower torque pulsations: the lower frequency of torque pulsation in a n -phase machine is caused by the harmonic of order $2n \pm 1$ injected by the power supply.
- Lower harmonic content in the DC-link currents of the power converters that feed the electromechanical drives.
- Improved power distribution per phase, decreasing the current rating through each phase when the number of phases increases for a given nominal power, which makes possible a smaller deterioration of the converters.
- High torque density: some designs allow to increase the torque production capability by means of the injection of current harmonic components in the stator.
- Fault-tolerant capability: a n -phase machine with one or multiple phases in fault condition can operate without requiring external equipment as long as the number of faulty phases is no more than $(n - 3)$, at the expense of lower torque and current ratings.

Multiphase machines are traditionally classified depending on the winding arrangement like symmetrical or asymmetrical machines. Symmetrical machines are formed by consecutive phase windings equally displaced $2\pi/n$, while asymmetrical machines are constituted by independent sets of windings. In addition, multiphase machines can be also classified by the number of odd or even phases they possess and if the number of phases is multiple of three. On the other hand, multiphase induction machines can be classified depending on the winding distribution as machines with concentrated or distributed windings. Multiphase induction machine with concentrated windings generate a high harmonic flux content when a sinusoidal stator voltage is applied, which can be used to enhance the electrical torque production. It must be noted that in the case of permanent magnet multiphase machines this is always possible. However, this flux harmonic content only generates electromagnetic losses in the induction machine if the distributed winding topology is used.

The research work developed in this field is very broad, finding papers that explore the different advances in the area [14,15,22–26]. They show that symmetrical five-phase and asymmetrical six-phase machines with isolated neutrals are the most popular considering the design, modeling and control of the drive. The control methods used in multiphase drives are, in

principle, an extension of those used in three-phase drives. Thus, Scalar Control was one of the first techniques to be studied [27–29]. Subsequently, the effort focused on Vector Control [30–32] and Direct Torque Control [33,34]. The Predictive Control has very recently been applied in these drives, focusing on its use as a current controller [35–39]. All these schemes will be discussed in more depth throughout this chapter.

This section has presented multiphase drives as an interesting technology, constituted by different types of machines and control techniques. Their special benefits, compared to classical three-phase machines, have made them attractive not only within the research community, but also in some industrial applications. Therefore, the requirement for continuous research on the topic is justified in order to meet industry and safety standards while exploiting their benefits at reasonable costs.

2.2 Modeling of the multiphase drive

In this section, the model of the induction machine with distributed windings is deduced in the first place, considering the general case of n phases. The complexity of the model will be greater than for three-phase machines due to the increase in the number of phases. Firstly, the physical model of the drive is described. From this model, applying the Clarke transformation, the complexity of the model is simplified, remaining the machine described in orthogonal planes. Being a machine with only one frequency-domain subspace, all the electromagnetic energy conversion is mapped exclusively in one of the planes, so the losses produced when operating the machine will be mapped in the remaining planes. Subsequently, the model is described in a general reference frame and a greater simplification can be achieved, reaching a certain analogy with the control of a DC machine. The model is then particularized for the five-phase case, which in the end will be the one used in the development of this Thesis.

Next, the models of five-phase machines with two frequency-domain subspaces are analyzed, i.e. induction machine with concentrated windings and permanent magnet synchronous machine. These designs allow a greater use of the magnetic flux in the air gap of the machine, generating the electromagnetic energy conversion in two planes, thus obtaining an improvement in the performance of the system. Note that model of these three types of machines will be used in the different speed control schemes that are evaluated in this work.

Finally, the model of the power converter that supplies the multiphase machine is studied, with the aim of completing the modeling of the multiphase drive. The study is firstly focused on the model of the n -leg two-level power converter and then particularized to the five-leg case.

2.2.1 Multiphase machines with one frequency-domain subspace: distributed winding induction machine case

Induction machines (IM) are one of the most used electromechanical devices in industrial applications due to their low production and maintenance costs. The general theory of electrical machines and multiphase systems has enough tools to define the model of the system, considering an arbitrary number of phases. The generalization of Fortescue and Clarke is the basis for the

extension of the vector models currently used [40,41]. These research works propose different mathematical transformations to replace the representation originally expressed in phase variables (voltages, currents, fluxes...) by an equivalent representation whose advantage is the simplification of the dynamic equations of the system that describe the operation of the multiphase machine. So far, multiple works have been developed focusing on the modeling of multiphase machines, differentiating between machines with an arbitrary odd or even number of phases [42–44] and if the number of phases is multiple of three [45–47]. This subsection describes the general modeling of symmetrical distributed windings induction machines (DW-IM) with an odd number of phases.

Considerations for modeling

The symmetrical n -phase IM (Fig. 2.1) consists of n windings with an electrical displacement evenly distributed in the stator ($\vartheta = 2\pi/n$). These windings have a sinusoidal spatial distribution along the stator, configured in p pairs of poles. The machine rotor is a squirrel cage topology whose modeling behavior can be considered equivalent to n inductive loads interconnected in parallel. The following hypotheses have also been assumed:

- All the machine windings are identical and equally distributed around the stator and rotor.
- The magnetization characteristic of the ferromagnetic material is assumed to be linear, therefore the effects of magnetic field saturation are negligible.
- The couplings due to leakage inductances, reluctance changes dependent on the rotor position and core losses due to eddy currents are not considered.
- The variations due to temperature or frequency, as well as non-linearities are also neglected.
- The machine air gap is considered to be uniform and of constant density, disregarding its variation due to rotor eccentricities or stator and rotor slots.

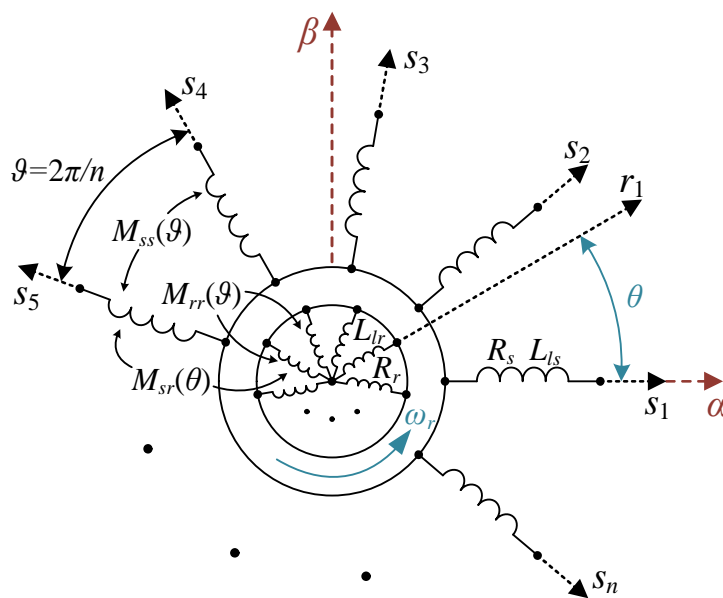


Figure 2.1. Schematic of the symmetrical n -phase induction machine.

Model in phase variables (physical model)

Taking into account the above considerations, the symmetrical n -phase IM can be modeled by the following set of differential equations, obtained by analyzing the magnetic coupling of the stator and rotor circuits:

$$[v_s] = [R_s] \cdot [i_s] + \frac{d}{dt}[\lambda_s] = [R_s] \cdot [i_s] + [L_{ss}] \cdot \frac{d}{dt}[i_s] + \frac{d}{dt}([L_{sr}(\theta)] \cdot [i_r]) \quad (2.1)$$

$$[v_r] = [R_r] \cdot [i_r] + \frac{d}{dt}[\lambda_r] = [R_r] \cdot [i_r] + [L_{rr}] \cdot \frac{d}{dt}[i_r] + \frac{d}{dt}([L_{rs}(\theta)] \cdot [i_s]) \quad (2.2)$$

$$\theta = \int_0^t \omega_r \cdot dt \quad (2.3)$$

In these equations v , i and λ denote voltage, current and flux variables, respectively, while the s and r subscripts identify the stator and rotor variables, respectively. The instantaneous rotor coordinate with respect to the stator is represented by θ , while ω_r is the rotor electrical velocity. The voltage, current and flux vectors are defined in (2.4)–(2.9), being the variables corresponding to each phase represented by the subscripts 1, 2, 3, ..., n , where it can be noted that the rotor phase voltages are null because of considering the case of a squirrel cage asynchronous IM.

$$[v_s] = [v_{s1} \ v_{s2} \ v_{s3} \ \cdots \ v_{sn}]^T \quad (2.4)$$

$$[v_r] = [v_{r1} \ v_{r2} \ v_{r3} \ \cdots \ v_{rn}]^T = [0 \ 0 \ 0 \ \cdots \ 0]^T \quad (2.5)$$

$$[i_s] = [i_{s1} \ i_{s2} \ i_{s3} \ \cdots \ i_{sn}]^T \quad (2.6)$$

$$[i_r] = [i_{r1} \ i_{r2} \ i_{r3} \ \cdots \ i_{rn}]^T \quad (2.7)$$

$$[\lambda_s] = [\lambda_{s1} \ \lambda_{s2} \ \lambda_{s3} \ \cdots \ \lambda_{sn}]^T \quad (2.8)$$

$$[\lambda_r] = [\lambda_{r1} \ \lambda_{r2} \ \lambda_{r3} \ \cdots \ \lambda_{rn}]^T \quad (2.9)$$

Stator and rotor windings possess N_s and N_r turns, respectively, so the transformation ratio in the stator-rotor coupling (k_w) is defined according to equation (2.10). The components of the voltage, current and flux rotor variables referred to the stator are obtained from the real rotor components $[v'_r]$, $[i'_r]$ and $[\lambda'_r]$, respectively, through equations (2.11)–(2.13):

$$k_w = \frac{N_s}{N_r} \quad (2.10)$$

$$[i_r] = \frac{1}{k_w} \cdot [i'_r] \quad (2.11)$$

$$[v_r] = k_w \cdot [v'_r] \quad (2.12)$$

$$[\lambda_r] = k_w \cdot [\lambda'_r] \quad (2.13)$$

The impedance matrices are defined as described in equations (2.14)–(2.18), where $[I_n]$ is the identity matrix of order n , the stator and rotor resistances are R_s and R'_r , respectively, the mutual inductance is represented by M , while L_{ls} and L_{lr} designate the stator and rotor leakage inductances, respectively.

$$[R_s] = R_s \cdot [I_n] \quad (2.14)$$

$$[R_r] = R_r \cdot [I_n] = k_w^2 \cdot R'_r \cdot [I_n] \quad (2.15)$$

$$[L_{ss}] = L_{ls} \cdot [I_n] + [M_{ss}(\vartheta)] \quad (2.16)$$

$$[L_{rr}] = L_{lr} \cdot [I_n] + [M_{rr}(\vartheta)] \quad (2.17)$$

$$[L_{sr}(\theta)] = [L_{rs}(\theta)]^T = [M_{sr}(\theta)] \quad (2.18)$$

where $[M_{ss}(\vartheta)]$, $[M_{rr}(\vartheta)]$ and $[M_{sr}(\theta)]$ are defined as follows:

$$[M_{ss}(\vartheta)] = [M_{rr}(\vartheta)] = M \cdot \begin{bmatrix} 1 & \cos(\vartheta) & \cos(2\vartheta) & \cdots & \cos((n-1)\vartheta) \\ \cos((n-1)\vartheta) & 1 & \cos(\vartheta) & \cdots & \cos((n-2)\vartheta) \\ \cos((n-2)\vartheta) & \cos((n-1)\vartheta) & 1 & \cdots & \cos((n-3)\vartheta) \\ \vdots & \vdots & \vdots & \ddots & \vdots \\ \cos(\vartheta) & \cos(2\vartheta) & \cos(3\vartheta) & \cdots & 1 \end{bmatrix} \quad (2.19)$$

$$[M_{sr}(\theta)] = M \cdot \begin{bmatrix} \cos(\Delta_1) & \cos(\Delta_2) & \cos(\Delta_3) & \cos(\Delta_4) & \cdots & \cos(\Delta_n) \\ \cos(\Delta_n) & \cos(\Delta_1) & \cos(\Delta_2) & \cos(\Delta_3) & \cdots & \cos(\Delta_{n-1}) \\ \cos(\Delta_{n-1}) & \cos(\Delta_n) & \cos(\Delta_1) & \cos(\Delta_2) & \cdots & \cos(\Delta_{n-2}) \\ \cos(\Delta_{n-2}) & \cos(\Delta_{n-1}) & \cos(\Delta_n) & \cos(\Delta_1) & \cdots & \cos(\Delta_{n-3}) \\ \vdots & \vdots & \vdots & \vdots & \ddots & \vdots \\ \cos(\Delta_2) & \cos(\Delta_3) & \cos(\Delta_4) & \cos(\Delta_5) & \cdots & \cos(\Delta_1) \end{bmatrix} \quad (2.20)$$

and the angle Δ_k is determined through the following expression:

$$\Delta_k = \theta + (k-1) \cdot \vartheta \quad \text{with } k = 1, 2, 3, \dots, n \quad (2.21)$$

The electromagnetic torque T_{em} , generated as a function of the stator and rotor phase currents, is obtained by means of the magnetic coenergy function (W_{co}) of the machine, as shown in the next equation:

$$T_{em} = \frac{dW_{co}}{d\theta} = \frac{p}{2} \cdot \begin{bmatrix} [i_s] \\ [i_r] \end{bmatrix}^T \cdot \begin{bmatrix} [L_{ss}] & [L_{sr}(\theta)] \\ [L_{rs}(\theta)] & [L_{rr}] \end{bmatrix} \cdot \begin{bmatrix} [i_s] \\ [i_r] \end{bmatrix} \quad (2.22)$$

From this equation and using the inductance matrices described in equations (2.16)–(2.21), the following matrix expression for the electromagnetic torque is obtained:

$$T_{em} = p \cdot [i_s]^T \cdot \frac{d}{d\theta} [L_{sr}(\theta)] \cdot [i_r] \quad (2.23)$$

Analytically developing the above expression, the electromagnetic torque is obtained from the next equation:

$$\begin{aligned} T_{em} = & -p \cdot M \cdot \left\{ (i_{s1} \cdot i_{r1} + i_{s2} \cdot i_{r2} + i_{s3} \cdot i_{r3} + \dots + i_{sn} \cdot i_{rn}) \cdot \sin(\theta) \right. \\ & + (i_{s1} \cdot i_{r2} + i_{s2} \cdot i_{r3} + i_{s3} \cdot i_{r4} + \dots + i_{sn} \cdot i_{r1}) \cdot \sin(\theta - \vartheta) \\ & + (i_{s1} \cdot i_{r3} + i_{s2} \cdot i_{r4} + i_{s3} \cdot i_{r5} + \dots + i_{sn} \cdot i_{r2}) \cdot \sin(\theta - 2\vartheta) \\ & \vdots \\ & \left. + (i_{s1} \cdot i_{rn} + i_{s2} \cdot i_{r1} + i_{s3} \cdot i_{r2} + \dots + i_{sn} \cdot i_{r(n-1)}) \cdot \sin(\theta - (n-1)\vartheta) \right\} \end{aligned} \quad (2.24)$$

The generated electromagnetic torque is in turn mechanically coupled to the load applied on the machine shaft, verifying the following differential equation:

$$J_m \cdot \frac{d\omega_m}{dt} = T_{em} - T_L - B_m \cdot \omega_m \quad (2.25)$$

being ω_m the mechanical speed of the rotor shaft ($\omega_r = p \cdot \omega_m$), T_L the load torque applied to the machine, J_m the rotational inertial constant and B_m the friction coefficient of the rotor-load bearings.

Clarke decoupled model (stationary reference frame)

The previously described model based on phase variables presents as main drawback the dependence of the rotor position in the definition of the inductance matrices and in the determination of the electromagnetic torque. This difficulty can be overcome using the Vector Space Decomposition (VSD) theory, which considers the machine variables in a stationary reference frame. Thus, the Clarke transformation is applied to the model described in (2.1)–(2.21) in the previous subsection, by means of the square matrix $[C_n]$ of order n presented in (2.26). The machine is represented through the transformed components in a new space defined by $(n-1)/2$ two-dimensional orthogonal planes (called α - β , x_1 - y_1 , x_2 - y_2 , ...), whose components are the projections of the original space (phase variables) to the new reference frame, plus an axis that contains the homopolar component (z -component). Since the planes that constitute the new space are orthogonal, they will be completely decoupled from each other, achieving an important simplification in the machine model.

$$[C_n] = \frac{2}{n} \cdot \begin{bmatrix} 1 & \cos(\vartheta) & \cos(2\vartheta) & \cdots & \cos((n-1)\cdot\vartheta) \\ 0 & \sin(\vartheta) & \sin(2\vartheta) & \cdots & \sin((n-1)\cdot\vartheta) \\ 1 & \cos(2\vartheta) & \cos(4\vartheta) & \cdots & \cos(2(n-1)\cdot\vartheta) \\ 0 & \sin(2\vartheta) & \sin(4\vartheta) & \cdots & \sin(2(n-1)\cdot\vartheta) \\ \vdots & \vdots & \vdots & \ddots & \vdots \\ 1 & \cos\left(\frac{(n-1)\cdot\vartheta}{2}\right) & \cos\left(\frac{(n-1)\cdot2\vartheta}{2}\right) & \cdots & \cos\left(\frac{(n-1)\cdot(n-1)\cdot\vartheta}{2}\right) \\ 0 & \sin\left(\frac{(n-1)\cdot\vartheta}{2}\right) & \sin\left(\frac{(n-1)\cdot2\vartheta}{2}\right) & \cdots & \sin\left(\frac{(n-1)\cdot(n-1)\cdot\vartheta}{2}\right) \\ \frac{1}{2} & \frac{1}{2} & \frac{1}{2} & \cdots & \frac{1}{2} \end{bmatrix} \quad (2.26)$$

The coefficient used in this transformation is $2/n$ in order to obtain the property of keeping invariant the electrical magnitudes. In different research works [15,20,48], it is used the transformation coefficient $\sqrt{(2/n)}$, giving rise to a power invariant transformation. Applying the matrix to the machine model, pre-multiplying $[C_n]$ in (2.1) and (2.2):

$$[C_n] \cdot [v_s] = [C_n] \cdot [R_s] \cdot [C_n]^{-1} \cdot [C_n] \cdot [i_s] + [C_n] \cdot [L_{ss}] \cdot [C_n]^{-1} \cdot \frac{d}{dt}([C_n] \cdot [i_s]) + \frac{d}{dt}([C_n] \cdot [L_{sr}(\theta)] \cdot [C_n]^{-1} \cdot [C_n] \cdot [i_r]) \quad (2.27)$$

$$[0] = [C_n] \cdot [R_r] \cdot [C_n]^{-1} \cdot [C_n] \cdot [i_r] + [C_n] \cdot [L_{rr}] \cdot [C_n]^{-1} \cdot \frac{d}{dt}([C_n] \cdot [i_r]) + \frac{d}{dt}([C_n] \cdot [L_{rs}(\theta)] \cdot [C_n]^{-1} \cdot [C_n] \cdot [i_s]) \quad (2.28)$$

The phase variables are now transformed into the new reference frame. The new voltage, current and flux vectors are defined as follows:

$$\begin{bmatrix} v_{s\alpha} \\ v_{s\beta} \\ v_{sx_1} \\ v_{sy_1} \\ \vdots \\ v_{sx_{(n-3)/2}} \\ v_{sy_{(n-3)/2}} \\ v_{sz} \end{bmatrix} = [C_n] \cdot [v_s]; \quad \begin{bmatrix} i_{s\alpha} \\ i_{s\beta} \\ i_{sx_1} \\ i_{sy_1} \\ \vdots \\ i_{sx_{(n-3)/2}} \\ i_{sy_{(n-3)/2}} \\ i_{sz} \end{bmatrix} = [C_n] \cdot [i_s]; \quad \begin{bmatrix} \lambda_{s\alpha} \\ \lambda_{s\beta} \\ \lambda_{sx_1} \\ \lambda_{sy_1} \\ \vdots \\ \lambda_{sx_{(n-3)/2}} \\ \lambda_{sy_{(n-3)/2}} \\ \lambda_{sz} \end{bmatrix} = [C_n] \cdot [\lambda_s] \quad (2.29)$$

$$\begin{bmatrix} v'_{r\alpha} \\ v'_{r\beta} \\ v'_{rx_1} \\ v'_{ry_1} \\ \vdots \\ v'_{rx_{(n-3)/2}} \\ v'_{ry_{(n-3)/2}} \\ v'_{rz} \end{bmatrix} = [C_n] \cdot [v_r]; \quad \begin{bmatrix} i'_{r\alpha} \\ i'_{r\beta} \\ i'_{rx_1} \\ i'_{ry_1} \\ \vdots \\ i'_{rx_{(n-3)/2}} \\ i'_{ry_{(n-3)/2}} \\ i'_{rz} \end{bmatrix} = [C_n] \cdot [i_r]; \quad \begin{bmatrix} \lambda'_{r\alpha} \\ \lambda'_{r\beta} \\ \lambda'_{rx_1} \\ \lambda'_{ry_1} \\ \vdots \\ \lambda'_{rx_{(n-3)/2}} \\ \lambda'_{ry_{(n-3)/2}} \\ \lambda'_{rz} \end{bmatrix} = [C_n] \cdot [\lambda_r] \quad (2.30)$$

The stator and rotor resistance and inductance matrices with the new transformation are:

$$[C_n] \cdot [R_s] \cdot [C_n]^{-1} = [R_s] \quad (2.31)$$

$$[C_n] \cdot [R_r] \cdot [C_n]^{-1} = [R_r] \quad (2.32)$$

$$[C_n] \cdot [L_{ss}] \cdot [C_n]^{-1} = L_{ls} \cdot [I_n] + M \cdot \begin{bmatrix} \frac{n}{2} & 0 & 0 & 0 & \cdots & 0 \\ 0 & \frac{n}{2} & 0 & 0 & \cdots & 0 \\ 0 & 0 & 0 & 0 & \cdots & 0 \\ 0 & 0 & 0 & 0 & \cdots & 0 \\ \vdots & \vdots & \vdots & \vdots & \ddots & \vdots \\ 0 & 0 & 0 & 0 & \cdots & 0 \end{bmatrix} = \begin{bmatrix} L_s & 0 & 0 & 0 & \cdots & 0 \\ 0 & L_s & 0 & 0 & \cdots & 0 \\ 0 & 0 & L_{ls} & 0 & \cdots & 0 \\ 0 & 0 & 0 & L_{ls} & \cdots & 0 \\ \vdots & \vdots & \vdots & \vdots & \ddots & \vdots \\ 0 & 0 & 0 & 0 & \cdots & L_{ls} \end{bmatrix} \quad (2.33)$$

$$[C_n] \cdot [L_{sr}(\theta)] \cdot [C_n]^{-1} = \frac{n}{2} \cdot M \cdot \begin{bmatrix} \cos(\theta) & -\sin(\theta) & 0 & 0 & \cdots & 0 \\ \sin(\theta) & \cos(\theta) & 0 & 0 & \cdots & 0 \\ 0 & 0 & 0 & 0 & \cdots & 0 \\ 0 & 0 & 0 & 0 & \cdots & 0 \\ \vdots & \vdots & \vdots & \vdots & \ddots & \vdots \\ 0 & 0 & 0 & 0 & \cdots & 0 \end{bmatrix} \quad (2.34)$$

$$[C_n] \cdot [L_{rr}] \cdot [C_n]^{-1} = L_{lr} \cdot [I_n] + M \cdot \begin{bmatrix} \frac{n}{2} & 0 & 0 & 0 & \cdots & 0 \\ 0 & \frac{n}{2} & 0 & 0 & \cdots & 0 \\ 0 & 0 & 0 & 0 & \cdots & 0 \\ 0 & 0 & 0 & 0 & \cdots & 0 \\ \vdots & \vdots & \vdots & \vdots & \ddots & \vdots \\ 0 & 0 & 0 & 0 & \cdots & 0 \end{bmatrix} = \begin{bmatrix} L_r & 0 & 0 & 0 & \cdots & 0 \\ 0 & L_r & 0 & 0 & \cdots & 0 \\ 0 & 0 & L_{lr} & 0 & \cdots & 0 \\ 0 & 0 & 0 & L_{lr} & \cdots & 0 \\ \vdots & \vdots & \vdots & \vdots & \ddots & \vdots \\ 0 & 0 & 0 & 0 & \cdots & L_{lr} \end{bmatrix} \quad (2.35)$$

$$[C_n] \cdot [L_{rs}(\theta)] \cdot [C_n]^{-1} = \frac{n}{2} \cdot M \cdot \begin{bmatrix} \cos(\theta) & \sin(\theta) & 0 & 0 & \cdots & 0 \\ -\sin(\theta) & \cos(\theta) & 0 & 0 & \cdots & 0 \\ 0 & 0 & 0 & 0 & \cdots & 0 \\ 0 & 0 & 0 & 0 & \cdots & 0 \\ \vdots & \vdots & \vdots & \vdots & \ddots & \vdots \\ 0 & 0 & 0 & 0 & \cdots & 0 \end{bmatrix} \quad (2.36)$$

where $L_s = L_{ls} + L_m$ and $L_r = L_{lr} + L_m$ are the stator and rotor inductance in the new reference frame, respectively, while $L_m = (n/2) \cdot M$ is the new mutual inductance.

Taking into account the aforementioned considerations, the Clarke decoupled model is described by a set of voltage equations in every subspace, which will be separately studied below.

• *Model in the α - β subspace:*

The voltage equations in this subspace are:

$$\begin{bmatrix} v_{s\alpha} \\ v_{s\beta} \end{bmatrix} = \begin{bmatrix} R_s & 0 \\ 0 & R_s \end{bmatrix} \cdot \begin{bmatrix} i_{s\alpha} \\ i_{s\beta} \end{bmatrix} + \frac{d}{dt} \left(\begin{bmatrix} L_s & 0 \\ 0 & L_s \end{bmatrix} \cdot \begin{bmatrix} i_{s\alpha} \\ i_{s\beta} \end{bmatrix} \right) + L_m \cdot \begin{bmatrix} \cos(\theta) & -\sin(\theta) \\ \sin(\theta) & \cos(\theta) \end{bmatrix} \cdot \begin{bmatrix} i'_{r\alpha} \\ i'_{r\beta} \end{bmatrix} \quad (2.37)$$

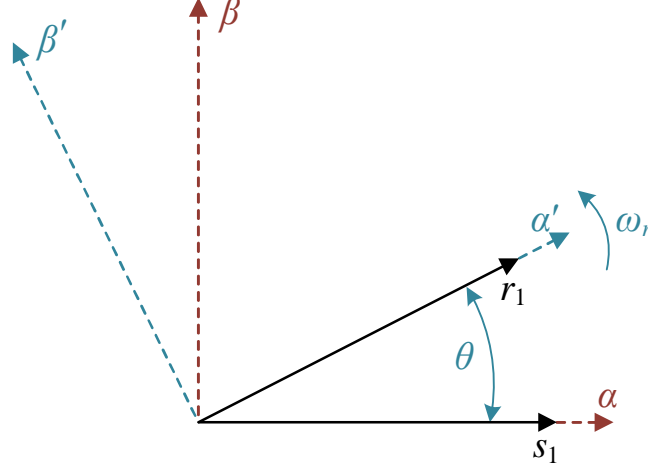
$$\begin{bmatrix} 0 \\ 0 \end{bmatrix} = \begin{bmatrix} R_r & 0 \\ 0 & R_r \end{bmatrix} \cdot \begin{bmatrix} i'_{r\alpha} \\ i'_{r\beta} \end{bmatrix} + \frac{d}{dt} \left(\begin{bmatrix} L_r & 0 \\ 0 & L_r \end{bmatrix} \cdot \begin{bmatrix} i'_{r\alpha} \\ i'_{r\beta} \end{bmatrix} \right) + L_m \cdot \begin{bmatrix} \cos(\theta) & \sin(\theta) \\ -\sin(\theta) & \cos(\theta) \end{bmatrix} \cdot \begin{bmatrix} i_{s\alpha} \\ i_{s\beta} \end{bmatrix} \quad (2.38)$$

This set of equations represents the components of the α - β plane, where the fundamental of the flux is mapped and, therefore, it is the plane where the electromechanical energy conversion takes place. After the application of the transformation, the rotor and stator variables are referred to different reference frames (Fig. 2.2). The stator variables are associated with a stationary reference frame (α - β), while the rotor variables are linked to a reference frame fixed to the rotor (α' - β') that is rotating at a speed ω_r . This maintains the dependence of some inductances on the instantaneous rotor coordinate θ , as it happened in the case of the model in phase variables. In order to avoid this situation, all the variables must be represented with respect to the same reference frame (stationary reference frame in this case), using the following rotation matrix for the rotor variables:

$$[T_r(\theta)] = \begin{bmatrix} \cos(\theta) & -\sin(\theta) \\ \sin(\theta) & \cos(\theta) \end{bmatrix}; \quad [T_r(\theta)]^{-1} = [T_r(\theta)]^T = [T_r(-\theta)] \quad (2.39)$$

Applying this rotation matrix, the new rotor variables are transformed as follows:

$$\begin{bmatrix} v_{r\alpha} \\ v_{r\beta} \end{bmatrix} = [T_r(\theta)] \cdot \begin{bmatrix} v'_{r\alpha} \\ v'_{r\beta} \end{bmatrix}; \quad \begin{bmatrix} i_{r\alpha} \\ i_{r\beta} \end{bmatrix} = [T_r(\theta)] \cdot \begin{bmatrix} i'_{r\alpha} \\ i'_{r\beta} \end{bmatrix}; \quad \begin{bmatrix} \lambda_{r\alpha} \\ \lambda_{r\beta} \end{bmatrix} = [T_r(\theta)] \cdot \begin{bmatrix} \lambda'_{r\alpha} \\ \lambda'_{r\beta} \end{bmatrix} \quad (2.40)$$


 Figure 2.2. Reference frames of stator (α - β) and rotor (α' - β') variables.

Therefore, the stator voltage equation in the α - β subspace will be:

$$\begin{bmatrix} v_{s\alpha} \\ v_{s\beta} \end{bmatrix} = \begin{bmatrix} R_s & 0 \\ 0 & R_s \end{bmatrix} \cdot \begin{bmatrix} i_{s\alpha} \\ i_{s\beta} \end{bmatrix} + \frac{d}{dt} \left(\begin{bmatrix} L_s & 0 \\ 0 & L_s \end{bmatrix} \cdot \begin{bmatrix} i_{s\alpha} \\ i_{s\beta} \end{bmatrix} + L_m \cdot \begin{bmatrix} i_{r\alpha} \\ i_{r\beta} \end{bmatrix} \right) \quad (2.41)$$

With the aim of obtaining the rotor voltage equation, it is necessary to pre-multiply equation (2.38) by $[T_r(\theta)]$:

$$\begin{aligned} \begin{bmatrix} 0 \\ 0 \end{bmatrix} &= \underbrace{[T_r(\theta)] \cdot \begin{bmatrix} R_r & 0 \\ 0 & R_r \end{bmatrix} \cdot [T_r(-\theta)]}_{\boxed{a}} \cdot \underbrace{[T_r(\theta)] \cdot \begin{bmatrix} i'_{r\alpha} \\ i'_{r\beta} \end{bmatrix}}_{\boxed{b}} \\ &+ \underbrace{[T_r(\theta)] \cdot \frac{d}{dt} \left(\begin{bmatrix} L_r & 0 \\ 0 & L_r \end{bmatrix} \cdot \begin{bmatrix} i'_{r\alpha} \\ i'_{r\beta} \end{bmatrix} \right)}_{\boxed{c}} + \underbrace{[T_r(\theta)] \cdot \frac{d}{dt} \left(L_m \cdot \begin{bmatrix} \cos(\theta) & \sin(\theta) \\ -\sin(\theta) & \cos(\theta) \end{bmatrix} \cdot \begin{bmatrix} i_{s\alpha} \\ i_{s\beta} \end{bmatrix} \right)}_{\boxed{d}} \end{aligned} \quad (2.42)$$

where:

$$\boxed{a} = [T_r(\theta)] \cdot \begin{bmatrix} R_r & 0 \\ 0 & R_r \end{bmatrix} \cdot [T_r(-\theta)] = \begin{bmatrix} R_r & 0 \\ 0 & R_r \end{bmatrix} \quad (2.42a)$$

$$\boxed{b} = [T_r(\theta)] \cdot \begin{bmatrix} i'_{r\alpha} \\ i'_{r\beta} \end{bmatrix} = \begin{bmatrix} i_{r\alpha} \\ i_{r\beta} \end{bmatrix} \quad (2.42b)$$

$$\begin{aligned} \boxed{c} &= [T_r(\theta)] \cdot \frac{d}{dt} \left(\begin{bmatrix} L_r & 0 \\ 0 & L_r \end{bmatrix} \cdot \begin{bmatrix} i'_{r\alpha} \\ i'_{r\beta} \end{bmatrix} \right) = [T_r(\theta)] \cdot \frac{d}{dt} \left(\begin{bmatrix} L_r & 0 \\ 0 & L_r \end{bmatrix} \cdot [T_r(-\theta)] \cdot \begin{bmatrix} i_{r\alpha} \\ i_{r\beta} \end{bmatrix} \right) = \\ &= \frac{d\theta}{dt} \cdot \begin{bmatrix} 0 & L_r \\ -L_r & 0 \end{bmatrix} \cdot \begin{bmatrix} i_{r\alpha} \\ i_{r\beta} \end{bmatrix} + \begin{bmatrix} L_r & 0 \\ 0 & L_r \end{bmatrix} \cdot \frac{d}{dt} \begin{bmatrix} i_{r\alpha} \\ i_{r\beta} \end{bmatrix} \end{aligned} \quad (2.42c)$$

$$\begin{aligned} \boxed{d} &= [T_r(\theta)] \cdot \frac{d}{dt} \left(L_m \cdot \begin{bmatrix} \cos(\theta) & \sin(\theta) \\ -\sin(\theta) & \cos(\theta) \end{bmatrix} \cdot \begin{bmatrix} i_{s\alpha} \\ i_{s\beta} \end{bmatrix} \right) = [T_r(\theta)] \cdot \frac{d}{dt} \left(L_m \cdot [T_r(-\theta)] \cdot \begin{bmatrix} i_{s\alpha} \\ i_{s\beta} \end{bmatrix} \right) \\ &= \frac{d\theta}{dt} \cdot \begin{bmatrix} 0 & L_m \\ -L_m & 0 \end{bmatrix} \cdot \begin{bmatrix} i_{s\alpha} \\ i_{s\beta} \end{bmatrix} + \begin{bmatrix} L_m & 0 \\ 0 & L_m \end{bmatrix} \cdot \frac{d}{dt} \begin{bmatrix} i_{s\alpha} \\ i_{s\beta} \end{bmatrix} \end{aligned} \quad (2.42d)$$

Finally, the model in the α - β subspace can be summarized with the following expressions, taking into account that $d\theta/dt = \omega_r$:

$$v_{s\alpha} = R_s \cdot i_{s\alpha} + L_s \cdot \frac{di_{s\alpha}}{dt} + L_m \cdot \frac{di_{r\alpha}}{dt} = R_s \cdot i_{s\alpha} + \frac{d\lambda_{s\alpha}}{dt} \quad (2.43)$$

$$\lambda_{s\alpha} = L_s \cdot i_{s\alpha} + L_m \cdot i_{r\alpha} \quad (2.44)$$

$$v_{s\beta} = R_s \cdot i_{s\beta} + L_s \cdot \frac{di_{s\beta}}{dt} + L_m \cdot \frac{di_{r\beta}}{dt} = R_s \cdot i_{s\beta} + \frac{d\lambda_{s\beta}}{dt} \quad (2.45)$$

$$\lambda_{s\beta} = L_s \cdot i_{s\beta} + L_m \cdot i_{r\beta} \quad (2.46)$$

$$0 = R_r \cdot i_{r\alpha} + L_r \cdot \frac{di_{r\alpha}}{dt} + L_m \cdot \frac{di_{s\alpha}}{dt} + \omega_r \cdot (L_r \cdot i_{r\beta} + L_m \cdot i_{s\beta}) = R_r \cdot i_{r\alpha} + \frac{d\lambda_{r\alpha}}{dt} + \omega_r \cdot \lambda_{r\beta} \quad (2.47)$$

$$\lambda_{r\alpha} = L_r \cdot i_{r\alpha} + L_m \cdot i_{s\alpha} \quad (2.48)$$

$$\lambda_{r\beta} = L_r \cdot i_{r\beta} + L_m \cdot i_{s\beta} \quad (2.49)$$

$$0 = R_r \cdot i_{r\beta} + L_r \cdot \frac{di_{r\beta}}{dt} + L_m \cdot \frac{di_{s\beta}}{dt} - \omega_r \cdot (L_r \cdot i_{r\alpha} + L_m \cdot i_{s\alpha}) = R_r \cdot i_{r\beta} + \frac{d\lambda_{r\beta}}{dt} - \omega_r \cdot \lambda_{r\alpha} \quad (2.50)$$

• *Model in the x_k - y_k subspaces:*

The variables in the stator and rotor are only coupled in the α - β plane, while for the remaining $(n-3)/2$ planes notice that there is no coupling between stator and rotor. For that reason:

$$\begin{bmatrix} v_{rx_k} \\ v_{ry_k} \end{bmatrix} = \begin{bmatrix} v'_{rx_k} \\ v'_{ry_k} \end{bmatrix}; \quad \begin{bmatrix} i_{rx_k} \\ i_{ry_k} \end{bmatrix} = \begin{bmatrix} i'_{rx_k} \\ i'_{ry_k} \end{bmatrix}; \quad \begin{bmatrix} \lambda_{rx_k} \\ \lambda_{ry_k} \end{bmatrix} = \begin{bmatrix} \lambda'_{rx_k} \\ \lambda'_{ry_k} \end{bmatrix} \quad (2.51)$$

The model for these subspaces can be deduced from equations (2.27)–(2.36):

$$v_{sx_k} = R_s \cdot i_{sx_k} + L_{ls} \cdot \frac{di_{sx_k}}{dt} = R_s \cdot i_{sx_k} + \frac{d\lambda_{sx_k}}{dt} \quad (2.52)$$

$$\lambda_{sx_k} = L_{ls} \cdot i_{sx_k} \quad (2.53)$$

$$v_{sy_k} = R_s \cdot i_{sy_k} + L_{ls} \cdot \frac{di_{sy_k}}{dt} = R_s \cdot i_{sy_k} + \frac{d\lambda_{sy_k}}{dt} \quad (2.54)$$

$$\lambda_{sy_k} = L_{ls} \cdot i_{sy_k} \quad (2.55)$$

$$0 = R_r \cdot i_{rx_k} + L_{lr} \cdot \frac{di_{rx_k}}{dt} = R_r \cdot i_{rx_k} + \frac{d\lambda_{rx_k}}{dt} \quad (2.56)$$

$$\lambda_{rx_k} = L_{lr} \cdot i_{rx_k} \quad (2.57)$$

$$0 = R_r \cdot i_{ry_k} + L_{lr} \cdot \frac{di_{ry_k}}{dt} = R_r \cdot i_{ry_k} + \frac{d\lambda_{ry_k}}{dt} \quad (2.58)$$

$$\lambda_{ry_k} = L_{lr} \cdot i_{ry_k} \quad (2.59)$$

where $k = 1, 2, 3, \dots, (n-3)/2$.

• *Model in the z-component:*

On the other hand, in equations (2.60)–(2.63) the resulting model in the z -axis is presented, where the homopolar component is projected. In this axis, there will never be coupling between the stator and rotor because of considering the rotor as a set of short-circuited windings. In any case, currents in this axis will be zero if a star connection is used.

$$v_{sz} = R_s \cdot i_{sz} + L_{ls} \cdot \frac{di_{sz}}{dt} = R_s \cdot i_{sz} + \frac{d\lambda_{sz}}{dt} \quad (2.60)$$

$$\lambda_{sz} = L_{ls} \cdot i_{sz} \quad (2.61)$$

$$v_{rz} = R_r \cdot i_{rz} + L_{lr} \cdot \frac{di_{rz}}{dt} = R_r \cdot i_{rz} + \frac{d\lambda_{rz}}{dt} \quad (2.62)$$

$$\lambda_{rz} = L_{lr} \cdot i_{rz} \quad (2.63)$$

Finally, the expression of the electromagnetic torque can be obtained from equation (2.23), transforming the phase variables into the new stationary reference frame, as stated below:

$$T_{em} = p \cdot [i_s]^T \cdot \frac{d}{d\theta} [L_{sr}(\theta)] \cdot [i_r] = p \cdot \begin{bmatrix} i_{s\alpha} \\ i_{s\beta} \\ i_{sx_1} \\ i_{sy_1} \\ \vdots \\ i_{sz} \end{bmatrix}^T \cdot \underbrace{\left[[C_n]^T \right]^{-1} \cdot \frac{d}{d\theta} [L_{sr}(\theta)] \cdot [C_n]^{-1} \right]}_{[a]} \cdot \begin{bmatrix} i'_{r\alpha} \\ i'_{r\beta} \\ i'_{rx_1} \\ i'_{ry_1} \\ \vdots \\ i'_{rz} \end{bmatrix} \quad (2.64)$$

$$\begin{aligned}
\boxed{a} &= \left[[C_n]^T \right]^{-1} \cdot \frac{d}{d\theta} [L_{sr}(\theta)] \cdot [C_n]^{-1} = \frac{d}{d\theta} \left(\left[[C_n]^T \right]^{-1} \cdot [L_{sr}(\theta)] \cdot [C_n]^{-1} \right) = \\
&= \frac{d}{d\theta} \left(\left(\frac{n}{2} \right)^2 \cdot M \cdot \begin{bmatrix} \cos(\theta) & -\sin(\theta) & 0 & 0 & \cdots & 0 \\ \sin(\theta) & \cos(\theta) & 0 & 0 & \cdots & 0 \\ 0 & 0 & 0 & 0 & \cdots & 0 \\ 0 & 0 & 0 & 0 & \cdots & 0 \\ \vdots & \vdots & \vdots & \vdots & \ddots & \vdots \\ 0 & 0 & 0 & 0 & \cdots & 0 \end{bmatrix} \right) = \\
&= \left(\frac{n}{2} \right)^2 \cdot M \cdot \begin{bmatrix} -\sin(\theta) & -\cos(\theta) & 0 & 0 & \cdots & 0 \\ \cos(\theta) & -\sin(\theta) & 0 & 0 & \cdots & 0 \\ 0 & 0 & 0 & 0 & \cdots & 0 \\ 0 & 0 & 0 & 0 & \cdots & 0 \\ \vdots & \vdots & \vdots & \vdots & \ddots & \vdots \\ 0 & 0 & 0 & 0 & \cdots & 0 \end{bmatrix}
\end{aligned} \tag{2.64a}$$

Making some substitutions and applying the rotation matrix to the rotor variables to set all the variables in the stationary reference system, the torque expression remains:

$$\begin{aligned}
T_{em} &= p \cdot \left(\frac{n}{2} \right)^2 \cdot M \cdot \begin{bmatrix} i_{s\alpha} \\ i_{s\beta} \end{bmatrix}^T \cdot \begin{bmatrix} -\sin(\theta) & -\cos(\theta) \\ \cos(\theta) & -\sin(\theta) \end{bmatrix} \cdot [T_r(-\theta)] \cdot \begin{bmatrix} i_{r\alpha} \\ i_{r\beta} \end{bmatrix} = \\
&= p \cdot \frac{n}{2} \cdot L_m \cdot \begin{bmatrix} i_{s\alpha} \\ i_{s\beta} \end{bmatrix}^T \cdot \begin{bmatrix} -\sin(\theta) & -\cos(\theta) \\ \cos(\theta) & -\sin(\theta) \end{bmatrix} \cdot \begin{bmatrix} \cos(\theta) & \sin(\theta) \\ -\sin(\theta) & \cos(\theta) \end{bmatrix} \cdot \begin{bmatrix} i_{r\alpha} \\ i_{r\beta} \end{bmatrix}
\end{aligned} \tag{2.65}$$

Lastly, it is obtained:

$$T_{em} = p \cdot \frac{n}{2} \cdot L_m \cdot (i_{r\alpha} \cdot i_{s\beta} - i_{r\beta} \cdot i_{s\alpha}) \tag{2.66}$$

As expected, the variables in the x_k - y_k subspaces, as well as in the z -component, are not present in the torque equation showing that the useful transformation of energy occurs only in the α - β subspace (remember that the distributed winding case is currently considered). Other expressions widely used in the literature to determine the electromagnetic torque appear in (2.67)–(2.69), easily obtained by making some substitutions. This is of special importance for control purposes where different schemes are implemented depending on the selected torque expression. It should be noted that in these expressions, the factor $n/2$ will not appear when a power invariant transformation is applied.

$$T_{em} = p \cdot \frac{n}{2} \cdot (\lambda_{s\alpha} \cdot i_{s\beta} - \lambda_{s\beta} \cdot i_{s\alpha}) \tag{2.67}$$

$$T_{em} = p \cdot \frac{n}{2} \cdot (i_{r\alpha} \cdot \lambda_{r\beta} - i_{r\beta} \cdot \lambda_{r\alpha}) \tag{2.68}$$

$$T_{em} = p \cdot \frac{n}{2} \cdot \frac{L_m}{L_r} \cdot (\lambda_{r\alpha} \cdot i_{s\beta} - \lambda_{r\beta} \cdot i_{s\alpha}) \quad (2.69)$$

Model in the d - q reference frame (rotating reference frame)

In the Clarke decoupled model, it was highlighted that the variables are referred to a static reference frame fixed to the stator of the machine, allowing a considerable simplification of the machine model. In addition, only the components of the α - β plane are involved in the torque production. However, under transient conditions these components present an oscillating nature that must be avoided to ensure an adequate control. It is possible to perform a new transformation of variables, expressing them in a rotating reference frame (d - q), where the new components have a non-oscillating nature, in other words, constant in steady state and varying in transient state [49]. The change of reference frame is obtained through matrix transformations applied to the Clarke decoupled model. Since the stator and rotor are coupled only in the α - β plane, the transformations will only affect the electrical variables defined in such plane, while the other subspaces remain as they were detailed in the previous section.

For the development of the new model, consider a d - q reference frame that rotates at a speed ω_a , whose instantaneous position with respect to the stationary frame is defined by the coordinate θ_a (see Fig. 2.3), which in turn is related to the speed ω_a as follows:

$$\theta_a = \int_0^t \omega_a \cdot dt \quad (2.70)$$

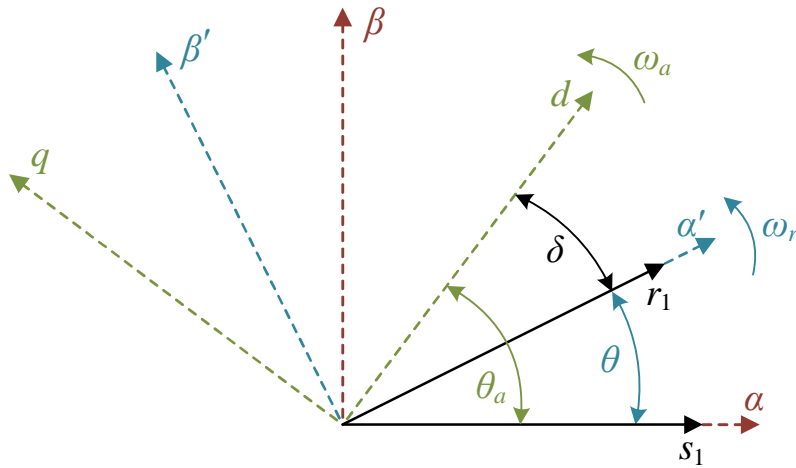


Figure 2.3. Rotating reference frame (d - q).

In the same way, the rotor reference frame (α' - β') is rotating at a speed ω_r and its coordinate referred to the stationary reference frame is given by the variable θ . Likewise, the rotor position with respect to the d - q reference frame is defined by the coordinate δ that depends at each instant on the slip speed ω_{sl} (relative speed between the rotating and the rotor reference frames), according to the following equation:

$$\delta = \theta_a - \theta = \int_0^t (\omega_a - \omega_r) \cdot dt = \int_0^t \omega_{sl} \cdot dt \quad (2.71)$$

Thus, the rotation matrices of the stator and rotor variables are detailed in equations (2.72) and (2.73), respectively. The voltage, current and flux vectors in the stationary reference frame are now transformed into the new reference system, see equations (2.74) and (2.75).

$$[P_{sn}] = \begin{bmatrix} \cos(\theta_a) & \sin(\theta_a) & 0 & 0 & \cdots & 0 \\ -\sin(\theta_a) & \cos(\theta_a) & 0 & 0 & \cdots & 0 \\ 0 & 0 & 1 & 0 & \cdots & 0 \\ 0 & 0 & 0 & 1 & \cdots & 0 \\ \vdots & \vdots & \vdots & \vdots & \ddots & \vdots \\ 0 & 0 & 0 & 0 & \cdots & 1 \end{bmatrix}; \quad [P_{sn}]^{-1} = [P_{sn}]^T \quad (2.72)$$

$$[P_{rn}] = \begin{bmatrix} \cos(\delta) & \sin(\delta) & 0 & 0 & \cdots & 0 \\ -\sin(\delta) & \cos(\delta) & 0 & 0 & \cdots & 0 \\ 0 & 0 & 1 & 0 & \cdots & 0 \\ 0 & 0 & 0 & 1 & \cdots & 0 \\ \vdots & \vdots & \vdots & \vdots & \ddots & \vdots \\ 0 & 0 & 0 & 0 & \cdots & 1 \end{bmatrix}; \quad [P_{rn}]^{-1} = [P_{rn}]^T \quad (2.73)$$

$$\begin{bmatrix} v_{sd} \\ v_{sq} \\ v_{sx_1} \\ v_{sy_1} \\ \vdots \\ v_{sx_{(n-3)/2}} \\ v_{sy_{(n-3)/2}} \\ v_{sz} \end{bmatrix} = [P_{sn}] \cdot \begin{bmatrix} v_{s\alpha} \\ v_{s\beta} \\ v_{sx_1} \\ v_{sy_1} \\ \vdots \\ v_{sx_{(n-3)/2}} \\ v_{sy_{(n-3)/2}} \\ v_{sz} \end{bmatrix}; \quad \begin{bmatrix} i_{sd} \\ i_{sq} \\ i_{sx_1} \\ i_{sy_1} \\ \vdots \\ i_{sx_{(n-3)/2}} \\ i_{sy_{(n-3)/2}} \\ i_{sz} \end{bmatrix} = [P_{sn}] \cdot \begin{bmatrix} i_{s\alpha} \\ i_{s\beta} \\ i_{sx_1} \\ i_{sy_1} \\ \vdots \\ i_{sx_{(n-3)/2}} \\ i_{sy_{(n-3)/2}} \\ i_{sz} \end{bmatrix}; \quad \begin{bmatrix} \lambda_{sd} \\ \lambda_{sq} \\ \lambda_{sx_1} \\ \lambda_{sy_1} \\ \vdots \\ \lambda_{sx_{(n-3)/2}} \\ \lambda_{sy_{(n-3)/2}} \\ \lambda_{sz} \end{bmatrix} = [P_{sn}] \cdot \begin{bmatrix} \lambda_{s\alpha} \\ \lambda_{s\beta} \\ \lambda_{sx_1} \\ \lambda_{sy_1} \\ \vdots \\ \lambda_{sx_{(n-3)/2}} \\ \lambda_{sy_{(n-3)/2}} \\ \lambda_{sz} \end{bmatrix} \quad (2.74)$$

$$\begin{bmatrix} v_{rd} \\ v_{rq} \\ v_{rx_1} \\ v_{ry_1} \\ \vdots \\ v_{rx_{(n-3)/2}} \\ v_{ry_{(n-3)/2}} \\ v_{rz} \end{bmatrix} = [P_{rn}] \cdot \begin{bmatrix} v'_{r\alpha} \\ v'_{r\beta} \\ v_{rx_1} \\ v_{ry_1} \\ \vdots \\ v_{rx_{(n-3)/2}} \\ v_{ry_{(n-3)/2}} \\ v_{rz} \end{bmatrix}; \quad \begin{bmatrix} i_{rd} \\ i_{rq} \\ i_{rx_1} \\ i_{ry_1} \\ \vdots \\ i_{rx_{(n-3)/2}} \\ i_{ry_{(n-3)/2}} \\ i_{rz} \end{bmatrix} = [P_{rn}] \cdot \begin{bmatrix} i'_{r\alpha} \\ i'_{r\beta} \\ i_{rx_1} \\ i_{ry_1} \\ \vdots \\ i_{rx_{(n-3)/2}} \\ i_{ry_{(n-3)/2}} \\ i_{rz} \end{bmatrix}; \quad \begin{bmatrix} \lambda_{rd} \\ \lambda_{rq} \\ \lambda_{rx_1} \\ \lambda_{ry_1} \\ \vdots \\ \lambda_{rx_{(n-3)/2}} \\ \lambda_{ry_{(n-3)/2}} \\ \lambda_{rz} \end{bmatrix} = [P_{rn}] \cdot \begin{bmatrix} \lambda'_{r\alpha} \\ \lambda'_{r\beta} \\ \lambda_{rx_1} \\ \lambda_{ry_1} \\ \vdots \\ \lambda_{rx_{(n-3)/2}} \\ \lambda_{ry_{(n-3)/2}} \\ \lambda_{rz} \end{bmatrix} \quad (2.75)$$

Notice that the transformation is effective only in the α - β plane, whereas the other planes remain invariant. Therefore, the stator and rotor voltage equations in the secondary planes are the same as in the previous case. Meanwhile, to obtain the new equations for the α - β plane, the

transformation presented in (2.72)–(2.75) is applied to equations (2.37) and (2.38). In this way, for the stator voltage equation, it is necessary to pre-multiply (2.37) by $[P_{sn}]$, while the rotor voltage equation is calculated pre-multiplying (2.38) by $[P_m]$. The resulting model, after the application of the proposed transformation, is defined by the next set of voltage equations:

$$v_{sd} = R_s \cdot i_{sd} + L_s \cdot \frac{di_{sd}}{dt} - L_s \cdot \omega_a \cdot i_{sq} + L_m \cdot \frac{di_{rd}}{dt} - L_m \cdot \omega_a \cdot i_{rq} = R_s \cdot i_{sd} + \frac{d\lambda_{sd}}{dt} - \omega_a \cdot \lambda_{sq} \quad (2.76)$$

$$v_{sq} = R_s \cdot i_{sq} + L_s \cdot \frac{di_{sq}}{dt} + L_s \cdot \omega_a \cdot i_{sd} + L_m \cdot \frac{di_{rq}}{dt} + L_m \cdot \omega_a \cdot i_{rd} = R_s \cdot i_{sq} + \frac{d\lambda_{sq}}{dt} + \omega_a \cdot \lambda_{sd} \quad (2.77)$$

$$0 = R_r \cdot i_{rd} + L_r \cdot \frac{di_{rd}}{dt} - L_r \cdot \omega_{sl} \cdot i_{rq} + L_m \cdot \frac{di_{sd}}{dt} - L_m \cdot \omega_{sl} \cdot i_{sq} = R_r \cdot i_{rd} + \frac{d\lambda_{rd}}{dt} - \omega_{sl} \cdot \lambda_{rq} \quad (2.78)$$

$$0 = R_r \cdot i_{rq} + L_r \cdot \frac{di_{rq}}{dt} + L_r \cdot \omega_{sl} \cdot i_{rd} + L_m \cdot \frac{di_{sq}}{dt} + L_m \cdot \omega_{sl} \cdot i_{sd} = R_r \cdot i_{rq} + \frac{d\lambda_{rq}}{dt} + \omega_{sl} \cdot \lambda_{rd} \quad (2.79)$$

where the flux components in the d – q plane are defined as follows:

$$\lambda_{sd} = L_s \cdot i_{sd} + L_m \cdot i_{rd} \quad (2.80)$$

$$\lambda_{sq} = L_s \cdot i_{sq} + L_m \cdot i_{rq} \quad (2.81)$$

$$\lambda_{rd} = L_r \cdot i_{rd} + L_m \cdot i_{sd} \quad (2.82)$$

$$\lambda_{rq} = L_r \cdot i_{rq} + L_m \cdot i_{sq} \quad (2.83)$$

Proceeding analogously to what was done in the previous case, the generated electromagnetic torque is defined by the following expression:

$$T_{em} = p \cdot \frac{n}{2} \cdot L_m \cdot (i_{rd} \cdot i_{sq} - i_{rq} \cdot i_{sd}) \quad (2.84)$$

As in the stationary case, other expressions for the electromagnetic torque appear in (2.85)–(2.87). The use of some of them is very common in different control strategies, with the aim of reducing the number of calculations required when the model is represented in certain reference frames. Again, the factor $n/2$ will not appear when a power invariant transformation is applied.

$$T_{em} = p \cdot \frac{n}{2} \cdot (\lambda_{sd} \cdot i_{sq} - \lambda_{sq} \cdot i_{sd}) \quad (2.85)$$

$$T_{em} = p \cdot \frac{n}{2} \cdot (i_{rd} \cdot \lambda_{rq} - i_{rq} \cdot \lambda_{rd}) \quad (2.86)$$

$$T_{em} = p \cdot \frac{n}{2} \cdot \frac{L_m}{L_r} \cdot (\lambda_{rd} \cdot i_{sq} - \lambda_{rq} \cdot i_{sd}) \quad (2.87)$$

The model in the rotating reference frame offers important simplifications on which the different control strategies are based. The model presented in equations (2.43)–(2.63), referred to a stationary reference frame, is a particular case where ω_a is zero. Another interesting case is the resulting model when the d -axis is fixed to the rotor flux, having projection only in this axis. This is the basis for the Rotor Field Oriented Control architecture [14,50], described in more detail in Section 2.3.1. Another considered option consists in the alignment of the reference frame to the stator flux, which is typically used in the Direct Torque Control [51,52]. These last two alternatives also generate an important simplification in the estimation of the electromagnetic torque.

2.2.2 Five-phase distributed winding induction machine: a case study

Since the main interest of this work is to serve as basic research for a later application in low- and medium-power electrical systems (such as electric propulsion application in electric vehicles), a five-phase system is selected as case study. In this subsection, the generalized model described above is particularized to the symmetrical five-phase machine, which constitutes an important part of this Thesis.

The model in phase variables corresponds to equations (2.1)–(2.21), particularizing for $n = 5$. The stator and rotor phase variables are represented by the vectors $[\mu_s]$ and $[\mu_r]$, respectively, where μ represents each variable (voltage, current or flux) and the phases are identified with the subscripts a, b, c, d and e :

$$[\mu_s] = [\mu_{sa} \quad \mu_{sb} \quad \mu_{sc} \quad \mu_{sd} \quad \mu_{se}]^T \quad (2.88)$$

$$[\mu_r] = [\mu_{ra} \quad \mu_{rb} \quad \mu_{rc} \quad \mu_{rd} \quad \mu_{re}]^T \quad (2.89)$$

Clarke decoupled model (stationary reference frame)

The transformation matrix applied to the model based on phase variables is presented in equation (2.90), obtaining the new variables in the stationary reference frame, equations (2.91)–(2.94). The model in this reference frame is composed of two orthogonal planes, namely α – β (exclusive plane of energy conversion) and x – y , plus the homopolar z -component.

$$[C_5] = \frac{2}{5} \cdot \begin{bmatrix} 1 & \cos(\vartheta) & \cos(2\vartheta) & \cos(3\vartheta) & \cos(4\vartheta) \\ 0 & \sin(\vartheta) & \sin(2\vartheta) & \sin(3\vartheta) & \sin(4\vartheta) \\ 1 & \cos(2\vartheta) & \cos(4\vartheta) & \cos(6\vartheta) & \cos(8\vartheta) \\ 0 & \sin(2\vartheta) & \sin(4\vartheta) & \sin(6\vartheta) & \sin(8\vartheta) \\ \frac{1}{2} & \frac{1}{2} & \frac{1}{2} & \frac{1}{2} & \frac{1}{2} \end{bmatrix} \quad (2.90)$$

$$\begin{bmatrix} v_{s\alpha} \\ v_{s\beta} \\ v_{sx} \\ v_{sy} \\ v_{sz} \end{bmatrix} = R_s \cdot \begin{bmatrix} i_{s\alpha} \\ i_{s\beta} \\ i_{sx} \\ i_{sy} \\ i_{sz} \end{bmatrix} + \frac{d}{dt} \begin{bmatrix} \lambda_{s\alpha} \\ \lambda_{s\beta} \\ \lambda_{sx} \\ \lambda_{sy} \\ \lambda_{sz} \end{bmatrix} \quad (2.91)$$

$$\begin{bmatrix} 0 \\ 0 \\ 0 \\ 0 \\ 0 \end{bmatrix} = R_r \cdot \begin{bmatrix} i_{r\alpha} \\ i_{r\beta} \\ i_{rx} \\ i_{ry} \\ i_{rz} \end{bmatrix} + \frac{d}{dt} \begin{bmatrix} \lambda_{r\alpha} \\ \lambda_{r\beta} \\ \lambda_{rx} \\ \lambda_{ry} \\ \lambda_{rz} \end{bmatrix} + \begin{bmatrix} 0 & \omega_r & 0 & 0 & 0 \\ -\omega_r & 0 & 0 & 0 & 0 \\ 0 & 0 & 0 & 0 & 0 \\ 0 & 0 & 0 & 0 & 0 \\ 0 & 0 & 0 & 0 & 0 \end{bmatrix} \cdot \begin{bmatrix} \lambda_{r\alpha} \\ \lambda_{r\beta} \\ \lambda_{rx} \\ \lambda_{ry} \\ \lambda_{rz} \end{bmatrix} \quad (2.92)$$

$$\begin{bmatrix} \lambda_{s\alpha} \\ \lambda_{s\beta} \\ \lambda_{sx} \\ \lambda_{sy} \\ \lambda_{sz} \end{bmatrix} = \begin{bmatrix} L_s & 0 & 0 & 0 & 0 \\ 0 & L_s & 0 & 0 & 0 \\ 0 & 0 & L_{ls} & 0 & 0 \\ 0 & 0 & 0 & L_{ls} & 0 \\ 0 & 0 & 0 & 0 & L_{ls} \end{bmatrix} \cdot \begin{bmatrix} i_{s\alpha} \\ i_{s\beta} \\ i_{sx} \\ i_{sy} \\ i_{sz} \end{bmatrix} + \begin{bmatrix} L_m & 0 & 0 & 0 & 0 \\ 0 & L_m & 0 & 0 & 0 \\ 0 & 0 & 0 & 0 & 0 \\ 0 & 0 & 0 & 0 & 0 \\ 0 & 0 & 0 & 0 & 0 \end{bmatrix} \cdot \begin{bmatrix} i_{r\alpha} \\ i_{r\beta} \\ i_{rx} \\ i_{ry} \\ i_{rz} \end{bmatrix} \quad (2.93)$$

$$\begin{bmatrix} \lambda_{r\alpha} \\ \lambda_{r\beta} \\ \lambda_{rx} \\ \lambda_{ry} \\ \lambda_{rz} \end{bmatrix} = \begin{bmatrix} L_r & 0 & 0 & 0 & 0 \\ 0 & L_r & 0 & 0 & 0 \\ 0 & 0 & L_{lr} & 0 & 0 \\ 0 & 0 & 0 & L_{lr} & 0 \\ 0 & 0 & 0 & 0 & L_{lr} \end{bmatrix} \cdot \begin{bmatrix} i_{r\alpha} \\ i_{r\beta} \\ i_{rx} \\ i_{ry} \\ i_{rz} \end{bmatrix} + \begin{bmatrix} L_m & 0 & 0 & 0 & 0 \\ 0 & L_m & 0 & 0 & 0 \\ 0 & 0 & 0 & 0 & 0 \\ 0 & 0 & 0 & 0 & 0 \\ 0 & 0 & 0 & 0 & 0 \end{bmatrix} \cdot \begin{bmatrix} i_{s\alpha} \\ i_{s\beta} \\ i_{sx} \\ i_{sy} \\ i_{sz} \end{bmatrix} \quad (2.94)$$

Model in the d - q reference frame (rotating reference frame)

Finally, applying the transformation to obtain the model in the d - q rotating reference frame defined in equations (2.95) and (2.96), the stator and rotor variables in the new reference frame are achieved, equations (2.97)–(2.100). On the other hand, the electromagnetic torque can be obtained in one or the other reference frame using equations (2.66)–(2.69) and (2.84)–(2.87), respectively, particularizing for $n = 5$.

$$[P_{s5}] = \begin{bmatrix} \cos(\theta_a) & \sin(\theta_a) & 0 & 0 & 0 \\ -\sin(\theta_a) & \cos(\theta_a) & 0 & 0 & 0 \\ 0 & 0 & 1 & 0 & 0 \\ 0 & 0 & 0 & 1 & 0 \\ 0 & 0 & 0 & 0 & 1 \end{bmatrix} \quad (2.95)$$

$$[P_{r5}] = \begin{bmatrix} \cos(\delta) & \sin(\delta) & 0 & 0 & 0 \\ -\sin(\delta) & \cos(\delta) & 0 & 0 & 0 \\ 0 & 0 & 1 & 0 & 0 \\ 0 & 0 & 0 & 1 & 0 \\ 0 & 0 & 0 & 0 & 1 \end{bmatrix} \quad (2.96)$$

$$\begin{bmatrix} v_{sd} \\ v_{sq} \\ v_{sx} \\ v_{sy} \\ v_{sz} \end{bmatrix} = R_s \cdot \begin{bmatrix} i_{sd} \\ i_{sq} \\ i_{sx} \\ i_{sy} \\ i_{sz} \end{bmatrix} + \frac{d}{dt} \begin{bmatrix} \lambda_{sd} \\ \lambda_{sq} \\ \lambda_{sx} \\ \lambda_{sy} \\ \lambda_{sz} \end{bmatrix} + \begin{bmatrix} 0 & -\omega_a & 0 & 0 & 0 \\ \omega_a & 0 & 0 & 0 & 0 \\ 0 & 0 & 0 & 0 & 0 \\ 0 & 0 & 0 & 0 & 0 \\ 0 & 0 & 0 & 0 & 0 \end{bmatrix} \cdot \begin{bmatrix} \lambda_{rd} \\ \lambda_{rq} \\ \lambda_{rx} \\ \lambda_{ry} \\ \lambda_{rz} \end{bmatrix} \quad (2.97)$$

$$\begin{bmatrix} 0 \\ 0 \\ 0 \\ 0 \\ 0 \end{bmatrix} = R_r \cdot \begin{bmatrix} i_{rd} \\ i_{rq} \\ i_{rx} \\ i_{ry} \\ i_{rz} \end{bmatrix} + \frac{d}{dt} \begin{bmatrix} \lambda_{rd} \\ \lambda_{rq} \\ \lambda_{rx} \\ \lambda_{ry} \\ \lambda_{rz} \end{bmatrix} + \begin{bmatrix} 0 & -\omega_{sl} & 0 & 0 & 0 \\ \omega_{sl} & 0 & 0 & 0 & 0 \\ 0 & 0 & 0 & 0 & 0 \\ 0 & 0 & 0 & 0 & 0 \\ 0 & 0 & 0 & 0 & 0 \end{bmatrix} \cdot \begin{bmatrix} \lambda_{rd} \\ \lambda_{rq} \\ \lambda_{rx} \\ \lambda_{ry} \\ \lambda_{rz} \end{bmatrix} \quad (2.98)$$

$$\begin{bmatrix} \lambda_{sd} \\ \lambda_{sq} \\ \lambda_{sx} \\ \lambda_{sy} \\ \lambda_{sz} \end{bmatrix} = \begin{bmatrix} L_s & 0 & 0 & 0 & 0 \\ 0 & L_s & 0 & 0 & 0 \\ 0 & 0 & L_{ls} & 0 & 0 \\ 0 & 0 & 0 & L_{ls} & 0 \\ 0 & 0 & 0 & 0 & L_{ls} \end{bmatrix} \cdot \begin{bmatrix} i_{sd} \\ i_{sq} \\ i_{sx} \\ i_{sy} \\ i_{sz} \end{bmatrix} + \begin{bmatrix} L_m & 0 & 0 & 0 & 0 \\ 0 & L_m & 0 & 0 & 0 \\ 0 & 0 & 0 & 0 & 0 \\ 0 & 0 & 0 & 0 & 0 \\ 0 & 0 & 0 & 0 & 0 \end{bmatrix} \cdot \begin{bmatrix} i_{rd} \\ i_{rq} \\ i_{rx} \\ i_{ry} \\ i_{rz} \end{bmatrix} \quad (2.99)$$

$$\begin{bmatrix} \lambda_{rd} \\ \lambda_{rq} \\ \lambda_{rx} \\ \lambda_{ry} \\ \lambda_{rz} \end{bmatrix} = \begin{bmatrix} L_r & 0 & 0 & 0 & 0 \\ 0 & L_r & 0 & 0 & 0 \\ 0 & 0 & L_{lr} & 0 & 0 \\ 0 & 0 & 0 & L_{lr} & 0 \\ 0 & 0 & 0 & 0 & L_{lr} \end{bmatrix} \cdot \begin{bmatrix} i_{rd} \\ i_{rq} \\ i_{rx} \\ i_{ry} \\ i_{rz} \end{bmatrix} + \begin{bmatrix} L_m & 0 & 0 & 0 & 0 \\ 0 & L_m & 0 & 0 & 0 \\ 0 & 0 & 0 & 0 & 0 \\ 0 & 0 & 0 & 0 & 0 \\ 0 & 0 & 0 & 0 & 0 \end{bmatrix} \cdot \begin{bmatrix} i_{sd} \\ i_{sq} \\ i_{sx} \\ i_{sy} \\ i_{sz} \end{bmatrix} \quad (2.100)$$

2.2.3 Extension to multiphase machines with two frequency-domain subspaces: a second case example using the five-phase concentrated winding induction machine

The model studied in the previous section describes the multiphase induction machine assuming a sinusoidal distribution of the field along the air gap. Another alternative is to use different distributions in the machine windings in order to increase its efficiency. It has been proved that if the stator windings are concentrated, instead of distributed, the air gap field can have a rectangular or trapezoidal profile instead of sinusoidal. With these new profiles a better use of

the field is achieved because there are values close to saturation not only at one point in the magnetic core, as in the case of sinusoidal profiles [53]. With the appearance of multiphase machines, the designs based on concentrated windings could be experimentally implemented and have been modeled and studied in [42–44,54,55]. The model in phase variables, considering the stator formed by an arbitrary number of phases and the rotor with an arbitrary number of bars, has been analyzed in [42,43], where a study of the generated harmonic components is also included considering the particular case of five-, seven- and nine-phase machines.

Clarke decoupled model (stationary reference frame)

The model in the stationary reference system considering a concentrated winding induction machine (CW-IM) has been shown in [44,54,55], where the experimental results of a real five-phase machine are compared. In all these research works an improvement of the efficiency in the generation of the electromagnetic torque has been described. The study of the effect of harmonic components on the behavior of the system for five-phase machines has revealed that, in addition to the fundamental component (plane α - β), the third harmonic (plane x - y) also contributes to the torque generation. This is due to the fact that the stator and the rotor are also magnetically coupled in the x - y plane. In the system model, both planes are independent and are described by the VSD using the transformation matrix $[C_5]$ defined in equation (2.101). This matrix transforms the phase variables (a , b , c , d , and e) into a reference frame formed by the orthogonal planes α - β and x - y , as follows:

$$[C_5] = \sqrt{\frac{2}{5}} \cdot \begin{bmatrix} 1 & \cos(\vartheta) & \cos(2\vartheta) & \cos(3\vartheta) & \cos(4\vartheta) \\ 0 & \sin(\vartheta) & \sin(2\vartheta) & \sin(3\vartheta) & \sin(4\vartheta) \\ 1 & \cos(2\vartheta) & \cos(4\vartheta) & \cos(6\vartheta) & \cos(8\vartheta) \\ 0 & \sin(2\vartheta) & \sin(4\vartheta) & \sin(6\vartheta) & \sin(8\vartheta) \\ \frac{1}{\sqrt{2}} & \frac{1}{\sqrt{2}} & \frac{1}{\sqrt{2}} & \frac{1}{\sqrt{2}} & \frac{1}{\sqrt{2}} \end{bmatrix} \quad (2.101)$$

$$\begin{bmatrix} v_{s\alpha} \\ v_{s\beta} \\ v_{sx} \\ v_{sy} \\ v_{sz} \end{bmatrix} = R_s \cdot \begin{bmatrix} i_{s\alpha} \\ i_{s\beta} \\ i_{sx} \\ i_{sy} \\ i_{sz} \end{bmatrix} + \frac{d}{dt} \begin{bmatrix} \lambda_{s\alpha} \\ \lambda_{s\beta} \\ \lambda_{sx} \\ \lambda_{sy} \\ \lambda_{sz} \end{bmatrix} \quad (2.102)$$

$$\begin{bmatrix} 0 \\ 0 \\ 0 \\ 0 \\ 0 \end{bmatrix} = \begin{bmatrix} R_{r1} & 0 & 0 & 0 & 0 \\ 0 & R_{r1} & 0 & 0 & 0 \\ 0 & 0 & R_{r3} & 0 & 0 \\ 0 & 0 & 0 & R_{r3} & 0 \\ 0 & 0 & 0 & 0 & R_{rz} \end{bmatrix} \cdot \begin{bmatrix} i_{r\alpha} \\ i_{r\beta} \\ i_{rx} \\ i_{ry} \\ i_{rz} \end{bmatrix} + \frac{d}{dt} \begin{bmatrix} \lambda_{r\alpha} \\ \lambda_{r\beta} \\ \lambda_{rx} \\ \lambda_{ry} \\ \lambda_{rz} \end{bmatrix} + \begin{bmatrix} 0 & \omega_r & 0 & 0 & 0 \\ -\omega_r & 0 & 0 & 0 & 0 \\ 0 & 0 & 0 & 3\omega_r & 0 \\ 0 & 0 & -3\omega_r & 0 & 0 \\ 0 & 0 & 0 & 0 & 0 \end{bmatrix} \cdot \begin{bmatrix} \lambda_{r\alpha} \\ \lambda_{r\beta} \\ \lambda_{rx} \\ \lambda_{ry} \\ \lambda_{rz} \end{bmatrix} \quad (2.103)$$

$$\begin{bmatrix} \lambda_{s\alpha} \\ \lambda_{s\beta} \\ \lambda_{sx} \\ \lambda_{sy} \\ \lambda_{sz} \end{bmatrix} = \begin{bmatrix} L_{s1} & 0 & 0 & 0 & 0 \\ 0 & L_{s1} & 0 & 0 & 0 \\ 0 & 0 & L_{s3} & 0 & 0 \\ 0 & 0 & 0 & L_{s3} & 0 \\ 0 & 0 & 0 & 0 & L_{ls} \end{bmatrix} \cdot \begin{bmatrix} i_{s\alpha} \\ i_{s\beta} \\ i_{sx} \\ i_{sy} \\ i_{sz} \end{bmatrix} + \begin{bmatrix} L_{m1} & 0 & 0 & 0 & 0 \\ 0 & L_{m1} & 0 & 0 & 0 \\ 0 & 0 & L_{m3} & 0 & 0 \\ 0 & 0 & 0 & L_{m3} & 0 \\ 0 & 0 & 0 & 0 & 0 \end{bmatrix} \cdot \begin{bmatrix} i_{r\alpha} \\ i_{r\beta} \\ i_{rx} \\ i_{ry} \\ i_{rz} \end{bmatrix} \quad (2.104)$$

$$\begin{bmatrix} \lambda_{r\alpha} \\ \lambda_{r\beta} \\ \lambda_{rx} \\ \lambda_{ry} \\ \lambda_{rz} \end{bmatrix} = \begin{bmatrix} L_{r1} & 0 & 0 & 0 & 0 \\ 0 & L_{r1} & 0 & 0 & 0 \\ 0 & 0 & L_{r3} & 0 & 0 \\ 0 & 0 & 0 & L_{r3} & 0 \\ 0 & 0 & 0 & 0 & L_{lr} \end{bmatrix} \cdot \begin{bmatrix} i_{r\alpha} \\ i_{r\beta} \\ i_{rx} \\ i_{ry} \\ i_{rz} \end{bmatrix} + \begin{bmatrix} L_{m1} & 0 & 0 & 0 & 0 \\ 0 & L_{m1} & 0 & 0 & 0 \\ 0 & 0 & L_{m3} & 0 & 0 \\ 0 & 0 & 0 & L_{m3} & 0 \\ 0 & 0 & 0 & 0 & 0 \end{bmatrix} \cdot \begin{bmatrix} i_{s\alpha} \\ i_{s\beta} \\ i_{sx} \\ i_{sy} \\ i_{sz} \end{bmatrix} \quad (2.105)$$

Model in the d - q reference frame (rotating reference frame)

For the development of the model in the rotating reference frame, consider the orthogonal planes d_1 - q_1 and d_3 - q_3 , associated with the fundamental component and the third harmonic, respectively. These planes rotate at a speed ω_{a1} and $3\omega_{a3}$, while the instantaneous positions with respect to the stationary frame are defined by the coordinates θ_{a1} and $3\theta_{a3}$, respectively. The rotation matrix is represented in (2.106), while the model of the five-phase machine is shown in (2.107)–(2.110).

$$[P_{s5}] = \begin{bmatrix} \cos(\theta_{a1}) & \sin(\theta_{a1}) & 0 & 0 & 0 \\ -\sin(\theta_{a1}) & \cos(\theta_{a1}) & 0 & 0 & 0 \\ 0 & 0 & \cos(3\theta_{a3}) & \sin(3\theta_{a3}) & 0 \\ 0 & 0 & -\sin(3\theta_{a3}) & \cos(3\theta_{a3}) & 0 \\ 0 & 0 & 0 & 0 & 1 \end{bmatrix} \quad (2.106)$$

$$\begin{bmatrix} v_{sd1} \\ v_{sq1} \\ v_{sd3} \\ v_{sq3} \\ v_{sz} \end{bmatrix} = R_s \cdot \begin{bmatrix} i_{sd1} \\ i_{sq1} \\ i_{sd3} \\ i_{sq3} \\ i_{sz} \end{bmatrix} + \frac{d}{dt} \begin{bmatrix} \lambda_{sd1} \\ \lambda_{sq1} \\ \lambda_{sd3} \\ \lambda_{sq3} \\ \lambda_{sz} \end{bmatrix} + \begin{bmatrix} 0 & -\omega_{a1} & 0 & 0 & 0 \\ \omega_{a1} & 0 & 0 & 0 & 0 \\ 0 & 0 & 0 & -3\omega_{a3} & 0 \\ 0 & 0 & 3\omega_{a3} & 0 & 0 \\ 0 & 0 & 0 & 0 & 0 \end{bmatrix} \cdot \begin{bmatrix} \lambda_{sd1} \\ \lambda_{sq1} \\ \lambda_{sd3} \\ \lambda_{sq3} \\ \lambda_{sz} \end{bmatrix} \quad (2.107)$$

$$\begin{bmatrix} 0 \\ 0 \\ 0 \\ 0 \\ 0 \end{bmatrix} = \begin{bmatrix} R_{r1} & 0 & 0 & 0 & 0 \\ 0 & R_{r1} & 0 & 0 & 0 \\ 0 & 0 & R_{r3} & 0 & 0 \\ 0 & 0 & 0 & R_{r3} & 0 \\ 0 & 0 & 0 & 0 & R_{rz} \end{bmatrix} \cdot \begin{bmatrix} i_{rd1} \\ i_{rq1} \\ i_{rd3} \\ i_{rq3} \\ i_{rz} \end{bmatrix} + \frac{d}{dt} \begin{bmatrix} \lambda_{rd1} \\ \lambda_{rq1} \\ \lambda_{rd3} \\ \lambda_{rq3} \\ \lambda_{rz} \end{bmatrix} + \begin{bmatrix} 0 & -\omega_{s1} & 0 & 0 & 0 \\ \omega_{s1} & 0 & 0 & 0 & 0 \\ 0 & 0 & 0 & -3\omega_{s3} & 0 \\ 0 & 0 & 3\omega_{s3} & 0 & 0 \\ 0 & 0 & 0 & 0 & 0 \end{bmatrix} \cdot \begin{bmatrix} \lambda_{rd1} \\ \lambda_{rq1} \\ \lambda_{rd3} \\ \lambda_{rq3} \\ \lambda_{rz} \end{bmatrix} \quad (2.108)$$

$$\begin{bmatrix} \lambda_{sd1} \\ \lambda_{sq1} \\ \lambda_{sd3} \\ \lambda_{sq3} \\ \lambda_{sz} \end{bmatrix} = \begin{bmatrix} L_{s1} & 0 & 0 & 0 & 0 \\ 0 & L_{s1} & 0 & 0 & 0 \\ 0 & 0 & L_{s3} & 0 & 0 \\ 0 & 0 & 0 & L_{s3} & 0 \\ 0 & 0 & 0 & 0 & L_{ls} \end{bmatrix} \cdot \begin{bmatrix} i_{sd1} \\ i_{sq1} \\ i_{sd3} \\ i_{sq3} \\ i_{sz} \end{bmatrix} + \begin{bmatrix} L_{m1} & 0 & 0 & 0 & 0 \\ 0 & L_{m1} & 0 & 0 & 0 \\ 0 & 0 & L_{m3} & 0 & 0 \\ 0 & 0 & 0 & L_{m3} & 0 \\ 0 & 0 & 0 & 0 & 0 \end{bmatrix} \cdot \begin{bmatrix} i_{rd1} \\ i_{rq1} \\ i_{rd3} \\ i_{rq3} \\ i_{rz} \end{bmatrix} \quad (2.109)$$

$$\begin{bmatrix} \lambda_{rd1} \\ \lambda_{rq1} \\ \lambda_{rd3} \\ \lambda_{rq3} \\ \lambda_{rz} \end{bmatrix} = \begin{bmatrix} L_{r1} & 0 & 0 & 0 & 0 \\ 0 & L_{r1} & 0 & 0 & 0 \\ 0 & 0 & L_{r3} & 0 & 0 \\ 0 & 0 & 0 & L_{r3} & 0 \\ 0 & 0 & 0 & 0 & L_{lr} \end{bmatrix} \cdot \begin{bmatrix} i_{rd1} \\ i_{rq1} \\ i_{rd3} \\ i_{rq3} \\ i_{rz} \end{bmatrix} + \begin{bmatrix} L_{m1} & 0 & 0 & 0 & 0 \\ 0 & L_{m1} & 0 & 0 & 0 \\ 0 & 0 & L_{m3} & 0 & 0 \\ 0 & 0 & 0 & L_{m3} & 0 \\ 0 & 0 & 0 & 0 & 0 \end{bmatrix} \cdot \begin{bmatrix} i_{sd1} \\ i_{sq1} \\ i_{sd3} \\ i_{sq3} \\ i_{sz} \end{bmatrix} \quad (2.110)$$

Finally, the expression of the electromagnetic torque is obtained in a very similar way to that conducted in the distributed windings case, taking into account this time that the third harmonic components also contribute to the torque generation, as it appears in the following expressions:

$$T_{em} = T_{em1} + T_{em3} \quad (2.111)$$

$$T_{em1} = p \cdot L_{m1} \cdot (i_{rd1} \cdot i_{sq1} - i_{rq1} \cdot i_{sd1}) \quad (2.112)$$

$$T_{em3} = 3p \cdot L_{m3} \cdot (i_{rd3} \cdot i_{sq3} - i_{rq3} \cdot i_{sd3}) \quad (2.113)$$

2.2.4 Multiphase machines with two frequency-domain subspaces: a third case example using the five-phase permanent magnet synchronous machine

A permanent magnet synchronous machine (PMSM) is a machine that uses rotor permanent magnets to produce the air gap magnetic field rather than using rotor field windings. This machine has attracted the interest of researchers and industry for its use in many applications (electric vehicles, ship propulsion and aerospace applications, to name a few), being its model studied in several research works [56–59]. The properties of the permanent magnet will affect directly the performance of the machine. The earliest manufactured magnet material was hardened steel. Magnets made in steel were easily magnetized, however they could hold very low energy and were easy to demagnetize. In recent years other magnet materials such as Aluminum Nickel and Cobalt alloys, Strontium Ferrite or Barium Ferrite, Samarium Cobalt and Neodymium Iron-Boron have been developed and used for constructing permanent magnets [60].

In this subsection, a model of the five-phase PMSM is initially developed in phase variables form. In order to simplify the model by removing the time variation of inductance terms, a transformation is applied and the so-called d_1 – q_1 – d_3 – q_3 – z model of the machine is constructed.

Model in phase variables (physical model)

The model of the five-phase PMSM in the reference frame constituted by phase variables can be written as follows. The stator voltage equation is given by (2.114)–(2.115), where R_s , i_s and λ_s are the stator resistance, current and flux linkage vectors, respectively, see (2.116)–(2.118).

$$[v_s] = [R_s] \cdot [i_s] + \frac{d}{dt} [\lambda_s] \quad (2.114)$$

$$[v_s] = [v_{sa} \ v_{sb} \ v_{sc} \ v_{sd} \ v_{se}]^T \quad (2.115)$$

$$[R_s] = R_s \cdot [I_5] \quad (2.116)$$

$$[i_s] = [i_{sa} \ i_{sb} \ i_{sc} \ i_{sd} \ i_{se}]^T \quad (2.117)$$

$$[\lambda_s] = [\lambda_{sa} \ \lambda_{sb} \ \lambda_{sc} \ \lambda_{sd} \ \lambda_{se}]^T \quad (2.118)$$

The air gap flux linkages are presented in (2.119). On one hand, $[L_{ss}]$ is the stator inductance matrix, see (2.120)–(2.121), where L_{ls} is the leakage inductance of the stator phases and M is the mutual inductance between phases. On the other hand, $[\lambda_m]$ is the established flux linkage matrix due to the permanent magnets viewed from the stator phase windings, see (2.122), where λ_{m1} and λ_{m3} are the amplitude of fundamental and third harmonic components of magnet flux linkages.

$$[\lambda_s] = [L_{ss}] \cdot [i_s] + [\lambda_m] \quad (2.119)$$

$$[L_{ss}] = L_{ls} \cdot [I_5] + [M_{ss}(\vartheta)] \quad (2.120)$$

$$[M_{ss}(\vartheta)] = M \cdot \begin{bmatrix} 1 & \cos(\vartheta) & \cos(2\vartheta) & \cos(3\vartheta) & \cos(4\vartheta) \\ \cos(4\vartheta) & 1 & \cos(\vartheta) & \cos(2\vartheta) & \cos(3\vartheta) \\ \cos(3\vartheta) & \cos(4\vartheta) & 1 & \cos(\vartheta) & \cos(2\vartheta) \\ \cos(2\vartheta) & \cos(3\vartheta) & \cos(4\vartheta) & 1 & \cos(\vartheta) \\ \cos(\vartheta) & \cos(2\vartheta) & \cos(3\vartheta) & \cos(4\vartheta) & 1 \end{bmatrix} \quad (2.121)$$

$$[\lambda_m] = \lambda_{m1} \cdot \begin{bmatrix} \sin(\theta) \\ \sin\left(\theta - \frac{2\pi}{5}\right) \\ \sin\left(\theta - \frac{4\pi}{5}\right) \\ \sin\left(\theta - \frac{6\pi}{5}\right) \\ \sin\left(\theta - \frac{8\pi}{5}\right) \end{bmatrix} + \lambda_{m3} \cdot \begin{bmatrix} \sin 3(\theta) \\ \sin 3\left(\theta - \frac{2\pi}{5}\right) \\ \sin 3\left(\theta - \frac{4\pi}{5}\right) \\ \sin 3\left(\theta - \frac{6\pi}{5}\right) \\ \sin 3\left(\theta - \frac{8\pi}{5}\right) \end{bmatrix} \quad (2.122)$$

Model in the d - q reference frame (rotating reference frame)

In order to simplify the machine model, an arbitrary coordinate transformation is introduced, which transfers the variables of the machine into a reference frame rotating at an arbitrary angular speed. Including the effect of the third harmonic, a d_1 - q_1 - d_3 - q_3 - z transformation can be applied. The d_1 - q_1 plane is rotating at synchronous speed (ω_r), while the d_3 - q_3 plane is rotating at three times the synchronous speed ($3\omega_r$). The extended Park matrix is represented in (2.123), which is a combination of the Clarke and rotation matrices. By applying this transformation to the stator voltages and flux linkages equations, the model of the five-phase machine is obtained in (2.124)–(2.125).

$$[T_5] = \sqrt{\frac{2}{5}} \begin{bmatrix} \cos(\theta) & \cos\left(\theta - \frac{2\pi}{5}\right) & \cos\left(\theta - \frac{4\pi}{5}\right) & \cos\left(\theta - \frac{6\pi}{5}\right) & \cos\left(\theta - \frac{8\pi}{5}\right) \\ -\sin(\theta) & -\sin\left(\theta - \frac{2\pi}{5}\right) & -\sin\left(\theta - \frac{4\pi}{5}\right) & -\sin\left(\theta - \frac{6\pi}{5}\right) & -\sin\left(\theta - \frac{8\pi}{5}\right) \\ \cos 3(\theta) & \cos 3\left(\theta - \frac{2\pi}{5}\right) & \cos 3\left(\theta - \frac{4\pi}{5}\right) & \cos 3\left(\theta - \frac{6\pi}{5}\right) & \cos 3\left(\theta - \frac{8\pi}{5}\right) \\ \sin 3(\theta) & \sin 3\left(\theta - \frac{2\pi}{5}\right) & \sin 3\left(\theta - \frac{4\pi}{5}\right) & \sin 3\left(\theta - \frac{6\pi}{5}\right) & \sin 3\left(\theta - \frac{8\pi}{5}\right) \\ \frac{1}{\sqrt{2}} & \frac{1}{\sqrt{2}} & \frac{1}{\sqrt{2}} & \frac{1}{\sqrt{2}} & \frac{1}{\sqrt{2}} \end{bmatrix} \quad (2.123)$$

$$\begin{bmatrix} v_{sd1} \\ v_{sq1} \\ v_{sd3} \\ v_{sq3} \\ v_{sz} \end{bmatrix} = R_s \cdot \begin{bmatrix} i_{sd1} \\ i_{sq1} \\ i_{sd3} \\ i_{sq3} \\ i_{sz} \end{bmatrix} + \frac{d}{dt} \begin{bmatrix} \lambda_{sd1} \\ \lambda_{sq1} \\ \lambda_{sd3} \\ \lambda_{sq3} \\ \lambda_{sz} \end{bmatrix} + \begin{bmatrix} 0 & -\omega_r & 0 & 0 & 0 \\ \omega_r & 0 & 0 & 0 & 0 \\ 0 & 0 & 0 & 3\omega_r & 0 \\ 0 & 0 & -3\omega_r & 0 & 0 \\ 0 & 0 & 0 & 0 & 0 \end{bmatrix} \cdot \begin{bmatrix} \lambda_{sd1} \\ \lambda_{sq1} \\ \lambda_{sd3} \\ \lambda_{sq3} \\ \lambda_{sz} \end{bmatrix} \quad (2.124)$$

$$\begin{bmatrix} \lambda_{sd1} \\ \lambda_{sq1} \\ \lambda_{sd3} \\ \lambda_{sq3} \\ \lambda_{sz} \end{bmatrix} = \begin{bmatrix} L_{sd1} & 0 & 0 & 0 & 0 \\ 0 & L_{sq1} & 0 & 0 & 0 \\ 0 & 0 & L_{sd3} & 0 & 0 \\ 0 & 0 & 0 & L_{sq3} & 0 \\ 0 & 0 & 0 & 0 & L_{sz} \end{bmatrix} \cdot \begin{bmatrix} i_{sd1} \\ i_{sq1} \\ i_{sd3} \\ i_{sq3} \\ i_{sz} \end{bmatrix} + \begin{bmatrix} \lambda_{m1} \\ 0 \\ -\lambda_{m3} \\ 0 \\ 0 \end{bmatrix} \quad (2.125)$$

Finally, the expression of the electromagnetic torque is obtained as in the case of the IM with concentrated windings, considering that the third harmonic components also contribute to the torque generation, as it appears in the following expressions:

$$T_{em} = T_{em1} + T_{em3} \quad (2.126)$$

$$T_{em1} = p \cdot \left[(L_{sd1} - L_{sq1}) \cdot i_{sd1} \cdot i_{sq1} + \lambda_{m1} \cdot i_{sq1} \right] \quad (2.127)$$

$$T_{em3} = 3p \cdot \left[(L_{sq3} - L_{sd3}) \cdot i_{sd3} \cdot i_{sq3} + \lambda_{m3} \cdot i_{sq3} \right] \quad (2.128)$$

In conclusion, different types of multiphase machines have been presented along these subsections, focusing on symmetrical five-phase machines. Their mathematical models have thoroughly been analyzed in phase variables, stationary and rotating reference frames. If a five-phase machine with only one frequency-domain subspace is considered (IM with distributed windings), it has been demonstrated that the electromagnetic energy conversion occurs exclusively in one subspace (related to the fundamental components of the machine). Otherwise, in five-phase machines with two frequency-domain subspaces (IM with concentrated windings and PMSM), the components of two subspaces contribute to the torque generation, which in the end will improve the performance of the system. Once the multiphase has been modeled, the power converter is analyzed in the next subsection to complete the modeling of the multiphase drive.

2.2.5 Modeling of the multiphase power converter

The control of electrical machines is nowadays linked to power electronics since, in most cases, the primary source of electrical energy has a format in terms of amplitude, frequency and number of phases that is not compatible with that required by the machine. Therefore, a converter element must be introduced that performs the transformation tasks and this is where the power converter plays its role. Power converters are in charge of converting energy from AC to DC or vice versa, controlling its voltage, current and frequency characteristics. Depending of its nature or application requirements, different topologies can be found in the literature, distinguished by the number of phases they possess (single phase, three-phase or multiphase) and the number of voltage levels they use to synthesize the modulated current/voltage (two-level, multilevel). Currently, the most widespread type of converter structure for both three-phase and multiphase systems is the *back-to-back* topology, which allows greater control of the system power by decoupling the part of the machine from the grid to which it is connected, through a DC bus (DC-link from now on). Such topology is formed by two stages, usually a non-controlled rectifier and an inverter, electrically coupled through the mentioned DC-link. The described system has the capacity to operate in a wide range of frequencies in its output and to generate, by means of a suitable control algorithm, an output with a multi-frequency sinusoidal average value together with a small content of low-order harmonics. These converters are usually of two voltage levels, although lately the use of multilevel converters has been growing [61,62].

In this subsection, the study will be focused on the part of the voltage source inverter (VSI from now on) that feeds the multiphase machine, where the model and principle of operation of two-level multiphase inverters are described and particularized to the five-leg case. The VSI model is useful for the formulation of the control techniques proposed in this Thesis. Initially, the VSI scalar model is obtained, to finally define the vector model that is crucial for the description of the different control strategies.

VSI scalar model

In Fig. 2.4, the scheme of the n -leg two-level VSI is shown. It is considered that the DC-link is fed with a DC voltage source V_{dc} with a midpoint 0 (the DC-link is provided by an external low-impedance DC source). The converter is composed of $2n$ switches based on insulated-gate bipolar transistor (IGBT) and their corresponding anti-parallel free-wheeling diode, two for each phase, whose electrical ratings are able to withstand the entire DC-link voltage and the maximum rated current of the machine. The VSI output corresponds to each midpoint (1, 2, 3, ..., n) between these IGBTs. It is assumed, for simplicity, that the VSI output feeds a balanced load in star connection with inductive predominance (dominant characteristic in electrical machines), being N the common point. The phase voltages are defined by the variables v_{sk} where $k = \{1, 2, 3, \dots, n\}$.

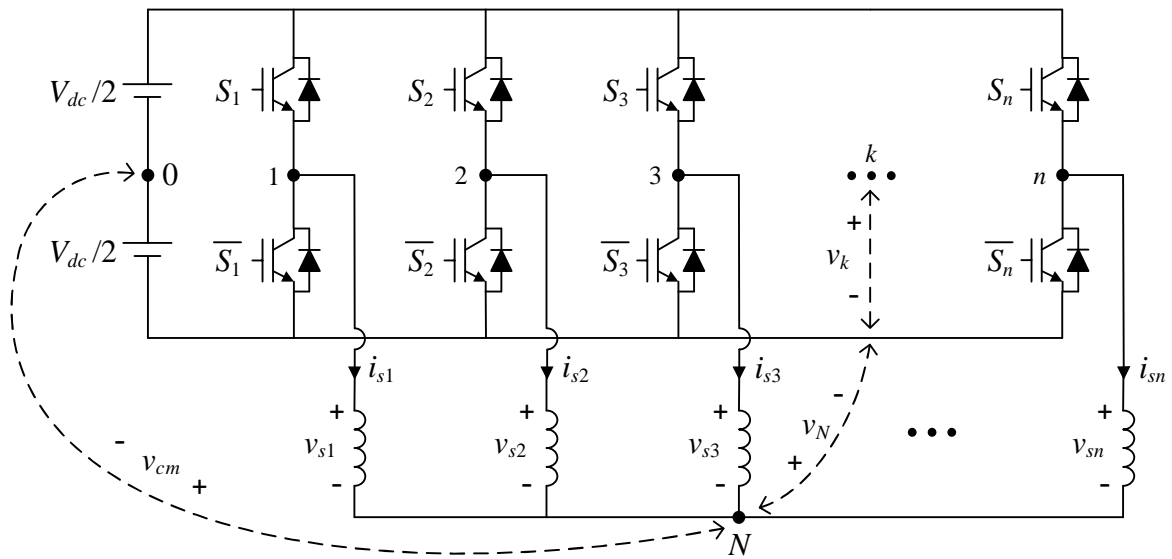


Figure 2.4. Schematic diagram of the n -leg two-level VSI.

For the presented scheme and in order to avoid short circuits, only one IGBT can be activated at the same time in each VSI leg. When both IGBTs of a same leg are OFF, there is no control over the load, so this state must be also avoided during normal operation of the VSI. Therefore, the IGBTs of each leg will switch alternately, also leaving a small dead time between their commutations to avoid transient short circuits. Thus, the state of each leg S_k can be defined using the binary logic, $S_k = \{0, 1\}$; so that $S_k = 1$ implies that the upper IGBT is ON and the lower one is OFF, while the opposite case is verified when $S_k = 0$. This allows that at the VSI output two voltage levels ($\pm V_{dc}/2$) are available with respect to the midpoint of the DC-link. The switching function of the VSI can be defined using the switching vector $[S_1 \ S_2 \ \dots \ S_n]^T$, where the superscript T indicates the transposition operation. For the n -leg VSI, in this case, there are 2^n switching states. The following study is conducted considering that n is an odd number.

The voltage v_k with respect to the negative DC-link bus can be defined based on the switching state of this leg, as indicated in the following equation:

$$v_k = V_{dc} \cdot S_k \quad (2.129)$$

This voltage v_k is related to the phase voltage v_{sk} and the voltage v_N (between the negative DC-link bus and the common point of the star connection, see Fig. 2.4), according to the next expression:

$$v_k = v_{sk} + v_N \quad (2.130)$$

For the studied case with balanced load, the sum of the phase voltages must be equal to zero. Adding all the equations obtained in each phase with the expression in (2.130) in conjunction with equation (2.129), it is achieved that the voltage v_N can be defined from the switching states in the following way:

$$v_N = \frac{1}{n} \sum_{i=1}^n v_i = \frac{V_{dc}}{n} \sum_{i=1}^n S_i \quad (2.131)$$

Replacing this equality in equation (2.130), the phase voltage is determined as:

$$v_{sk} = v_k - v_N = V_{dc} \cdot S_k - \frac{V_{dc}}{n} \sum_{i=1}^n S_i = V_{dc} \cdot \left[S_k - \frac{1}{n} \sum_{i=1}^n S_i \right] \quad (2.132)$$

The increase in the number of phases also produces an increment in the number of voltage levels v_{sk} capable of being generated by the VSI. This voltage can take $(2n - 1)$ different values between $(n - 1) \cdot V_{dc}/n$ and $-(n - 1) \cdot V_{dc}/n$, with steps of V_{dc}/n . For the sake of simplicity, the phase voltages defined in equation (2.132) as a function of the switching states are usually expressed using matrices, as indicated down below:

$$\begin{bmatrix} v_{s1} \\ v_{s2} \\ v_{s3} \\ \vdots \\ v_{sn-1} \\ v_{sn} \end{bmatrix} = \frac{V_{dc}}{n} \cdot \begin{bmatrix} (n-1) & -1 & -1 & \cdots & -1 & -1 \\ -1 & (n-1) & -1 & \cdots & -1 & -1 \\ -1 & -1 & (n-1) & \cdots & -1 & -1 \\ \vdots & \vdots & \vdots & \ddots & \vdots & \vdots \\ -1 & -1 & -1 & \cdots & (n-1) & -1 \\ -1 & -1 & -1 & \cdots & -1 & (n-1) \end{bmatrix} \cdot \begin{bmatrix} S_1 \\ S_2 \\ S_3 \\ \vdots \\ S_{n-1} \\ S_n \end{bmatrix} \quad (2.133)$$

The common-mode voltage v_{cm} of the VSI is defined as the voltage of the common point of the star connection with respect to the midpoint of the DC-link. This voltage can be defined using equation (2.131), in the following way:

$$v_{cm} = v_N - \frac{V_{dc}}{2} = \frac{V_{dc}}{n} \sum_{i=1}^n S_i - \frac{V_{dc}}{2} \quad (2.134)$$

This last expression indicates that the n -leg two-level VSI, under the described load conditions, presents $(n + 1)$ different values of common-mode voltage from $+V_{dc}/2$ to $-V_{dc}/2$, with incremental steps of V_{dc}/n . This corresponds to $(n + 1)/2$ voltage magnitude levels.

VSI vector model

For the development of this model, the procedure is analogous to that carried out to determine the vector model of the multiphase induction machine in Section 2.2.1. In order to facilitate and simplify the analysis of the mathematical model of the VSI, the Clarke transformation matrix $[C_n]$ is used, which is detailed in equation (2.135), where $\vartheta = 2\pi/n$.

$$[C_n] = \frac{2}{n} \cdot \begin{bmatrix} 1 & \cos(\vartheta) & \cos(2\vartheta) & \cdots & \cos((n-1)\cdot\vartheta) \\ 0 & \sin(\vartheta) & \sin(2\vartheta) & \cdots & \sin((n-1)\cdot\vartheta) \\ 1 & \cos(2\vartheta) & \cos(4\vartheta) & \cdots & \cos(2(n-1)\cdot\vartheta) \\ 0 & \sin(2\vartheta) & \sin(4\vartheta) & \cdots & \sin(2(n-1)\cdot\vartheta) \\ \vdots & \vdots & \vdots & \ddots & \vdots \\ 1 & \cos\left(\frac{(n-1)}{2}\cdot\vartheta\right) & \cos\left(\frac{(n-1)}{2}\cdot 2\vartheta\right) & \cdots & \cos\left(\frac{(n-1)}{2}\cdot(n-1)\cdot\vartheta\right) \\ 0 & \sin\left(\frac{(n-1)}{2}\cdot\vartheta\right) & \sin\left(\frac{(n-1)}{2}\cdot 2\vartheta\right) & \cdots & \sin\left(\frac{(n-1)}{2}\cdot(n-1)\cdot\vartheta\right) \\ \frac{1}{2} & \frac{1}{2} & \frac{1}{2} & \cdots & \frac{1}{2} \end{bmatrix} \quad (2.135)$$

This transformation matrix has the particularity of decomposing the n -dimensional space into orthogonal subspaces, formed by several two-dimensional planes and a one-dimensional component (homopolar axis). The information of each plane is contained in two consecutive rows of the matrix, while the last row defines the homopolar component. The n -dimension vector defined by the components in phase variables $[v_{s1}, v_{s2}, v_{s3}, \dots, v_{sn}]^T$, after the transformation, will be represented by the vector that contains the two-dimensional components of each plane and the homopolar one $[v_{sa}, v_{sb}, v_{sx1}, v_{sy1}, \dots, v_{sz}]^T$.

Five-leg two-level VSI

In this section the VSI is particularized to the five-leg case (Fig. 2.5) to control five-phase machines, which corresponds to the type of machine studied in this Thesis. In this case, the phase variables are identified by means of the letters a, b, c, d and e , respectively. For its operation, the VSI has $2^5 = 32$ different switching states. Each commutation is characterized by a switching vector defined by $[S_a S_b S_c S_d S_e]^T$, with $S_k = \{0,1\}$, following the nomenclature exposed in the generalized n -leg model. Therefore, the phase voltages are defined as a function of the switching states as indicated in the following equation:

$$\begin{bmatrix} v_{sa} \\ v_{sb} \\ v_{sc} \\ v_{sd} \\ v_{se} \end{bmatrix} = \frac{V_{dc}}{5} \cdot \begin{bmatrix} 4 & -1 & -1 & -1 & -1 \\ -1 & 4 & -1 & -1 & -1 \\ -1 & -1 & 4 & -1 & -1 \\ -1 & -1 & -1 & 4 & -1 \\ -1 & -1 & -1 & -1 & 4 \end{bmatrix} \cdot \begin{bmatrix} S_a \\ S_b \\ S_c \\ S_d \\ S_e \end{bmatrix} \quad (2.136)$$

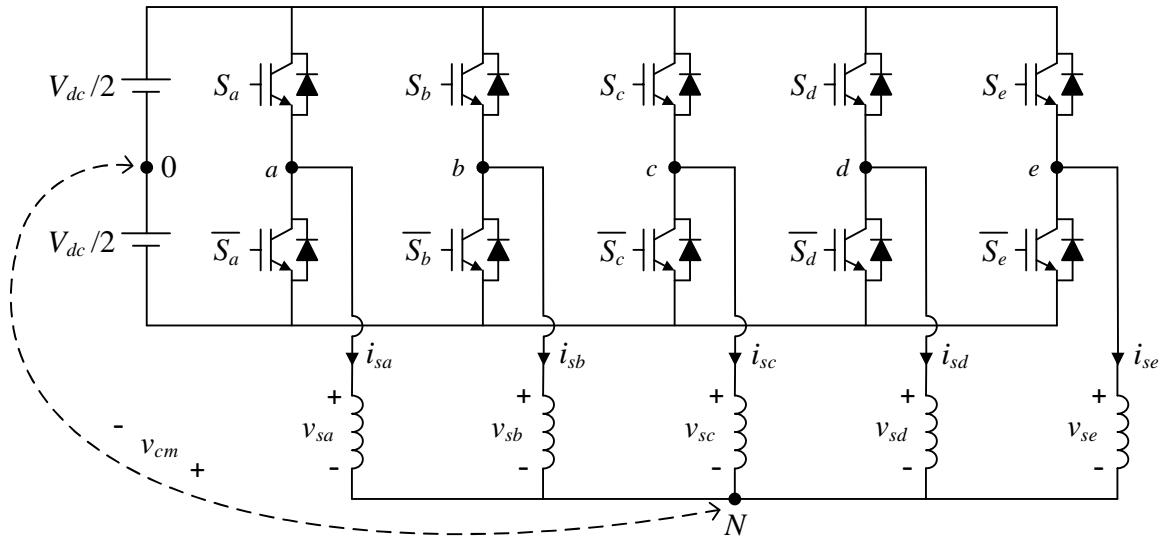


Figure 2.5. Five-leg two-level VSI with star-connected load.

Depending on the switching state, these phase voltages can have values of $\pm 4V_{dc}/5$, $\pm 3V_{dc}/5$, $\pm 2V_{dc}/5$, $\pm V_{dc}/5$ and 0, as it can be seen in Fig. 2.6, producing different load configurations from the point of view of the DC-link. The possible load configurations are {0,5}, {1,4}, {2,3}, {3,2}, {4,1} and {5,0}, where the first and second digits represent the number of legs connected to the positive and negative DC-link bus, respectively.

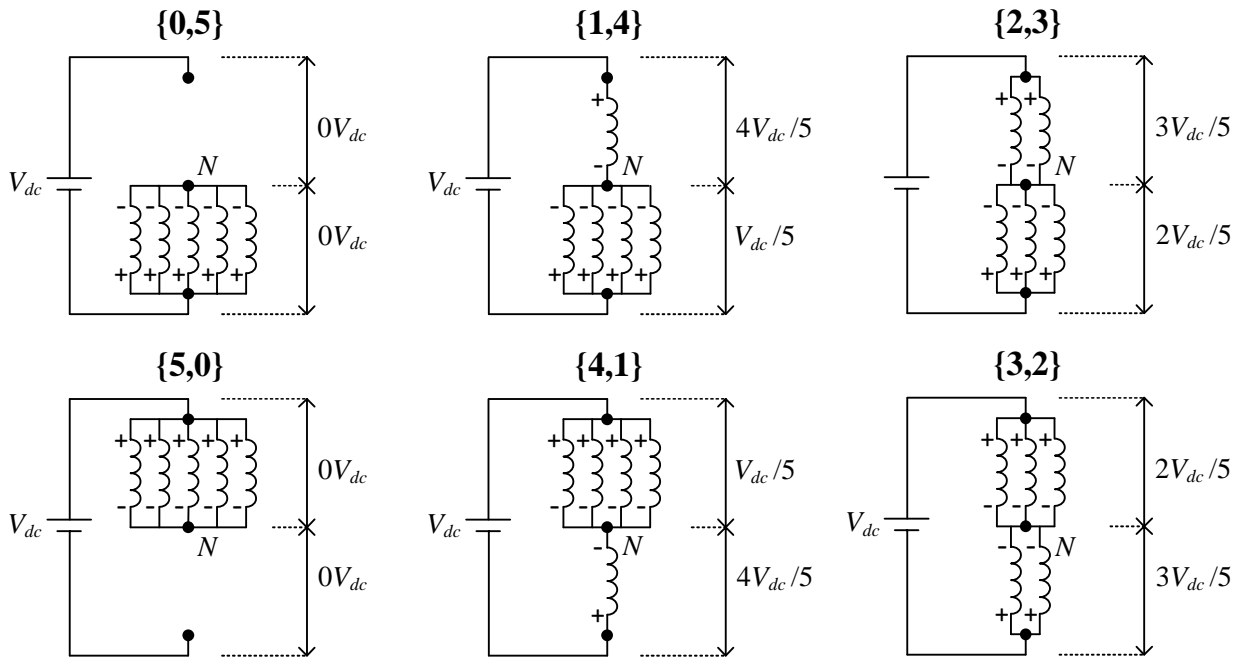


Figure 2.6. Five-leg two-level VSI load configuration scheme.

For the development of this VSI vector model, the Clarke transformation matrix is obtained from the one presented in the previous section in equation (2.135), particularizing with $\vartheta = 2\pi/5$ and $n = 5$:

$$\begin{bmatrix} v_{s\alpha} \\ v_{s\beta} \\ v_{sx} \\ v_{sy} \\ v_{sz} \end{bmatrix} = \frac{2}{5} \cdot \begin{bmatrix} 1 & \cos(9) & \cos(29) & \cos(39) & \cos(49) \\ 0 & \sin(9) & \sin(29) & \sin(39) & \sin(49) \\ 1 & \cos(29) & \cos(49) & \cos(69) & \cos(89) \\ 0 & \sin(29) & \sin(49) & \sin(69) & \sin(89) \\ \frac{1}{2} & \frac{1}{2} & \frac{1}{2} & \frac{1}{2} & \frac{1}{2} \end{bmatrix} \cdot \begin{bmatrix} v_{sa} \\ v_{sb} \\ v_{sc} \\ v_{sd} \\ v_{se} \end{bmatrix} \quad (2.137)$$

Applying this transformation, 30 active voltage vectors and 2 null vectors are defined. Figure 2.7 shows the two-dimensional projections obtained with every vector, identified with the decimal number equivalent of their respective switching state $[S_a S_b S_c S_d S_e]^T$, being S_a and S_e the most and the least significant bits, respectively. These vectors uniformly divide the space that they occupy in 10 sectors with a separation of $\pi/5$ between them. Likewise, the active voltage vectors can be classified according to their magnitude in long ($0.647V_{dc}$), medium ($0.4V_{dc}$) and short ($0.247V_{dc}$) vectors. The switching states that generate long vectors in the α - β plane correspond to those that generate short vectors in the x - y plane, and vice versa. The switching states corresponding to vectors of medium magnitude in the α - β plane, also generate medium vectors in the x - y plane. On the other hand, null vectors are generated by the same switching states in both planes. This transformation allows the detailed study of the harmonic components, since they are projected in certain planes. Particularly, the fundamental frequency together with the harmonics of order $10k \pm 1$ ($k = 0, 1, 2, \dots$) are mapped in the α - β plane, while the harmonics of order $10k \pm 3$ are related to the x - y plane. The homopolar component and the harmonics of order $5k$ are projected on the z -axis.

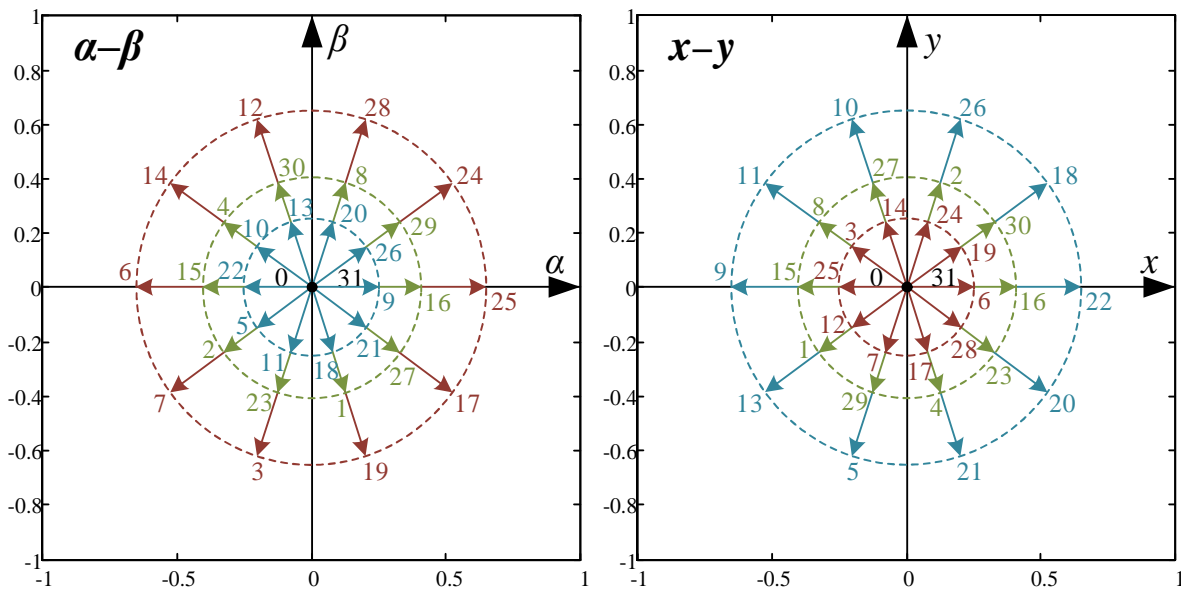


Figure 2.7. Mapping of the phase voltages of the five-leg VSI into the α - β (left plot) and x - y (right plot) planes.

Finally, the common-mode voltage, for this particular case, is defined by the following equation:

$$v_{cm} = \frac{V_{dc}}{5} \cdot (S_a + S_b + S_c + S_d + S_e) - \frac{V_{dc}}{2} \quad (2.138)$$

Analyzing equation (2.138), it is verified that there are three levels of voltage magnitude in common mode. The greatest magnitude ($0.5V_{dc}$) corresponds to the states [0 0 0 0 0] and [1 1 1 1 1] (null vectors), corresponding to the load configurations {0,5} and {5,0}, respectively, which produce a zero voltage in all phases. The states that have load configurations {1,4} and {4,1} generate a medium magnitude level ($0.3V_{dc}$). Lastly, the switching states that present load configurations {2,3} and {3,2} generate the lowest common-mode voltage ($0.1V_{dc}$). In addition, it should be noted that complementary switching states synthesize the same common-mode voltage magnitudes but with opposite signs.

2.3 State of the art in the multiphase drives control field

Multiphase drives control schemes are based mainly on the extension of traditional control techniques originally proposed for three-phase machines, where the additional degrees of freedom that multiphase drives possess are effectively exploited. The most common control strategy employed in research works is the Field Oriented Control technique, based on linear cascaded control loops and assisted by coordinate transformations and modulation stages. The multiphase machine is decomposed in multiple orthogonal $d-q$ subspaces (fundamental and harmonics components), being each set of $d-q$ variables independently controlled. The reference voltages are determined by the well-known proportional-integral controllers, which are inputs for the modulation stage based on PWM with a fixed frequency that generates the switching signals to the VSI. This method can be considered as an ‘average control’, in the way that the reference voltages (which are continuous signals) are synthesized by the PWM stage, producing discrete signals that correspond to the expected reference in average value.

An alternative to such technique is the ‘direct control’ strategy, which includes Direct Torque Control and Model-based Predictive Control as leading competitors. The main difference with Field Oriented Control is the way in which the VSI that supplies the multiphase machine is controlled. In ‘direct control’ the VSI switches are directly applied forcing the controlled variables to rapidly track their reference values, eliminating the PWM stage or other form of modulation.

A brief state of the art in the multiphase drives control field is done in this section to put the focus on the control techniques that will be applied in this work, without losing the environment perspective.

2.3.1 Field Oriented Control

Vector Control or Field Oriented Control (FOC), proposed at the end of the 60’s [63,64], is the most popular technique for the control of AC machines and its development completely displaced the use of DC machines in variable speed applications. The essence of this technique is to decouple the control of the flux (whether the stator, rotor or air gap flux) from the control of the electromagnetic torque, controlling both independently in the $d-q$ rotating reference frame. The

Rotor Field Oriented Control (RFOC) technique is the most widely used among the FOC strategies in industrial applications [15]. Now, consider the case of the five-phase induction machine with distributed windings. In this case, the rotor flux component is aligned with the d -axis, making that the rotor flux in the q -axis is null:

$$\lambda_{rd} = L_r \cdot i_{rd} + L_m \cdot i_{sd} \quad \rightarrow \quad i_{rd} = \frac{1}{L_r} \cdot (\lambda_{rd} - L_m \cdot i_{sd}) \quad (2.139)$$

$$\lambda_{rq} = L_r \cdot i_{rq} + L_m \cdot i_{sq} = 0 \quad \rightarrow \quad i_{rq} = -\frac{L_m}{L_r} \cdot i_{sq} \quad (2.140)$$

$$\frac{d\lambda_{rq}}{dt} = 0 \quad (2.141)$$

Substituting (2.139)–(2.141) in the equations of the rotor voltage (2.78)–(2.79) and in the equation of the torque (2.87), it is obtained:

$$\tau_r \cdot \frac{d\lambda_{rd}}{dt} + \lambda_{rd} = L_m \cdot i_{sd} \quad (2.142)$$

$$\omega_{sl} \cdot \tau_r \cdot \lambda_{rd} = L_m \cdot i_{sq} \quad (2.143)$$

$$T_{em} = p \cdot \frac{5}{2} \cdot \frac{L_m}{L_r} \cdot \lambda_{rd} \cdot i_{sq} \quad (2.144)$$

where $\tau_r = L_r/R_r$ represents the rotor time constant. The electromagnetic torque represented by (2.144) shows that it can be controlled by modifying the stator reference current i_{sq} and keeping the rotor flux λ_{rd} constant below the synchronism. Analyzing (2.142), it can be stated that the rotor flux is independent of the current i_{sq} , responsible for the torque production, and that the rotor flux value is determined solely by the stator current i_{sd} . The reference value of i_{sd} is usually established at its nominal value (constant reference flux and equal to the maximum possible one below the synchronization speed of the electromechanical drive), while i_{sq} is independently controlled. In addition, currents i_{sd} and i_{sq} are constants in steady state, facilitating their regulation.

There exist two main versions of the RFOC: the Indirect Rotor Flux Oriented Control (IRFOC) [30,31,63,65–72] and the Direct Rotor Flux Oriented Control (DRFOC) [32,64,73,74]. The difference between both techniques lies in the way of determining the angle of the rotor flux, necessary for the field orientation. DRFOC was proposed in [64], where flux sensors mounted in the air gap of the machine are used to determine directly this angle. It is also possible to implement DRFOC by estimating the position and magnitude of the vector flux with the current and voltage measurements, at the expense of increasing the computational burden of the control system. On the other hand, IRFOC was developed in [63], where the orientation of the flux vector is forced imposing the slip from the equations of the machine to guarantee the decoupling between the stator current components that regulate the flux and the torque. In this way, making use of (2.70) and (2.143), the equation presented in (2.145) is obtained, where the slip is estimated according to (2.143), considering the references of the current i_{sq} and the rotor flux in the d -axis. IRFOC is more

used than DRFOC since it decreases the number of required sensors, in addition to certain modifications in the machine for its assembly that would reduce the robustness of the system. However, the IRFOC technique requires a good knowledge of the rotor time constant τ_r to achieve a good orientation.

$$\theta_a = \int_0^t \omega_a \cdot dt = \int_0^t (\omega_r + \omega_{sl}) \cdot dt = \int_0^t \left(\omega_r + \frac{L_m \cdot i_{sq}^*}{\tau_r \cdot \lambda_{rd}^*} \right) \cdot dt \quad (2.145)$$

The IRFOC scheme for a five-phase induction machine with distributed windings is shown in Fig. 2.8. The technique is based on four independent control loops for speed, rotor flux and currents in the x - y plane. For the regulation of the above variables, proportional-integral (PI) controllers are used, which provide the controller with robustness against the main disadvantage of this control method, which is the need to know the parameters of the machine in order to achieve a correct orientation. The i_{sd} current is controlled through a PI based on the rotor flux error, while the i_{sq} current control is achieved through the outer speed PI regulator followed by an inner current loop (see Fig. 2.8). Finally, because it is a machine with distributed windings, the x - y stator reference currents are set to zero, since they do not contribute to the torque generation, so they must be limited to avoid undesired harmonics. The outputs of the PI controllers provide the reference values for the voltages in the d - q reference system, which are again transformed to the reference frame of phase variables to be processed by means of modulation algorithms in order to control the VSI.

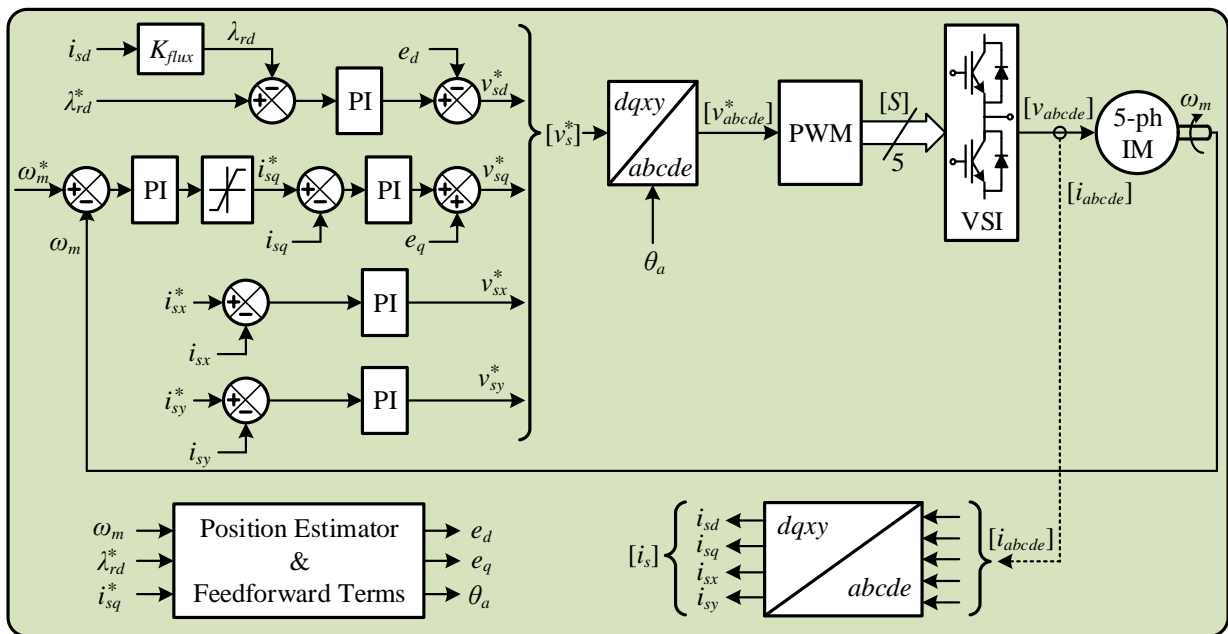


Figure 2.8. IRFOC control scheme applied to a five-phase IM with distributed windings.

For the implementation of this technique in multiphase machines, it was necessary to extend the modulation techniques to the multiphase case, developing mainly two types: Carrier Based Pulse Width Modulation (CBPWM) and Space Vector Pulse Width Modulation (SVPWM). In the

case of CBPWM, a comparison is made between the reference voltage waveform and a triangular modulation signal whose frequency corresponds to the switching frequency of the VSI. Conversely, in the SVPWM technique a combination of the different adjacent space vectors applied during different times is used to achieve the reference voltage. Many research works are found in the literature using both techniques in induction machines with different phase numbers [75–82] and including in some cases, for example, the reduction of the generated common-mode voltage [83,84] to extend the control criteria.

Modified FOC controllers have been successfully applied in induction machines with concentrated windings, as well as in permanent magnet synchronous machines. In these cases, the injection of harmonics is required to improve the performance in the electromagnetic torque generation. The controllers used in the additional planes (d_k-q_k) are analogous to those used in the d_1-q_1 plane, since it is verified that these planes also contribute to the torque generation. In order to enhance this torque generation, a non-zero reference current is required in these complementary planes, but it must be synchronized with the fundamental component. This is usually made by injecting a fixed percentage of the fundamental magnitude to achieve the desired flux profile. This scheme has been implemented in both types of machines with different number of phases [65,85–91]. For example, in [85] a five-phase concentrated windings induction machine is used, adjusting the injection percentage of the third harmonic to 15% of the fundamental to achieve a trapezoidal flux profile. In [65] a compensation loop is alternatively used in the injected current of the d_3-q_3 plane to maintain the synchronization between the two planes and produce a flux profile similar to the one previously obtained.

2.3.2 Direct Torque Control

Direct Torque Control (DTC) is a control strategy known for its fast flux and torque response, as well as its robustness with respect to the variation of the electrical parameters of the machine. Its origins go back to the mid-80's thanks to the innovative studies of Takahashi [92] and Depenbrock [93], when it seemed that the standardization of the FOC technique was taking place. This strategy has been widely studied in the case of three-phase drives [94] and has led to commercial devices in traditional drives [95]. Consequently, the technique has been extended to the multiphase field considering different types of machines [47,94], neutral connections [96,97] and drives without speed sensors [51]. Traditionally, its operating principle is based on a look-up table, which is calculated offline, used to select the most appropriate VSI state that will be applied on the machine. This selection is done taking into account the position of the flux vector and two error signals (stator flux and electromagnetic torque errors) obtained from the difference between the reference values and the estimated ones. The error signals are usually processed using a structure based on hysteresis comparators, thereby controlling the variables within that band. This strategy is called DTC based on switching tables (ST-DTC).

One of its main disadvantages is the generation of high torque/flux ripple and its high harmonic content in the current [33,34]. In the case of multiphase drives, since the controller has only two degrees of freedom (stator flux and electromagnetic torque), there is no chance for regulating the current and voltage components in the $x-y$ plane. In this sense, some DTC strategies have been developed that satisfy this additional requirement. For example, in [98,99] a

modification in the traditional control scheme is proposed, performing a two-step search to minimize the effect of low-order harmonics. Alternatively, the use of virtual vectors has been proposed to reduce the current distortion [51]. Some criteria have also been included in the selection process within the look-up table to improve its performance in the low-speed region and an optimization between the two zero vectors to minimize the obtained average switching frequency [52]. On the other hand, based on the virtual vectors defined in [51], a DTC scheme is presented in [100,101] to reduce the common-mode voltage generated by the VSI, defining new virtual vectors and avoiding the use of the zero vector.

Another disadvantage to be considered is that DTC does not generate a constant switching frequency, as in the case of FOC, which depends on the operating point and the bandwidth of the hysteresis controllers. The use of DTC schemes with PI regulators and SVPWM strategies (Space Vector Modulated Direct Torque Control or SVM-DTC) have also been proposed in [102], in order to compensate the variable switching frequency and the torque and flux ripple.

Operating principle of DTC

In order to deduce the operating principle of DTC, the five-phase IM with distributed windings is considered as a case example. Then, the control goal is reduced to the α - β plane (torque and flux regulation), while trying to nullify the x - y components. The study starts from the model of such machine expressed in the α - β - x - y stationary reference frame, described in Section 2.2.1. From equations (2.43) and (2.45), the variation in the stator flux in the α - β subspace can be defined, using vector notation, as:

$$\Delta \vec{\lambda}_{s\alpha\beta} = \int_0^t (\vec{v}_{s\alpha\beta} - R_s \cdot \vec{i}_{s\alpha\beta}) \cdot dt \quad (2.146)$$

If the voltage drop in the stator resistance is ignored in a small sampling time (T_s) for simplicity, the equation presented in (2.147) is obtained. From this expression, it is deduced that the variation in the modulus of the flux vector directly depends on the voltage vector applied during each sampling period.

$$\Delta \vec{\lambda}_{s\alpha\beta} \approx \vec{v}_{s\alpha\beta} \cdot T_s \quad (2.147)$$

With the aim of analyzing the behavior of the electromagnetic torque, equations (2.84)–(2.87) are combined, obtaining the following expression:

$$T_{em} = \frac{5}{2} \cdot \frac{p \cdot k_r}{\sigma \cdot L_s} \cdot (\vec{\lambda}_{r\alpha\beta} \times \vec{\lambda}_{s\alpha\beta}) = \frac{5}{2} \cdot \frac{p \cdot k_r}{\sigma \cdot L_s} \cdot \|\vec{\lambda}_{r\alpha\beta}\| \cdot \|\vec{\lambda}_{s\alpha\beta}\| \cdot \sin \gamma \quad (2.148)$$

$$\sigma = 1 - \left(\frac{L_m^2}{L_s \cdot L_r} \right) \quad (2.149)$$

$$k_r = \frac{L_m}{L_r} \quad (2.150)$$

where γ is the angle between stator and rotor flux vectors, named as the load angle. Since the rotor time constant is relatively larger with respect to that of the stator, it can be assumed that the rotor flux varies very slowly compared to the stator flux, and therefore γ remains fixed. Thus, any fast change in the angle between both vectors produces an increase or decrease in the magnitude of the torque, since it is proportional to the sine of the load angle γ . This change is obtained by the application of a voltage vector, as stated in equation (2.147). In Fig. 2.9, it can be seen the impact of a spatial voltage vector on both the magnitude of the stator flux and the load angle γ . Notice that Fig. 2.9a shows the phasor diagram based on the equations of the machine model (including the voltage drop in the stator resistance), while Fig. 2.9b presents the assumed approach for the control strategy. The impact on the load angle γ can be noted, considering that the response of the rotor flux is much slower than that of the stator, as discussed above.

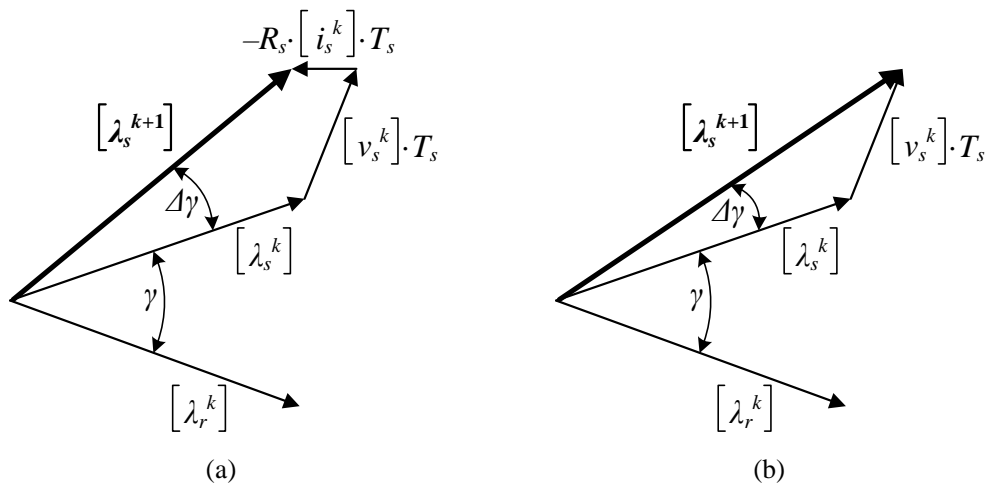


Figure 2.9. Impact of a voltage vector on both the stator flux and the load angle. (a) Phasor diagram of the real model of the machine. (b) Estimated phasor diagram for the application of DTC.

Different results will be obtained depending on the spatial voltage vector that is applied in each sampling time, creating the rotation direction of the machine flux. As stated in Section 2.2.5, for a five-leg two-level VSI there are 32 vectors (30 active and 2 null vectors) that can be selected to comply with the control criteria. Combining equations (2.136) and (2.137), the spatial voltage vectors in the α - β and x - y subspaces are obtained as a function of the switching state of the VSI. Figure 2.7 shows these vectors, where each vector is represented by the equivalent decimal number of the switching state of the VSI, $[S_a S_b S_c S_d S_e]^T$, defining ten sectors in each plane. Using the voltage vectors in the α - β plane, which are those that generate the torque in this type of machines, Fig. 2.10 presents the availability of spatial voltage vectors and the reference circular trajectory of the stator flux vector. The rotor flux vector with the load angle γ is also shown. In short, the spatial voltage vector can be divided in tangential and radial components with respect to the flux. The tangential component is the one that produces the change in the torque of the machine (it increases or decreases the sine of the angle γ), while the radial component is the one that modifies the stator flux magnitude (it increases or decreases the stator flux modulus). In this way, the flux and the electromagnetic torque can be controlled simultaneously with the applied spatial voltage vector.

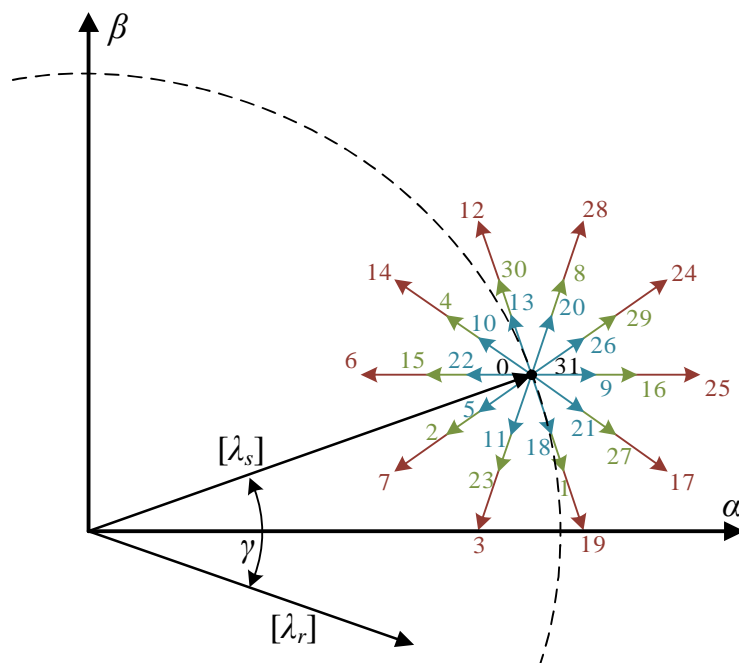


Figure 2.10. Diagram of the flux vectors together with the spatial voltage vectors available for the control.

Introduction of virtual voltage vectors

In multiphase machines the application of a spatial voltage vector does not only affect the voltages in the α - β plane, but also the voltages in the other planes (and therefore the currents). In the IM drive with distributed windings remember that the torque is only generated in the α - β plane, while currents in the x - y plane represent losses in the machine and should be limited to avoid undesired harmonics. Thus, a control strategy is required to minimize the currents in the x - y plane.

Note in Fig. 2.7 that there are 32 vectors with 4 different magnitudes: 2 null vectors (0), 10 short vectors ($0.247V_{dc}$), 10 medium vectors ($0.4V_{dc}$) and 10 long vectors ($0.647V_{dc}$). It can be seen that the switching states that represent long vectors in the α - β plane represent short vectors in the x - y plane (and vice versa), while switching states that produce medium vectors in the α - β plane also produce medium vectors in the x - y plane. In addition, long and medium vectors with the same direction in the α - β subspace, are equivalent to medium and short vectors with opposite directions in the x - y subspace. The same occurs with medium and short vectors in the α - β plane, since they are equivalent to medium and long vectors with opposite directions in the x - y plane. These geometrical characteristics make possible the definition of virtual voltage vectors that allow to minimize the currents in the x - y plane. This technique was firstly introduced in [51]. A virtual vector (VV_i) is a combination of two available voltage vector following a certain strategy. In this case, the strategy is to select adequate dwell time ratios (K_{v1} and K_{v2}) to generate zero average volts-per-second in the x - y subspace in order to minimize the copper losses in the machine. It is possible to define in each sector a long virtual vector (formed by a long and a medium vector in the α - β plane) and a short virtual vector (formed by a medium and a short vector in the α - β plane), as shown in equations (2.151) and (2.152). For example, consider the long virtual vector in the sector number 1 formed by the voltage vectors 25 and 16 (v_{25} and v_{16} , respectively), which are in the same direction in the α - β subspace and are opposite in the x - y subspace. By selecting adequate values of K_{v1} and K_{v2} , it is obtained zero average volts-per-second in the x - y subspace (see Fig.

2.11). Figure 2.12 shows all the virtual vectors in the α - β plane, being VV_{Li} the long virtual vectors and VV_{Si} the short ones. Furthermore, the dwell times of every vector in each sampling time T_s to achieve the minimization of the x - y currents are $K_{v1} = 0.618T_s$ and $K_{v2} = 0.382T_s$. It should be noted, however, that even in the case when virtual voltage vectors are used, the x - y currents are kept in open loop. Consequently, the machine must have low asymmetries and spatial harmonic content and/or high impedance in the x - y plane to reasonably limit the circulation of x - y currents. It is also important to highlight that x - y components do not contribute to the torque, but they increase the power losses in the electromechanical system. Then, a control goal is the cancellation of these components or, as it is done in DTC, the generation of the minimum possible values.

$$VV_{Li} = v_{Long} \cdot K_{v1} + v_{Medium} \cdot K_{v2} \quad (2.151)$$

$$VV_{Si} = v_{Medium} \cdot K_{v1} + v_{Short} \cdot K_{v2} \quad (2.152)$$

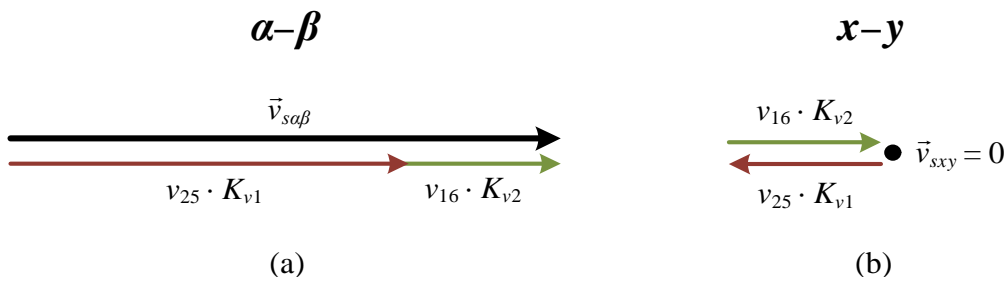


Figure 2.11. VV_{L1} projections in the (a) α - β and (b) x - y planes.

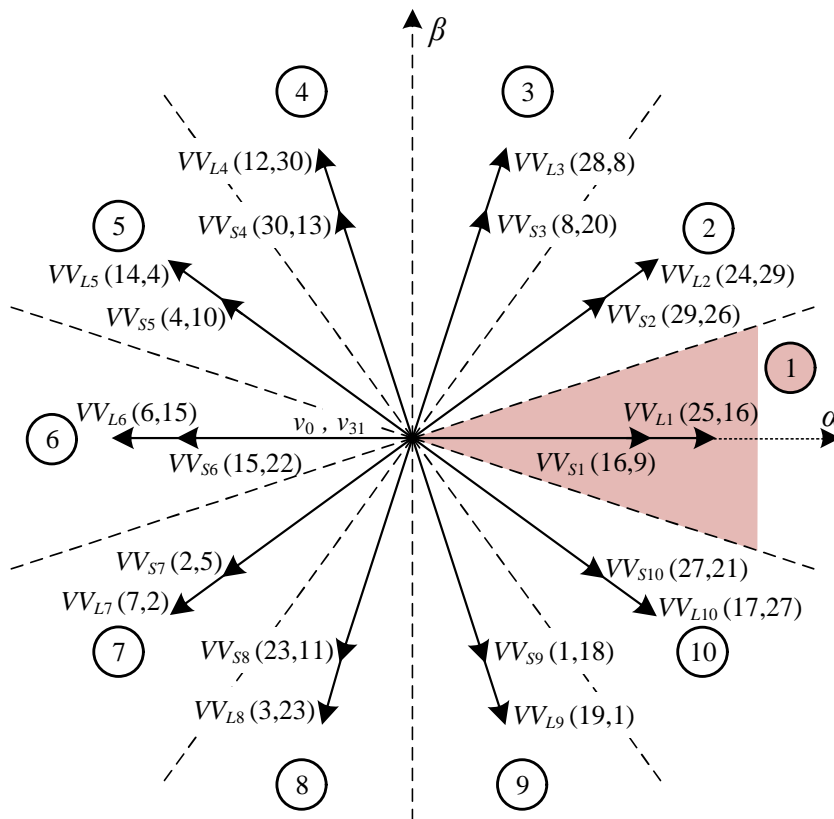


Figure 2.12. Virtual voltage vectors in the α - β plane.

Selection of voltage vectors (look-up tables)

To implement the DTC technique, the scheme presented in Fig. 2.13 is used. In this scheme, flux and torque estimators are considered (see Appendix B), whose outputs are compared with the reference values. By means of these outputs, the voltage vectors to be selected are determined using hysteresis comparators. On the one hand, the stator flux is maintained within a hysteresis band of minimum magnitude. For such purpose, a two-level comparator is proposed, which evaluates when the flux magnitude is higher or lower than the reference quantity. On the other hand, the electromagnetic torque is also maintained within a hysteresis band ΔT_{em} . In this case, a five-level comparator is used, leading to two possible error levels (one higher than the other) in both rotation directions of the machine and a zero error level. Finally, it must be considered that at low speeds the effect of neglecting the voltage drop in the stator resistance produces an appreciable drop in the stator flux vector when it is positioned at the limit of some sector [52]. Therefore, a comparator with two speed levels that defines the low-speed band is also proposed, because at low speed the effect of the voltage drop on the stator resistance cannot be neglected. The low-speed threshold is defined as ω_{mth} . Hereunder, it is presented the mathematical expressions to generate the error signals that will serve as criteria for selecting the appropriate voltage vector to satisfy the control requirements:

$$\begin{aligned} \lambda_s^* &> \|\vec{\lambda}_{s\alpha\beta}\| & d\lambda &= +1 \\ \lambda_s^* &\leq \|\vec{\lambda}_{s\alpha\beta}\| & d\lambda &= -1 \end{aligned} \quad (2.153)$$

$$\begin{aligned} T_{em}^* &\geq T_{em} + \frac{\Delta T_{em}}{2} & dT &= +2 \\ T_{em} + \frac{\Delta T_{em}}{2} &> T_{em}^* > T_{em} + \frac{\Delta T_{em}}{4} & dT &= +1 \\ T_{em} + \frac{\Delta T_{em}}{4} &\geq T_{em}^* \geq T_{em} - \frac{\Delta T_{em}}{4} & dT &= 0 \\ T_{em} - \frac{\Delta T_{em}}{4} &< T_{em}^* < T_{em} - \frac{\Delta T_{em}}{2} & dT &= -1 \\ T_{em}^* &\leq T_{em} - \frac{\Delta T_{em}}{2} & dT &= -2 \end{aligned} \quad (2.154)$$

$$\begin{aligned} \omega_m &> \omega_{mth} & d\omega &= +1 \\ \omega_m &\leq \omega_{mth} & d\omega &= -1 \end{aligned} \quad (2.155)$$

being $d\lambda$, dT and $d\omega$ the outputs of the flux, torque and speed comparators, respectively.

The selection of the voltage vector to be applied in each sampling time is carried out through a look-up table (see Table 2.1) that contains all the virtual vectors that must be selected according to the three outputs of the controllers and the sector where the stator flux is currently located. The selected virtual vectors correspond to a certain combination of switching states that are directly applied to the VSI, without needing to apply a PWM modulation block.

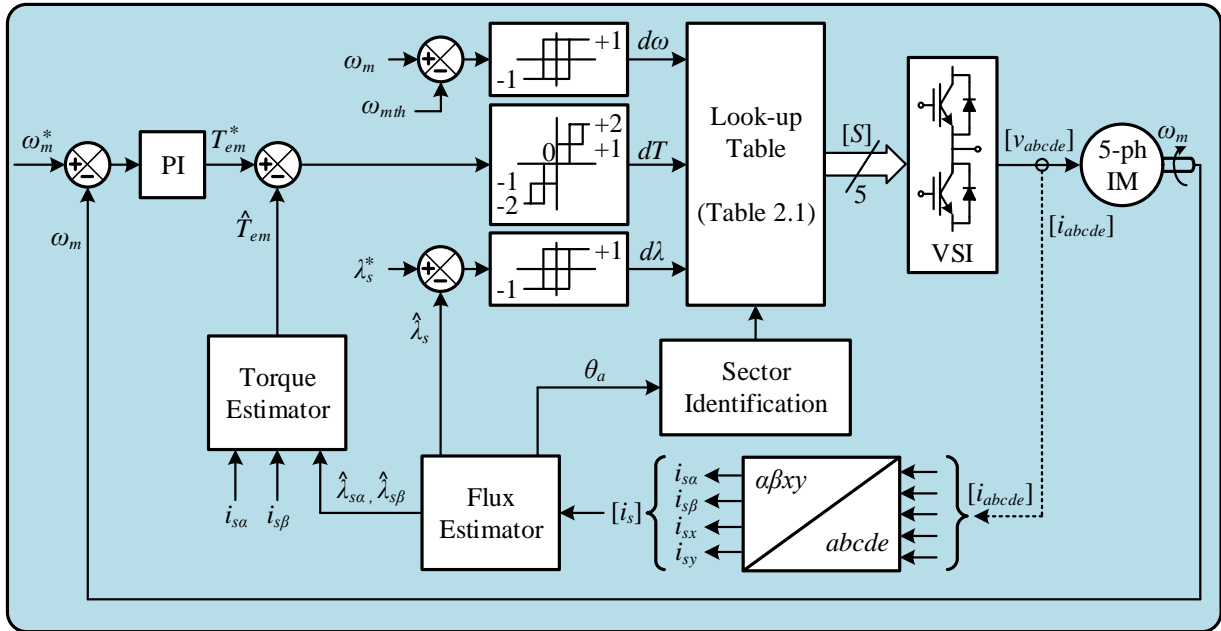


Figure 2.13. DTC scheme applied to a five-phase IM with distributed windings.

Table 2.1. Look-up table for the DTC controller

$d\lambda$	dT	$d\omega$	Position of stator flux (Sector)										
			1	2	3	4	5	6	7	8	9	10	
+1	+2	+1	VV _{L3}	VV _{L4}	VV _{L5}	VV _{L6}	VV _{L7}	VV _{L8}	VV _{L9}	VV _{L10}	VV _{L1}	VV _{L2}	
		-1	VV _{L2}	VV _{L3}	VV _{L4}	VV _{L5}	VV _{L6}	VV _{L7}	VV _{L8}	VV _{L9}	VV _{L10}	VV _{L1}	
	+1	+1	VV _{S3}	VV _{S4}	VV _{S5}	VV _{S6}	VV _{S7}	VV _{S8}	VV _{S9}	VV _{S10}	VV _{S1}	VV _{S2}	
		-1	VV _{S2}	VV _{S3}	VV _{S4}	VV _{S5}	VV _{S6}	VV _{S7}	VV _{S8}	VV _{S9}	VV _{S10}	VV _{S1}	
	0	+1	v ₀	v ₃₁	v ₀	v ₃₁	v ₀	v ₃₁	v ₀	v ₃₁	v ₀	v ₃₁	
		-1	v ₀	v ₃₁	v ₀	v ₃₁	v ₀	v ₃₁	v ₀	v ₃₁	v ₀	v ₃₁	
	-1	+1	VV _{S9}	VV _{S10}	VV _{S1}	VV _{S2}	VV _{S3}	VV _{S4}	VV _{S5}	VV _{S6}	VV _{S7}	VV _{S8}	
		-1	VV _{S10}	VV _{S1}	VV _{S2}	VV _{S3}	VV _{S4}	VV _{S5}	VV _{S6}	VV _{S7}	VV _{S8}	VV _{S9}	
	-2	+1	VV _{L9}	VV _{L10}	VV _{L1}	VV _{L2}	VV _{L3}	VV _{L4}	VV _{L5}	VV _{L6}	VV _{L7}	VV _{L8}	
		-1	VV _{L10}	VV _{L1}	VV _{L2}	VV _{L3}	VV _{L4}	VV _{L5}	VV _{L6}	VV _{L7}	VV _{L8}	VV _{L9}	
	-1	+2	+1	VV _{L4}	VV _{L5}	VV _{L6}	VV _{L7}	VV _{L8}	VV _{L9}	VV _{L10}	VV _{L1}	VV _{L2}	VV _{L3}
			-1	VV _{L5}	VV _{L6}	VV _{L7}	VV _{L8}	VV _{L9}	VV _{L10}	VV _{L1}	VV _{L2}	VV _{L3}	VV _{L4}
+1		+1	VV _{S4}	VV _{S5}	VV _{S6}	VV _{S7}	VV _{S8}	VV _{S9}	VV _{S10}	VV _{S1}	VV _{S2}	VV _{S3}	
		-1	VV _{S5}	VV _{S6}	VV _{S7}	VV _{S8}	VV _{S9}	VV _{S10}	VV _{S1}	VV _{S2}	VV _{S3}	VV _{S4}	
0		+1	v ₃₁	v ₀	v ₃₁	v ₀	v ₃₁	v ₀	v ₃₁	v ₀	v ₃₁	v ₀	
		-1	v ₃₁	v ₀	v ₃₁	v ₀	v ₃₁	v ₀	v ₃₁	v ₀	v ₃₁	v ₀	
-1		+1	VV _{S8}	VV _{S9}	VV _{S10}	VV _{S1}	VV _{S2}	VV _{S3}	VV _{S4}	VV _{S5}	VV _{S6}	VV _{S7}	
		-1	VV _{S7}	VV _{S8}	VV _{S9}	VV _{S10}	VV _{S1}	VV _{S2}	VV _{S3}	VV _{S4}	VV _{S5}	VV _{S6}	
-2		+1	VV _{L8}	VV _{L9}	VV _{L10}	VV _{L1}	VV _{L2}	VV _{L3}	VV _{L4}	VV _{L5}	VV _{L6}	VV _{L7}	
		-1	VV _{L7}	VV _{L8}	VV _{L9}	VV _{L10}	VV _{L1}	VV _{L2}	VV _{L3}	VV _{L4}	VV _{L5}	VV _{L6}	

2.3.3 Model-based Predictive Control

An alternative to DTC is the Predictive Control, which can be also considered as a direct control method. This technique was developed in the 70's and has recently found a wide variety of applications in the control of multiphase drives. This is due to its advantages, among which the conceptual simplicity and the flexibility of its schemes to include constraints or non-linearity in the control strategy are the most remarkable ones. However, its implementation requires a computational cost higher than that required by other traditional methods, at the same time as it is highly dependent on the model used. This last issue requires an exact knowledge of all the parameters that are used to model the controlled system. A classification of the different Predictive Control schemes used in electrical drives is presented in [103], where it is emphasized that the Model-based Predictive Control (MPC) schemes are the best adapted to the control of electrical drives.

MPC is based on an accurate model of the system that is used to predict the future behavior of the system variables through time, in order to select the optimal value of the control variables (the VSI switching states) by minimizing a cost function [103,104]. This technique can be divided in two wide categories as shown in Fig. 2.14, i.e. Continuous-Control-Set MPC (CCS-MPC) and Finite-Control-Set MPC (FCS-MPC), being the main differences between them the way in which the optimization is performed and how the control actions are applied. In CCS-MPC, an average model of the system is defined and controlled with the purpose of generating continuous reference signals, being necessary to include a modulator in order to obtain the required switching signals [103,104]. This will result in having a fixed switching frequency, making that this MPC technique in particular can be considered as an 'average control' technique. On the other hand, FCS-MPC takes advantage of the limited number of switching states available in the power converter for solving the optimization problem using a simple and easy iterative algorithm. Thus, the control objective represented by a cost function, which is usually composed by the errors between the reference and predicted values of the system variables, is evaluated at every sampling period and the switching state that ensures a lower cost function is selected to be directly applied during the next cycle.

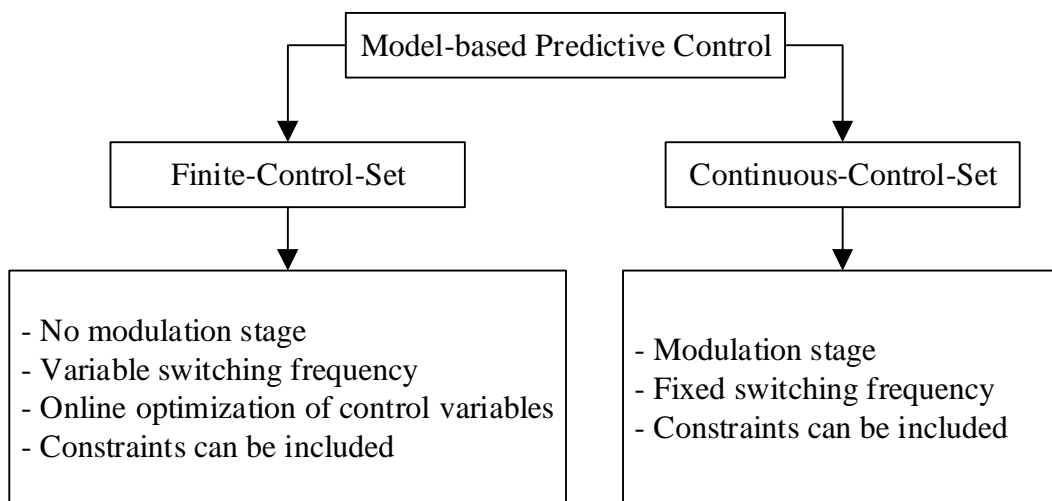


Figure 2.14. Model-based Predictive Control methods.

Many research works in the multiphase machine area are related to the FCS-MPC controller because of its formulation simplicity, inherent adaptation to power electronic circuits and its discrete nature [35,38,105–107]. Most of its applications are related to the current regulation, while only few works extend its utility to the flux and torque regulation [108–110]. Among the advantages of FCS-MPC, it can be noted its capability to include additional control objectives, such as commutation losses, common-mode voltages and low-order harmonics reduction [111]. Moreover, systems nonlinearities and different limits and constraints can be added at the same time, greatly increasing the flexibility and reach of this control strategy [112]. On the other hand, the main drawback is the high amount of calculations needed in order to solve the optimization problem online. Because of the required computational effort, its implementation has been for a long time restricted to slow systems. However, the revolutionary development of microprocessors and the advance in real-time solutions make now possible the implementation of MPC for fast systems with shorter time steps, becoming an established control technique in power electronics and electrical drives [104].

Different strategies have been carried out using the FCS-MPC method trying to mitigate the computational cost problem. In [35,105] a pseudo-optimal search criterion is used that allows to reduce the set of possible voltage vectors and, consequently, the computational cost, as well as to ensure a suitable switching frequency for the operation of the machine. Other schemes present modifications with respect to the one developed in [35], with the aim of minimizing the reference tracking error and the low-order harmonics that appear in the stator currents. Thus, in [36] a technique is developed that adds a modulation algorithm between the optimal vector [S_{opt}] and the zero vector [S_0] in order to reduce the tracking error with the reference current. The dwell times are determined by minimizing an error function where the contribution of each vector is linearly approximated. In all the above schemes, a subset of switching states was defined among all those available in the VSI. The technique presented in [39], called Restrained Search Predictive Control, avoids the discard of vectors. The selected vectors for the optimization process are defined during each sampling period, imposing restrictions on the total number of permissible commutations and preventing consecutive commutations in the same VSI leg in consecutive periods. The obtained results allow the reduction of the computational burden, as well as of the average switching frequency by limiting the number of commutations.

As mentioned before, the FCS-MPC technique is based on a mathematical model of the system to predict its future behavior. This model depends on the machine parameters, which are usually estimated using offline techniques [113,114]. However, parameters may not be precisely estimated or they can change during the operation of the system, being these changes rarely captured in the model. As a consequence, the parameters uncertainty may lead to inaccurate prediction of the system variables, deteriorating the performance and stability of the predictive algorithm. Recent research works deal with this problem, proposing new methods to improve the robustness of the Predictive Control [115,116]. Future trends can look for including parameters supervision and online model actualization to improve the stability and robustness of the controller.

Operating principle of FCS-MPC

In order to implement the FCS-MPC technique, the scheme presented in Fig. 2.15 is used, where the five-phase IM with distributed windings is considered as a case example. The control

action is obtained solving an optimization problem at each sampling period, where a discretized model of the real system, also called predictive model, is used to predict the system output. For this purpose, a forward Euler method is used, and the discretized model is applied to estimate the stator current values in the next sampling period $k + 1$, $[i_s^{k+1}]$, using the measured mechanical speed and stator currents in the instant k , ω_m^k and $[i_s^k]$, respectively. Once the prediction is done, the controller determines the next switch configuration $[S_{opt}^{k+1}]$ to be applied in the VSI in order to minimize a predefined cost function J . This cost function represents the control objective of the FCS-MPC method, being in the considered case the tracking of the reference currents, see equation (2.156). Notice that the reference value in the instant $k + 1$ is required and can be assumed equal to the value in the instant k since the sampling period T_s is enough small compared with the dynamic behaviour of the system. Therefore, the reference can be considered constant along T_s . Additionally, different cost functions can be used to include different control constraints (DC-link voltage balancing, switching stress minimization, common-mode voltage reduction, stator current harmonic minimization...) and depending on the specific application. For instance, a different cost function in order to reduce the VSI losses or the stator current harmonic content is proposed in [104], where weighting factors are also introduced to weight the control action between current tracking and losses reduction. This is one of the advantages of the FCS-MPC technique, a flexible control method where different constraints can be easily introduced without increasing the complexity of the algorithm. Finally, the applied switching state $[S_{opt}^{k+1}]$ is obtained through an exhaustive search process, where the predictive model is computed for every available switching state ($2^5 = 32$ for a five-phase machine) to find the future stator current that minimizes J . This process is detailed in the flow diagram shown in Fig. 2.16.

$$J = (i_{s\alpha}^{*k+1} - i_{s\alpha}^{k+1})^2 + (i_{s\beta}^{*k+1} - i_{s\beta}^{k+1})^2 + (i_{sx}^{*k+1} - i_{sx}^{k+1})^2 + (i_{sy}^{*k+1} - i_{sy}^{k+1})^2 \quad (2.156)$$

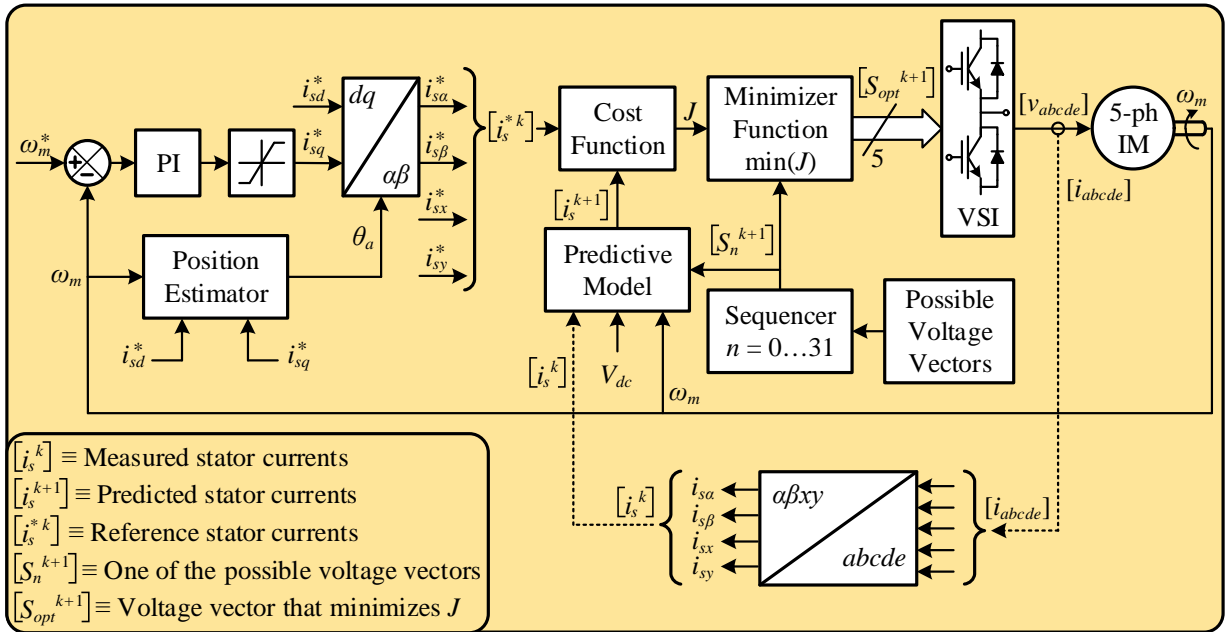


Figure 2.15. FCS-MPC control scheme.

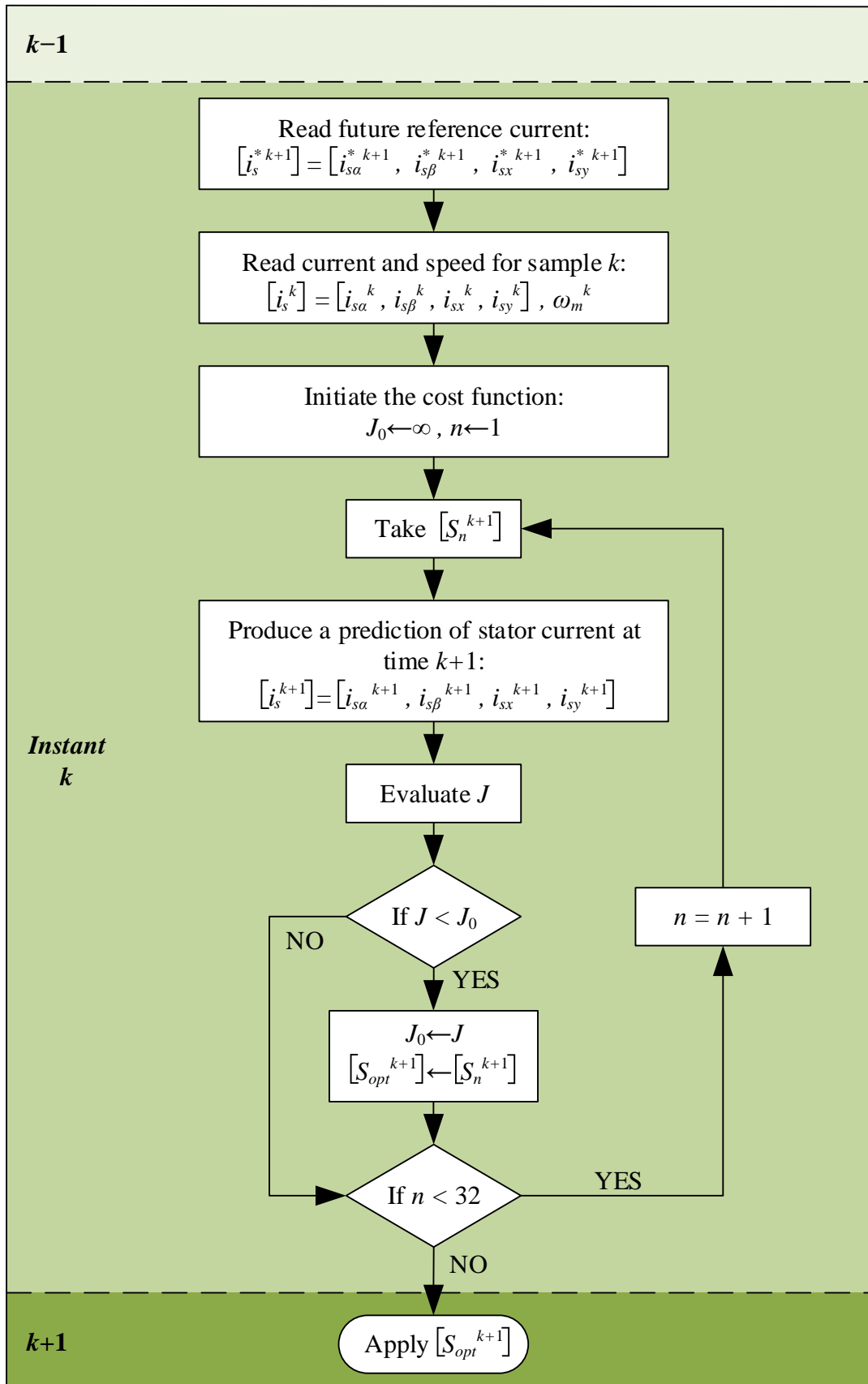


Figure 2.16. Flow diagram of the FCS-MPC method.

Notice that the ideal case where variables can be measured, predicted and controlled instantaneously at time k is not feasible in real-time applications. However, this problem can be solved if a two-step prediction is considered, where the control action is determined to be applied in the next sampling period $k + 1$. In this way, a complete sampling period T_s is available to develop the algorithm. Of course, the sampling period T_s must be higher than the sum of the measurement, calculation and control action times. On the other hand, the prediction horizon N_p can be defined as the number of future states in time that the controller predicts in order to select the most suitable control action [117]. The shortest prediction horizon can be defined as $N_p = 1$, where variables are measured in the instant k , while the optimum switching state is calculated for $k + 1$ and applied at $k + 1$. It has been demonstrated that larger prediction horizon results in better performance [118]. In this case ($N_p \geq 2$), the behavior of the electrical machine is predicted for future instants ($k + 2$, $k + 3$, ...), while the optimum VSI switching state is selected to be applied at time $k + 1$ (see Fig. 2.17). However, the increase in the prediction horizon results in higher computational cost, making difficult the real-time implementation of the method in low- and medium-power drive applications [119].

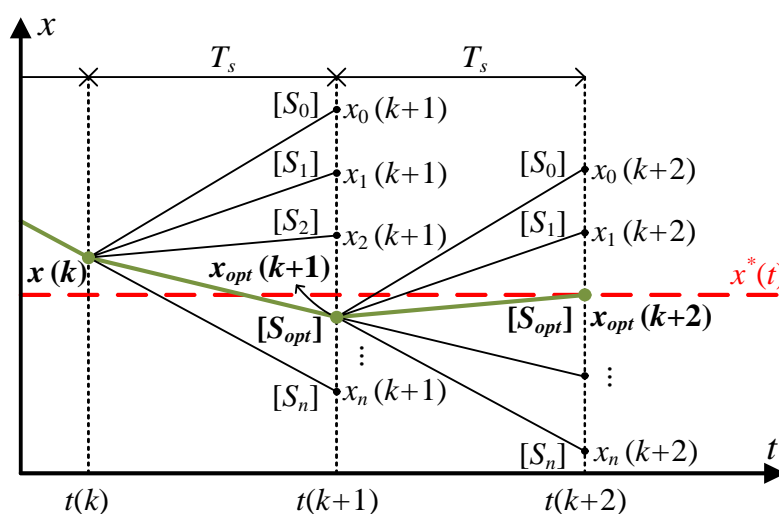


Figure 2.17. FCS-MPC prediction horizon principle.

In order to implement the FCS-MPC in a Digital Signal Processor (DSP), the equations of the machine model must be represented in a discrete-time state-space form [108,120]. This is done in Appendix A for each case example analyzed in this Thesis.

2.4 Performance limits

The industrial demand of higher requirements in the peak torque and power density of modern motor drives is forcing a large increment in their reliability levels [121], introducing stringent controllers with the ability of managing failure mechanisms and critical electrical limits. The fault-tolerant capability is the property that enables the drive to continue operating properly in the event of a failure in one (or more) of its components, ensuring the speed or torque reference tracking.

On the other hand, the optimal control of modern power drives involves the consideration of electrical constraints in the regulator strategy, including voltage and current limits imposed by the power converter and the electrical machine or the magnetization level limit due to the iron core. This section presents the state of the art of the controllers used to face the different analysis conditions that will be studied in this Thesis, more specifically the tolerance to open-phase faults in the multiphase electrical machine and the inclusion of electrical limits in the control strategy.

2.4.1 Tolerance to open-phase faults

In the case of conventional three-phase electrical drives, fault tolerance is only possible if extra equipment or some redundancy are available [121]. Conversely, in multiphase drives, fault tolerance is an inherent characteristic due to the higher number of phases they possess, without the need of using extra equipment. In other words, fault tolerance is obtained through an adequate post-fault control strategy, which is possible thanks to the extra degrees of freedom that multiphase systems present. From the point of view of safety, this inherent capacity is specially appreciated in aerospace and traction applications [122–124], where reliability is a fundamental aspect. In addition, there are applications where the post-fault operation provides an economical benefit, as in the case of offshore wind farms, where corrective maintenance may be delayed depending on the weather conditions [125].

The term ‘fault tolerance’ in multiphase drives is broad since the fault may occur in any of the elements of the system, including both VSI and machine faults that may lead to short-circuit (phase [126], VSI switch [127], interturn [128]) or open-circuit (phase [129], VSI switch [130], or line [131]) faults. Figure 2.18 shows a schematic with several fault possibilities in the case of a five-phase machine, either induction or permanent magnet, supplied by a five-leg two-level VSI. Note the large number of types of electrical faults that can occur in the system, being short-circuit and open-circuit faults the most common ones. However, the most widely studied case in the literature in recent years is the fault tolerance against open-phase faults, whose recent progresses are studied in this section.

On the other hand, the management of a fault is mainly composed of three stages, namely: fault detection, fault isolation and post-fault control implementation. Both fault detection and isolation techniques have been developed based on the specific characteristics of the system. In principle, the well-known detection techniques for conventional three-phase drives are applicable to multiphase systems. It is possible, however, to use the extra degrees of freedom to design new fault detection methods. For example, the components of the secondary plane allow to detect and locate the affected phase [132–134]. Once the fault has been detected and isolated, it is necessary to implement an adequate post-fault control strategy that guarantees the correct tracking of the reference currents values. Note that the study of the fault detection and isolation is out of scope of this Thesis, focusing in the development of post-fault control strategies. In order to develop this new control technique and ensure the proper operation of the system after the fault, it is necessary to establish new limits and reference current values, limiting the operating range of the system, as well as to reconfigure its model. These actions are analyzed in the following sections.

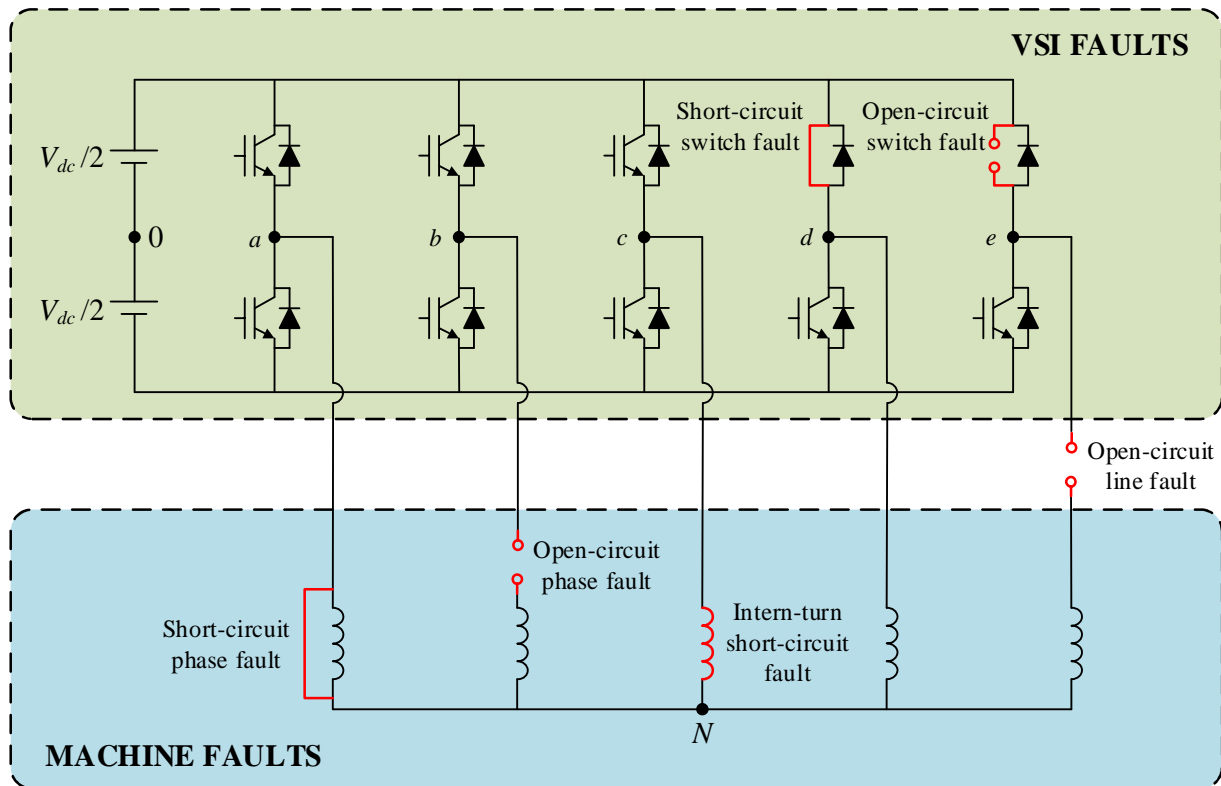


Figure 2.18. Schematic of different types of faults in a five-phase drive.

Current limits in open-phase fault operation

The post-fault operation in multiphase drives is only possible under certain operating limits, since the integrity of the healthy parts must be safeguarded. When the system operates in pre-fault situation, all stator currents in steady state have the same RMS values and their limit is defined by the rated value of the drive. However, after the loss of one or more phases due to an open-phase fault, the waveform and RMS values of stator currents can be heterogeneous, while the limit that they can reach is undefined. It is necessary, therefore, to establish the maximum allowed value of the currents in the post-fault situation. If no current limit is set, the pre-fault rated torque can be achieved after the fault. However, since the number of phases is lower and they are asymmetrically distributed, the rated value of the currents can be exceeded, with the consequent risk for the system integrity. Therefore, the drive could be damaged by causing an excessive thermal stress in the electrical machine or by exceeding the rated current values of the semiconductors. There are different criteria in the literature when establishing the limits of post-fault currents:

1. Limiting the currents to the nominal RMS value as in pre-fault situation, allowing to safeguard the health of the system, but lowering the amount of torque/speed available for post-fault operation [135,136]. This procedure is termed *approach 1* in what follows.
2. Allowing phase currents to exceed the RMS pre-fault value (within the electrical limits of the drive), but maintaining the same pre-fault copper losses [129,137]. This second procedure is termed *approach 2* from now on.

Approach 1 is clearly on the safe side since device ratings are not surpassed and the thermal stress is reduced after the fault. On the contrary, *approach 2* is less conservative and does not

guarantee that the thermal stress in every location of the electrical machine is not increased in post-fault operation. The adoption of one or another criterion will be done according to the needs of the application and the characteristics of the system.

Optimal reference currents in open-phase fault operation

In addition to the adoption of a criterion that sets the maximum value of the currents, their reference values must be recalculated to avoid an undesired behavior in the system. The new reference values will be established by the type of fault, as well as by the characteristics of the electrical drive used. If the open-phase fault is analyzed, the heterogeneity caused by the fault generates a higher torque ripple if the same pre-fault references are maintained [138–140]. Regardless of the adopted post-fault control strategy and the type of machine, there are some common features of the post-fault reference current calculation:

- The remaining healthy currents must generate a rotating magnetomotive force (MMF) in the air gap that describes a circular path and cancels the electromagnetic torque ripple.
- The sum of the currents must be zero if the machine is star-connected with isolated neutral point.
- Healthy currents present symmetry with respect to the location of the faulty phases.

The most used post-fault strategies to define the new reference currents are described down below, as well as their interaction with the selected criterion to set the maximum value of the currents:

1. Minimum copper loss (MCL) criterion [131,141]. Given a certain reference torque, the model of the machine is used to calculate the current values that generate the desired torque and, at the same time, produce the minimum copper losses. This criterion does not restrict the maximum RMS value of the currents, so a risk situation due to thermal damage can be generated if such value is not limited by any of the criteria described in the previous section. This option typically results in unequal RMS phase currents.
2. Maximum torque (MT) criterion [131,135,142]. Reference currents are calculated to provide the reference torque on average, but the fundamental components of phase currents are forced to have equal magnitudes. As in the MCL criterion, it is necessary to set a maximum admissible value for the phase currents.

For example, if the MCL criterion is adopted together with *approach 2* from the previous section, current peaks that cause magnetic saturation and hot spots in the machine can occur. Alternatively, the choice of the MCL criterion together with *approach 1* implies a heterogeneous distribution of the phase currents that reduces the torque production. In the case of selecting *approach 1* for the MT strategy, the torque production will be higher and it will help to avoid the magnetic saturation of the core.

The application of these criteria presents significantly different results when the reference currents are sinusoidal [136,138,140,143,144] and when higher order current harmonics are present [131,135,141,142,145,146].

In the case of IM drives with distributed windings and neglecting the spatial harmonics, in other words, with sinusoidal reference currents, it is usual to calculate the α - β reference currents

in order to generate the desired rotating MMF. These α - β currents can follow a circular [136,140,144] or ellipsoidal [138,143] trajectory, depending on the transformation matrix used, but in all cases the machine is driven with a rotating MMF as before the fault. Meanwhile, x - y reference currents are set according to the open-circuit restriction and the selected post-fault criterion (MCL or MT). When spatial harmonics cannot be neglected, the current harmonics become torque-related and the x - y current components under either MCL or MT criteria generate low frequency torque pulsations. To overcome this problem, in [144] it is suggested that x - y components follow a circular trajectory, although higher copper losses and lower torque production are found.

The injection of current harmonics in post-fault situation presents an additional complexity and has become one of the focus of scientific interest when optimizing the stator current waveforms in permanent magnet machines. Both MCL and MT criteria have been considered in the literature [131,135,141,147], with either one or two open-phase faults. Online and offline procedures have been proposed to calculate the reference currents, based on scalar and vector methods, obtaining similar results [141,148].

Modeling and control techniques in open-phase fault operation

When a fault occurs in the electrical drive, the physical model varies. The fault in the system causes that new restrictions must be added, as it has previously been exposed, being necessary to reconfigure the model and the controller of the system to adapt them to the new situation. Although it is possible to use the general phase variable model, the use of the VSD for control purposes is well recognized and more usual. The VSD is performed with the healthy model using the generalized Clarke transformation for n phases [C_n]. This decomposition splits currents and voltages in several subspaces that can be independently controlled. However, when the machine operates under an open-phase fault, these subspaces are no longer independent due to the loss of degrees of freedom caused by the fault. There are two possible procedures when this situation occurs: the VSD can be performed using the same transformation matrix [C_n] that was used in pre-fault situation [136,144,149] or using a new reduced-order transformation matrix [C_{n-m}], where m is the number of phases in open-circuit [140,143,145]. If the same transformation matrix is maintained as in pre-fault situation, the electrical and torque equations remain the same. Focusing on the current control, this choice minimizes the changes in the post-fault control scheme and maintains a circular trajectory in the α - β currents [136]. Conversely, if an orthogonal reduced-order transformation matrix is used, as in [138,143], a model with non-constant parameters is obtained, where the α - β currents describe an ellipsoidal trajectory but the number of voltage and current components is equal to the number of remaining degrees of freedom ($n - m$). Another option is presented in [130,140], where non-orthogonal reduced-order transformation matrices are used to obtain the same model that was obtained in pre-fault situation.

On the other hand, a common feature of the post-fault control schemes is the use of the RFOC method, with an outer PI speed controller that generates the reference torque. Nevertheless, there are different strategies regarding the inner current loops, as described below.

- *Hysteresis current control:*

Since the d - q reference currents are no longer constant in the rotating reference frame and possess an oscillating nature, a simple choice is to control currents in the natural reference system using hysteresis controllers with a high bandwidth [17,123,135,141,145,146,150,151]. These controllers are known to be susceptible to noise and generate a variable switching frequency.

- *Robust current control:*

The use of fuzzy logic and sliding mode current control in association with the RFOC method has been suggested in [143] and [152], respectively. The control is performed in the synchronous reference frame using the Park rotation matrix. Although a reduced-order transformation matrix [C_{n-m}] is used that alters the electrical parameters of the equations, the implementation of a robust control allows to cope with these variations.

- *Dual PI control:*

The standard control for electrical machine uses RFOC with PI controllers and PWM, therefore, a simple choice is to extend this scheme for the post-fault situation. Although a direct extension of the RFOC has been suggested in [138,149,153], the bandwidth of the PI controllers is not very wide, which may compromise the tracking of non-constant currents. For this reason, in [136,144,154] it has been proposed the use of resonant controllers, making possible the control of unbalanced reference currents. The α - β currents are controlled in the synchronous and asynchronous reference systems (using the Park transformation matrix and its inverse, respectively) to track positive and negative sequences. The use of the standard transformation matrix [C_n] makes the post-fault RFOC scheme very similar to that of pre-fault situation, while the use of resonant controllers helps to follow the non-circular behavior of the x - y components.

- *MPC:*

The MPC technique has recently been extended to post-fault situation in [140,155]. In contrast to other current controllers, it is necessary to know the voltage that supplies the system, so a reduced-order transformation matrix is preferred in this case. Since this technique is based on the model of the system, the oscillation of the neutral voltage needs to be directly addressed by the estimation of the back electromotive force (EMF) induced in the faulty phase. This control strategy is extended in [130], where the operation of the free-wheeling diode of the VSI is allowed, showing that this post-fault control is also applicable with minimum performance degradation.

2.4.2 Electrical limits in the control strategy

Regarding the inclusion of electrical limits in the control strategy, optimal control techniques have appeared as a viable candidate to this end [156,157]. Many algorithms have been so far proposed in the scientific literature based on this industrial requirement [158]. For instance, the switching frequency and the current control limit are considered in [159] to avoid an excessive temperature increment in the critical components of the system. Optimal d - q current control

vectors are estimated to maximize the drive's efficiency and speed-torque performance within the temperature and voltage constraints. The reference flux is also evaluated to guarantee the maximum torque capability over the entire speed range of induction [160–163] or permanent magnet [164,165] machines. More recently, different optimal controllers are presented and experimentally compared in [166], where permanent magnet synchronous motors are again considered. Most, if not all, of these scientific studies focus on conventional three-phase drives, where one d - q reference subspace appears and an analytical expression of the optimal reference stator current that respects the imposed constraints can be easily obtain. The machine flux is usually weakened (the d -current component is reduced) to respect the imposed voltage limit, adjusting at the same time the q -current component with the aim of not exceeding the current limit.

However, the situation becomes much more complex when a multiphase electromechanical drive is considered. Optimal controllers can enhance the benefits of using multiphase machines, but the appearance of multiple orthogonal d - q control subspaces involved in the torque production of the multiphase drive highly complicates the extraction of the maximum torque under electrical limits and constraints. The problem of applying an optimal controller in a multiphase drive is in relation with the difficulty to obtain analytical expressions for the electrical references in the orthogonal d - q sets from the electrical phase limits, where a dependency appears. In general terms, the peak value of the phase voltage (current) depends on the voltages (currents) in each d - q subspace, which are unrelated and of different frequencies, magnitudes and phase shifts. This dependency has recently been simplified using offline assumptions to force an analytical relation between the electrical references in the orthogonal d - q subspaces, obtaining a kind of suboptimal controller. This is the case in [167,168], where the worst-case scenario is considered, assuming that all d - q voltage (current) components reach their peak values at the same time instant. This in fact gives safety performance margins in the system, but the obtained results cannot be considered as optimal. An interesting alternative based on offline look-up tables appears in [112]. In this case, d - q reference currents are generated using a preliminary minimization technique that finds the minimum of a constrained nonlinear multivariable function. These values are then placed in reference tables to be used in the control strategy. A significant consequence is that steady-state reference values are found and used in look-up tables, and the defined controller has the ability of managing failure mechanisms and critical electrical limits.

A potential and never explored alternative for the definition of optimal regulators can be the use of model-based techniques, where a model of the real system is applied to estimate its future performance, for solving the optimization and control problems. It is noteworthy that MPC techniques have been widely used to solve control problems in electrical applications with power converters [169]. Different control objectives and/or constraints are easily included, and MPC has been proposed for controlling multiphase drives giving a high flexibility, as stated in Section 2.3.3. However, none of these proposals considers failure mechanisms or electrical limits for the drive in the control strategy. More recently, a simulation study states that optimal reference currents can be obtained using model-based methods [170], using then classical PI controllers to regulate the electric drive.

2.5 Review on graphical formalisms for control

This section is focused on a brief review concerning the tools developed for graphical representation of the models of systems, each with a particular purpose but all having a strong common point, i.e. to illustrate and to organize the model of a system in different interacting subsystems. In this sense, the Causal Ordering Graph and the Energetic Macroscopic Representation are graphical formalisms applied to the models of electromechanical systems that have been developed within the Control team of the L2EP laboratory, where this work is conducted.

From a general point of view, a system is composed of inputs and outputs, being its modeling an expression of its outputs from its inputs. Electromechanical systems can be decomposed into elementary interconnected subsystems that manage energy (dissipation, storage and transformation), being modeled using differential equations with state variables. These variables are associated with energy and are dependent on inputs and time according to the integral causality [171]. When inputs change, the state variables reach a different steady state after the transient period, which means that outputs are always consequence of inputs.

The Causal Ordering Graph (COG) is a graphical description that was introduced in 1996 to describe power electronics and electrical machines for developing their control [172,173]. It exclusively uses the integral causality, on the contrary of the well-known Bond Graph that authorizes the derivative causality [174]. Thanks to a strict respect of the integral causality, specific to any physical system, the COG formalism constitutes a simple and systematic method for description of systems, in order to prepare their control. In this way, the inversion of COG is the basis of the inversion-based control theory, yielding the control structure of the system with measurements and controllers. In this theory, the control structure is considered as an inversion of the causal path because the control has to define the appropriated inputs $u_{inv}(t)$ to be applied from the desired output $y_{ref}(t)$ (see Fig. 2.19).

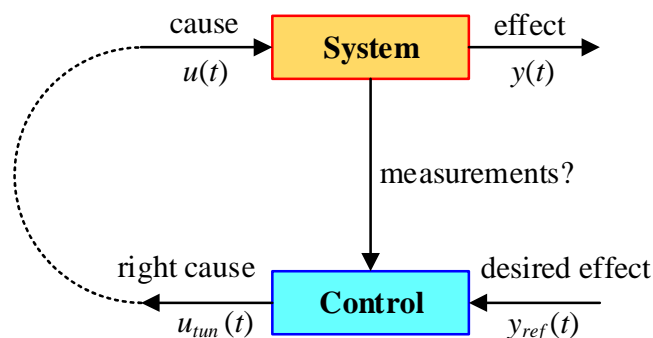


Figure 2.19. Inversion-based control principle.

On the other hand, the Energetic Macroscopic Representation (EMR) is a more macroscopic description for modeling and control of complex electromechanical systems. It is based on the action-reaction principle to organize the system as interconnected subsystems according to the integral causality. This description highlights energetic properties of the system (energy accumulation, conversion and distribution) and an inversion-based control can be also systematically deduced from EMR using inversion rules. EMR has been introduced in 2000 within

the L2EP laboratory for research development in complex electromechanical drives, especially multi-drives systems [175]. Since then, it has been applied to different applications, such as traction or wind energy conversion systems, among others [176–180].

Compared with other graphical description tools (such as Bond Graph or COG), EMR has a more global energetic view and it is perfectly adapted to the deduction of control structures of electromechanical systems with multiple inputs. This technique is focused not only on the system structure, but also on the system function. EMR gives insight into the real energy operation of the system and allows a deep understanding of its potentialities from a dynamic point of view. In short, the distinct features of EMR lie in its clarity of physical concepts, as well as its physical causality and its functional modeling rather than a structural modeling. It hence contributes significantly to the design of control and energy management of the system.

Considering the above, EMR can be effectively applied to the vector model of the VSI and multiphase machine assembly, with the aim of deducing its control structure. The development of this graphical representation for a five-phase PMSM and its subsequent inversion-based control are presented here as a case example of application. The system can be decomposed into several interconnected subsystems using four basic EMR elements (Fig. 2.20):

- Energy sources (green ovals) that are the terminals of the system, delivering and/or receiving energy.
- Accumulation elements (orange rectangles with diagonal line), which represent the energy storage and lead to state variables.
- Conversion elements (various orange pictograms), which convert energy without energy accumulation.
- Coupling elements (orange overlapped pictograms) for energy distribution.

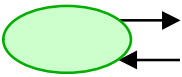
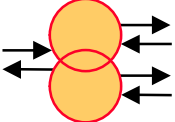
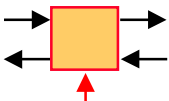
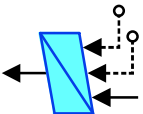
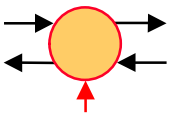
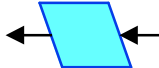
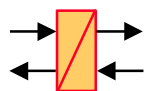
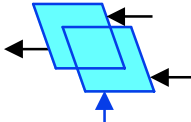
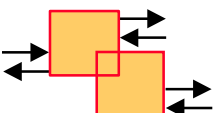

	Source element (energy source)		Multi-physical coupling element (energy distribution)
	Mono-physical conversion element		Indirect inversion (closed-loop control)
	Multi-physical conversion element		Direct inversion (open-loop control)
	Accumulation element (energy storage)		Coupling inversion (energy criteria)
	Mono-physical coupling element (energy distribution)		Strategy element

Figure 2.20. EMR pictograms.

Taking into account such methodology, the EMR structure of a five-phase PMSM is presented in Fig. 2.21. The DC bus is considered as an equivalent DC source that imposes the voltage on the VSI, which reacts by imposing the current I_{VSI} . The VSI is an electrical converter, which defines the voltage vectors v_s from the DC-link voltage V_{dc} , and currents i_s from machine currents, by acting on the switching states S . Note that this formalism allows to represent graphically the vector model of the drive, showing the decoupling subspaces that constitute the drive. In this way, EMR represent graphically the energy flows associated to each subspace, emphasizing the property of harmonics distribution. According to the Generalized Vectorial Formalism (GVF), the real multiphase machine can be considered as an equivalent set of several fictitious machines [1,2], associated with each frequency-domain subspace. Depending on the dimension of the specific subspace with which it is associated, the fictitious machine will be either single-phase or two-phase. For the considered case of a five-phase machine, there are:

- Two two-phase fictitious machines, called main machine (MM) and secondary machine (SM), related to the d_1-q_1 and d_3-q_3 subspaces, respectively.
- One single-phase fictitious machine, called homopolar machine (HM) and related to the z -component.

Then, the EMR structure of the five-phase PMSM is defined by two blocks for each fictitious machine: an accumulation element that represents the equivalent stator windings and an electromechanical conversion that yields the torque. Finally, the machine shaft is an accumulation element, which yields the rotation speed ω_m from the machine torque T_{em} and the load torque T_L .

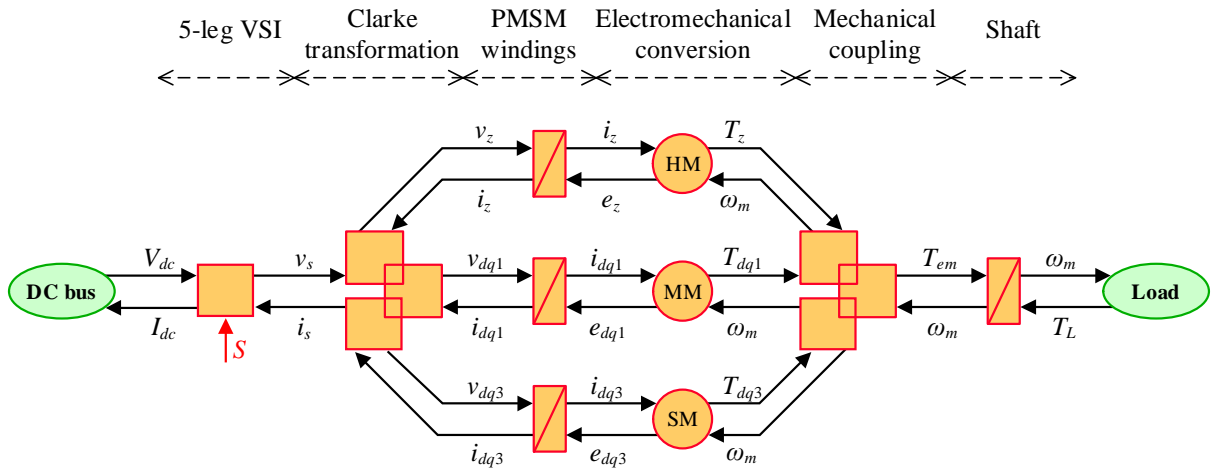


Figure 2.21. EMR for a five-phase PMSM.

EMR specifies all the causal relations of the multiphase machine. As a result, the control structure of the drive becomes more systematic by the inversion of the energy chain. In order to define the control structure, the inversion principle is applied to each subsystem defined by EMR. There are three basic inversion rules:

- Conversion elements are directly inverted. This inversion requires neither measurements nor controllers.
- Accumulation elements are inverted using a closed-loop controller.

- Inversions of coupling elements require input criteria, which lead to an organization of the energy distribution.

All control subsystems are depicted by blue parallelograms presented in Fig. 2.20 because they only handle information. Controllers contain an oblique bar inside (see Fig. 2.20). In this point, it is possible to differentiate between maximum control structure and practical control structure.

- *Maximum control structure:*

This control structure is obtained by means of a step-by-step inversion of the system decomposed into elementary subsystems. Such control structure is deduced through the following stages:

- Decomposition of the system into elementary subsystems.
- Determination of the tuning chain: from the tuning input to the global output to be controlled.
- Step-by-step inversion of the tuning chain using the previous inversion rules.

All variables are first considered as measurable. At this stage the control structure requires a maximum of controllers and sensors. For this reason, it is called maximum control structure. This control scheme is composed of cascaded loops, which enable limitation of internal variables.

- *Practical control structure:*

The maximum control structure is not always adapted for a real-time implementation. More practical control structures can be deduced using the following stages:

- Simplifications of the control.
- Estimation of non-measurable variables.
- Finally, the controller can be tuned and the real-time implementation can be done.

For the case of the five-phase PMSM, the practical control scheme is shown in Fig. 2.22. The control structure is a simple and graphical way of defining the control of the electrical drive. The classical FOC technique is used as example, with an outer speed and inner current controllers. Note that, as some variables are non-measurable, estimations are required. They are generally estimated using the relationships obtained through the model. For example, the estimation of the $d-q$ currents and the back EMF terms are obtained from the measurement of the present phase currents and the speed (see pink pictograms in the middle part of Fig. 2.22).

Despite the interest of this tool to help in the development of the control structure of multiphase machines, its implementation in this Thesis is out of scope. The application of EMR would be very useful if new control structures had to be designed, but this is not the case since well-presented and already defined control techniques will be considered along this Thesis. Remember that the focus of this work is the study of direct control techniques (DTC and MPC as maximum representatives) to face different limit situations. Then, the use of EMR is not necessary. Note also that the application of EMR to these techniques has already been considered in other research works, for example to DTC in [181].

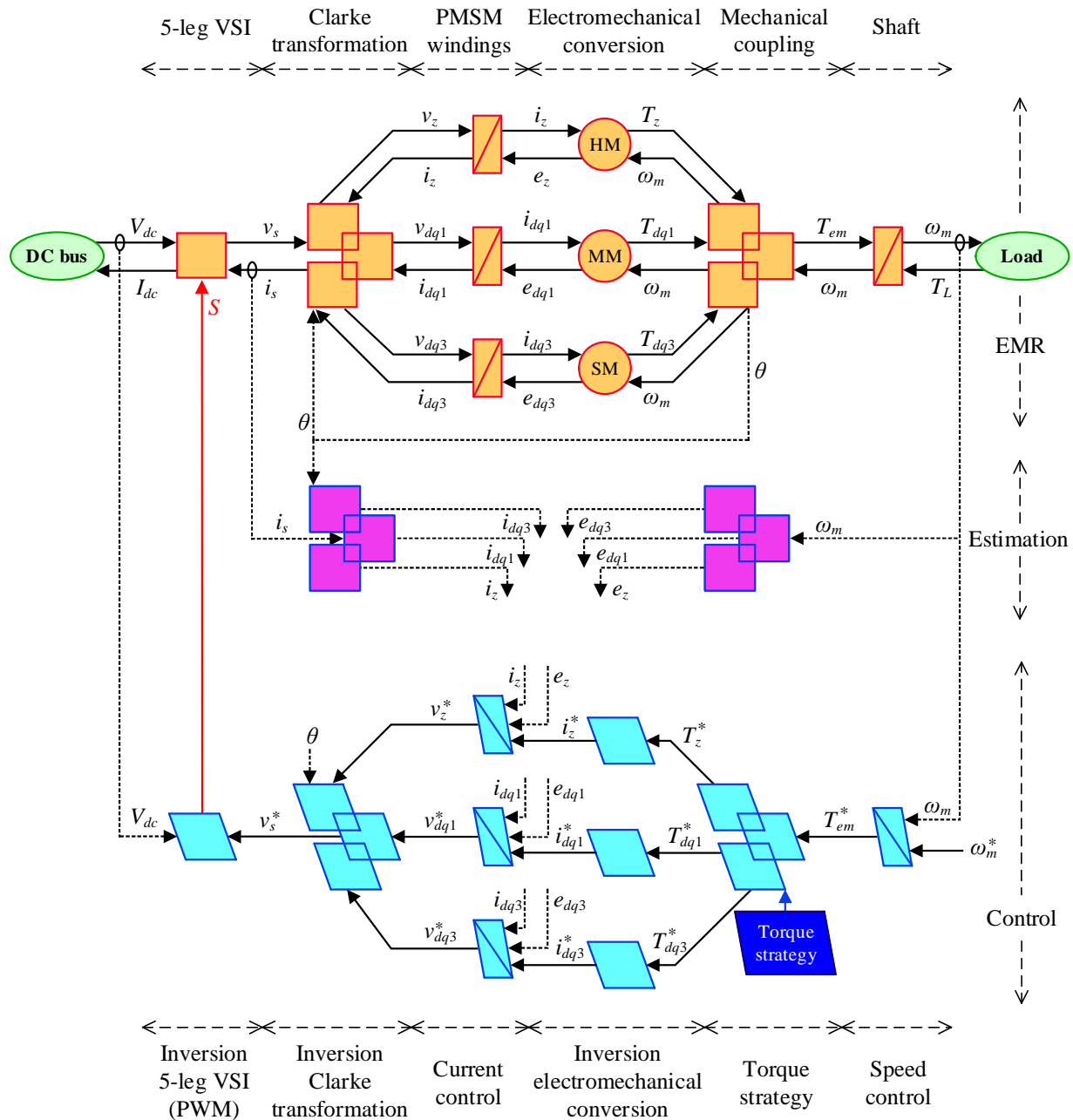


Figure 2.22. Practical control scheme for a five-phase PMSM.

2.6 Chapter conclusions

In this chapter, the basic concepts of multiphase drives have been presented, showing that these machines possess a number of benefits that makes them ideal to be an alternative to conventional three-phase drives in certain applications, where the number of phases results not only in better performance but also in higher reliability. Different types of multiphase machines were presented, taking special attention on symmetrical five-phase machines (permanent magnet and distributed/concentrated winding induction machines), used as case examples throughout this work and whose mathematical models were extensively analyzed in phase variables and in

stationary/rotating reference frames. Traditional control techniques were presented showing the evolution from the three-phase case to their implementation in the multiphase field. Specifically, the studied techniques were FOC, DTC and MPC. Although this Thesis work focuses on DTC and MPC as control strategies, it seems interesting to highlight their characteristics and operation mode with respect to FOC, since it is the control strategy used par excellence in the vast majority of electromechanical drives for industrial applications. In addition, different graphical formalisms for multiphase drives have also been studied in this chapter, putting a greater emphasis on the EMR structure.

Even though multiphase machines have been very studied in recent years, the state of maturity of this type of drives in what concerns the exploitation of its advantages has not yet been reached. In this regard, special interest should be given to the fault tolerance that, despite being one of the advantages that most supports the use of multiphase drives over conventional three-phase ones, has been poorly studied if it is compared with the healthy case. This Thesis tries to advance in the study and implementation of different post-fault control strategies that allow to improve the fault tolerance of multiphase electrical drives in variable speed applications. In Chapter 3, the DTC technique is proposed to manage the open-phase fault operation of the multiphase machine and its performance is compared with different state-of-the-art methods. Since DTC has as main characteristic the regulation of only two control variables (flux and torque) and has come to be considered as an alternative in the conventional three-phase case to FOC, it seems appropriate to face its study in cases in which the number of degrees of freedom of the multiphase system is similar to that of the three-phase system.

On the other hand, in relation with the obtainment of an optimal technique that includes the limits in the control strategy, this Thesis goes beyond the mentioned proposals in Section 2.4.2 to increase the torque performance of the electrical drive. In this case, DTC loses the interest as a regulation method since these limit conditions cause an increase in the number of variables and degrees of freedom to be controlled. Model-based techniques are then applied in this work to solve the optimization and control problems. A novel MPC regulator is consequently introduced in order to *i*) generate online optimal reference currents considering current, voltage and magnetization level limits, *ii*) extract the maximum torque of the machine, and *iii*) guarantee the closed-loop performance of the system (current tracking). Such controller generates online optimal reference currents by means of a MPC stage that respects the imposed electrical constraints. Then, a control stage based on the FCS-MPC technique is applied for the current regulation. This contribution will be further analyzed in Chapter 4.

Chapter 3

Controller with one Frequency-Domain Subspace: The DTC Case

This chapter is focused on the use of DTC to study the tolerance to the open-phase operation of the multiphase drive. The fault-tolerant capability of multiphase drives is an interesting intrinsic advantage for safety-critical applications, where recent research has demonstrated the effectiveness of FOC schemes to perform ripple-free post-fault operation. DTC has been widely used as an alternative to traditional FOC methods for three-phase drives. Despite this technique may not be seen as a competitor in the multiphase field because it is based on the ability to regulate only two degrees of freedom (flux and torque in the machine), the conventional DTC scheme has also been extended to multiphase drives in recent times, using hysteresis regulators to independently track the desired torque and flux in symmetrical five-phase IM drives. Applying this method, the control cannot focus on more than one frequency-domain subspace (α - β plane normally). Any action in the x - y subspace must be an open-loop current regulation, in order to limit undesired harmonics if a distributed winding topology is considered, which is usually done by the definition of virtual voltage vectors that generate zero voltage in the non-controlled subspaces. However, no extension to manage the post-fault operation of the drive is found in the literature. When the number of degrees of freedom decreases due to the open-phase fault situation, the drawback of using DTC in multiphase drives may be mitigated, being interesting to study this technique under these circumstances.

This chapter will assess the first obtained results in the Thesis, where a novel fault-tolerant DTC scheme is presented using a five-phase distributed winding IM as a case example. The modeling of the system is analyzed in **Section 3.1**, showing the effect of the open-phase fault occurrence in the physical system. The DTC method applied during the faulty operation of the machine is described in **Section 3.2**, studying the necessities of the controller to manage the new operating situation. Some preliminary simulation results based on a MATLAB[®] & Simulink[®] environment are presented in **Section 3.3**, where the ability of the modified DTC technique managing the post-fault operation of the multiphase drives is studied. The performance of the proposed method is also experimentally validated in a real test rig based on a five-phase distributed winding IM drive considering an open-phase fault condition, with the aim of verifying the preliminary analysis. **Section 3.4** provides different tests that analyze steady and transient states, including the transition from pre- to post-fault operation. Obtained results prove the interest of the proposal, which ensures the open-phase fault-tolerant capability of DTC controlled five-phase IM

drives. The performance of DTC compared with other RFOC techniques based on proportional resonant regulators and MPC techniques is carried out in **Section 3.5** when an open-phase fault appears in the five-phase IM drive, providing both simulation and experimental results in order to conclude the strengths and weaknesses of the analyzed methods. This chapter ends with the most relevant conclusions in **Section 3.6**.

3.1 Modeling of an open-phase fault situation

The system under study in this initial part of the Thesis is based on a five-phase IM with a squirrel-cage rotor and symmetrically distributed stator windings (with a fixed spatial displacement of $\vartheta = 2\pi/5$ between windings). A simplified scheme of the drive is shown in Fig. 3.1, where the machine is powered by a five-leg two-level VSI. This type of machine can be modeled in a stationary reference frame with a set of voltage equilibrium equations obtained from the stator and rotor electromagnetic circuits. This model under healthy operation (i.e. operation without faults) was studied in Section 2.2.2. On the other hand, the model of the VSI was presented in Section 2.2.5.

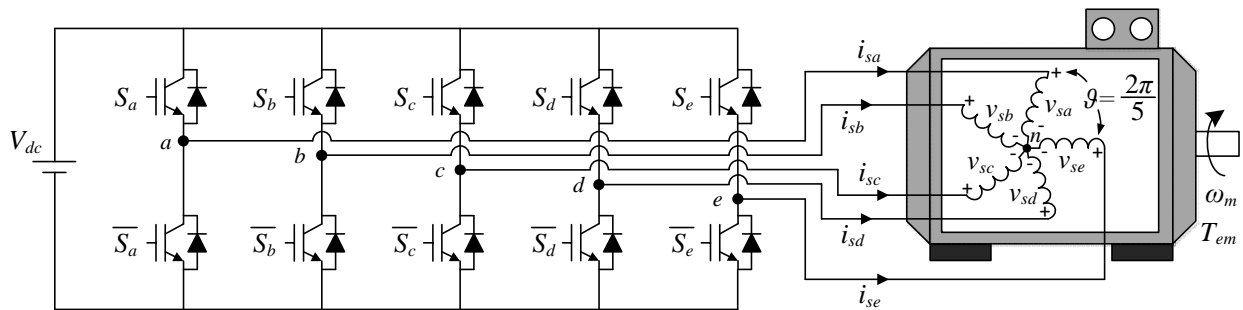


Figure 3.1. Schematic diagram of the five-phase IM drive.

Note that during the healthy operation of the multiphase drive, the equilibrium equation presented in (3.1) is verified. However, the machine becomes asymmetrical when an open-phase fault occurs and the sum of the remaining healthy stator phase voltages is no longer zero. Since the five-phase machine is symmetrical, the analysis when the fault appears can consider any faulty phase without lack of generality. Then, phase ‘a’ will be considered like the faulty phase from now on, being $i_{sa} = 0$. In any case, one degree of freedom is lost in the multiphase drive when the fault appears, and a fixed relationship between α - and x -current components is obtained, as it is stated in (3.2). It is then necessary to include the induced back EMF of the phase ‘a’, obtained from the neutral voltage evaluation [140], in the new equilibrium stator phase voltage equation (3.3), which is obtained from (2.136).

$$0 = v_{sa} + v_{sb} + v_{sc} + v_{sd} + v_{se} \quad (3.1)$$

$$i_{sa} = 0 = i_{s\alpha} + i_{sx} \Rightarrow i_{sx} = -i_{s\alpha} \quad (3.2)$$

$$\begin{bmatrix} v_{sb} \\ v_{sc} \\ v_{sd} \\ v_{se} \end{bmatrix} = \frac{V_{dc}}{4} \cdot \begin{bmatrix} 3 & -1 & -1 & -1 \\ -1 & 3 & -1 & -1 \\ -1 & -1 & 3 & -1 \\ -1 & -1 & -1 & 3 \end{bmatrix} \cdot \begin{bmatrix} S_b \\ S_c \\ S_d \\ S_e \end{bmatrix} - \frac{L_m \cdot \left(\frac{di_{s\alpha}}{dt} + \frac{di_{r\alpha}}{dt} \right)}{4} \cdot \begin{bmatrix} 1 \\ 1 \\ 1 \\ 1 \end{bmatrix} \quad (3.3)$$

Equation (3.3) links switching states and stator phase voltages of healthy phases, being the back EMF of the phase ‘a’ the second term on the right-hand side. This back EMF term can be neglected, as it is shown in [140], and will not be considered in what follows for the sake of simplicity. Stator/rotor impedance asymmetries of the machine appear during the fault operation that lead to non-circular trajectories of the stator currents in the α - β plane. The modified Clarke transformation matrix presented in [140] and shown in (3.4) can be used in the post-fault operation to compensate these asymmetries. Then, a symmetrical post-fault model of the machine is obtained, as well as circular trajectories of the stator currents in the α - β plane, and the same set of equations in α - β - x - y coordinates is generated in healthy and post-fault conditions. Consequently, the same model of the drive under healthy and fault conditions is used, which simplifies the treatment of the fault. However, the open-phase fault situation is characterized by four healthy phases, as it is stated in equations (3.5) and (3.6), while the number of switching states is reduced from $2^5 = 32$ to $2^4 = 16$.

$$[C_{POST}] = \frac{2}{5} \cdot \begin{bmatrix} \cos(\vartheta) - 1 & \cos(2\vartheta) - 1 & \cos(3\vartheta) - 1 & \cos(4\vartheta) - 1 \\ \sin(\vartheta) & \sin(2\vartheta) & \sin(3\vartheta) & \sin(4\vartheta) \\ \sin(2\vartheta) & \sin(4\vartheta) & \sin(6\vartheta) & \sin(8\vartheta) \\ 1 & 1 & 1 & 1 \end{bmatrix} \quad (3.4)$$

$$\begin{bmatrix} v_{s\alpha} & v_{s\beta} & v_{sy} & v_{sz} \end{bmatrix}^T = [C_{POST}] \cdot \begin{bmatrix} v_{sb} & v_{sc} & v_{sd} & v_{se} \end{bmatrix}^T \quad (3.5)$$

$$\begin{bmatrix} i_{s\alpha} & i_{s\beta} & i_{sy} & i_{sz} \end{bmatrix}^T = [C_{POST}] \cdot \begin{bmatrix} i_{sb} & i_{sc} & i_{sd} & i_{se} \end{bmatrix}^T \quad (3.6)$$

3.2 DTC scheme in open-phase fault operation

As stated before, traditional DTC methods have been successfully extended to five-phase drives, despite this technique is able to control only two degrees of freedom. Nevertheless, some advances have recently been achieved in the application of switching tables DTC techniques for the healthy operation of the drive [51,52]. This technique was presented in Section 2.3.2, where the scheme of the controller is detailed in Fig. 2.13. It is based on torque and flux hysteresis comparators, considering also the effect of neglecting the stator resistance at low speeds with a speed threshold called ω_{mth} (100 rpm in this case). Different virtual voltage vectors were defined in Fig. 2.12 for control purposes, as well as the look-up table to select the adequate vector every sampling time (see Table 2.1).

Some modifications must be applied when an open-phase fault occurs in order to ensure the post-fault operation of the multiphase drive. The overall aim must be the extension of the control

technique to the post-fault situation, where the fault reduces the number of controllable variables (only α -, β - and y -current components, while x -current component is found to be $i_{sx} = -i_{sy}$), being α - β and x - y subspaces no longer orthogonal. In this case, the proposed fault-tolerant DTC scheme is implemented applying a MCL-type criterion, which reduces copper losses in the faulty operation and is designed with the following considerations:

- New VV_i values are obtained to take into account that there are only 16 available voltage vectors in post-fault operation, as it is illustrated in Fig. 3.2.
- The additional degree of freedom (y -current component) is used to obtain zero average volts-per-seconds in the y direction during the post-fault operation of the drive. This should be equivalent to the MCL criterion assuming that machine asymmetries do not exist, because the stator current component in the y -axis (i_{sy}) will be low and close to zero [144,182,183]. The existence of some degree of asymmetry is then regarded as a non-modelled effect that may cause some disturbance in the current regulation.

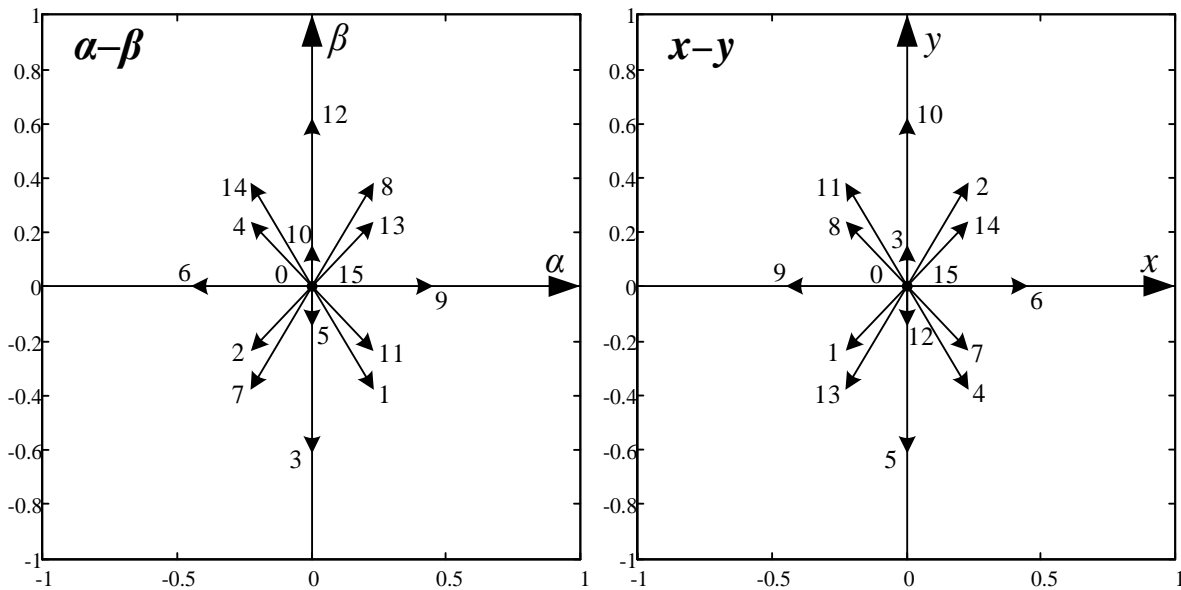


Figure 3.2. Available voltage vectors in the α - β (left plot) and x - y (right plot) planes in open-phase fault operation.

Eight sectors appear in the open-phase fault situation, which leads to eight VV_i in the α - β plane defined as:

$$VV_i = v_i \cdot K_{v1} + v_j \cdot K_{v2} \quad (3.7)$$

where v_i and v_j are two available voltage vectors (see Fig. 3.2), while K_{v1} and K_{v2} are the dwell time ratios that define VV_i with the condition $i_{sy} = 0$. Sectors 1 and 5 are exceptions and only use one vector since it does not produce voltage in the y direction. The obtained post-fault VV_i and sectors are depicted in Fig. 3.3, and the new obtained dwell time ratios are shown in Table 3.1. The look-up table that takes into account the open-phase fault situation is detailed in Table 3.2, where the applied stator voltage vector is the null voltage vector (v_0 or v_{15}) or VV_i , with $i = 1 \dots 8$.

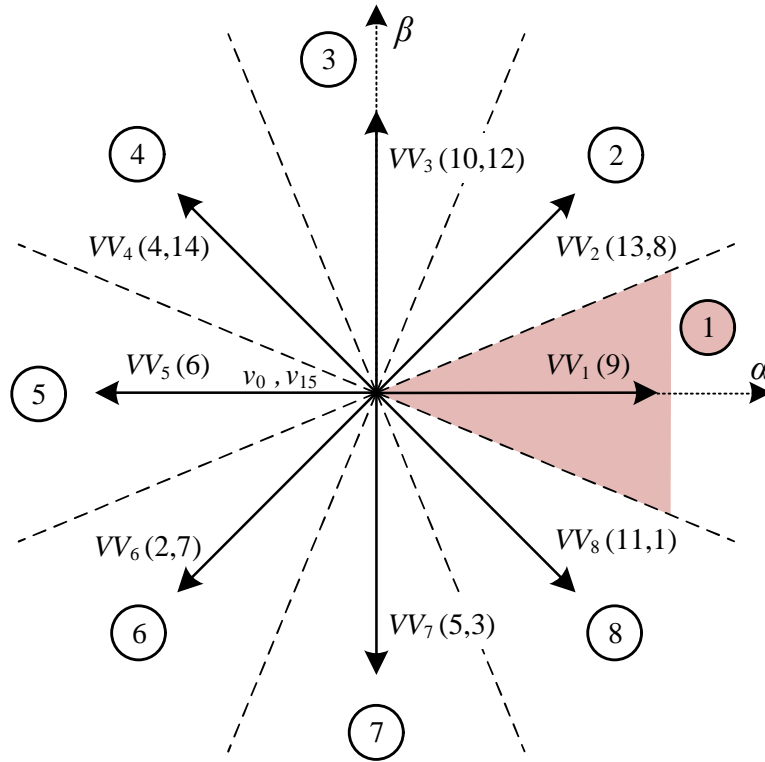

 Figure 3.3. Virtual voltage vectors (VV_i) in the α - β subspace during open-phase fault operation.

Table 3.1. Dwell times during the open-phase fault operation.

Dwell Time	Virtual voltage vectors							
	VV_1 (9)	VV_2 (13,8)	VV_3 (10,12)	VV_4 (4,14)	VV_5 (6)	VV_6 (2,7)	VV_7 (5,3)	VV_8 (11,1)
K_{v1}	1	0.382	0.191	0.382	1	0.382	0.191	0.382
K_{v2}	-	0.618	0.809	0.618	-	0.618	0.809	0.618

Table 3.2. Look-up table for the DTC controller in post-fault situation.

$d\lambda$	dT	Position of stator flux (Sector)							
		1	2	3	4	5	6	7	8
+1	+1	VV_2	VV_3	VV_4	VV_5	VV_6	VV_7	VV_8	VV_1
	-1	VV_8	VV_1	VV_2	VV_3	VV_4	VV_5	VV_6	VV_7
	0	v_0	v_{15}	v_0	v_{15}	v_0	v_{15}	v_0	v_{15}
-1	+1	VV_4	VV_5	VV_6	VV_7	VV_8	VV_1	VV_2	VV_3
	-1	VV_6	VV_7	VV_8	VV_1	VV_2	VV_3	VV_4	VV_5
	0	v_{15}	v_0	v_{15}	v_0	v_{15}	v_0	v_{15}	v_0

The post-fault DTC technique is detailed in Fig. 3.4. The controller includes an outer PI-based speed control loop and two inner torque and flux hysteresis regulators ($d\lambda$ and dT error signals). Notice that the low-speed region cannot be considered like in healthy case, because of the defined sectors and VV_i values. Finally, electrical torque and flux estimators (see Appendix B) are used to

currents. Then, electrical losses are minimized at the expense of unequal peaks of the phase currents, as it can be appreciated in Fig. 3.5b. Notice also that the α - β stator current vector describes a circular trajectory using the proposed DTC controller during the post-fault situation, being $i_{sx} = -i_{sa}$ and i_{sy} nearly null (see Fig. 3.5d).

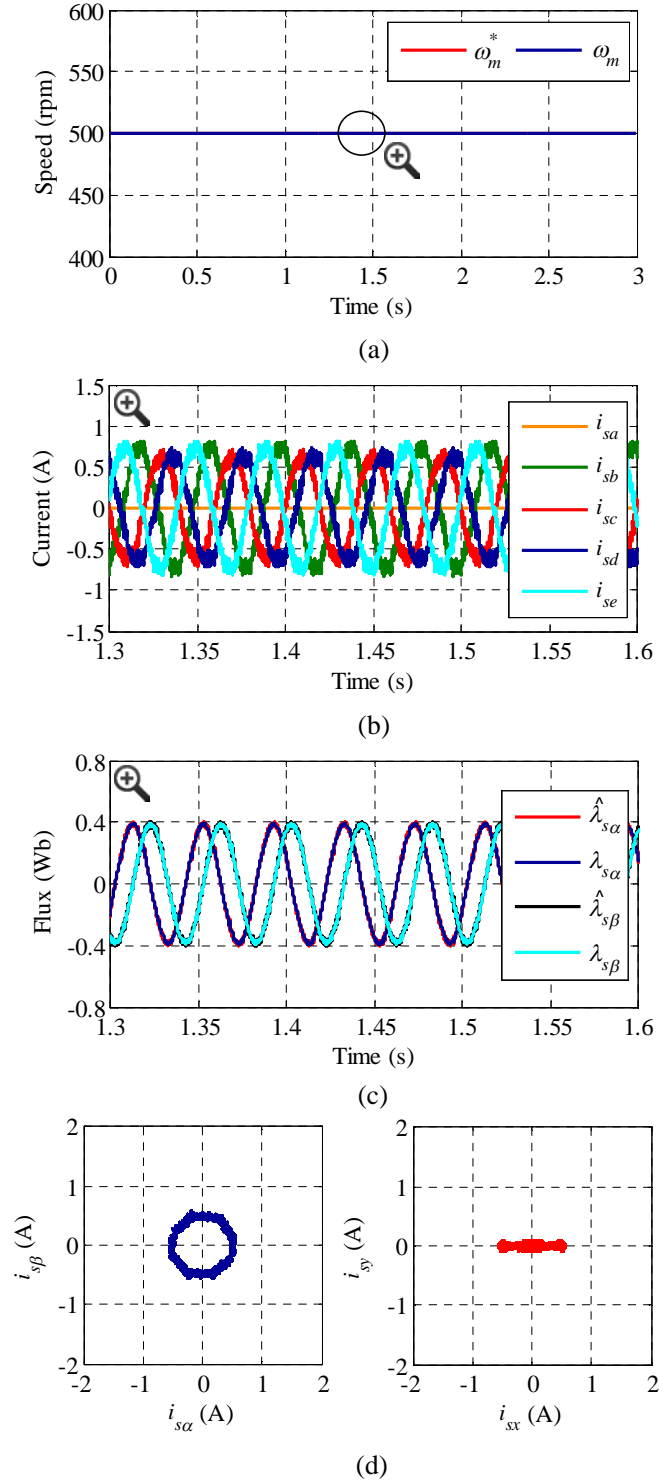


Figure 3.5. Simulation of the steady-state operation in post-fault mode of a 5-phase DW-IM drive. The reference speed is settled at 500 rpm. (a) Speed response. (b) Zoomed-in stator phase currents. (c) Zoom-in of the estimated and obtained stator flux waveforms. (d) Current trajectories in the α - β and x - y planes.

A reversal test has been performed during the post-fault operation of the drive and the reference speed has been changed from 500 to -500 rpm. The obtained results are shown in Fig. 3.6, where it can be seen an adequate performance of the motor speed using the DTC controller, Fig. 3.6a. The typical waveforms in the α - β plane of the stator phase currents and the stator flux are obtained during the zero-speed crossing operating point, see Fig. 3.6b and Fig. 3.6c, respectively.

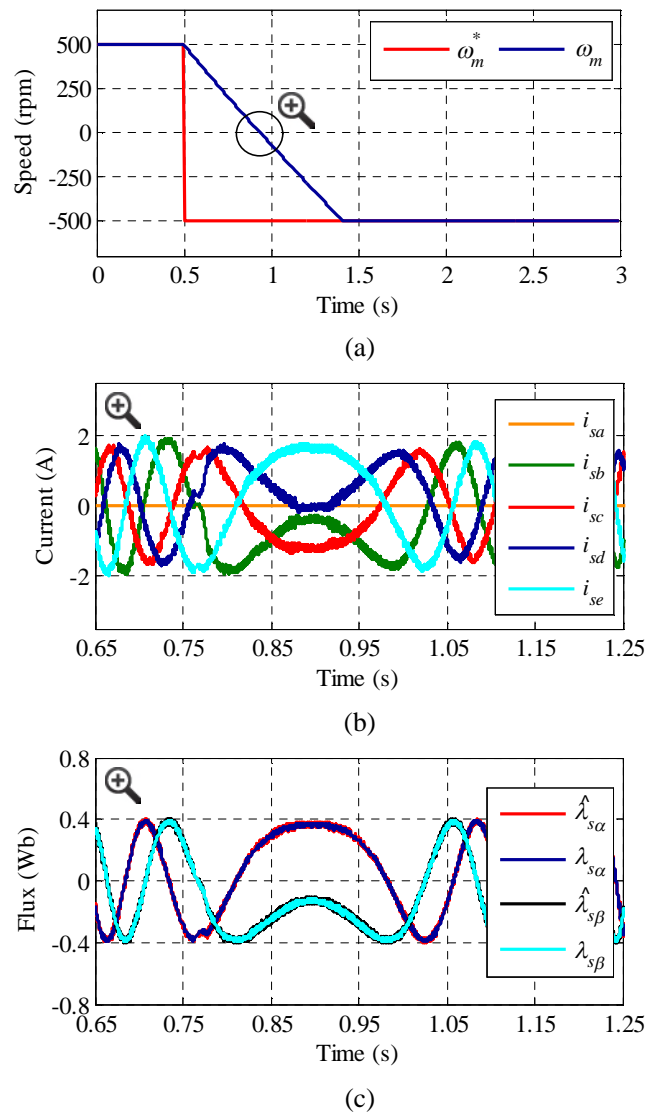


Figure 3.6. Simulation reversal test during the post-fault operation of a 5-phase DW-IM drive. A change in the reference speed from 500 to -500 rpm is applied. (a) Speed response. (b) Stator phase current and (c) stator flux waveforms in the α - β plane during the zero-speed crossing operating point.

The performance of the DTC controller when the fault appears is finally assessed. The reference speed is set to 500 rpm, as in previous tests. Figure 3.7 summarizes the obtained results from pre- to post-fault operation. The open-phase fault is simulated in phase ‘a’ at $t = 0.2$ s, and the fault detection delay is not considered during the test. Therefore, the transition between healthy and faulty models occurs as soon as the fault is generated. Figure 3.7a shows the speed response, where it can be observed that the transition is done without any impact on the motor speed, being

smoothly performed. Stator phase currents vary from healthy to faulty operation, as well as α - β stator currents, as plotted in Fig. 3.7b and Fig. 3.7c, respectively. When the fault appears and thanks to the proposed control strategy, the x -current component becomes sinusoidal ($i_{sx} = -i_{s\alpha}$) while the y -current component is nearly null, as it is observed in Fig. 3.7d.

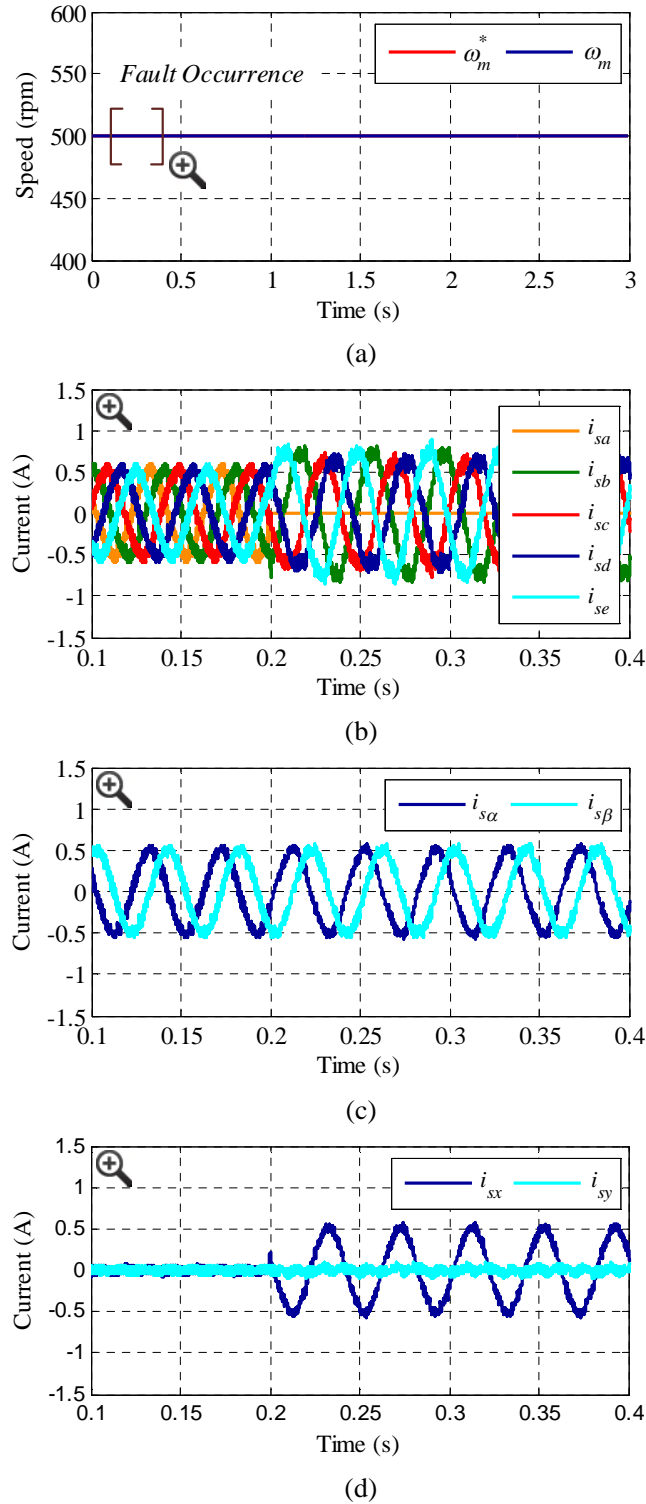


Figure 3.7. Simulation of the transition from pre- to post-fault operation of a 5-phase DW-IM drive. The fault appearance is at $t = 0.2$ s. (a) Speed response. Zoomed-in (b) phase, (c) α - β and (d) x - y currents before ($t < 0.2$ s) and after ($t > 0.2$ s) the fault occurrence.

3.4 Experimental validation in a real test rig

In order to prove the viability and assess the performance of the proposed fault-tolerant DTC scheme, different experimental tests have been performed on a three-phase IM rewound to have five phases with 30 slots and three pole pairs. This machine is available in the Electronic Engineering Laboratory of the University of Seville. The electrical and mechanical parameters of the five-phase IM are the same as the ones presented in the previous section (see Table C.1 in Appendix C). It is important to mention that during the following experimental tests the reference stator flux (λ_s^*) is set to 0.389 Wb, the applied sampling frequency is 10 kHz and the hysteresis bands of the torque and flux regulators are programmed to be at 1.06% and 1.29% of the rated values, respectively. On the other hand, the electrical machine is driven by two conventional three-phase VSIs from SEMIKRON (two SKS-22F modules where five over six power legs are used). The DC-link voltage is set to 300 V during all the experimental tests using an external DC power supply. The electronic control unit is based on a MSK28335 board and a Texas Instruments TMS320F28335 Digital Signal Processor (DSP). A digital encoder (GHM510296R/2500) and the enhanced quadrature encoder pulse peripheral of the DSP are used to measure the rotor mechanical speed ω_m . The load torque (T_L), which is demanded in the tests, is set by an independently controlled DC machine that is mechanically coupled to the five-phase machine. The experimental test rig is shown in Fig. 3.8, where some photographs of the system are included.

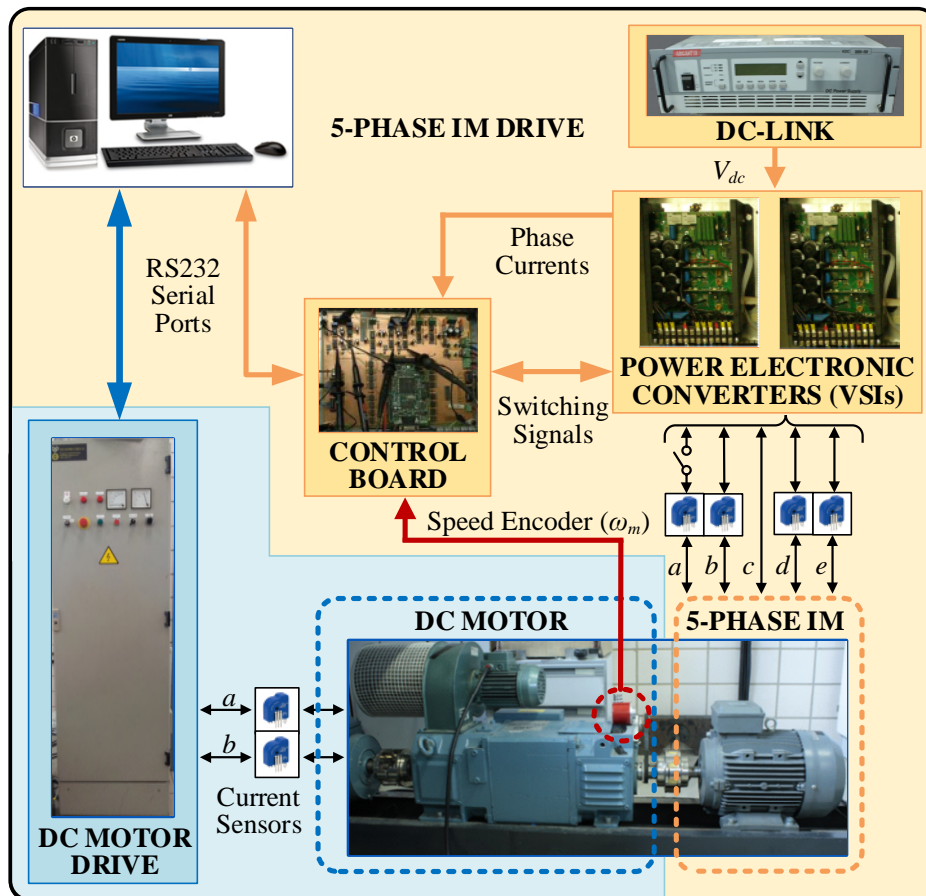


Figure 3.8. Graphical scheme of the experimental test rig based on a symmetrical five-phase distributed winding IM drive.

The behavior of the proposed DTC controller during the open-phase fault operation of the drive is firstly analyzed assuming a null load torque condition and forcing a step in the reference speed from 0 to 500 rpm that is applied at $t = 0.1$ s. Figure 3.9 shows the obtained results: the mechanical speed (upper plot), estimated electrical torque (middle figure) and stator flux (lower illustration) behaviors. It can be observed that the proposed post-fault DTC scheme provides an accurate tracking of the reference speed and electrical torque. The performance of the estimated stator flux is also shown in Fig. 3.9c, where a circle is obtained in the α - β plane polar diagram and the estimated stator flux vector has a controlled behavior in order to drive the multiphase system.

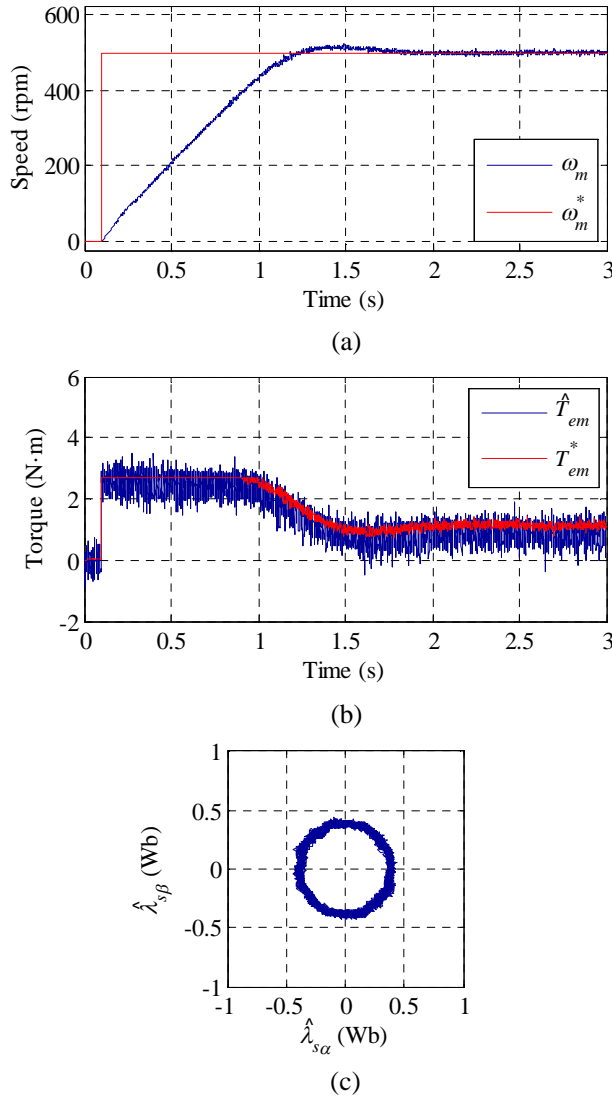


Figure 3.9. Experimental test of the speed step response for a 5-phase DW-IM drive. The reference speed is changed from 0 to 500 rpm at $t = 0.1$ s, while no load torque condition is assumed. (a) Speed response. (b) Estimated electrical torque. (c) Estimated stator flux in the α - β plane.

A reversal speed test is afterwards generated, where a change in the reference speed from 500 to -500 rpm is forced at $t = 0.2$ s, being the results shown in Fig. 3.10. The system is again operated in open-phase post-fault procedure, being null the load torque imposed by the DC machine. Appropriate tracking is again observed in the speed and the estimated electrical torque evolution,

as it can be seen in Figs. 3.10a and 3.10b, respectively, and the stator current performance in the α - β plane around the zero-speed crossing operating point is shown in detail in Fig. 3.10c.

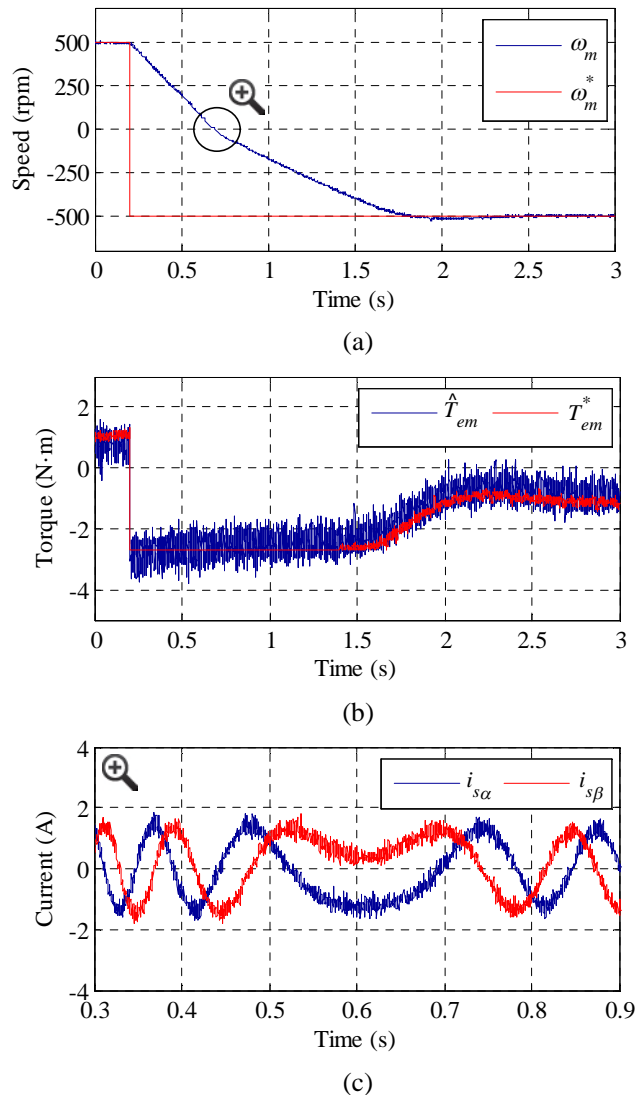


Figure 3.10. Experimental speed reversal test for a 5-phase DW-IM drive. The reference speed is changed from 500 to -500 rpm at 0.2 s. (a) Speed and (b) torque reference tracking. (c) Stator currents in the α - β plane at the zero-speed crossing point.

The rejection properties of the proposed DTC scheme are also studied when a change in the load torque is applied. The obtained results are summarized in Fig. 3.11, where the demanded load torque is varied while the reference speed is kept constant at 500 rpm. The DC machine is initially programmed to apply a zero load torque in opposition to the multiphase drive's electrical torque. Then, the load torque is forced to become about half of the nominal one ($T_L = 0.5 \cdot T_n$) at $t = 1.1$ s. It is observed a slight drop in the speed, although the controller successfully manages the disturbance, Fig. 3.11a. The estimated electrical torque is also regulated to be the referred one in steady and transient states, as it is shown in Fig. 3.11b, while stator currents in the α - β plane produce a circular trajectory in steady state with $T_L = 0$ and $T_L = 0.5 \cdot T_n$ conditions, as it is illustrated in left plots of Fig. 3.11c and Fig. 3.11d, respectively. This is the desired situation to

guarantee a controlled electrical torque in the multiphase drive. Flat lines are also observed in the x - y plane polar diagrams in steady state, see right drawings in Figs. 3.11c and 3.11d, which is in accordance with the applied post-fault MCL criterion where $i_{sx} = -i_{s\alpha}$ and i_{sy} should be regulated around a null reference value.

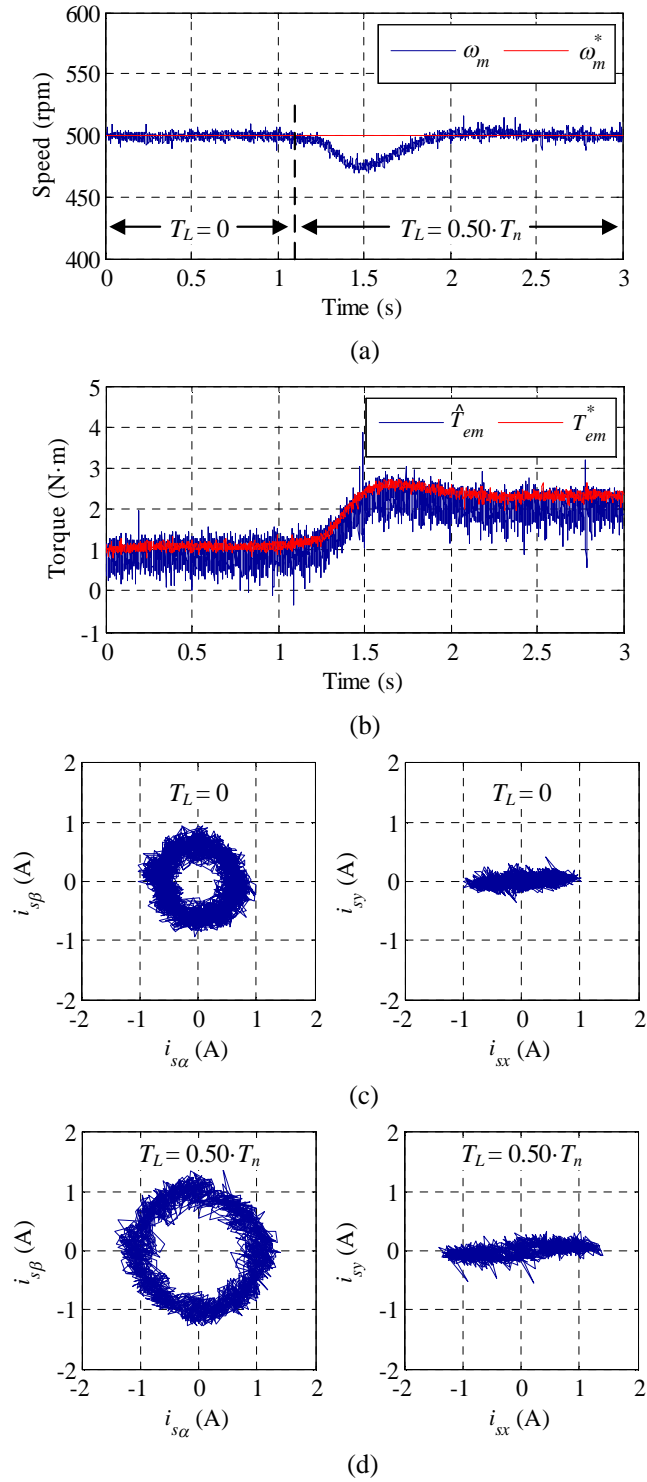


Figure 3.11. Experimental load torque rejection test for a 5-phase DW-IM drive. A change from 0 to 50% of the nominal load torque is applied at $t = 1.1$ s. (a) Speed response. (b) Estimated electrical torque behavior. Stator current performance in α - β and x - y planes in steady state with (c) null and (d) 50% of the nominal torque, respectively.

The transition between pre- and post-fault operation is analyzed in Fig. 3.12, where an open-phase fault is generated in phase ‘a’ at $t = 0.2$ s with a constant speed of 500 rpm and the system is instantaneously reconfigured. Left plots show the speed evolution while right figures display the estimated electrical torque response considering a demanded load torque of 28%, 50% and 70% of the nominal one in Figs. 3.12a, 3.12b and 3.12c, respectively. It is found that the fault occurrence does not affect the speed operation and the reference torque is accurately followed when the multiphase drive is working in the low load torque condition ($T_L = 0.28 \cdot T_n$), Fig. 3.12a. A quite similar situation (not exactly the same because a small deviation on the reference speed tracking is obtained just after the fault occurrence) is observed when the load torque is about 50% of the nominal one, Fig. 3.12b, which corresponds to the maximum controllable post-fault torque operation when the MCL post-fault control criterion is used. On the contrary, the proposed DTC scheme is not able to control the mechanical speed when the applied load torque exceeds the maximum controllable one in post-fault operation, as it is shown in Fig. 3.12c.

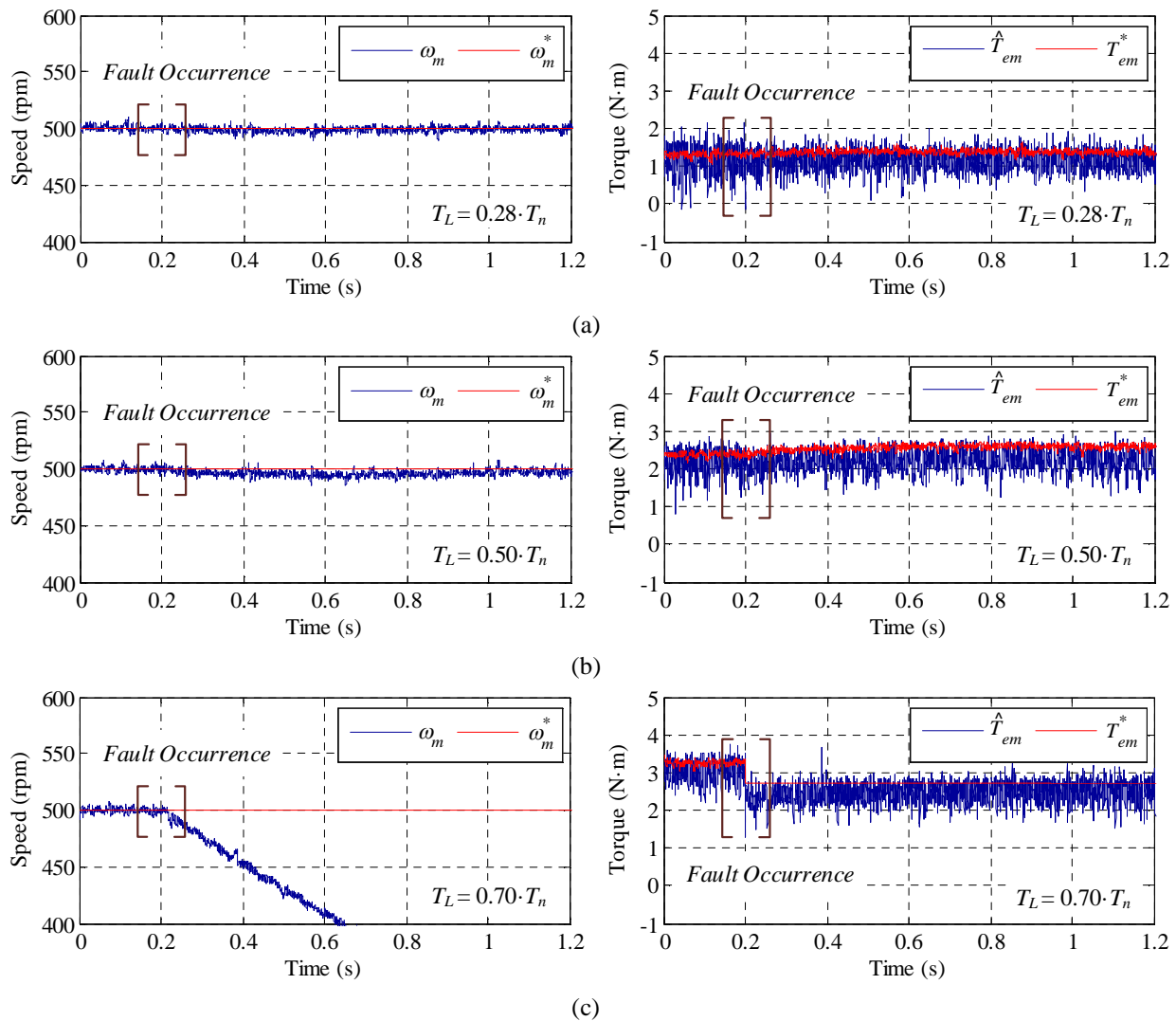


Figure 3.12. Experimental test of the transition from pre- to post-fault operation of a 5-phase DW-IM drive considering instantaneous control reconfiguration when the fault appears at $t = 0.2$ s. A reference speed of 500 rpm is assumed with an applied load torque of (a) 28%, (b) 50% and (c) 70% of the nominal one. The speed and estimated torque response is depicted in left and right plots, respectively.

The obtained healthy stator currents before and after the fault are shown in Fig. 3.13, where an increment in their magnitudes is noticed to compensate the open-phase fault situation; the magnitude of stator currents 'b' and 'e' are equal and larger than the magnitude of stator currents in phases 'c' and 'd', which is in accordance with the MCL criterion [182].

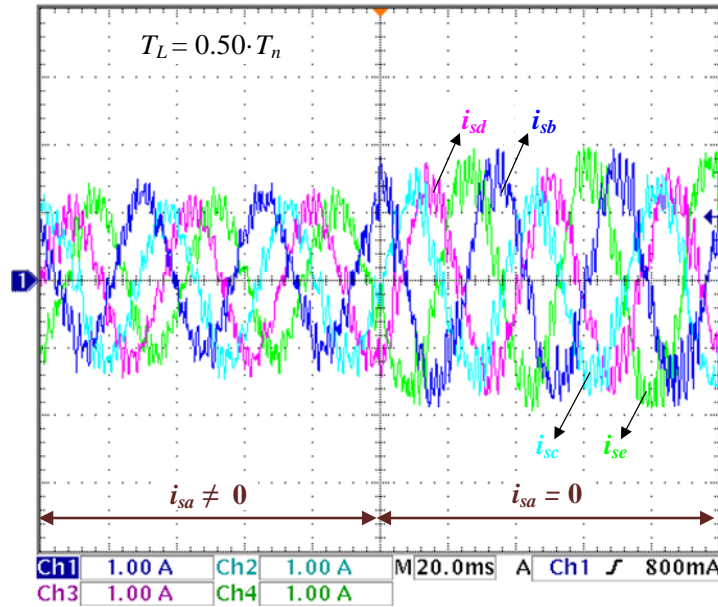


Figure 3.13. Healthy stator phase currents from the current probes when the open-phase fault appears in a 5-phase DW-IM drive and instantaneous control reconfiguration is used. The applied reference speed is 500 rpm and the demanded load torque is about 50% of the nominal one.

The low-speed operation of the drive is finally observed in Fig. 3.14, where a constant reference speed of 50 rpm is maintained from pre- to post-fault operation with constant load torques of 28% and 50% of the nominal one, Fig. 3.14a and 3.14b, respectively. Appropriate tracking of the reference speed (left figures) and the electrical torque (right plots) is obtained.

Note that the performed tests presented in this section consider that the open-phase fault condition occurs in phase 'a' and the fault occurrence is emulated by opening a power relay connected in series with the faulty phase. In the case that the fault occurs in a phase different from phase 'a', there are two valid solutions that can be used. The first one requires recalculating the transformation matrix and obtaining new voltage vectors in post-fault situation, new virtual vectors with their respective dwell times and a new look-up table. Then, it is necessary to keep all these parameters in the DSP's memory. When the fault happens, the controller must select the correct matrix, virtual vectors and look-up table, and use them to control the multiphase drive. This is a viable implementation alternative as long as the DSP's memory is more than sufficient for the control method. The second solution would need to readjust the order of the machine phases in order to establish the faulty power leg as phase 'a'. This is also possible thanks to the symmetry of the multiphase drive and allows to use the same transformation matrix $[C_{POST}]$, see equation (3.4), independently of the faulty phase. This second approach would also use the same virtual vectors and look-up table defined for phase 'a' but shows an important implementation drawback in comparison with the previous one: the General Purpose Input/Output (GPIO) modules that are

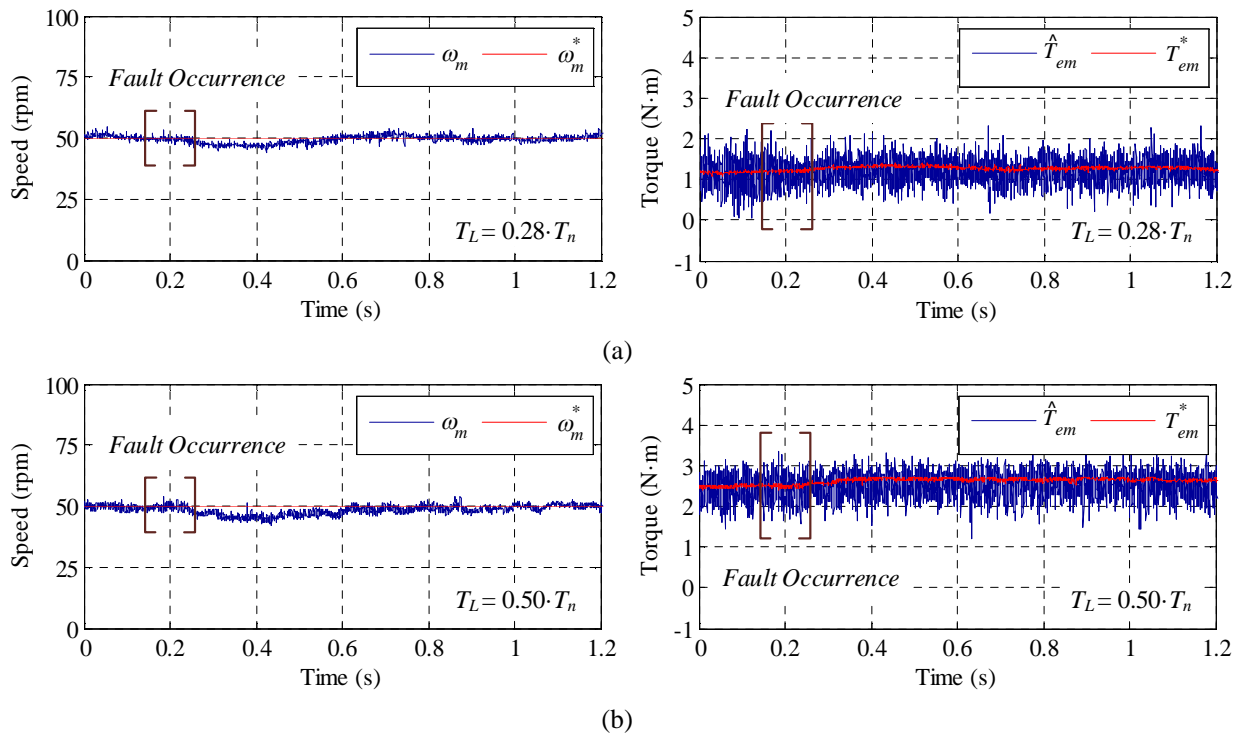


Figure 3.14. Experimental test of the low-speed operation of the 5-phase DW-IM drive. The reference speed is set to 50 rpm, while load torques of (a) 28% and (b) 50% of the nominal one are applied. The speed response and the estimated electrical torque are depicted in left and right plots, respectively. The fault is forced at $t = 0.2$ s.

used in the DSP to control the power converter (switching signals) need to be readjusted. In addition, the computational cost is slightly higher than in the first case, and what it is worse, a transition in the control action is introduced if the GPIO modules are reassigned, worsening the performance of the controlled system when managing the faulty situation.

To summarize, this study has extended the DTC technique to the open-phase fault operation of a symmetrical five-phase IM drive. Obtained experimental results analyze the performance of the proposed controller during the faulty operation of the drive. From these preliminary results it can be concluded that the proposed DTC strategy is a viable control alternative for symmetrical five-phase IM drives to FOC or MPC methods when the considered limit situation is the appearance of an open-phase fault. This conclusion extends the interest of DTC controllers in the multiphase drives' field because it is stated for the first time their utility during the faulty operation of the system, although more simulation and experimental results must be obtained to analyze their comparative performance, which is done in the next section.

3.5 A comparative analysis using conventional RFOC methods

This section complements the analysis presented in previous sections, validating through simulation and experimentation the interest of using DTC controllers in five-phase IM drives when open-phase fault conditions appear, compared with different state-of-the-art control methods. The

fault situation has recently been managed in five-phase IM drives using RFOC techniques with inner proportional resonant or predictive current controllers [155]. Then, the comparative advantages and disadvantages of applying these different control methods in healthy and open-phase fault situations are detailed, introducing a powerful tool for the controller selection for professional engineers interested in using multiphase drives in final applications.

3.5.1 RFOC techniques in open-phase fault operation

After the open-phase fault occurs, the remaining degree of freedom (the y -current component if the faulty phase is 'a', as stated before) needs to be established according to a certain strategy. Different criteria have recently been adopted in the literature in relation with ensuring post-fault operation and minimum copper losses, minimum derating (i.e. maximum load torque) or minimum torque ripple [144,182,183], as it was presented in Section 2.4.1. The MCL criterion is adopted in this case to obtain a fair comparison between RFOC and DTC methods.

When MCL is used with RFOC techniques, the y -current reference, which does not contribute to the torque production, is set to zero ($i_{sy}^* = 0$). The losses are then minimized and the efficiency of the system is improved. Notice that this criterion, as it is stated in [182], leads to unequal peaks in the phase currents and does not achieve the maximum post-fault available torque. The maximum references in the α - β plane to impose a rotating circle-shaped MMF are $i_{sa,max}^* = 0.6813 \cdot I_{sn} \cdot \sin(\omega t)$ and $i_{sb,max}^* = -0.6813 \cdot I_{sn} \cdot \cos(\omega t)$ in this case, being I_{sn} the nominal stator current value [182].

Figure 3.15 shows the scheme of RFOC controllers considered in this case [140,144]. The control is implemented in a synchronous reference frame (d - q), being the q -current reference obtained using the speed error and a PI-based controller, whereas the d -current reference is a constant value that provides the rated flux in steady-state operation. The inner fault-tolerant current controllers are implemented considering proportional resonant regulators (PR from now on) and Finite-Control-Set Model-based Predictive Current Control (PCC in what follows). Notice that the MCL criterion is imposed in this analysis ($i_{sx}^* = -i_{sa}$, $i_{sy}^* = 0$).

When a conventional RFOC method is used to manage the open-phase fault operation, PI controllers in secondary planes (x - y in this case) are substituted by PR regulators to cope with the oscillating nature of the references ($i_{sx}^* = -i_{sa}$ and $i_{sy}^* = 0$, as a consequence of the post-fault control criterion). This method is proposed in [144], where PR regulators are implemented adding the outputs of two independent PI controllers to track positive and negative sequences of the x - y stator reference currents, obtaining the reference voltages (v_{sx}^* and v_{sy}^*). Inner current controllers related to the d - q plane are PI-based, which include two feedforward terms (e_d and e_q) to improve the controller performance. Then, the obtained d - q reference voltages are first converted into the stationary frame (α - β plane) by means of the inverse Park matrix, then grouped with the obtained x - y reference voltages into α - β - x - y reference voltages and finally transformed into reference phase voltages using [C5], detailed in (2.90), to obtain a switching PWM pattern for the VSI.

The PCC scheme detailed in [140] includes an inner predictive stator current controller as the main difference with the PR technique. This predictive controller is based on the discretization of the post-fault five-phase IM drive model (predictive model in Fig. 3.15). Using this predictive model, the future stator current values, $[i_s^{k+1}]$, can be obtained in faulty operation with the measured stator currents, $[i_s^k]$, mechanical speed, ω_m , and DC-link voltage, V_{dc} . The control

objective of the predictive controller lies on defining a cost function J and finding the switching state to be applied, $[S_{opt}^{k+1}]$, that minimizes this cost function (see Fig. 3.15). This optimum value $[S_{opt}^{k+1}]$ is obtained computing the predictive model for every available switching state $[S_n^{k+1}]$ to obtain the future stator current and find the one that minimizes J . The cost function considered in this work is based on the difference between the reference and the predicted stator currents and it is shown in equation (3.8). Note that the reference stator currents are converted from the synchronous $d-q$ frame to the stationary $\alpha-\beta$ using the Park transformation and the MCL criterion is again applied ($i_{sx}^* = -i_{sa}, i_{sy}^* = 0$), while the measured stator phase currents $[i_{bcde}]$ are transformed into $\alpha-\beta-y$ coordinates using the matrix $[C_{POST}]$, see equation (3.4).

$$J = \left(i_{s\alpha}^{*k+1} - i_{s\alpha}^{k+1}\right)^2 + \left(i_{s\beta}^{*k+1} - i_{s\beta}^{k+1}\right)^2 + \left(i_{sy}^{*k+1} - i_{sy}^{k+1}\right)^2 \quad (3.8)$$

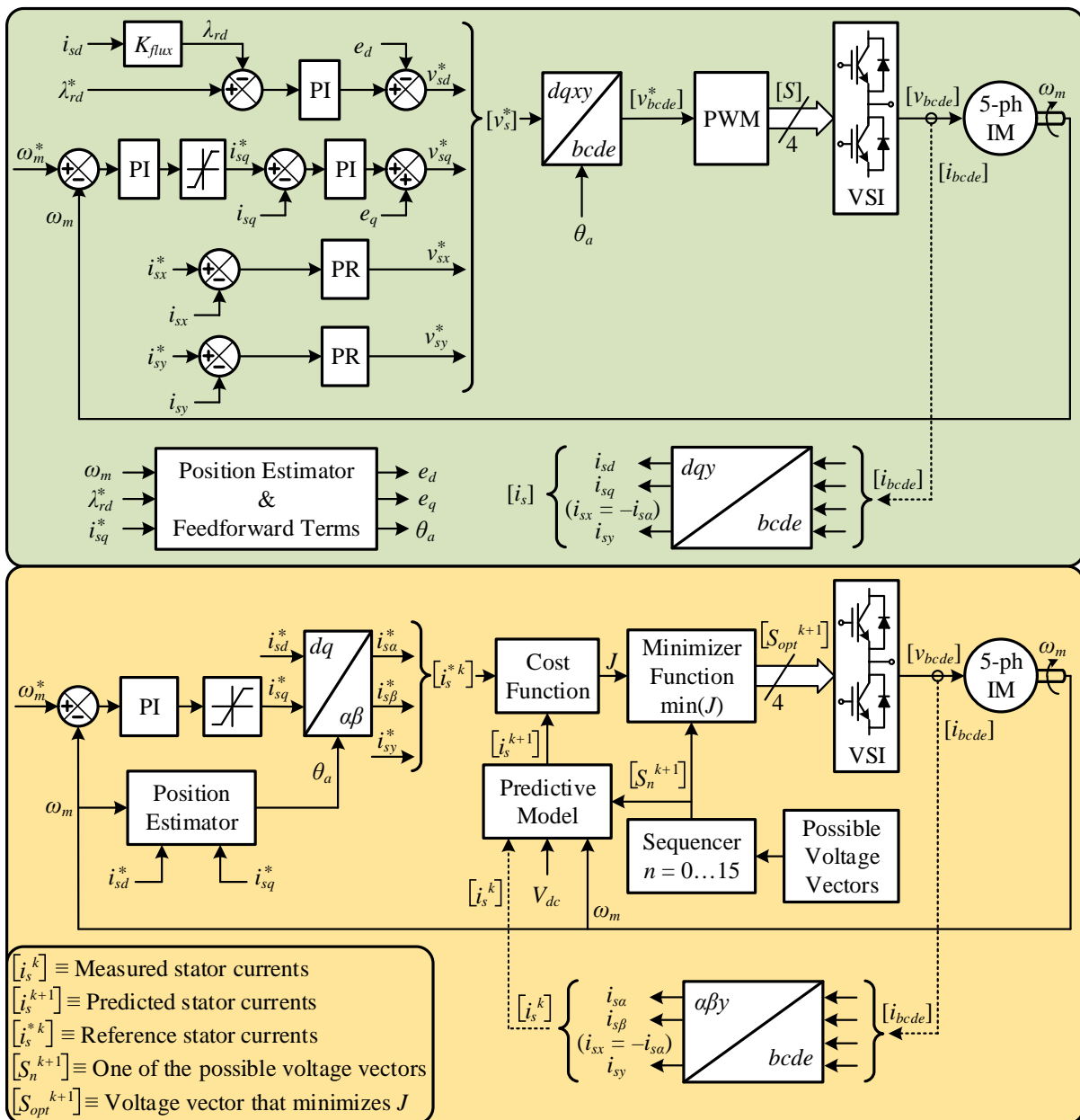


Figure 3.15. RFOC scheme based on PR (upper plot) and PCC (bottom plot) controllers.

3.5.2 Simulation results

RFOC and DTC control methods are implemented in a five-phase distributed winding IM drive, modeled using a MATLAB® & Simulink® environment. The electrical and mechanical parameters of the five-phase IM are the same as in previous sections (see Table C.1 in Appendix C). Figures 3.16 to 3.20 summarize the obtained results, where a DC-link voltage of 300 V is used.

Figure 3.16 shows the evolution of the stator currents in stationary frames using DTC and RFOC controllers in the open-phase fault operation when the reference speed is 500 rpm and the applied load torque is 25% of the nominal one. The obtained results using the DTC controller, Fig. 3.16c, are worse than the ones obtained using RFOC techniques, Figs. 3.16a and 3.16b. The harmonic content (amplitude of the ripple in the circular plots) is superior using DTC in the α - β and x - y planes. Notice that the PR current controller offers the best performance in this test, Fig. 3.16a.

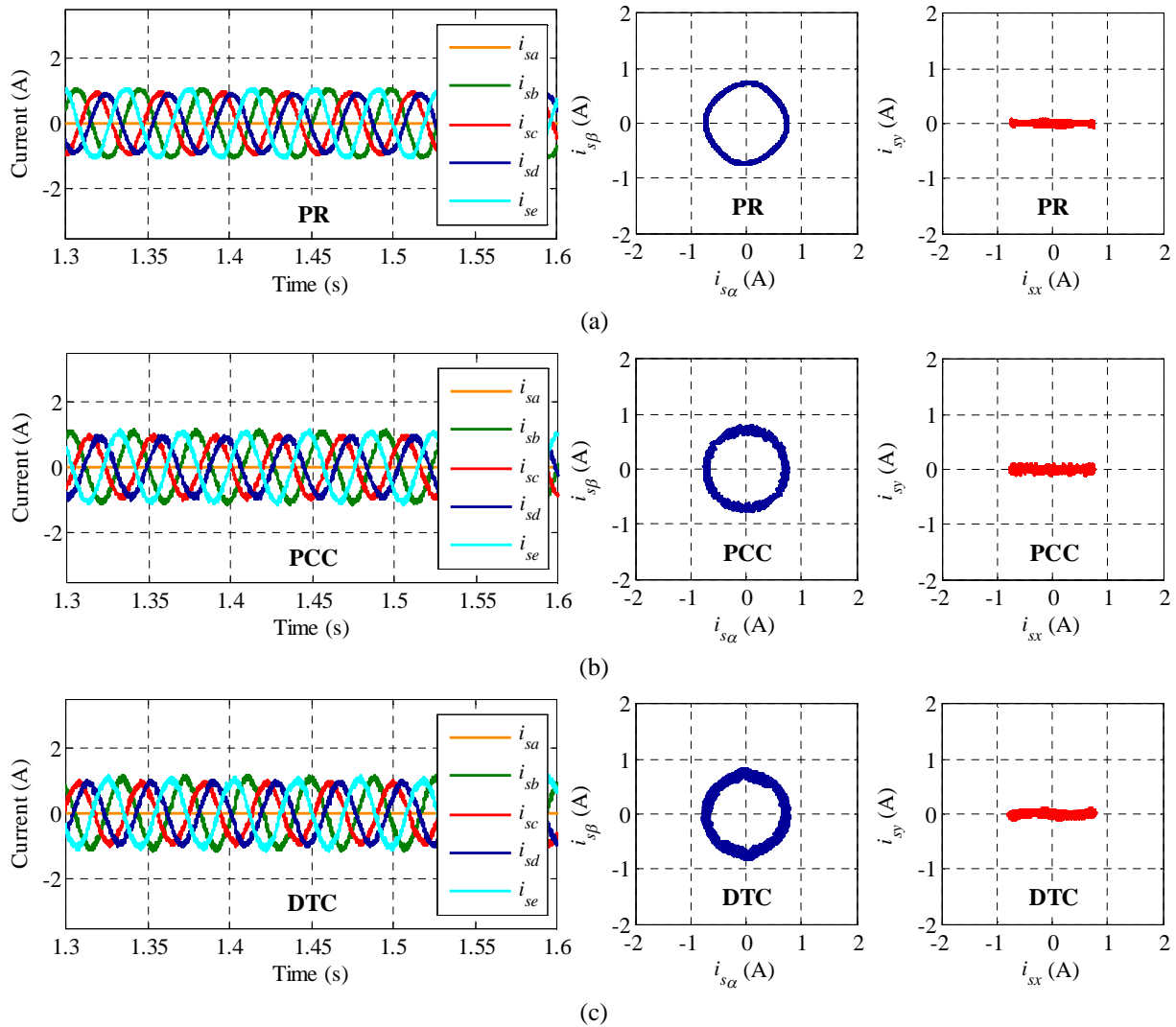


Figure 3.16. Simulation performance comparison of the steady-state operation of a 5-phase DW-IM drive, with a reference speed of 500 rpm and a load torque of about 25% of the nominal one. Stator phase currents (left-hand side plots) and evolution in the α - β (middle plots) and x - y (right-hand side plots) planes, implementing (a) PR, (b) PCC and (c) DTC controllers, respectively.

Figure 3.17 depicts the evolution of the stator currents in stationary frames but using a load torque of 50% of the nominal one. The same conclusions are reached, showing that DTC presents the worst response among the applied controllers. Notice that higher current ripples appear in this test comparing with the previous one, being this a consequence of approaching the maximum load torque that the speed controller can manage in the open-phase fault operation.

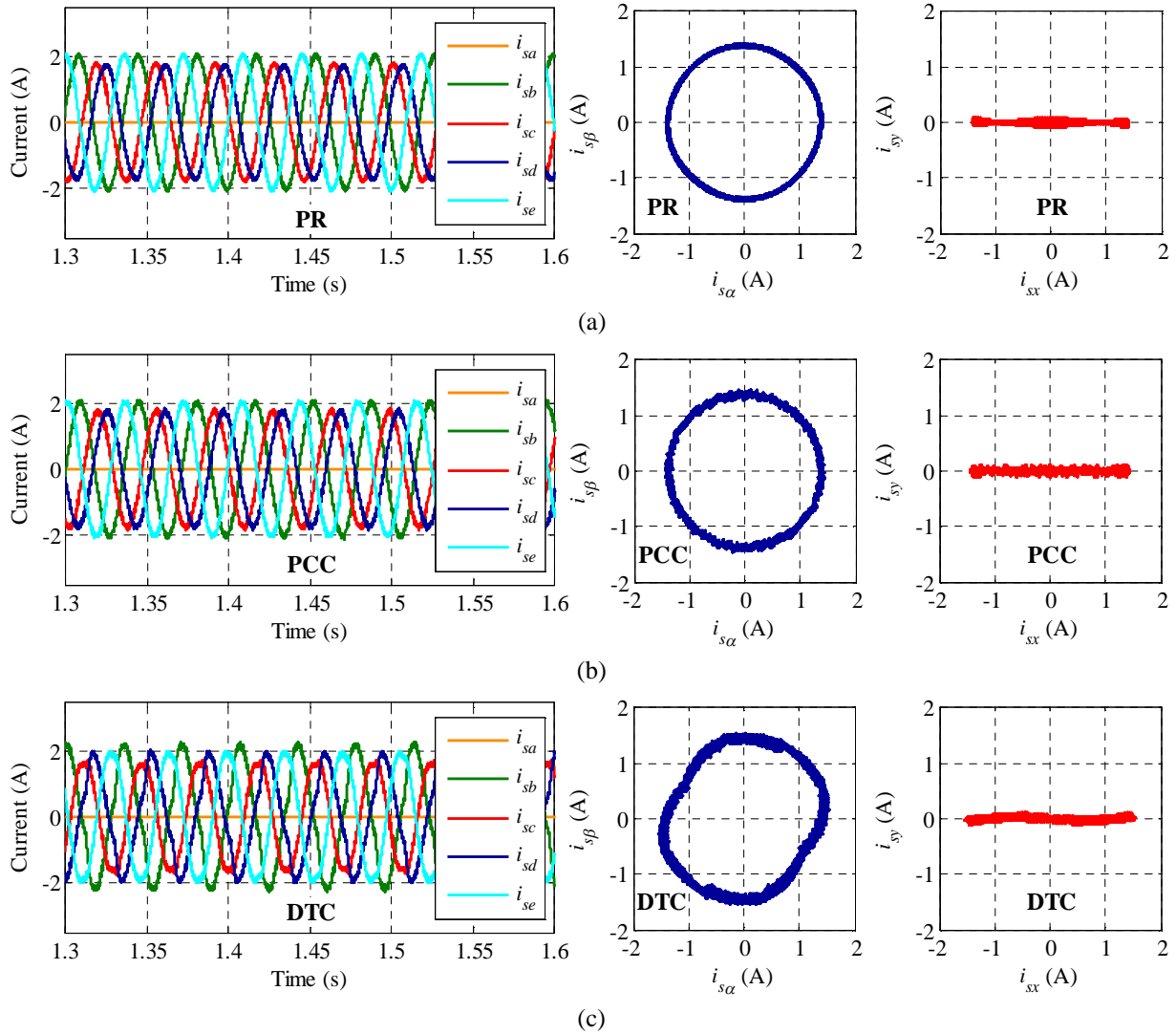


Figure 3.17. Simulation performance comparison of the steady-state operation of a 5-phase DW-IM drive, with a reference speed of 500 rpm and a load torque of about 50% of the nominal one. Stator phase currents (left-hand side plots) and evolution in the α - β (middle plots) and x - y (right-hand side plots) planes, implementing (a) PR, (b) PCC and (c) DTC controllers, respectively.

Figure 3.18 compares the speed response of the system using DTC and RFOC controllers in the open-phase fault operation when the reference speed is first changed from 500 to 300 rpm, and then from 300 to 400 rpm. A load torque of 25% of the nominal one is used. Although similar speed responses are obtained (upper plot), a detailed analysis of the responses (lower figures) shows that the DTC controller (blue traces) generates larger overshoots and poorer responses than the RFOC controllers with PCC technique (yellow traces), while offers similar responses than RFOC with PR controllers (green traces).

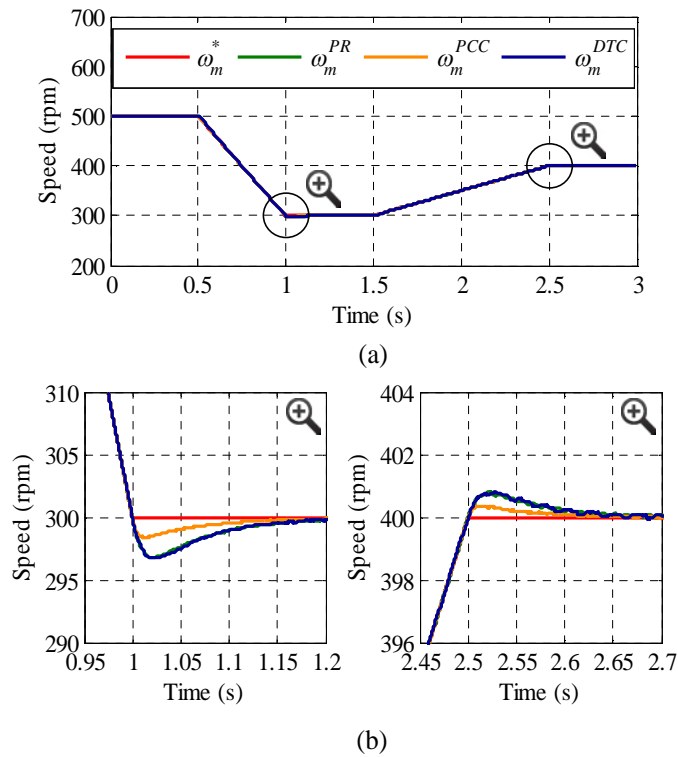


Figure 3.18. Simulation performance comparison when the reference speed is changed in a 5-phase DW-IM drive using a load torque of about 25% of the nominal one. (a) Speed response. (b) Zoom-in of the speed tracking.

The speed responses when a reversal test is done (from 500 rpm to -500 rpm in Fig. 3.19) show again slightly better performances when RFOC method with PCC controllers are used. However, all the control techniques offer a similar performance when a change in the load torque is applied, as it is shown in Fig. 3.20, where the load torque is changed from 0% to 25% of the nominal one at 500 rpm. These results prove that RFOC methods are not clearly superior to DTC techniques from the system performance perspective. Nevertheless, notice that the computational cost is much higher using RFOC methods, particularly if PCC technique is applied, which favors the real-time implementation of the DTC technique in modern microprocessors.

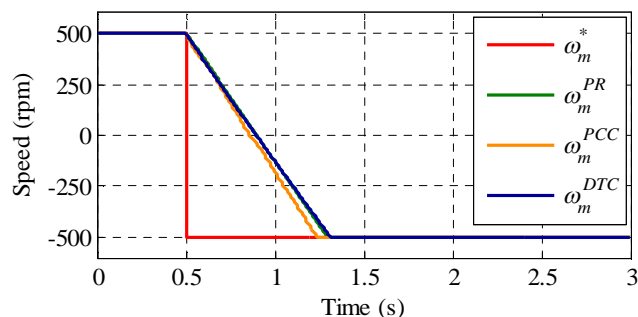


Figure 3.19. Simulation performance comparison of the speed response if a reversal test from 500 to -500 rpm is carried out in a 5-phase DW-IM drive.

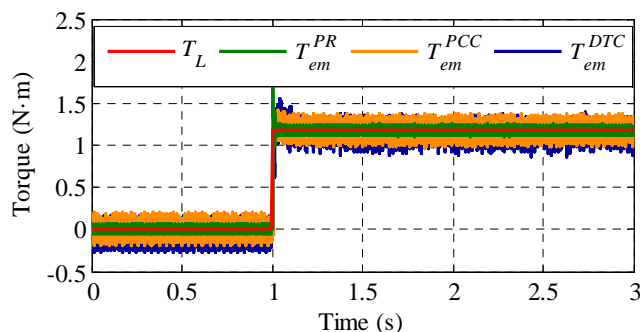


Figure 3.20. Simulation performance comparison of the generated electrical torque in a 5-phase DW-IM drive when the load torque is changed from 0% to 25% of the nominal one. The reference speed is maintained at 500 rpm during the test.

3.5.3 Experimental assessment

RFOC and DTC methods have been implemented in a lab-scale multiphase system to compare the performance results. The experimental test rig was described in Section 3.4 and shown in Fig. 3.8. The experiments are performed with a constant reference stator current in the d -axis of 0.57 A for RFOC methods, with an equivalent reference stator flux of 0.435 Wb in the DTC scheme. The hysteresis bands of the DTC torque and flux regulators are programmed at 0.77% and 1.15% of the rated values, respectively. The proportional and integral constants of the PI and PR controllers used in this study are shown in Table 3.3 and were adjusted using a trial and error procedure. The configured control sampling time is 0.1 ms in PCC and DTC methods, and 0.4 ms in PR, giving a similar switching frequency of about 2.5 kHz in all cases. Figures 3.21 to 3.25 summarize the obtained results that include the performance of the system in steady and transient states and show the performance from pre- to post-fault situations.

Table 3.3. Proportional and integral parameters of PI and PR controllers.

Controller	PR		PCC		DTC	
	K_p	K_i	K_p	K_i	K_p	K_i
Speed PI	0.15	6	0.08	6	0.25	5
d -current PI	336	18	-	-	-	-
q -current PI	80	390	-	-	-	-
x -current PR	12.5	322	-	-	-	-
y -current PR	12.5	322	-	-	-	-

The steady-state performance in faulty operation is firstly examined, driving the motor at 500 rpm when different load torques are demanded. Figure 3.21 shows the evolution of the stator currents using RFOC and DTC controllers when the applied load torque is $0.28 \cdot T_n$ (about half of the maximum achievable post-fault torque when the MCL criterion is used [140]). Regardless of the control strategy, stator currents in phases ‘ b ’ and ‘ e ’ are equal in magnitude and possess unequal peak values compared to stator phase currents ‘ c ’ and ‘ d ’ (see left plots in Fig. 3.21), being the obtained results in accordance with the applied MCL criterion [182]. Since the MMF remains

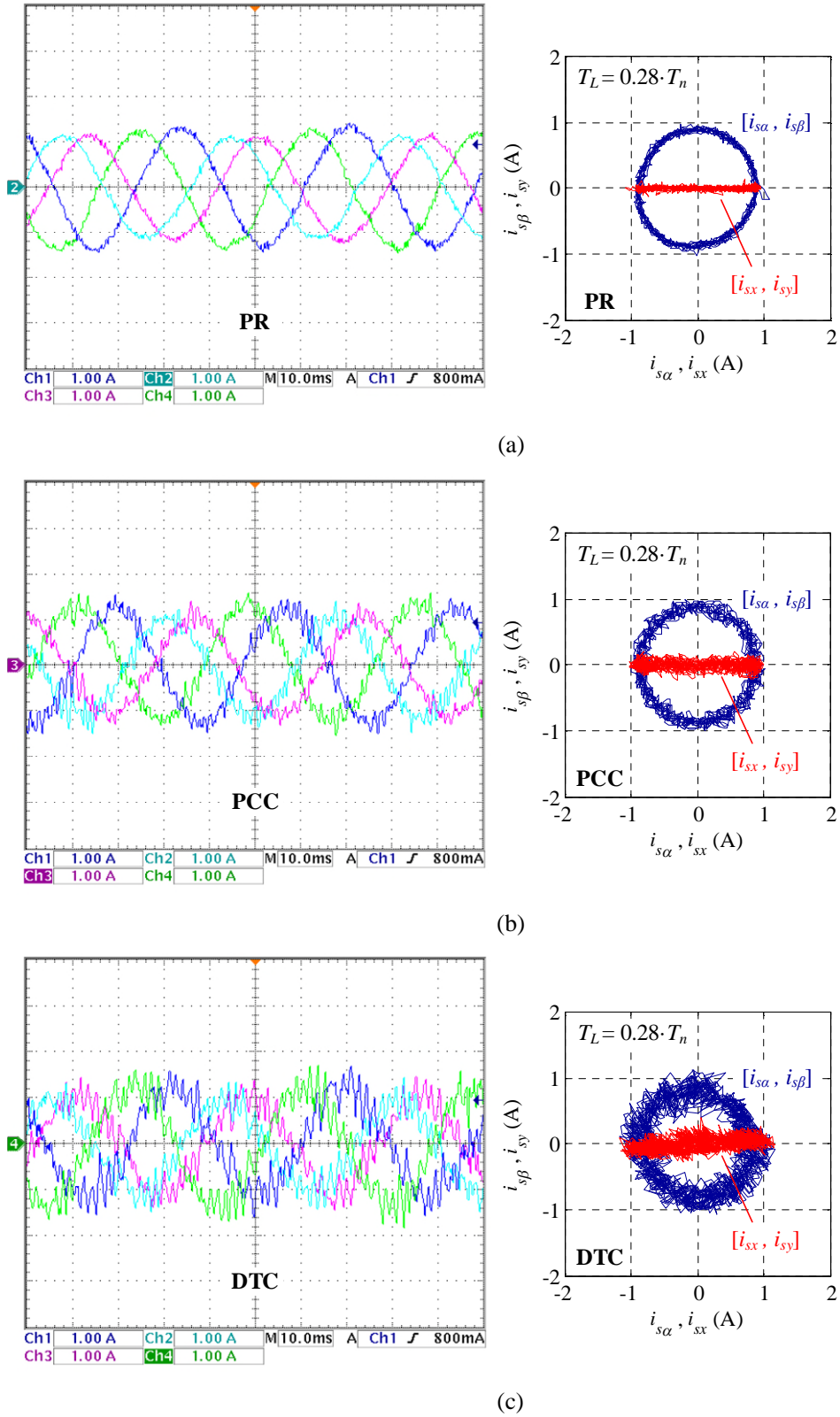


Figure 3.21. Experimental performance comparison of the steady-state faulty operation of a 5-phase DW-IM drive. The reference speed is set to 500 rpm and a load torque of 28% of the nominal one is required. Stator phase currents obtained from the current probes and stator phase currents in α - β and x - y planes (left and right plots, respectively), while (a) PR, (b) PCC and (c) DTC controllers are used.

the same in healthy and faulty operations, a circular trajectory is obtained in the α - β currents, see blue circles in right plots of Fig. 3.21. However, a horizontal line is observed in the x - y plane because $i_{sx} = -i_{sa}$ and i_{sy} is nearly null, see red line in right plots of Fig. 3.21. The main difference between the controllers is that the harmonic content is higher using DTC in the α - β and x - y planes, while the use of PR controllers with RFOC techniques offers the best performance in steady state.

If the maximum post-fault torque in steady state with the MCL criterion is applied ($0.56 \cdot T_n$) [140], the obtained results are summarized in Fig. 3.22. Similar conclusions are achieved when RFOC methods are analyzed (Figs. 3.22a and 3.22b). Notice that the reference speed is controlled during the test (right-hand side plots), while the difference between both methods is the harmonic

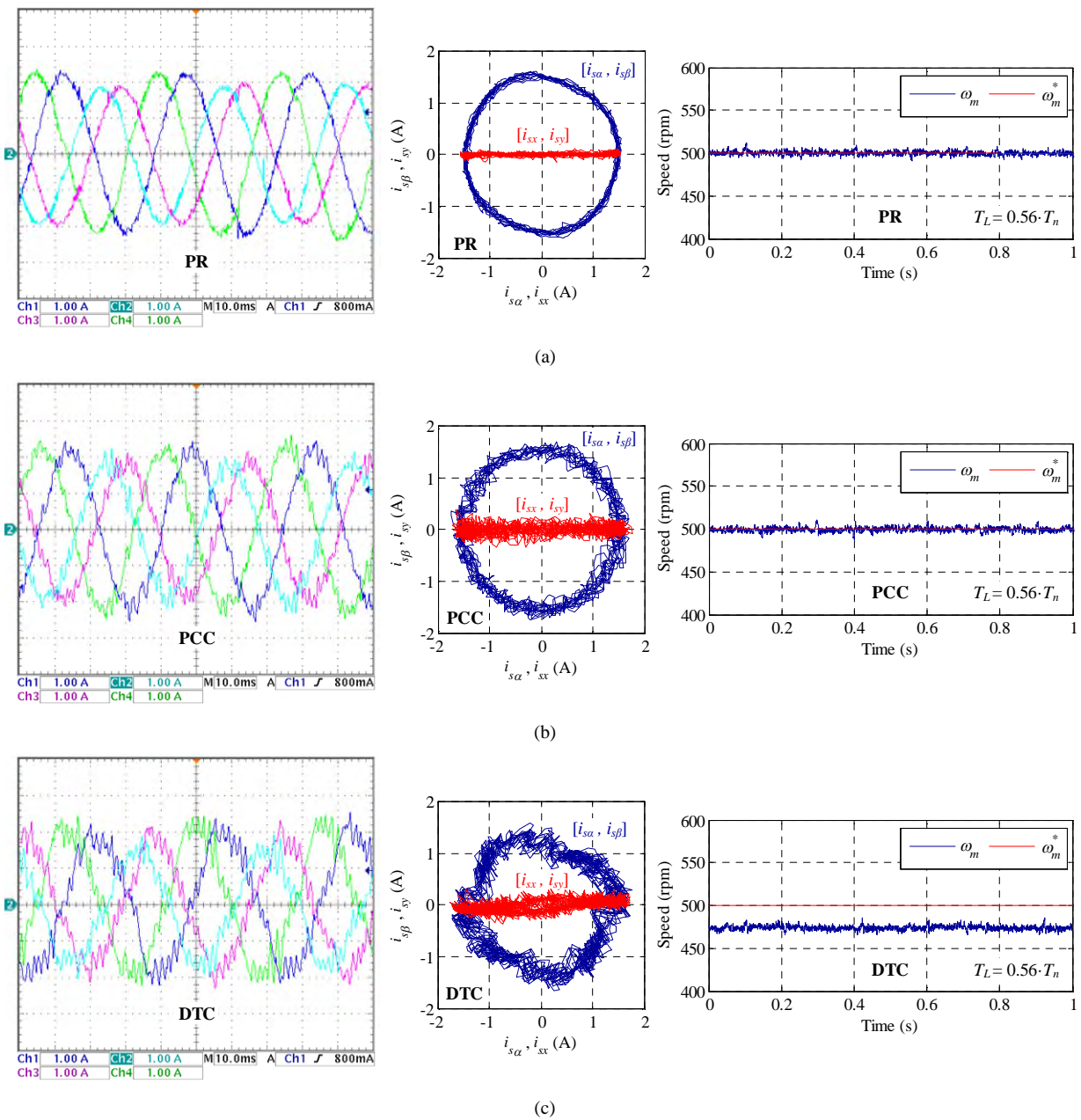


Figure 3.22. Experimental performance comparison of the steady-state faulty operation of a 5-phase DW-IM drive. The reference speed is set to 500 rpm and a load torque of 56% of the nominal one is required. Stator phase currents obtained from the current probes and stator phase currents in α - β and x - y planes (left and right plots, respectively), while (a) PR, (b) PCC and (c) DTC controllers are used.

content in the stator phase currents and the circular plots of currents in α - β and x - y planes (left-hand side and middle plots). The situation changes when the DTC method is used (Fig. 3.22c): the speed is not regulated, α - β currents do not describe a circular trajectory and peak values of stator phase currents are different. This is a consequence of using virtual voltage vectors of lower amplitude than the available voltage vectors, which reduces the harmonic content of DTC at the expense of also reducing the DC-link utilization. It can be then concluded that the maximum load torque that DTC can manage in post-fault operation is lower than using RFOC techniques.

The compared dynamic performance in faulty operation using the different control schemes is then analyzed. A reversal speed test is done, where the reference speed is changed from 500 to -500 rpm at $t = 0.2$ s, while no electrical load torque is demanded to the multiphase drive using the controlled DC machine. Figure 3.23 shows the obtained results, presenting the DTC technique lower settling times and overshoots than RFOC methods, left plots of Fig. 3.23. The harmonic content in the stator currents is lower using RFOC techniques, as it is illustrated in the zoom-in of the α - β stator currents at the zero-speed crossing instant, right plots of Fig. 3.23.

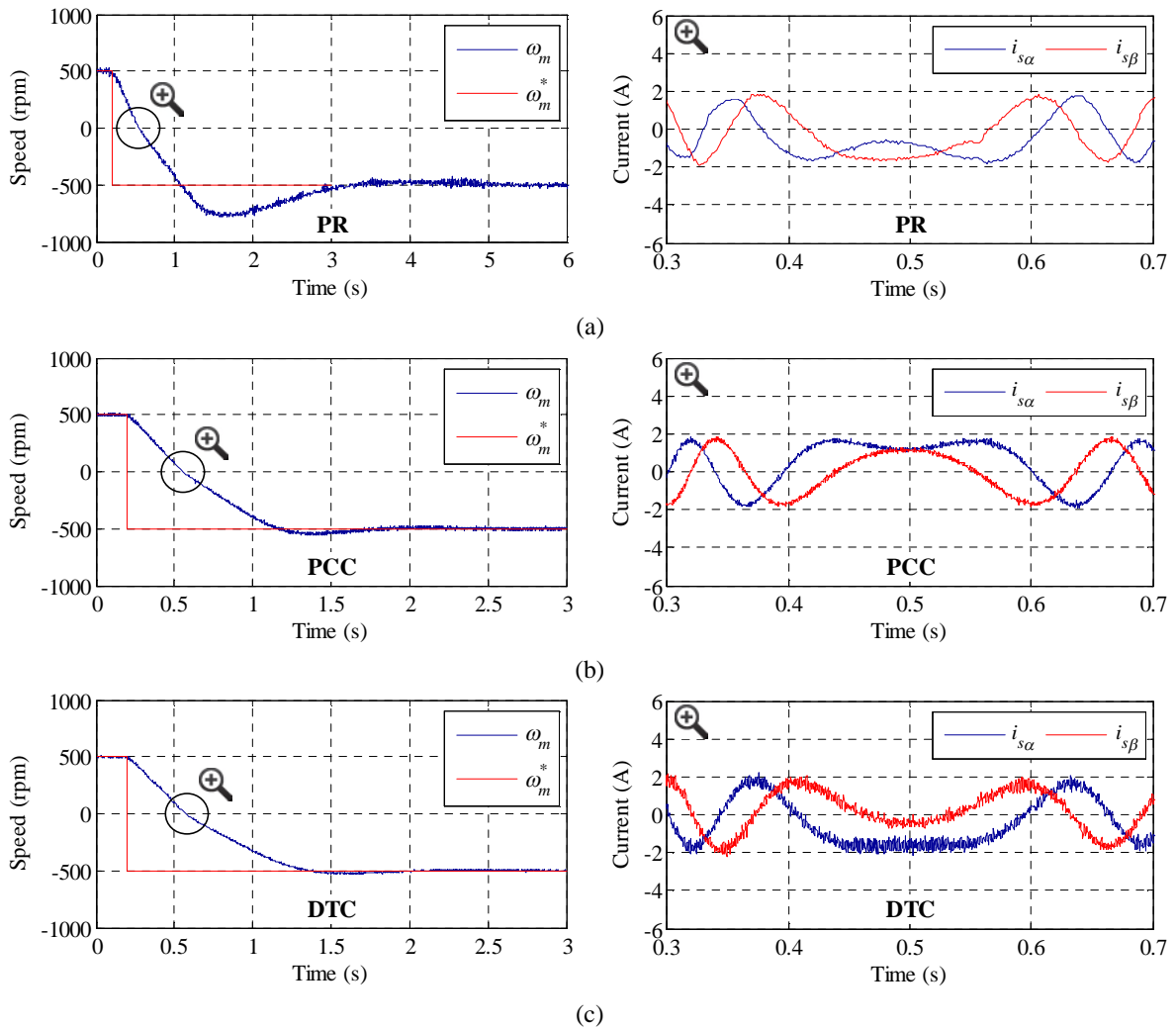


Figure 3.23. Experimental comparison of the dynamic performance of a 5-phase DW-IM drive in faulty operation. The reference speed is changed from 500 to -500 rpm at $t = 0.2$ s, while no electrical load torque is demanded. Speed response and stator current waveforms in the α - β plane at the zero-speed crossing point (left and right plots, respectively), when (a) PR, (b) PCC and (c) DTC controllers are used.

Next, the transition from pre- to post-fault operation is studied in Fig. 3.24, showing the performance of the system. Note that a delay of 40 ms between the fault occurrence and the control action is considered to take into account the fault detection process. The motor is driven at 500 rpm, before and after the fault occurrence, with a constant load torque of $0.50 \cdot T_n$. It is interesting to note the degradation of the speed tracking when the PCC method is used, see left plot of Fig. 3.24b, where the speed of the system drops to about 480 rpm. The control action is also poor when the PR method is used, see right plot of Fig. 3.24a, where the harmonic content in the electrical torque is the highest among the considered control methods. In this case, an oscillating ripple at double the fundamental frequency appears due to the q -current oscillation because of a negative sequence current that cannot be regulated by the outer PI-based speed and flux d - q controllers [144,155]. This is not the case when DTC is used (Fig. 3.24c), being a more robust control method in the experiment. Once the post-fault controllers are activated at 0.24 s, the control action is recovered and the speed is regulated in all cases. In particular, DTC shows a higher settling time.

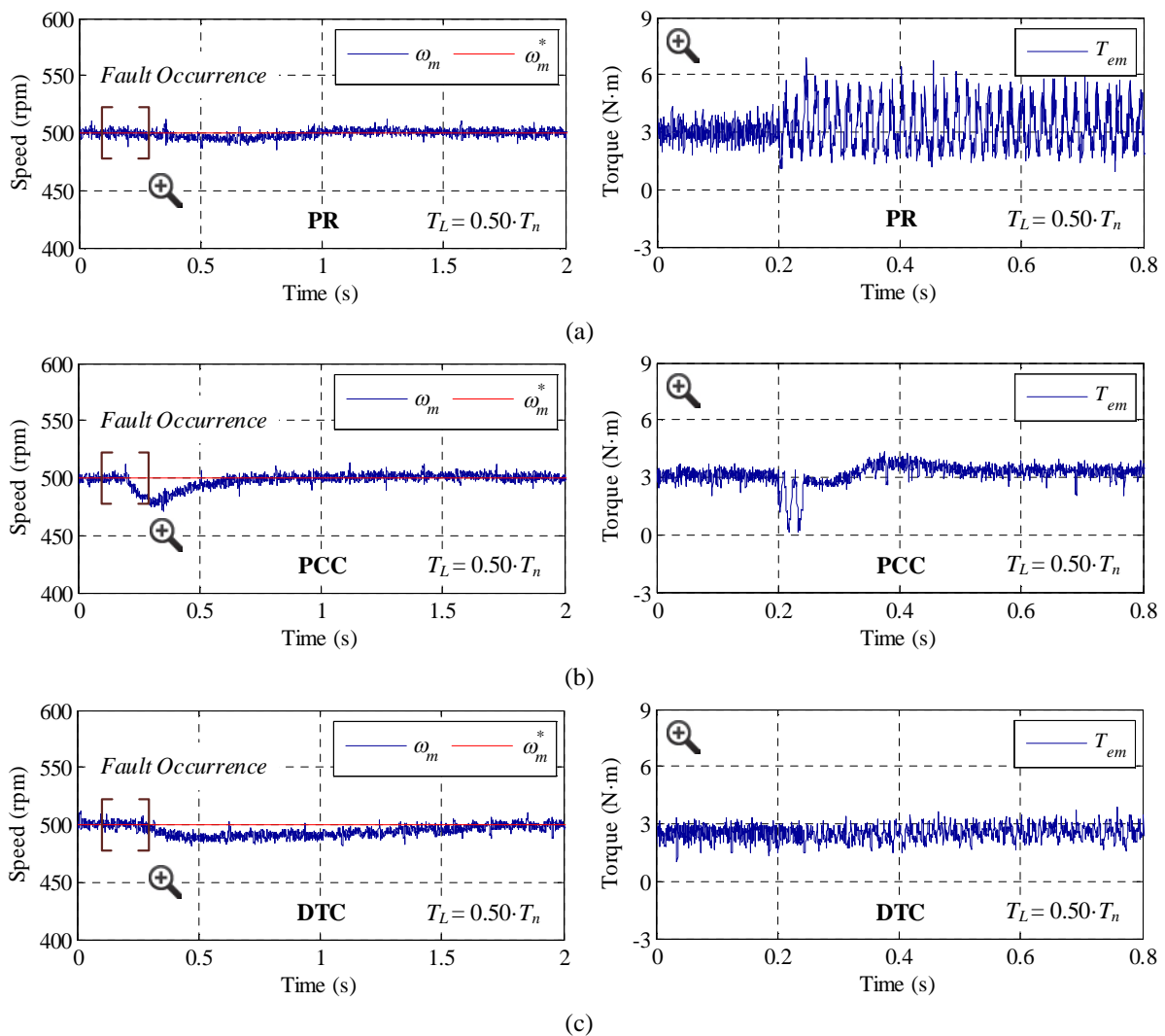


Figure 3.24. Experimental performance comparison of the pre- to post-fault transition under realistic conditions (a delay of 40 ms in the fault detection is assumed) in a 5-phase DW-IM drive. A load torque of about 50% of the nominal one and a reference speed of 500 rpm are used. Speed response and zoom-in of the generated electrical torque at the fault occurrence instant (left and right plots, respectively), when (a) PR, (b) PCC and (c) DTC techniques are considered.

The low-speed operation of the drive is finally analyzed in Fig. 3.25. A delay of 40 ms between the fault occurrence and the control action is again considered. A constant load of $0.50 \cdot T_n$ is applied, and a reference speed of 50 rpm is set. Similar responses are obtained using the different controllers, although the DTC method takes longer to settle down to its steady-state speed, left-hand side of Fig. 3.25c. The PR method offers an oscillating ripple at double the fundamental frequency, like in the previous test, right-hand side of Fig. 3.25a.

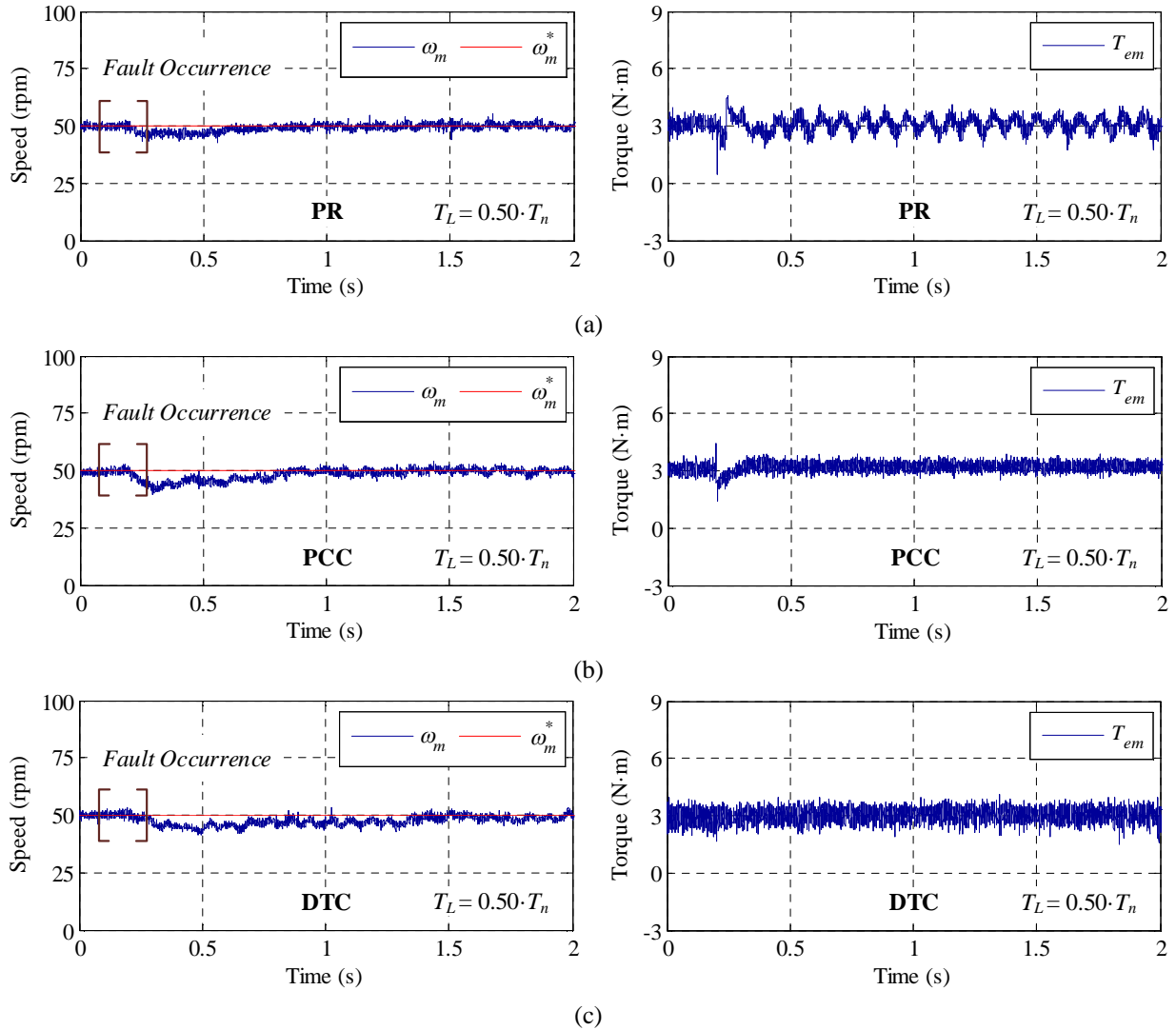


Figure 3.25. Experimental performance comparison of the pre- to post-fault transition at low-speed operation of a 5-phase DW-IM drive, where a delay of 40 ms in the fault detection process is assumed. A load torque of about 50% of the nominal one and a reference speed of 50 rpm are used. Speed response and generated electrical torque (left and right plots, respectively), when considering (a) PR, (b) PCC and (c) DTC techniques.

A qualitative comparative analysis between the studied control schemes is summarized in Table 3.4, and the obtained assumptions can be detailed as follows:

- Different fault detection delays (from 20 to 100 ms) have also been tested in the analyzed transitions from pre- to post-fault situation, concluding that the DTC method maintains the control action during the transition and shows the highest robustness in the study.
- A change in the model of the physical system is imperative when PCC and DTC methods are used, while the PR technique does not require this change.
- The controller must be redefined if PR and DTC techniques are used (substitution of conventional PI controllers and definition of a new look-up table, respectively) when the fault appears. In contrast, a change in the cost function is only needed after the fault detection when PCC is used.
- The computational cost of the implemented algorithms shows the lowest value for the DTC method and the largest one for the PCC technique.
- The quality of the obtained stator current in terms of harmonic content depicts the lowest values for the PR method, while the DTC technique produces the highest current ripple.
- The maximum obtained torque in faulty situation is higher (roughly about 10%) with RFOC methods.

All in one it can be concluded that there is no ideal controller to manage the open-phase fault appearance. If robustness, simplicity or computational cost are the desirable characteristics, the DTC method offers the best performance. However, if the quality of the obtained stator current or the maximum post-fault electrical torque are demanded in post-fault operation, the RFOC techniques are superior.

Table 3.4. Qualitative comparison between RFOC and DTC methods in open-phase fault operation.

Closed-loop system performance	PR	PCC	DTC
Speed tracking error when the fault appears	Negligible	High	Slight
Torque tracking loss in control during the delay	Yes	Yes	No
Robustness against fault detection delay	↓	↓↓	↑↑
Change in the Clarke transformation matrix	No	Yes	Yes
Reconfiguration of the controller	Yes	No	Yes
Computational cost	↑	↑↑	↓
Harmonic content in stator currents	↓	↑	↑↑
Maximum available torque	56% of T_n	56% of T_n	50% of T_n

3.6 Chapter conclusions

In this chapter, the limit situation of the loss of a phase in the machine has been analyzed. The considered direct control strategy to handle this situation has been the DTC method. Although the use of DTC is not habitual in the multiphase drives' field due to the intrinsic limitations of the method that only manages two degrees of freedom, it has recently been demonstrated that it is possible to apply it to five-phase machines as long as a series of virtual voltage vectors are created to impose zero voltage in the non-controllable x - y plane. This allows DTC to be successfully applied when the machine does not have asymmetries in its design, something that does not have

to coincide with reality. In any case, if the considered limit situation is the loss of a phase, the number of controllable degrees of freedom in the system are close to those of the conventional three-phase case, where DTC can be considered as a quite competitive alternative to FOC. This justifies considering the DTC technique as an interesting strategy for the five-phase case and the limit situation of loss of some degree of freedom in the control.

Therefore, this chapter has extended the DTC technique to the open-phase fault operation of a symmetrical five-phase distributed windings IM drive, used as a case example. Obtained simulation and experimental results analyze the performance of the proposed controller during the faulty operation of the drive, concluding that the speed, torque and flux references are maintained after the fault occurrence if the applied load torque is within the maximum torque that the post-fault control scheme can manage. A detailed comparative analysis between DTC and RFOC controllers has also been presented. Obtained results show that the DTC method has the capacity of managing lower maximum electrical torques than RFOC techniques. Higher harmonic content is also obtained in the stator phase current when the DTC technique is applied, as it occurs in the three-phase case. However, the use of a post-fault DTC is a viable option that proves to increase the robustness against fault detection delays while simplicity and low computational cost are preserved. This results in an interesting alternative to RFOC methods in industry applications where the reliability needs to be increased and the drive must be operated in safety conditions until a corrective maintenance is carried out.

However, when the considered limit situation implies the control of other degrees of freedom in the system (constraints in voltages, currents...), in this case DTC does not seem to be an interesting control alternative due to its limitations. It is advisable, therefore, to propose direct control alternatives that allow a high number of variables to be controlled. In the next chapter, the MPC method will be analyzed as a direct control technique where a greater number of degrees of freedom can be included in the control strategy.

Chapter 4

Controller with two Independent Frequency-Domain Subspaces: The MPC Case

The optimal control of modern power drives requires the consideration of electrical constraints in the regulator strategy, including voltage and current limits imposed by the power converter and the electrical machine or the magnetic saturation due to the iron core. This issue has been extensively analyzed in conventional three-phase drives but rarely studied in multiphase ones, where optimal controllers that take into account electrical limits are barely considered despite the current interest of the multiphase technology in high power density, wide speed range or fault-tolerant applications. As stated at the end of Chapter 3, the DTC technique loses interest in this situation since it is able to control only two degrees of freedom and does not permit the inclusion of electrical limits in the controller. Then, another direct control strategy that manages a greater number of degrees of freedom is required for this issue. In this sense, the MPC method appears as a candidate to this end, being in addition a control strategy that offers a high flexibility facing multi-input multi-output systems subject to constraints.

In this chapter, a generalized optimal controller using MPC techniques is introduced. The proposed control method is valid for conventional and multiphase drives, and it is based on two cascaded predictive stages. First, a CCS-MPC stage generates the optimal reference stator current complying with the electrical limits of the drive to exploit the maximum performance characteristic. Then, a FCS-MPC controller regulates the stator current and generates the switching state in the power converter. Two different topologies of five-phase machines are utilized as modern high-performance drives case examples for the experimental validation of the two-stage predictive technique: a five-phase PMSM and a five-phase IM with concentrated windings. These are common multiphase drives that can be considered as systems with two independent frequency-domain subspaces to be regulated, where fundamental and third harmonic currents are orthogonal components involved in the torque production. Real-time simulations based on OPAL-RT technologies and experimental results are provided to analyze the utility of the proposed controller, where optimal reference currents are generated, steady and transient states are studied, and performance conclusions are obtained.

This chapter is organized as follows. The electrical limits that will be included in the control strategy are detailed in **Section 4.1**. Then, the proposed optimal control scheme is introduced in **Section 4.2**, focusing on the study of the two control stages based on predictive techniques. The validation of the control strategy is analyzed in **Section 4.3**, which is divided in two parts. First, a

preliminary performance analysis of the technique is done prior to its implementation in a real system, using a real-time simulation environment based on OPAL-RT technologies. Next, the controller is implemented in a real test rig to experimentally validate the closed-loop performance of the entire system. Finally, this chapter ends with the most relevant conclusions in **Section 4.4**.

4.1 Electrical constraints for the optimal control strategy

The imposed electrical limits will maximize the torque capability of the system without exceeding the safety values of the machine and the VSI. The voltage limit comes from the maximum DC-link voltage that the VSI can apply to the machine (maximum peak phase-to-phase voltage, V_{dc}). It is obtained in the flux-weakening region, where the available torque decreases when the drive operates above the base speed. On the other hand, current limits are imposed by the power converter and the machine. Power switches impose a maximum peak phase current value I_{VSI} , while the copper losses in the machine establish a maximum RMS phase current I_{RMS} . For the sake of simplicity, it is considered in this work that the RMS phase current never exceeds the maximum value. Then, the electrical constraints that will be considered are summarized here:

$$i_{phase}(t) \leq I_{VSI} \quad (4.1)$$

$$u_{phase-to-phase}(t) \leq V_{dc} \quad (4.2)$$

Note also that, in order to avoid the magnetic saturation in the machine, the maximum peak of the magnetic field must be limited. This Thesis tries to begin to consider this limitation in the control strategy but taking into account a series of starting hypotheses. In this way, a starting point is established in the study of the magnetic saturation and its inclusion in the control of multiphase machines. First, remember that the used model for the multiphase machine is linear and does not consider any non-linearity due to the magnetic field saturation, as it was stated in Section 2.2. Next, suppose that the machine is only fluxed with the first and third harmonic components, and they are synchronized. Therefore, the air-gap magnetic field H can be expressed as follows:

$$H(\varphi) = H_1 \cdot \cos(\varphi) - H_3 \cdot \cos(3\varphi) \quad (4.3)$$

where H_1 and H_3 are the amplitudes of every harmonic component, while the angle φ varies in the range $[-\pi/2, \pi/2]$.

Then, as the maximum value of H must be limited in order to avoid the magnetic saturation, this limitation can be forced in terms of the stator current in the d_1 - and d_3 -axes (if the magnetic effects of the rotor on the stator are neglected), writing (4.3) in the following way:

$$I_{M,max} = \max_{\varphi \in [-\pi/2, \pi/2]} \left\{ i_{sd1} \cdot \cos(\varphi) - \frac{i_{sd3}}{3} \cdot \cos(3\varphi) \right\} \leq I_{sd, rated} \quad (4.4)$$

where $I_{sd, rated}$ is the rated magnetizing current of the machine, i.e. the magnetizing current that produces the rated sinusoidal spatial distribution of the air-gap magnetic field. This equation is a

new electrical limit that must be taken into account in the control strategy. The solution of (4.4) yields to the expressions presented in (4.5) and (4.6), as it is explained in [168], which constitute the maximum d -current values in order to not exceed the maximum magnetization level considering the previous hypotheses.

$$i_{sd1,max} = \frac{2}{\sqrt{3}} \cdot I_{sd,rated} \quad (4.5)$$

$$i_{sd3,max} = \frac{1}{\sqrt{3}} \cdot I_{sd,rated} \quad (4.6)$$

4.2 Definition of an optimal controller using MPC techniques

The general scheme of the proposed control strategy applied to a five-phase machine is presented in Fig. 4.1, where the two main stages are identified. The optimization problem (first control stage) is an optimal reference current generator that finds the best way to divide currents between d - and q -axes. It can be considered as an extra part of the inner current controller (second control stage), where the FCS-MPC technique is used for the stator current regulation of the machine. Note that an outer PI-based speed control loop should be also considered to implement a variable speed drive based on the utilization of a multiphase machine. As it was mentioned at the beginning of the chapter, one interesting characteristic of the proposal is that different limits or constraints are easily included in the controller. A detailed description of this control scheme will be given throughout this section.

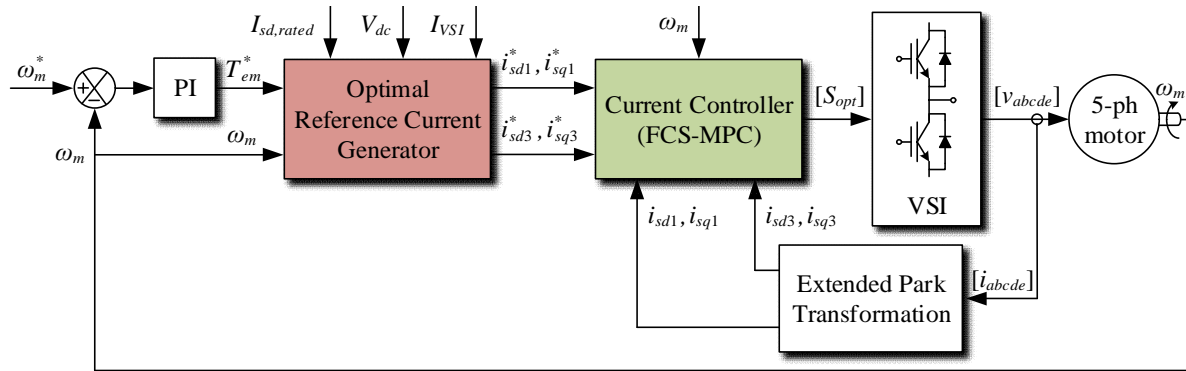


Figure 4.1. Scheme of the proposed optimal controller.

The first control stage is in charge of obtaining optimal references for the d - q currents using an optimization process based in a continuous MPC technique. The objective of this optimization stage is to get the expected torque along with the minimization of the copper losses, while respecting the defined maximum peak values of currents, voltages and the magnetization level. Consequently, the optimization problem to be solved is summarized in (4.7), where two weighting factors κ_i and κ_T are introduced in the objective function F to give more or less importance to the minimization of the copper losses with respect to the reference torque tracking. The selection of appropriate values for the weighting factors will be assessed in the following section. Note also

that it is required to discretize the model of the multiphase drive and the Euler method is used for this purpose. The discretized model is utilized to obtain the predicted phase voltages and currents that are used to compute the objective function and to calculate the peak values that constraint the optimization problem.

$$\begin{aligned} \min F &= \left[\kappa_i \cdot (i_{sd1}^2 + i_{sq1}^2 + i_{sd3}^2 + i_{sq3}^2) + \kappa_T \cdot (T_{em}^* - T_{em})^2 \right] \\ \text{subject to:} \\ I_{max} &= \text{peak}(i_{sa}, i_{sb}, i_{sc}, i_{sd}, i_{se}) \leq I_{VSI} \\ V_{max} &= \text{peak}(u_{ab}, u_{ac}, u_{ad}, u_{ae}) \leq V_{dc} \\ I_{M,max} &= \max_{\varphi \in [-\pi/2, \pi/2]} \left\{ i_{sd1} \cdot \cos(\varphi) - \frac{i_{sd3}}{3} \cdot \cos(3\varphi) \right\} \leq I_{sd,rated} \\ &\text{and respecting equations of the machine's model} \end{aligned} \quad (4.7)$$

Figure 4.2 summarizes the process to obtain the optimal d - q reference currents, where the proposed optimization problem in (4.7) is first rewritten in the standard form of a quadratic programming problem (see second block of Fig. 4.2). In this new quadratic programming form, $[z]$ is the primal optimization variable regrouping the states and inputs of the system's model, $[H]$ and $[h]$ are the quadratic and linear parts of the objective function, respectively, while matrices $[C]$, $[d]$ and $[E]$ represent the dynamics constraints. Since it is very difficult to solve this problem in real time, a change of variables is proposed with the aim of reducing the complexity (see third block of Fig. 4.2), where $[x]$ is the dual variable and $[M]$ represents the null space of $[C]$, i.e. $[C] \cdot [M] = 0$. The minimization problem resulting from this change of variables has less constraints and is finally solved through an iterative process based on the Primal-Dual Interior Point method for constrained nonlinear optimization, as it is detailed in [184].

Once the optimal reference currents have been determined, the second stage of the proposed controller is applied. This second stage is an inner stator current controller based on the FCS-MPC method, which is detailed in the flow diagram shown in Fig. 4.3 and in the block diagram of Fig. 4.4. The discretized model is again applied to estimate the stator current values in the next sampling period $k+1$, $[i_{sdq}^{k+1}]$, using the measured mechanical speed and stator currents in the instant k , ω_m^k and $[i_{sdq}^k]$ respectively. Once the prediction is done, the controller determines the next switch configuration $[S_{opt}]$ to be applied in the VSI in order to minimize a predefined cost function J , see equation (4.8). This cost function represents the control objective of the FCS-MPC method, being in this case the tracking of the optimal reference currents calculated by the optimization algorithm, although different cost functions can be used to include different control constraints and depending on the specific application. For instance, a different cost function in order to reduce the VSI losses or the stator current harmonic content is proposed in [104], where weighting factors are also introduced to weight the control action between current tracking and losses reduction. Finally, the applied switching state $[S_{opt}]$ is obtained through an exhaustive search process, where the predictive model is computed for every available switching state ($2^5 = 32$ for a five-phase machine) to find the future stator current that minimizes J .

$$J = \left(i_{sd1}^{*k+1} - i_{sd1}^{k+1}\right)^2 + \left(i_{sq1}^{*k+1} - i_{sq1}^{k+1}\right)^2 + \left(i_{sd3}^{*k+1} - i_{sd3}^{k+1}\right)^2 + \left(i_{sq3}^{*k+1} - i_{sq3}^{k+1}\right)^2 \quad (4.8)$$

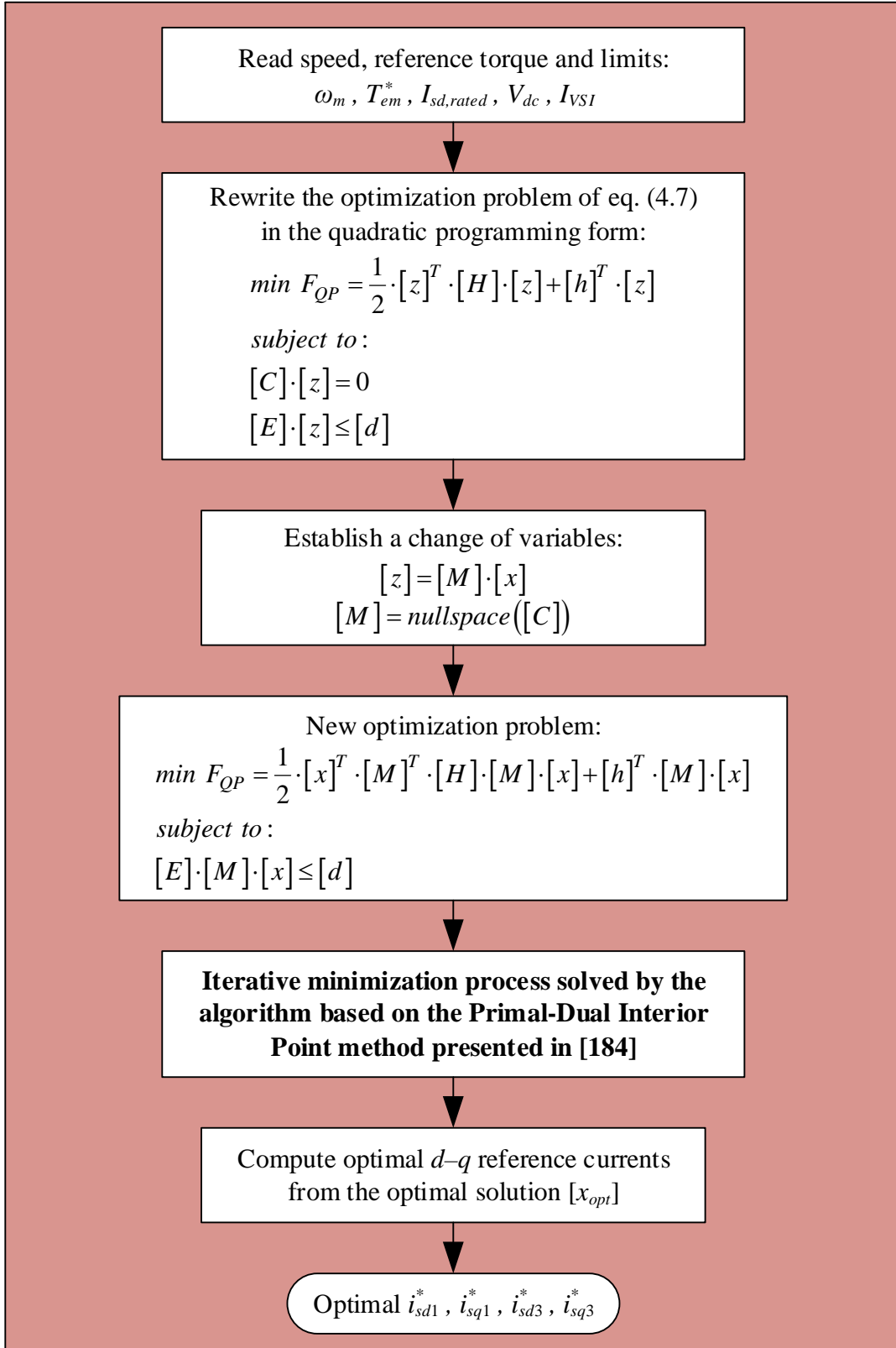


Figure 4.2. First MPC stage to implement the proposed technique: optimization process for the reference current generation.

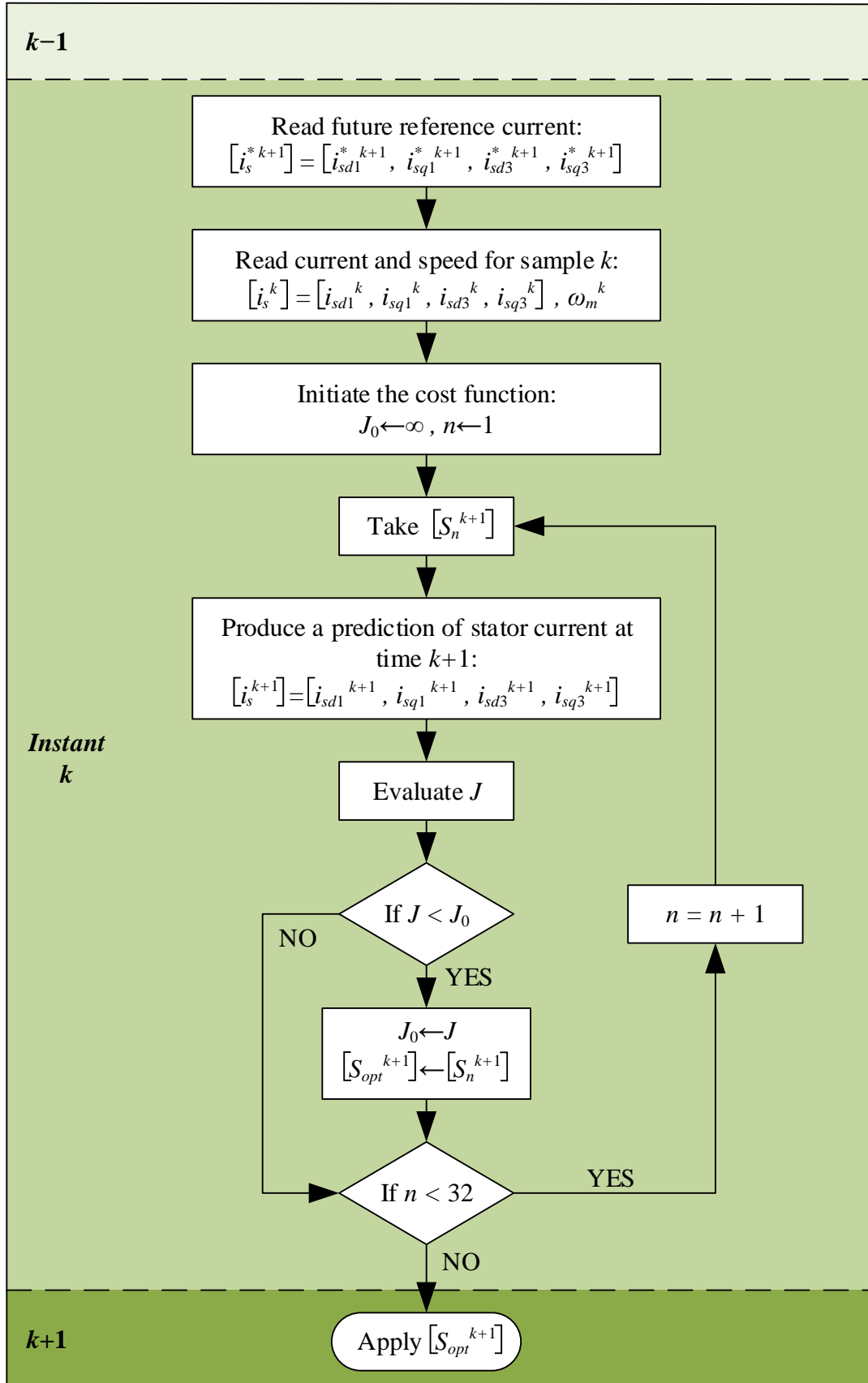


Figure 4.3. Second MPC stage to implement the proposed technique: FCS-MPC inner current controller.

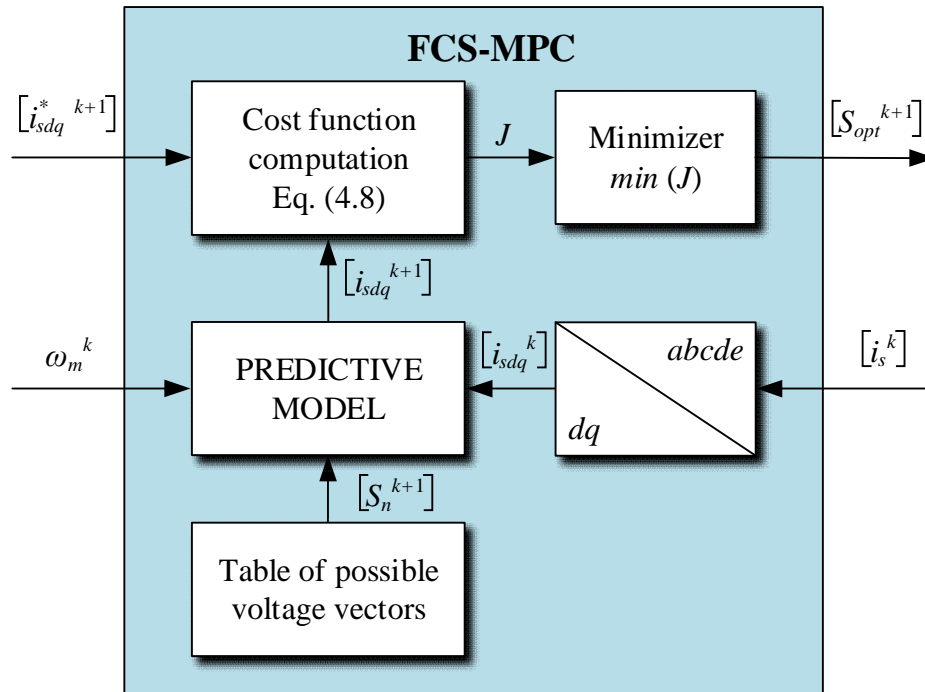


Figure 4.4. Block diagram of the second control stage based on the FCS-MPC method.

The optimal nature of the proposed technique is assured, since the optimization problem that leads to the optimal reference currents is convex and, therefore, it has only one optimal solution without local minima, checking the optimality condition and providing the optimal reference to the FCS-MPC controller. Then, the FCS-MPC stage uses a finite set of switching states, checking all of them to apply the optimal one that minimizes the designed cost function. Notice that a one-step prediction horizon is used in this study. Although better results are expected with longer prediction horizons, a bigger online calculation effort would be required and a prediction horizon equal to one should be enough to state the interest of the proposal.

4.3 Validation of the two-stage MPC method

This section is focused on the experimental verification of the optimal technique including in the system the limits that were previously introduced in Section 4.2. This verification is made using two different types of multiphase machine: a five-phase PMSM drive (case example #1), which is available in the laboratory L2EP of the École Nationale Supérieure d'Arts et Métiers – Campus de Lille, and a five-phase IM with concentrated windings (case example #2), which is available in the laboratory of the University of Seville. The following sections describe both systems and the different tests that have been carried out for every machine.

4.3.1 Case example #1: five-phase PMSM drive

A performance analysis of the proposed controller is done prior to its implementation in a real system, in the belief that the testing of the complex multiphase drive, under steady-state and

transient operating conditions, is a mandatory practice during both the controller development phase and before final system commissioning. A real-time simulation environment based on the OPAL-RT technology is selected for this purpose, to accelerate the analysis, to reduce risks associated with conducting tests on a physical system and to simplify its future implementation [185]. Notice that, despite a validation by a classical simulation could be enough, it can be very inconvenient in terms of the simulation speed. The utilization of FPGAs within the OPAL-RT environment allows a real-time simulation thanks to a hardware acceleration by multiple orders of magnitude. Furthermore, even though the proposed method is validated in a real-time simulation, the main hardware description language (HDL) design and software are developed in C and VHDL/System Generator, which can be directly transferred into an industrial application. The only difference would be the replacement of the OPAL-RT input/output interface with an appropriate industrial alternative, adding security checks for the possible overcurrent and faults.

A five-phase PMSM drive is used as a case example for these real-time simulations, whose parameters and the considered limits are detailed in Table C.2 in Appendix C. The model of this type of machine was studied in Section 2.2.4. The study is focused on the performance of the multiphase drive when online optimal reference currents are applied to get the reference torque, while minimizing the copper losses and respecting the defined maximum peaks values of currents and voltages (the maximum magnetization level is not considered in this case for the sake of simplicity). Then, the analysis is done in the open-loop torque regulation configuration to avoid any interference of the outer speed controller in the electrical performance of the system. The scheme of the technique to be applied in the five-phase PMSM drive using the OPAL-RT environment is presented in Fig. 4.5.

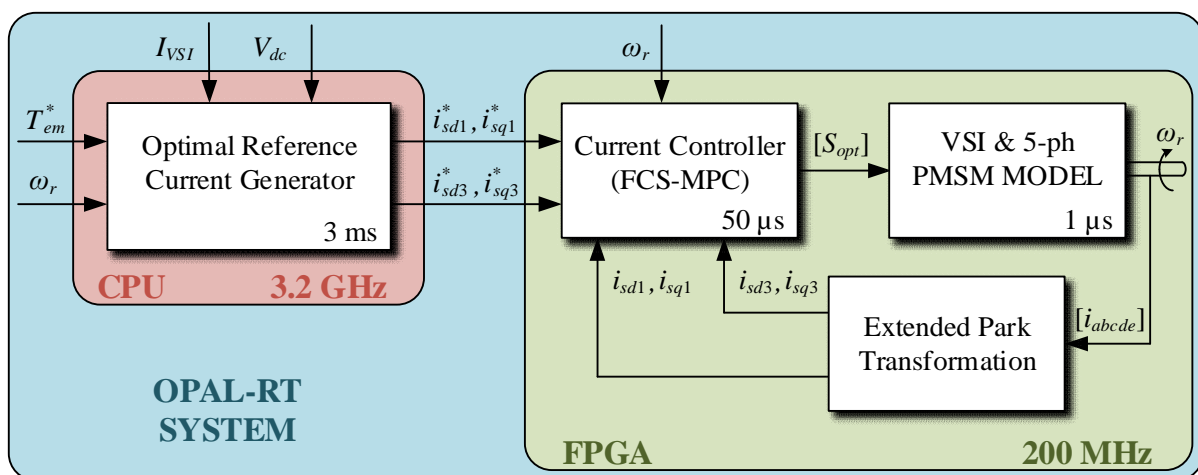


Figure 4.5. Description of the proposed technique in a real-time system based on OPAL-RT technologies for the case example #1.

In order to validate the proposed method, an experimental set-up system is programmed in a real-time system based on the OP5600 real-time simulator target platform complemented with the OP5607 extension module from OPAL-RT technologies. The Xilinx Virtex 7 FPGA of the OP5607 module is used for building the machine simulator and the FCS-MPC current controller, using an internal clock frequency of 200 MHz. On the other hand, the Intel Xeon CPU of the OP5600 platform is used to communicate with a host PC and to solve the optimal reference

generation, sending the obtained results to the FPGA as well as the reference inputs (such as the reference torque and speed). The CPU performance allows up to 3 ms of sampling time for the optimal reference current generator for single core mode, although further improvements could be obtained by parallelizing the solver. Notice, however, that the switching frequency is limited in real applications by the switching losses in the IGBT modules of the VSI. Then, the frequency of the FCS-MPC is set to 20 kHz due to this limitation, although the obtained frequency is lower. The obtained margin is employed in this case to reduce the resource use in the FPGA by further pipelining the mathematical operations in the predictor of the FCS-MPC controller.

Focusing on the machine simulator, it is running in the FPGA at 1 MHz with 1 μ s of sampling time. The model of the machine is discretized considering the forward Euler method since it is the easiest discretization process to be implemented. It also provides sufficient stability and precision for the used simulation time step (1 μ s), which it is much smaller than the smallest time constant of the machine. The inputs of the model are the mechanical load torque, phase voltages (or VSI switch configuration) and the DC-link voltage. The outputs are stator voltage and current values in both d - q and phase frames, along with the electrical torque and the speed of the machine. They are connected to four analog outputs of the OPAL-RT simulator and can be configured from the CPU part of the simulator.

The simulation model is split into multiple interconnected computation cores, which are responsible for various parts of the model. The general architecture of the FPGA implementation is shown in Fig. 4.6. The model is managed using a main controller that it is configured and supervised by the CPU part of the OPAL-RT simulator. Its main function is to generate synchronization signals, controlling the data flows between computation cores and insuring simulation synchronization with its time step. Other computation cores are: Park transformation, multiphase machine, torque estimator and mechanical model of the machine's rotor. The states of the simulation model are stored inside the corresponding cores and include the Park matrix, currents in d - q frame, the electrical torque, and the speed and position of the rotor, respectively.

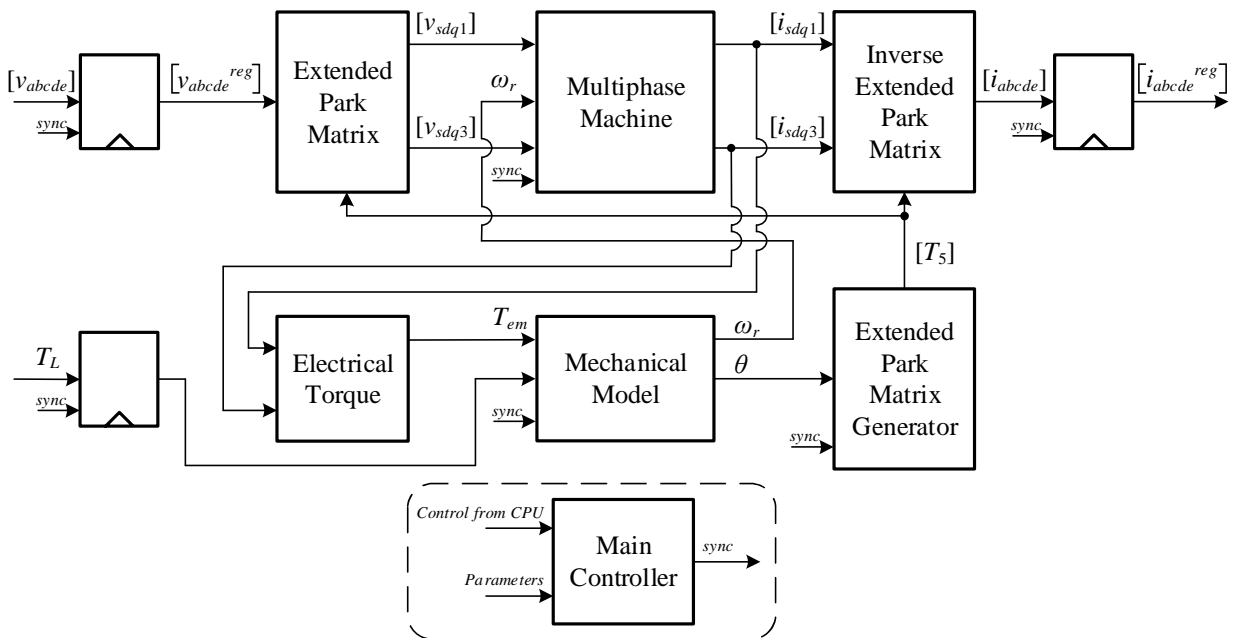


Figure 4.6. General architecture of the five-phase PMSM real-time model simulator in FPGA.

Computations are done in parallel and controlled through the synchronization signals. Figure 4.7 shows the computation timeline. First, the input voltages are converted from phase to d - q frame ($[v_{abcde}] \rightarrow [v_{sdq}]$) and the previous state currents from d - q to phase frame ($[i_{sdq}] \rightarrow [i_{abcde}]$), by using the Park matrix stored in the registers of its generator ($[T_5^k]$). Additionally, the new electrical torque (T_{em}^{k+1}) and speed (ω_r^{k+1}) are computed based on previous states of the model. Once the new speed is available, the new rotor position is found (θ^{k+1}) and the Park matrix is updated ($[T_5^{k+1}]$). When both new speed and d - q voltages are ready, new currents of first and third harmonic components can be calculated in parallel ($[i_{sdq1}^{k+1}]$ and $[i_{sdq3}^{k+1}]$, respectively), and a new simulation step can begin.

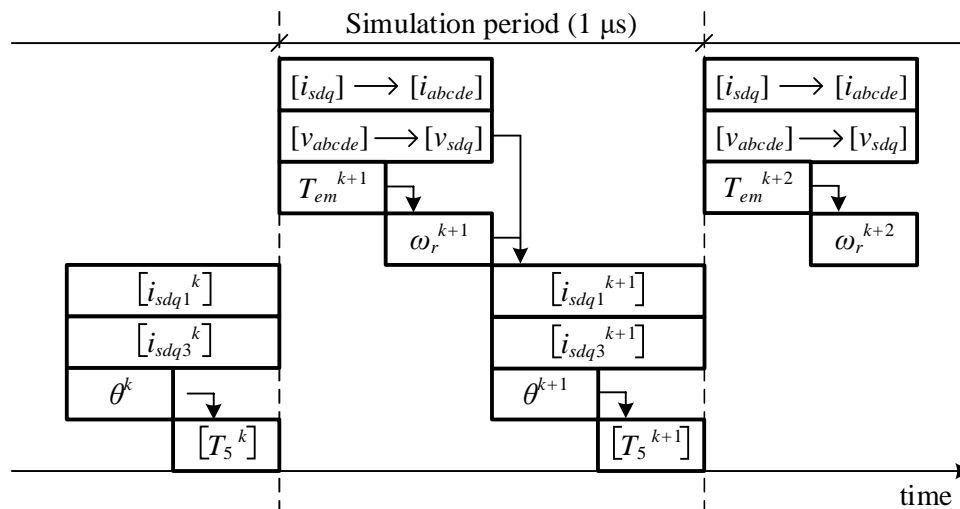


Figure 4.7. Computation timeline of the simulation model in the real-time system.

Since the extended Park matrix depends on the position of the rotor, each simulation step is generated using two look-up tables containing the values for sines and cosines, and it is stored in double registers. The extended Park matrix generator structure is shown in Fig. 4.8, where the sequencer is controlled by the external synchronization signal and iteratively populates the registers of the matrix using one of the look-up table and the corresponding rotor angle θ . Once the registers have been all written, they are stored in a second register array in such a way that the matrix changes instantly for the external cores. This approach allows to reduce the resource use in FPGA, taking advantage of the computation time of other cores of the model.

The main part of the simulation computation takes place in the multiphase machine core, based on d - q frame. The equations for first and third harmonic components are independent and can be simulated in parallel. Consider equations (2.124) and (2.125) in Section 2.2.4, which represent the voltages and fluxes of the machine. From these equations, the voltages of the fundamental component can be rewritten in the ordinary first-order differential equation form, as follows:

$$\frac{di_{sd1}}{dt} = \frac{1}{L_{sd1}} \cdot (v_{sd1} - R_s \cdot i_{sd1} + \omega_r \cdot L_{sq1} \cdot i_{sq1}) \quad (4.9)$$

$$\frac{di_{sq1}}{dt} = \frac{1}{L_{sq1}} \cdot (v_{sq1} - \omega_r \cdot L_{sd1} \cdot i_{sd1} - R_s \cdot i_{sq1} - \omega_r \cdot \lambda_{m1}) \quad (4.10)$$

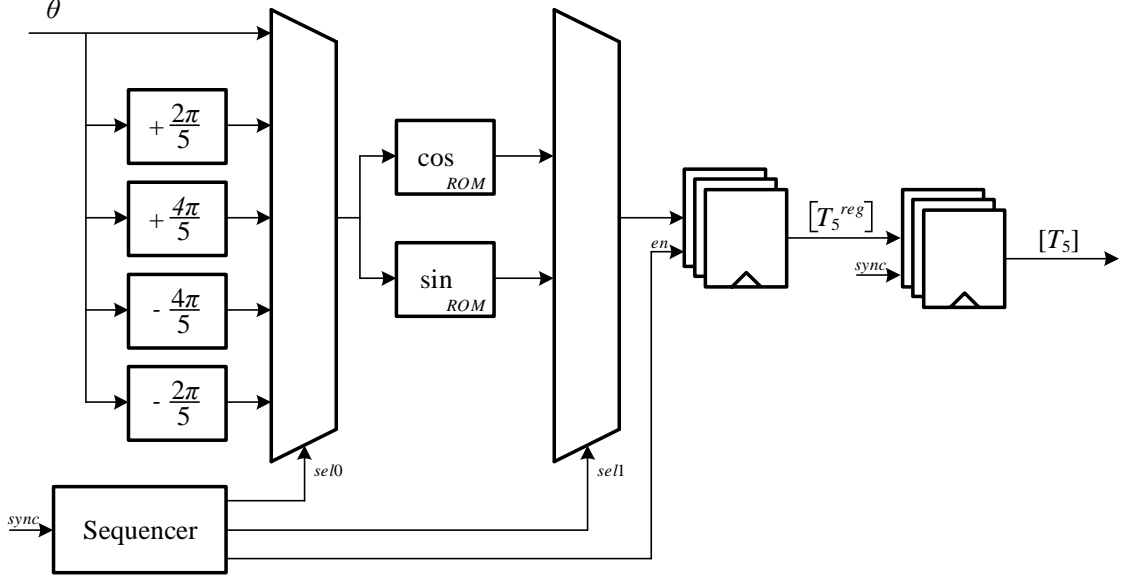


Figure 4.8. Extended Park matrix generator in the real-time system.

Then, new values for the currents are calculated at each simulation step using the following equations:

$$i_{sd1}^{k+1} = i_{sd1}^k + \frac{T_s}{L_{sd1}} \cdot (v_{sd1}^k - R_s \cdot i_{sd1}^k + \omega_r^k \cdot L_{sq1} \cdot i_{sq1}^k) \quad (4.11)$$

$$i_{sq1}^{k+1} = i_{sq1}^k + \frac{T_s}{L_{sq1}} (v_{sq1}^k - \omega_r^k \cdot L_{sd1} \cdot i_{sd1}^k - R_s \cdot i_{sq1}^k - \omega_r^k \cdot \lambda_{m1}) \quad (4.12)$$

being T_s a simulation step used for the modeling. The discretized equations for the third harmonic component can be obtained in a similar way. Summarizing, the equations for both subspaces can be written as follows:

$$\begin{pmatrix} i_{sd}^{k+1} \\ i_{sq}^{k+1} \end{pmatrix} = [\Gamma] \cdot \begin{pmatrix} v_{sd}^k \\ v_{sq}^k \end{pmatrix} + [\Phi] \cdot \begin{pmatrix} i_{sd}^k \\ i_{sq}^k \end{pmatrix} + [\Psi] \quad (4.13)$$

where $[\Gamma]$, $[\Phi]$ and $[\Psi]$ are matrices including parameters of the model and vary for each subspace (see Appendix A.3). These calculations define the core of the simulation and are implemented as a pipelined architecture. The previous values for the currents in $d-q$ frame are stored in registers controlled by the external synchronization signal and updated every simulation step.

Once the real-time simulation system has been described, and before presenting the obtained results, a preliminary analysis is done with the aim of selecting appropriate values for the weighting factors of the optimization problem of equation (4.7). For such purpose, the drive has been analytically studied (a simulation environment based on MATLAB[®] tools is used) within the valid operating region, where the ratio $\eta = \kappa_T/\kappa_i$ has been varied while the quadratic stator current $QI = i_{sd1}^2 + i_{sq1}^2 + i_{sd3}^2 + i_{sq3}^2$ and the torque quadratic error $QET = (T_{em}^* - T_{em})^2$ terms have been evaluated. With the intention of making a fair comparison, QI and QET have been represented in

a dimensionless manner, i.e. in terms of a percentage relative to their maximum values obtained in this test. Figure 4.9 depicts these dimensionless QI and QET values for one operating point (the reference speed is set at 50 rad/s with a torque of 10 N-m) and different η values. The crossing point of QI and QET curves represents a trade-off between copper losses reduction and torque tracking error. For example, the crossing point in the plotted case shows a value of $\eta = 22.47$, which corresponds to a 26.14% of copper losses and the same percentage of torque tracking error (both with respect to their maximum values in the test). It is interesting to mention that quite similar plots are obtained when different operating points are considered (Table 4.1 summarizes these results for different operating points). However, since the final objective is to control the machine at the desired speed and torque, the reduction of the torque tracking error must predominate and the η value should be higher than the ones of the crossing points. Therefore, a value of $\eta > 100$ seems to be an appropriate choice, guaranteeing good torque tracking in the system. In this case, the weighting factors are set to $\kappa_i = 1$ and $\kappa_T = 200$ to ensure good torque tracking in the whole operating region and, when it is also possible, reduce the copper losses in the multiphase machine.

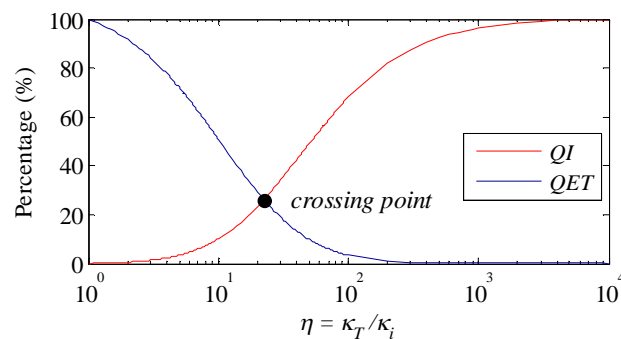


Figure 4.9. Evaluation of the dimensionless QI and QET terms using different η values when the PMSM is driven at a particular operating point (50 rad/s and 10 N-m).

Table 4.1. A representative set of obtained QI and QET curves in terms of their crossing points at different working conditions for case example #1.

Reference torque (N-m)	Mechanical speed (rad/s)			
	50	100	150	200
5	26.14%, $\eta = 22.47$	26.14%, $\eta = 22.47$	25.92%, $\eta = 26.71$	19.03%, $\eta = 56.22$
10	26.14%, $\eta = 22.47$	26.14%, $\eta = 22.47$	25.71%, $\eta = 27.81$	29.15%, $\eta = 59.06$
15	26.14%, $\eta = 22.47$	26.14%, $\eta = 22.47$	24.28%, $\eta = 29.65$	28.33%, $\eta = 31.04$

Different tests have been carried out to validate the proposed technique, using the machine parameters and limits detailed in Table C.2 (see Appendix C) as well as the aforementioned real-time system. First, the ability of the technique to generate optimal reference currents while respecting the limits over the entire speed range (from zero to the limit speed of the machine) is analyzed, summarizing Fig. 4.10 the obtained results. Figures 4.11 and 4.12 complement this analysis, showing the steady-state operation of the system in different operating points, including the operation without electrical limits, with one current or voltage limit and with the application of both limits. The dynamic behavior is also verified, and Fig. 4.13 summarizes the obtained

results. In this case, the multiphase machine is operated outside the feasible region to focus on the operation of the system when the voltage and current limits are applied.

The first set of tests includes the steady-state analysis of the controlled system in different operating points. A speed ramp is imposed to the machine from 0 rad/s to the limit speed of 240 rad/s, while the reference torque is always set higher than the maximum value (19.27 N·m, see Table C.2 in Appendix C), making that the peak value of phase currents is equal to the established limit (50 A) during the whole test. The maximum torque versus speed characteristic of the electrical machine is then obtained, once the steady-state operation of the system is reached, as it is shown in Fig. 4.10a (blue ink). Figure 4.10a also illustrates the considered case studies, when the electrical limits are not reached (reference points in region 1 or case 1), if the current limit must be applied (reference points in region 2 or case 2), if the voltage limit is considered (reference points in region 3 or case 3), and taking into account the voltage and current constraints (reference points in region 4 or case 4). The evolution of dq_1 and dq_3 currents is also plotted in Fig. 4.10b, showing the steady-state performance of the system depending on the operating point.

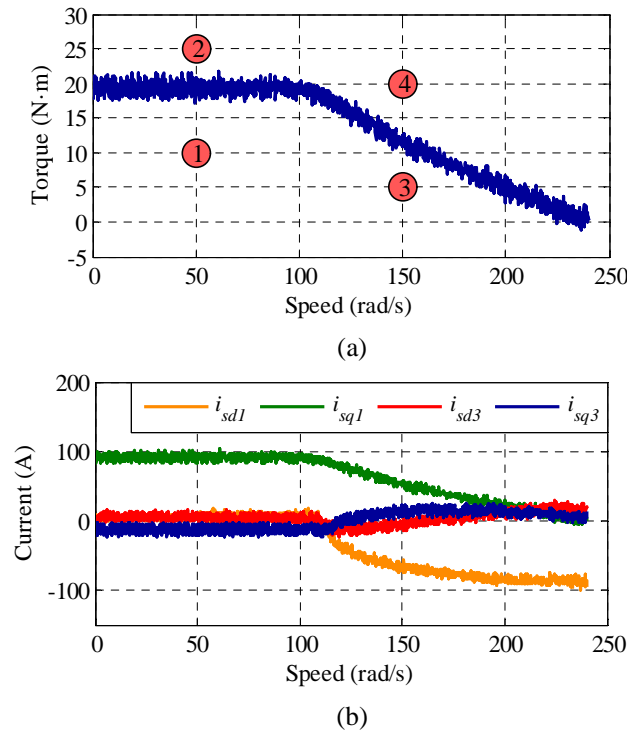


Figure 4.10. Real-time simulation for the steady-state analysis of the 5-phase PMSM drive, including a speed ramp test where the speed is varied in the machine from 0 rad/s to 240 rad/s and the reference torque is higher than the maximum value. (a) Obtained electrical torque versus speed characteristic of the system. (b) Evolution of dq_1 and dq_3 stator current values.

Notice that below the base speed (100 rad/s), the voltage limit is never reached, therefore obtained i_{sd1} and i_{sd3} values are equal to zero and the machine is not in the flux-weakening region. Furthermore, i_{sq1} is always positive to produce a positive electrical torque when the fundamental of the flux is applied, but i_{sq3} (which represents the third harmonic component of the stator current) is negative to guarantee that the maximum peak value for the phase current is not exceeded at the price of generating a negative electrical torque in the system. Once the base speed is reached, i_{sd1}

and i_{sd3} currents become negative in order to comply with the voltage limit. It is noteworthy that the machine is now operating in the well-known flux-weakening region and the system is also regulated in this case optimizing the third harmonic current components, i_{sd3} and i_{sq3} values, to be respectful with the established limits. This analysis shows that the optimal method manages the system taking into account the limits and following the real-time established optimization problem.

The previous analysis is complemented in Figs. 4.10 and 4.11, where the steady-state performance of the system in four different case studies (corresponding with the cases illustrated in Fig. 4.10a) is analyzed. These reference points are detailed in Table 4.2, where the applied reference torque and speed are shown. The evolution of the phase current is plotted in Figs. 4.11a and 4.12a in order to see if the current limit is reached in the analyzed cases. Notice that only one phase (phase ‘a’) is shown for the sake of clarity, but similar results are obtained for the rest of the stator current phases, from ‘b’ to ‘e’. Figures 4.11b and 4.12b depict all filtered phase-to-phase voltages (u) to find out that the voltage limits are regulated. When the machine operates and the established limits are not reached (case 1, Fig. 4.11a, left plot), it is observed that the obtained phase current using the optimal references from the proposed method (orange ink) is quite similar to the one corresponding with the analytical solution (green ink) that is found imposing the analytical optimal d - q reference currents from the copper losses point of view [141]:

$$i_{sd1}^* = 0 \quad (4.14)$$

$$i_{sq1}^* = \frac{\varepsilon_{sq1}}{\sum_{i=1,3} \varepsilon_{sqi}^2} \cdot T_{em}^* \quad (4.15)$$

$$i_{sd3}^* = 0 \quad (4.16)$$

$$i_{sq3}^* = \frac{\varepsilon_{sq3}}{\sum_{i=1,3} \varepsilon_{sqi}^2} \cdot T_{em}^* \quad (4.17)$$

being ε the speed-normalized back EMF. This result verifies a good similarity between the proposed technique and the analytical optimal solution if the constraints are not reached. In all the other cases, the current and voltage limits are considered and regulated by the proposed method, although the obtained current cannot be compared with any analytical optimal solution. Obtained results prove the reliability of the optimal technique, which complies the voltage and current limitations in every case study.

Table 4.2. Analyzed steady-state reference points in Figs. 4.11 and 4.12.

Case	Operation	Reference torque	Speed
1	Below the limits	10 N-m	50 rad/s
2	Under current limit	25 N-m	50 rad/s
3	Under voltage limit	5 N-m	150 rad/s
4	Under current and voltage limit	20 N-m	150 rad/s

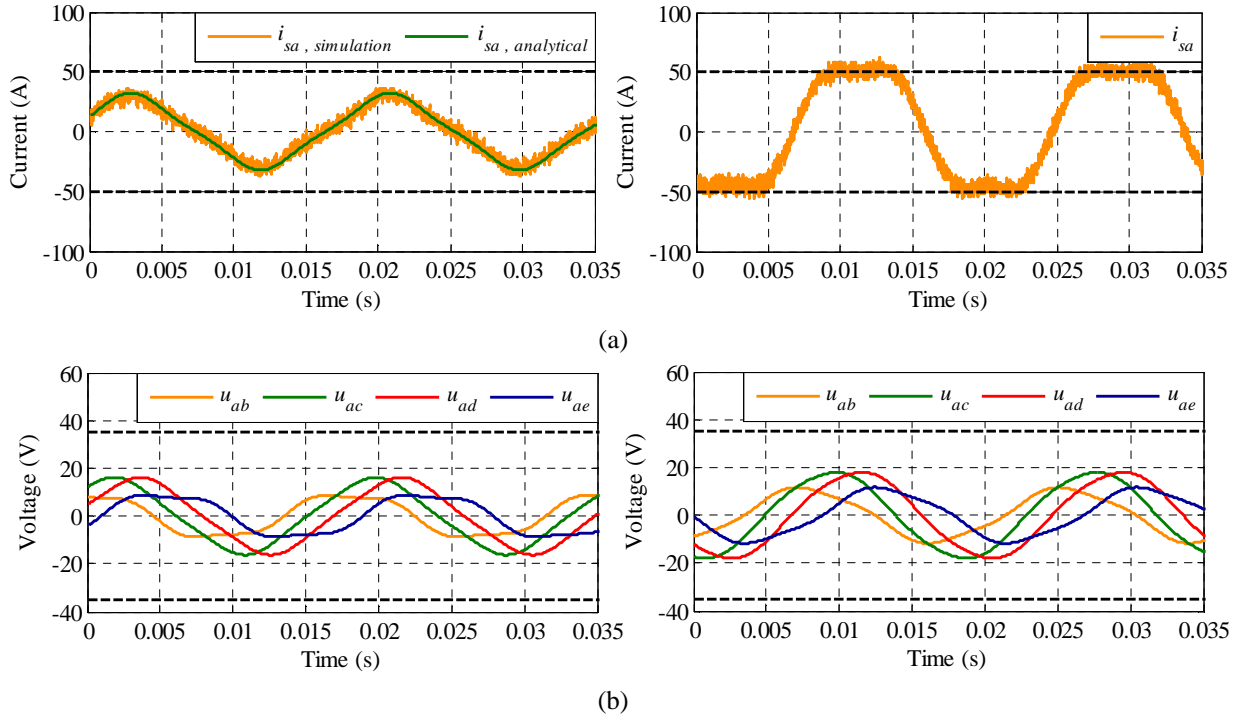


Figure 4.11. Real-time simulation of the steady-state operation of the 5-phase PMSM drive in cases 1 and 2: operation without considering voltage or current limits (left plots) and considering the current limit (right plots). (a) Stator phase current. (b) Filtered phase-to-phase stator voltages.

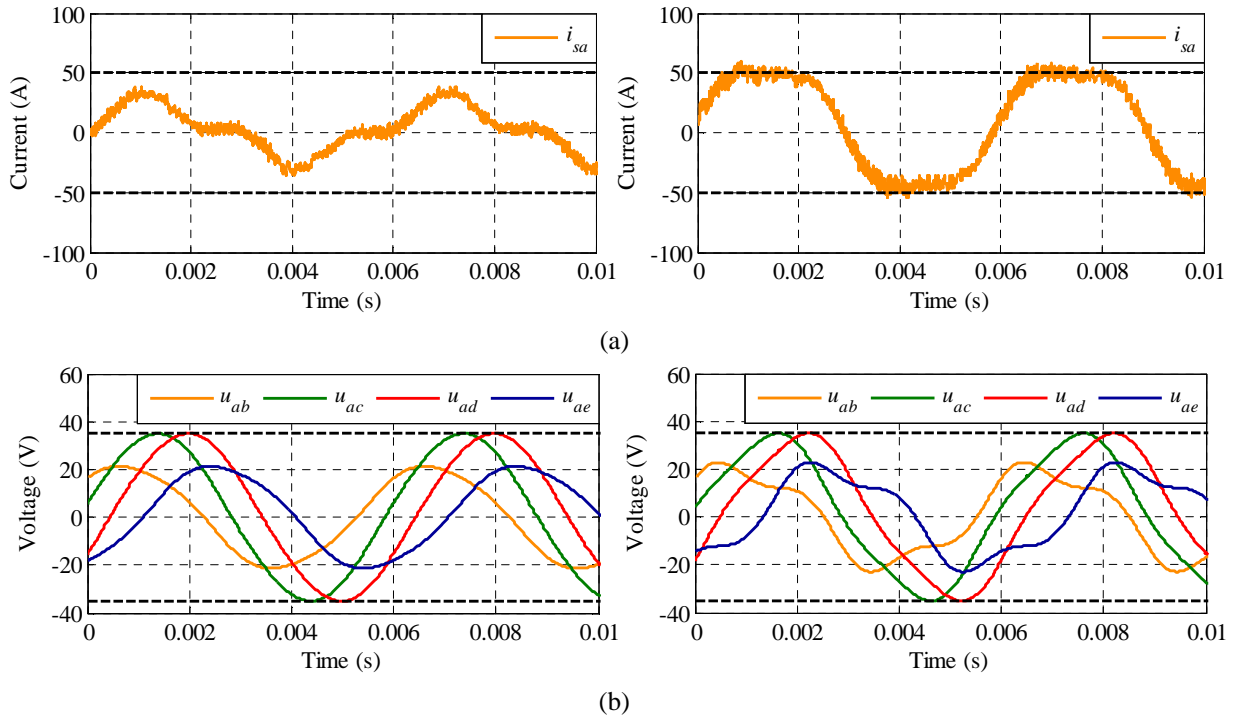


Figure 4.12. Real-time simulation of the steady-state operation of the 5-phase PMSM drive in cases 3 and 4: operation considering a voltage limit (left plots) and taking into account current and voltage limits (right plots). (a) Stator phase current. (b) Filtered phase-to-phase stator voltages.

Finally, the dynamic operation of the system using the proposed controller is analyzed imposing a reference torque step from 0 to 20 N-m (at $t = 0.01$ s approximately) while the machine is regulated at 150 rad/s during the whole test (the system is working over the base speed operating point). It is important to note that this reference point (20 N-m and 150 rad/s) is clearly out of the feasible region of the machine. The obtained torque response is shown in Fig. 4.13a, where the generated torque cannot achieve the reference. This is an expected performance because the reference point is out of the maximum torque versus speed characteristic of the machine. The obtained torque is about 12 N-m, which corresponds with the maximum available torque that the machine can produce operating at 150 rad/s (see Fig. 4.10a). On the other hand, the evolution of dq_1 and dq_3 currents is depicted in Fig. 4.13b. The machine is in the flux-weakening region during the whole experiment: i_{sd1} and i_{sd3} currents are not zero, being optimally adapted in real time to respect the voltage limit. Meanwhile, i_{sq1} and i_{sq3} currents are zero before $t = 0.01$ s because no generated torque is required. Once the reference torque step is applied, i_{sq1} and i_{sq3} currents become positive to maximize the produced torque while respecting the current limit. It is shown again that the obtained reference currents using this technique are appropriate and the proposed controller is viable. It is interesting to highlight that the obtained results do not consider the parameter uncertainty of the system, which is out of the scope of this work. Parameter uncertainty is a complex research field in electromechanical systems when MPC controllers are used [116], but also when conventional PI-PWM control techniques are applied, where the estimation of the rotor flux position is mandatory.

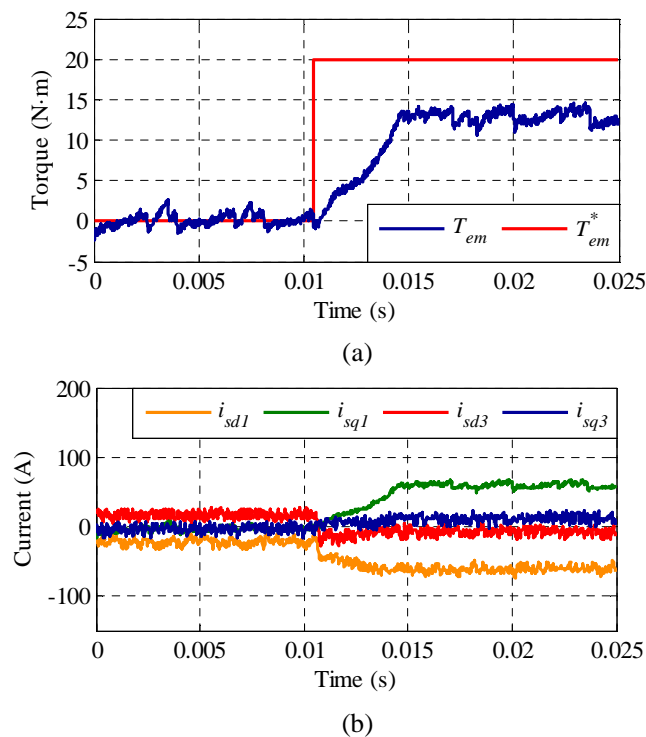


Figure 4.13. Real-time simulation of the dynamic response of the 5-phase PMSM drive using the proposed technique under current and voltage limits. The reference torque is changed from 0 to 20 N-m (at $t = 0.01$ s approximately), while the machine operates at 150 rad/s (above the base speed). (a) Torque response. (b) Evolution in dq_1 and dq_3 stator currents.

4.3.2 Case example #2: five-phase concentrated winding IM drive

While the test rig utilized in the case example #1 is based on a real-time simulator technology, an experimental system is available in Seville, where the feasibility of the proposed controller can be validated in a real system. This is done employing the same test rig of the experimental validations of Chapter 3 (see Fig. 3.8) but using a five-phase IM with concentrated windings, whose parameters and considered limits are gathered in Table C.3 of Appendix C. The machine is supplied by two three-phase inverters from SEMIKRON that are connected to a DC-link of 300 V from an independent DC power supply. The control algorithm is implemented in a TM320F28335 DSP placed on a MSK28335 Technosoft board. An external programmable load torque is also introduced by means of an independently controlled DC motor. Finally, the rotor mechanical speed is measured using a GHM510296R/2500 encoder that is coupled to the shaft of the multiphase IM.

In this case, the computational power and memory capacity of the DSP employed is not enough to solve online the optimization problem of the control strategy. A practical solution has been considered, which consists on calculate offline the optimal d - q reference currents through the optimization stage previously described in this chapter and store them in look-up tables whose inputs are the reference torque and speed. Such look-up tables are used by the DSP to implement the inner current controller through the FCS-MPC method.

As in the case example #1, a preliminary analysis is done to select appropriate values for the weighting factors used in the objective function F of the optimization problem. The drive is analyzed using a simulation environment based on MATLAB[®] tools. The ratio $\eta = \kappa_T/\kappa_i$ is varied while evaluating the quadratic stator current $QI = i_{sd1}^2 + i_{sq1}^2 + i_{sd3}^2 + i_{sq3}^2$ and the torque quadratic error $QET = (T_{em}^* - T_{em})^2$ terms. Figure 4.14 plots the obtained dimensionless QI and QET values for one operating point (the reference speed is set at 20 rad/s with a torque of 6 N-m) and different η values. The crossing point of QI and QET curves in this case shows a value of $\eta = 1.82$, with a 36.68% of copper losses and torque tracking error. Table 4.3 summarizes the obtained results for different operating points. Once again, this ratio should be higher than the ones of the crossing points, and a value of $\eta > 5$ seems to be an appropriate choice, guaranteeing good torque tracking in the system. In this case, the weighting factors are set to $\kappa_i = 1$ and $\kappa_T = 10$ to guarantee good torque tracking in the whole operating region, while reducing the copper losses in the machine.

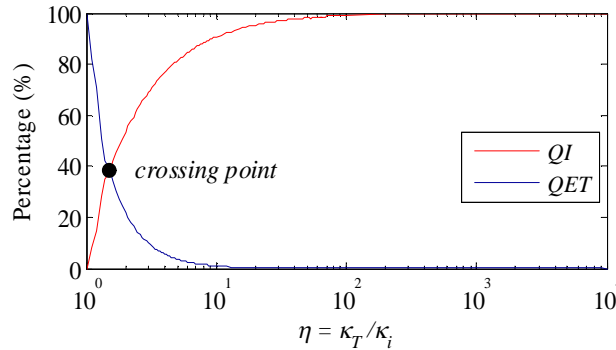


Figure 4.14. Evaluation of the dimensionless QI and QET terms using different η values when the 5-phase CW-IM is driven at a particular operating point (20 rad/s and 6 N-m).

Table 4.3. A representative set of obtained QI and QET curves in terms of their crossing points at different working conditions for case example #2.

Reference torque (N-m)	Mechanical speed (rad/s)				
	20	60	100	140	180
2	36.90%, $\eta=1.77$	36.90%, $\eta=1.77$	36.90%, $\eta=1.77$	26.95%, $\eta=3.29$	34.68%, $\eta=2.35$
4	36.72%, $\eta=1.81$	36.73%, $\eta=1.81$	34.53%, $\eta=2.28$	37.05%, $\eta=1.77$	37.91%, $\eta=1.69$
6	36.68%, $\eta=1.82$	36.65%, $\eta=1.82$	37.66%, $\eta=1.66$	34.96%, $\eta=1.60$	38.87%, $\eta=1.72$
8	36.66%, $\eta=1.83$	41.62%, $\eta=1.21$	37.42%, $\eta=1.75$	36.57%, $\eta=1.72$	38.29%, $\eta=1.51$

For the experimental tests, in this case the machine is closed-loop controlled, using the general scheme of the control strategy (see Fig. 4.1). The outer speed control loop is based on an Indirect Rotor Field Oriented Control (IRFOC) strategy, allowing the decoupling of the flux and the torque for the control purpose. In the d - q reference frame, it is assumed that fundamental and third harmonic rotor flux components are only attached to d_1 - and d_3 -axes, respectively, while no linkages exist on the q_1 - and q_3 -axes, as stated by (4.18). As a result, torque and flux productions are independently controlled, being i_{sd1} and i_{sd3} responsible of the regulation of the two rotor fluxes (fundamental and third harmonic), while i_{sq1} and i_{sq3} are related to the electrical torque production of first and third space harmonics, respectively.

$$\lambda_{rq1} = \frac{d\lambda_{rq1}}{dt} = 0 \quad ; \quad \lambda_{rq3} = \frac{d\lambda_{rq3}}{dt} = 0 \quad (4.18)$$

The present study starts by analyzing the ability of the reference current generator to produce optimal d - q references in all the speed range that produce the maximum torque while respecting the imposed limits and minimizing the copper losses. Five experimental tests have been conducted to study the steady-state performance of the system when the optimized references are applied in the available speed range. All the experiments have been carried out applying a constant reference speed of 20, 40, 60, 80 and 100 rad/s, and a load torque equal to the maximum available one to reach the electrical limits and force the optimization block action. The machine is driven to the steady state and the obtained results are shown in Fig. 4.15, where the mean values of the electrical torque and reference stator currents are plotted with filled circles. The maximum values of phase-to-phase stator voltages and phase stator currents (normalized to their limit values, V_{dc} and I_{VSI} , respectively) are shown in Fig. 4.15b, where two regions can be clearly identified. The third harmonic is fully exploited to produce the maximum torque while respecting the current limit in region 1, named constant torque region. The voltage limit is never reached and the flux-components of the current, i_{sd1} and i_{sd3} , do not exceed their maximum values of equations (4.5) and (4.6), respecting the maximum magnetization level. Region 2, or torque breakdown region, starts when the DC-link voltage becomes insufficient to inject the maximum phase current. When the voltage limit is reached, the flux-weakening is forced in the drive and the generated electrical torque is gradually reduced with the speed. Since the third harmonic component of the magnetic field requires an important portion of the DC-link voltage in detriment of the fundamental component, and this last component mostly generates the electrical torque in the machine, the reduction in dq_3 currents is larger than in dq_1 currents in region 2, being nearly zero at high speed.

An important issue in concentrated winding electrical drives is the torque enhancement due to the third harmonic injection. A comparison of the maximum obtained torque with and without third harmonic injection is detailed in Fig. 4.16, where previous experiments were reproduced forcing zero i_{sd3} and i_{sq3} values. Again, filled circles represent the obtained experimental results, and a significant increment in the obtained maximum torque can be observed (about 26% in region 1). It is important to remark that a MATLAB[®] simulation environment has been used in Figs. 4.15 and 4.16 to simulate the system and obtain the plotted curves in order to complete the results of the experimental analysis (filled circles), avoiding the record and memory limitations of the control board and reducing the number of experiments in the considered speed range.

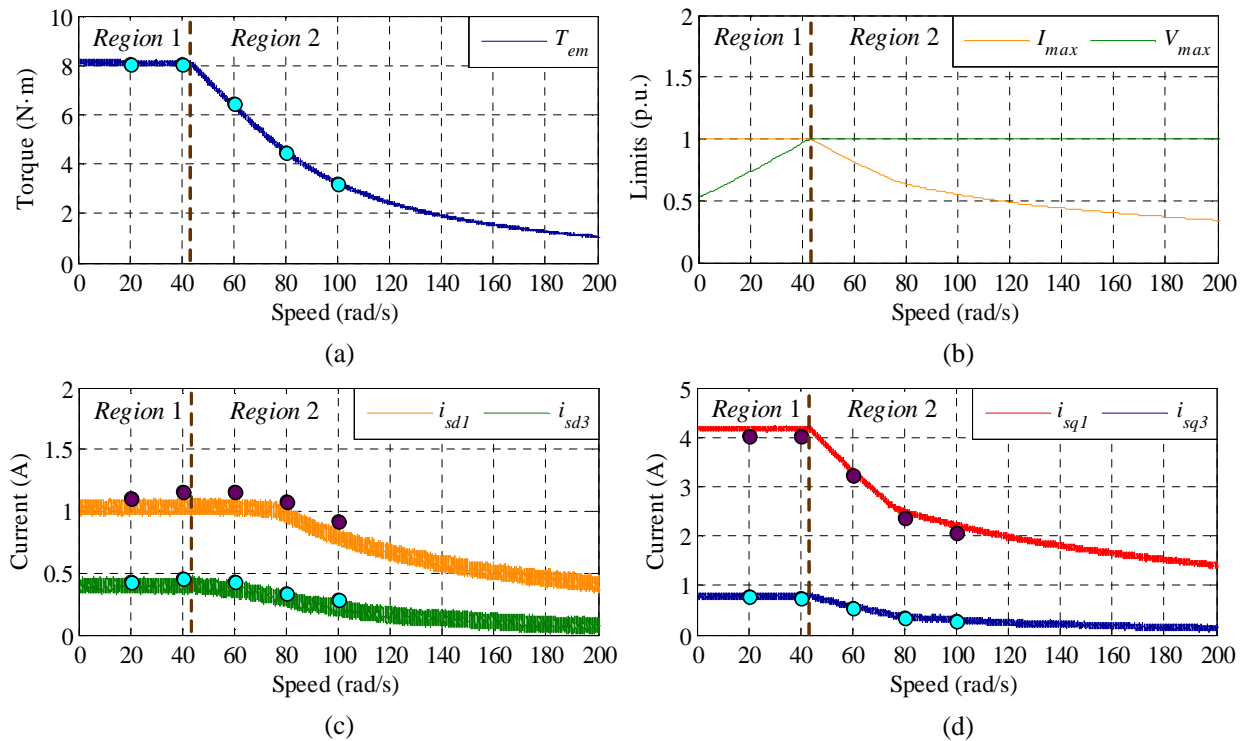


Figure 4.15. Experimental test for the steady-state analysis of the proposed controller using a 5-phase CW-IM drive. (a) Maximum obtained electrical torque versus speed. (b) Maximum phase-to-phase stator voltage and phase stator current (normalized to their limit values, V_{dc} and I_{VSI} , respectively). (c) Stator currents in d_1 - and d_3 -axes. (d) Stator currents in q_1 - and q_3 -axes.

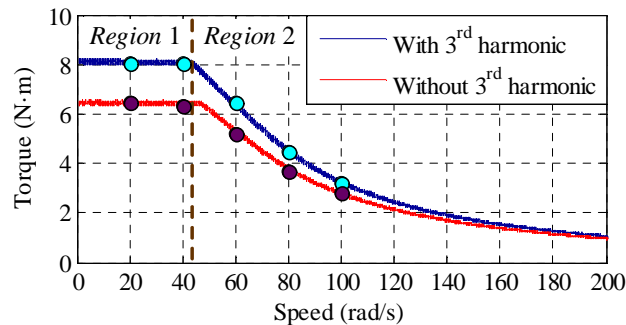


Figure 4.16. Maximum electrical torque in the experimental system based on the 5-phase CW-IM drive with and without the injection of third harmonic stator current components.

The previous analysis is complemented with some experimental tests to study the time performance of the controlled system. The first one is summarized in Fig. 4.17, where the maximum load torque is applied at a reference speed of 20 rad/s, being the system in steady state within the constant torque region (region 1). It can be observed a good tracking performance of the mechanical speed (Fig. 4.17a), while the values of the torque and dq_1 and dq_3 currents correspond to optimal values previously obtained (Figs. 4.17b, 4.17c and 4.17d respectively). Notice that the current limit is reached in the analyzed case, as it is shown in Fig. 4.17e, where the phase current 'a' is plotted. The rest of the stator currents in the multiphase machine have a similar behavior and they are omitted in the representation for the sake of clarity. The frequency decomposition of phase-to-phase voltages is depicted in Fig. 4.17f, where voltage u_{ac} is shown. Interestingly enough, two peaks appear corresponding with the fundamental and third harmonic components, showing that the voltage limit is not reached during the experiment.

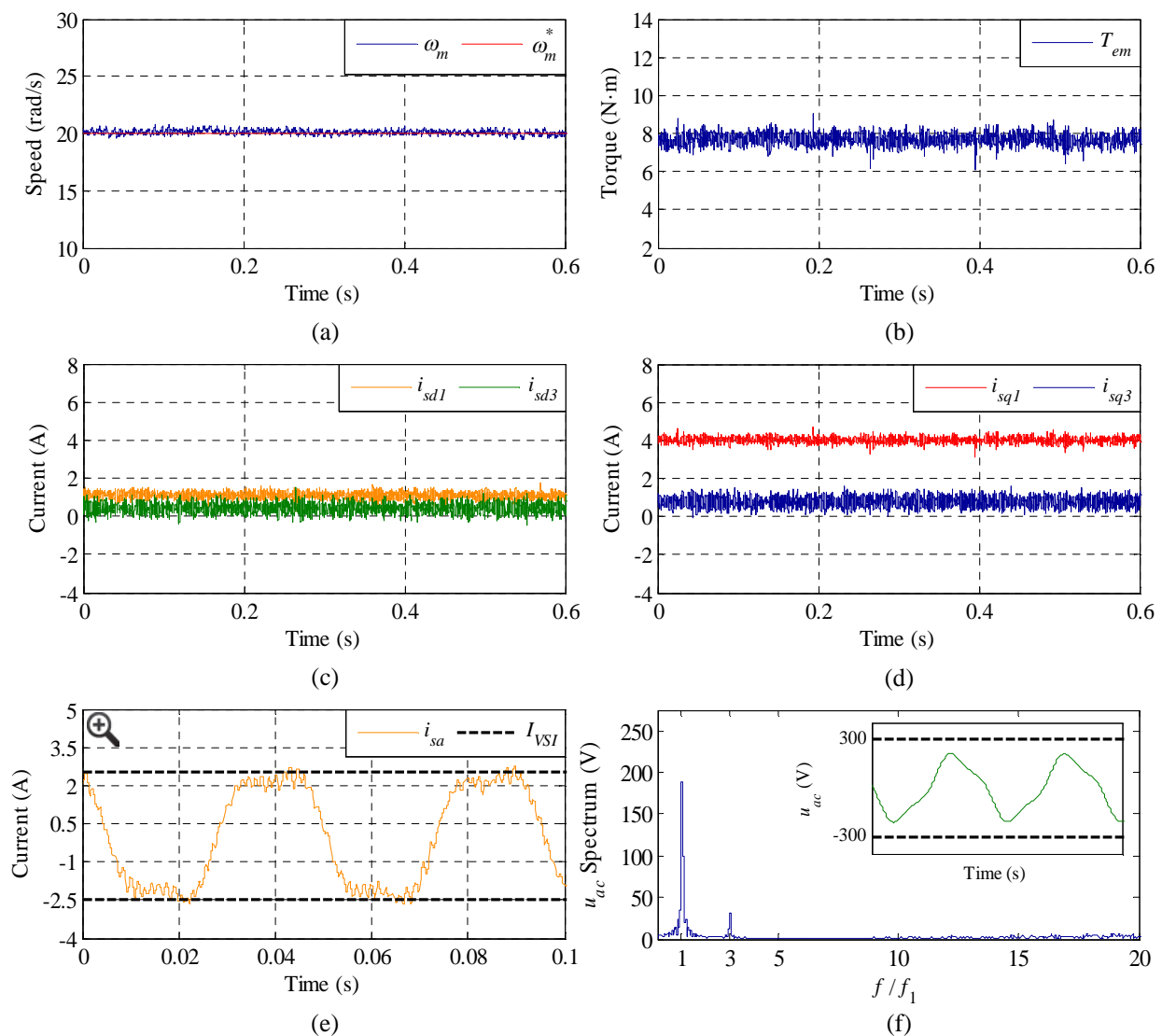


Figure 4.17. Experimental test of the 5-phase CW-IM drive when the maximum load torque is applied at a reference speed of 20 rad/s. (a) Measured mechanical speed versus the applied reference. (b) Obtained electrical torque. (c) Stator currents in d_1 - and d_3 -axes. (d) Stator currents in q_1 - and q_3 -axes. (e) Stator phase current 'a'. (f) Time-domain performance and frequency spectrum of phase-to-phase voltage u_{ac} .

A second experiment is presented in Fig. 4.18, where the torque breakdown region is considered. The machine is driven with a reference speed of 60 rad/s while the maximum allowable load torque at this speed is applied (about 6.4 N·m, see Fig. 4.18b). Under these conditions, the system is working with the optimal dq_1 and dq_3 stator current values obtained from the optimization stage (Figs. 4.18c and 4.18d), being the phase current value below the imposed limit (Fig. 4.18e, where only one stator phase current is again plotted for the sake of clarity, having a similar performance the rest of the stator currents). However, the voltage limit condition is reached, as it can be seen in Fig. 4.18f.

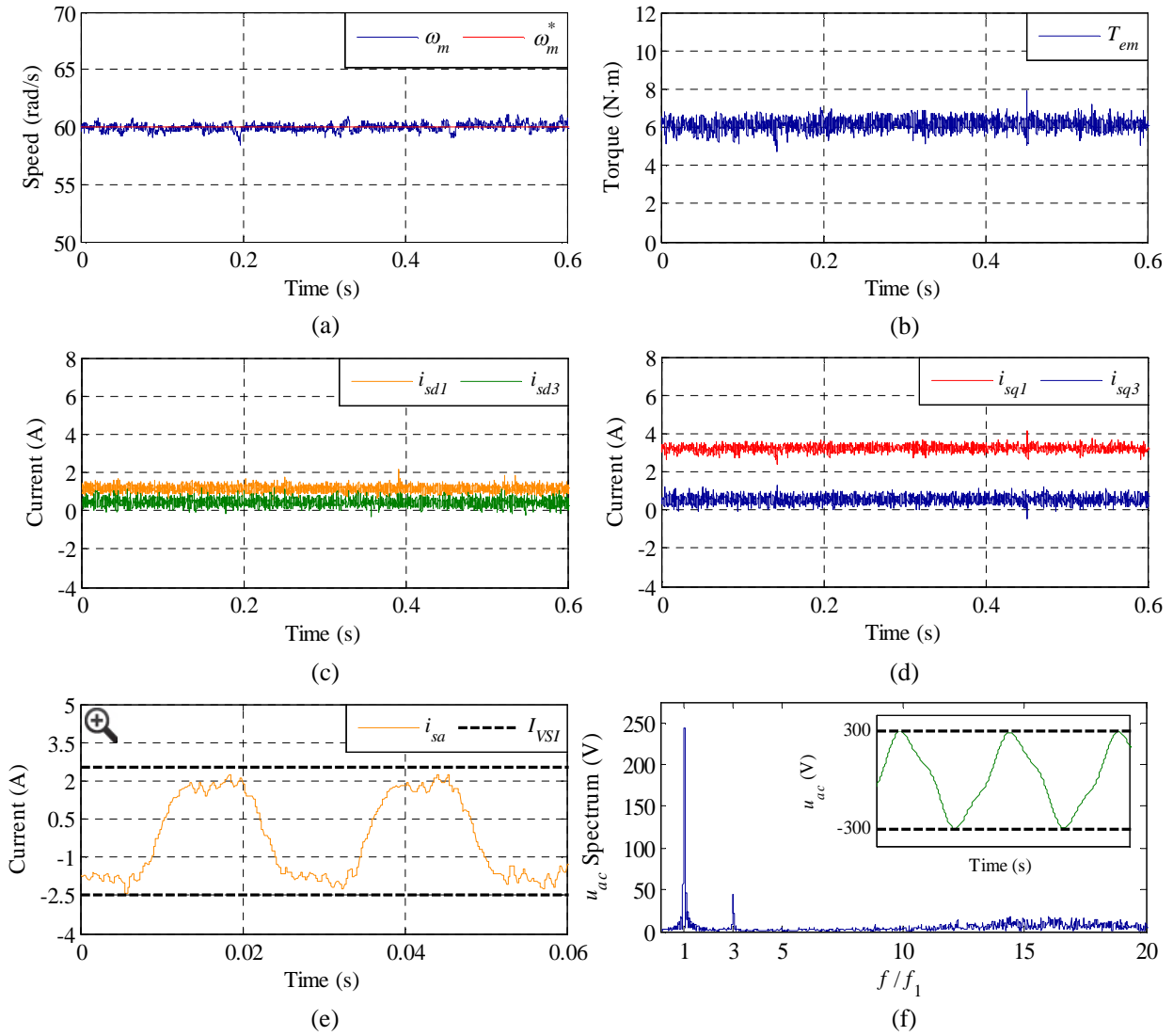


Figure 4.18. Experimental test of the 5-phase CW-IM drive when the maximum load torque is applied at a reference speed of 60 rad/s. (a) Measured mechanical speed versus the applied reference. (b) Obtained electrical torque. (c) Stator currents in d_1 - and d_3 -axes. (d) Stator currents in q_1 - and q_3 -axes. (e) Stator phase current 'a'. (f) Time-domain performance and frequency spectrum of phase-to-phase voltage u_{ac} .

The dynamic operation of the controlled system has also been studied in Figs. 4.19 and 4.20. First, a torque step test is presented in Fig. 4.19, where a reference speed of 20 rad/s is imposed and a load torque (T_L) step from 6.4 N·m to 8.13 N·m is applied. Notice that the starting system

conditions meet both current and voltage limits, ending with a maximum torque condition where the current limit is reached within the constant torque region, as it can be appreciated in Fig. 4.19e. A graphic representation of the operating point evolution is shown in Fig. 4.19f. From Figs. 4.19a and 4.19b it can be stated that the speed tracking performance is smooth and adequate, although a slight decrement in the value can be appreciated when the torque step is applied. Moreover, dq_1 and dq_3 currents (Figs. 4.19c and 4.19d) reach their optimal values, while q -current components increase with the torque.

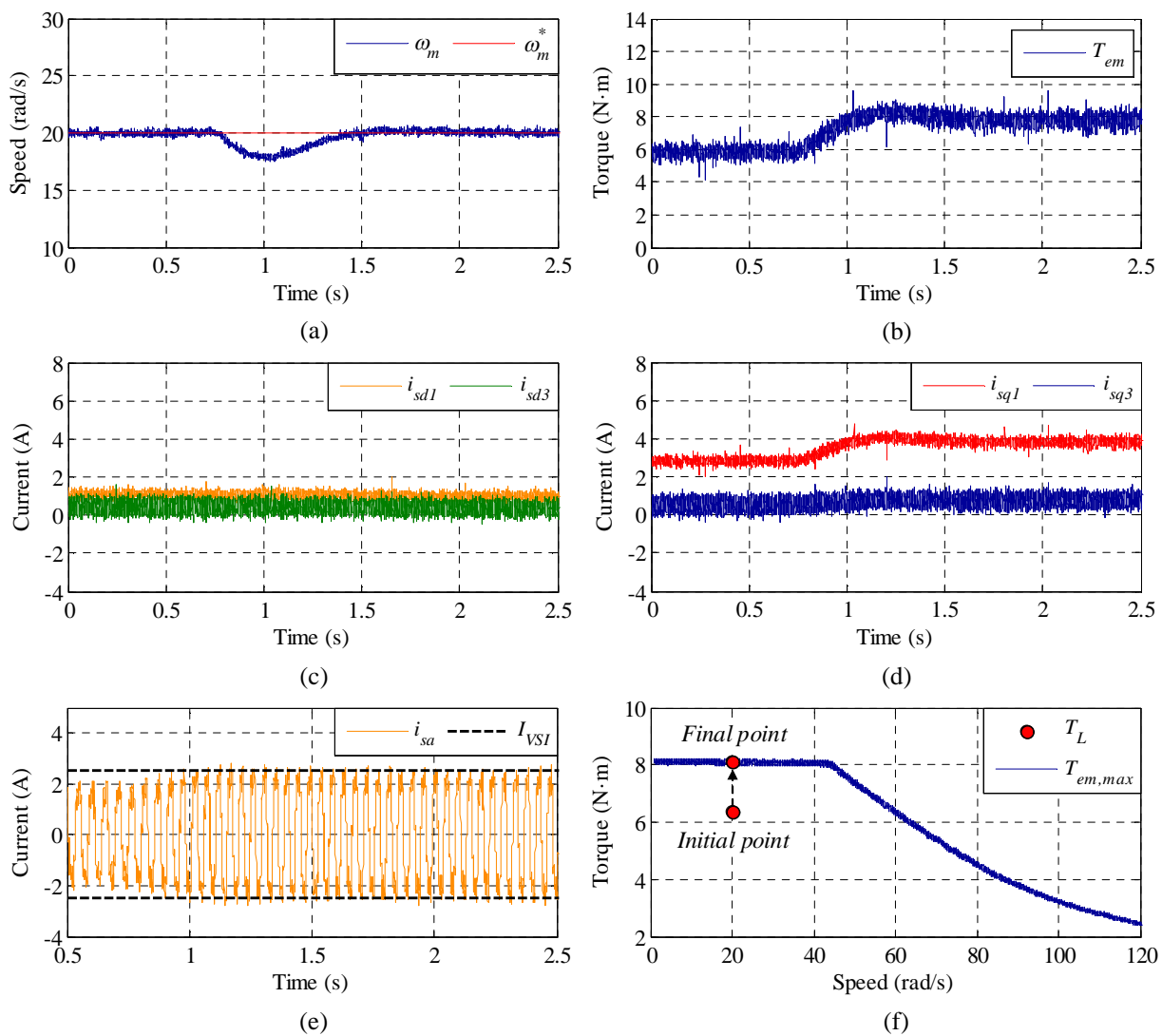


Figure 4.19. Experimental test of the dynamic response of the 5-phase CW-IM drive for a reference speed of 20 rad/s and a load torque step from 6.4 N·m to 8.13 N·m. (a) Measured mechanical speed versus the applied reference. (b) Obtained electrical torque. (c) Stator currents in d_1 - and d_3 -axes. (d) Stator currents in q_1 - and q_3 -axes. (e) Stator phase current ' a '. (f) System evolution in the maximum torque-speed curve.

Finally, a second dynamic test is obtained considering a speed step from 40 to 60 rad/s at a load torque of 6.4 N·m (the maximum available one when the system is operated at 60 rad/s), where the system enters in the torque breakdown region. The obtained results are presented in Fig. 4.20, where a schematic representation of the system evolution is plotted in Fig. 4.20f for a better

understanding of the experiment. The starting point of the experiment is below the electrical limits of the system. However, the voltage limit is reached when the speed step is applied in order to track the new reference speed as soon as possible. It can be appreciated that the stator current limit is also reached while the imposed reference speed step is tracked (see Fig. 4.20e), and dq_1 and dq_3 stator current components are regulated to their optimal values in Figs. 4.20c and 4.20d, respectively.

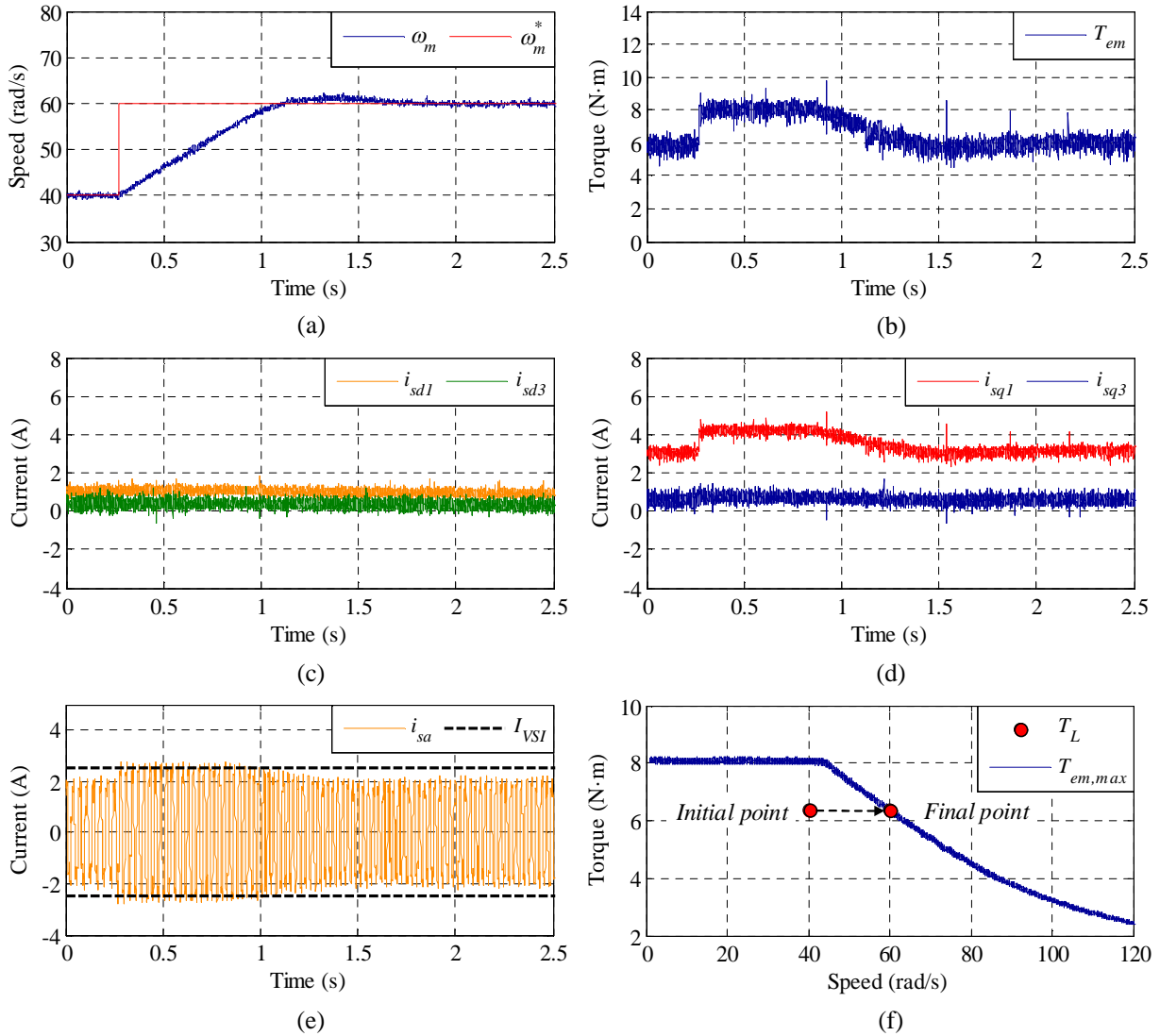


Figure 4.20. Experimental test of the dynamic response of the 5-phase CW-IM drive for a speed step from 40 to 60 rad/s and a load torque equal to 6.4 N·m (the maximum available at 60 rad/s). (a) Measured mechanical speed versus the applied reference. (b) Obtained electrical torque. (c) Stator currents in d_1 - and d_3 -axes. (d) Stator currents in q_1 - and q_3 -axes. (e) Stator phase current ‘ a ’. (f) System evolution in the maximum torque-speed curve.

All in one, the proposed controller based in MPC control techniques generates optimal reference currents taking into account the imposed voltage and current limits of the machine, as well as its maximum magnetization level, showing a good regulation of the electrical machine in steady and transient states.

4.4 Chapter conclusions

This chapter analyzes the optimal control of multiphase drives including electrical limits. The considered direct control strategy to manage this situation has been the MPC technique since the DTC method is not able to manage more than two degrees of freedom and optimal control implies not only flux and torque regulation. Therefore, an optimal current controller using MPC techniques is introduced, which allows the optimal utilization of the system's torque capability under voltage, current and magnetic limitations. First, a continuous predictive stage produces optimal reference currents, taking into account programmed electrical and magnetic constraints. Then, a predictive controller regulates the stator currents of the system in order to track the optimal references. The achievements of the two-stage MPC technique compared to classical methods can be summarized as follows:

- The proposed controller allows the consideration of electrical constraints in the regulator strategy, including voltage and current limits imposed by the power converter and the electrical machine. An important industrial demand, in relation with obtaining higher requirements in the peak torque and power density of modern motor drives, is then attended because an increment in the reliability levels of the drive is forced introducing stringent controllers with the ability of managing failure mechanisms and critical electrical limits.
- The PWM stage using an inner current controller based on the FCS-MPC method can be suppressed, which improves the closed-loop torque performance providing faster torque transient [186,187]. Note also that the tuning of the controller requires less effort in comparison to that of PI-PWM based methods.
- Although optimal controllers have previously been stated in the research bibliography, only suboptimal solutions have been raised up in the multiphase drives' field. In this particular research area, some simplifications and/or assumptions were considered in the control strategy to take into account the considered electrical limits, as stated before. However, the proposed method permits the online computation of the optimal reference current, ensuring the optimality condition of the problem.

The implementation of the technique in a real-time simulation environment based on OPAL-RT technologies is used as a previous step to validate the effectiveness of the proposal in steady-state and transient operating conditions, where optimal reference currents are generated, and the system is composed by a five-phase PMSM drive. Then, the interest of the proposed controller has been verified using one of the hottest electrical machine topologies due to its promising industry perspective, such as the five-phase IM with concentrated windings. The obtained results prove that the optimal reference current generator produces the best combination of the d - q reference currents to obtain the maximum torque while minimizing copper losses and respecting the imposed electrical limits, while an important enhancement in the torque production is achieved when the third harmonic component of the current is exploited. The dynamic operation of the system has also been tested, showing fast and smooth current and speed tracking performances. Although particular cases of multiphase drives have been used in this work, the proposal can be easily extended to n -phase multiphase machines, considering more complex cost functions and optimization problems.

Chapter 5

Conclusions and Future Research

5.1 Conclusions

The general objective of this Doctoral Thesis work has been the development of control techniques for multiphase machines, analyzing the tolerance of the drive to different limit operating conditions, such as electrical/magnetic constraints or failure situations such as an open-phase fault. Different direct control methods are proposed in the way of looking for alternatives to the Field Oriented Control (FOC) in the multiphase field that have not been addressed to date, in the same manner as the Direct Torque Control (DTC) is to FOC in the three-phase case. Experimental validations have been carried out to corroborate the initial approaches, using particular cases of five-phase drives that are available in the laboratories where this work is conducted. Nevertheless, all the proposed techniques can be easily extended to n -phase multiphase machines.

Firstly, the DTC technique was proposed to manage the open-phase fault operation of the multiphase machine. Note that the use of DTC in multiphase drives can be limited in normal operation due to the impossibility of regulating more than two degrees of freedom (electrical torque and stator flux). However, when faulty situations appear, the number of degrees of freedom in the system is reduced and the inconvenient of using the DTC method can also be mitigated, being the benefits similar to the ones obtained in conventional three-phase drives where DTC became long time ago a well-known interesting alternative to FOC methods in industry applications. The DTC technique has been effectively extended in this work to face the operation of the multiphase machine under an open-phase fault. The speed, torque and flux references are successfully tracked after the fault occurrence if the applied load torque is within the maximum torque that the post-fault control scheme can manage. Additionally, an experimental assessment between DTC and other methods has been carried out in this work, revealing that there is no ideal control technique to manage the open-phase fault appearance. If robustness, simplicity or computational cost are the desirable characteristics, the DTC method offers the best performance. Otherwise, if the quality of the obtained stator current in terms of harmonic distortion or the maximum post-fault electrical torque are demanded in post-fault operation, the most appropriate solution consists in the use of the RFOC techniques.

When the number of degrees of freedom increases, DTC seems to be an inadequate control method with the ability of regulating only the torque and flux in the drive. An interesting alternative from the direct control perspective can be the Model-based Predictive Control (MPC),

which has been successfully applied in recent times in the field. MPC has been shown as an excellent solution to optimize the torque capability of the multiphase drive under voltage, current and magnetic constraints imposed by the power converter and the electrical machine. In this regard, a novel technique constituted by two cascaded MPC stages is introduced, allowing the online computation of the optimal reference currents. The obtained experimental results prove that the method can generate an optimal combination of the d - q reference currents to obtain the maximum torque while minimizing copper losses and respecting the imposed electrical limitations.

Finally, it is noteworthy the internationalization of this work that has been developed within an international joint supervision agreement between Arts et Métiers and the University of Seville, being the PhD student funded by Arts et Métiers. This work has also been funded by two research projects supported by the Spanish government. Furthermore, the obtained research results have given rise to an important number of papers published in indexed journals, contributions in conferences of recognized prestige, as well as book chapters and registered patents (see Table 5.1).

Table 5.1. Summary of the internationalization derived from this Doctoral Thesis

Achievement	Number
Journal publications	10 (+ 2 under review)
Conference papers	5
Spanish patents	1
Book chapters	1
Participation in R&D projects	2

5.2 Future research

From this Thesis, various proposed tracks may be followed to extend the interest of multiphase machines in the scientific community, as detailed hereunder.

First, since the work presented here can be seen as a basic research, it may be complemented with some application-oriented research as a step to moving into real industry applications in low- and medium-power electrical systems, such as the development of a multiphase propulsion drive with application in electric vehicles. In this regard, this stage would involve the selection and integration of the electromagnetic drive and control technique for their analysis in the final application. The selection of the electronic control unit that allows the complete implementation of the control techniques is another issue to be taken into account. The technological advance in this field ensures the availability of a powerful unit for this purpose, especially bearing in mind the famous Moore's law, which is the observation that the number of transistors in a microprocessor doubles approximately every two years. This observation has been accurate for several decades, but inevitably the possibility of increasing capacity and reducing the size of integrated circuits has a limit and the rate of progress would reach saturation. This opens up new avenues of study, such as research with new materials (beyond silicon) and with new disciplines like the promising quantum computing. Whereas common digital computing uses binary digits (or bits), each of which is always one of two definite states (0 or 1), quantum computing uses quantum

bits (or qubits), which can be in superposition of states, giving rise to new logical gates that would make possible new algorithms.

Furthermore, some improvements or additional analyses strictly related to the content of this Thesis may be done. For example, this Thesis work tries to establish a starting point to include the limit of magnetic saturation in the control strategy, as stated in Section 4.1, where some assumptions were considered. However, this study may be continued with the utilization of a non-linear model of the machine to effectively take into account the mentioned limitation. Then, regarding the control strategy, the proposed controller in Chapter 4 may be enhanced in the future. A new optimization algorithm based on the CCS-MPC method may be used to generate optimal reference currents while considering both the electrical limits and the new non-linear model for the magnetic saturation. Going further, it would be very interesting the combination of the optimization and control stages using a more complex cost function to depict a novel proper online optimal controller. In this sense, the EMR formalism may be used as a powerful and useful tool to help in the development of this new control structure.

On the other hand, concerning the fault tolerance, an attractive option may be to include other features as a way of approaching to the final application. For example, a fast fault detection and localization process is required to achieve a self-reconfigurable fault-tolerant control in multiphase drives, which has not been considered in this Thesis. A possible future research work may consist on the implementation of different methods for the detection and isolation of the analyzed faults in the multiphase drive, including not only open-phase faults in the machine but also open-switch faults in the converter. This would lead to a more realistic treatment of the fault appearance.

Note finally that this work has been focused on the analysis of three particular five-phase machines with one or two frequency-domain control subspaces. Then, different number of phases, as well as different topologies should be considered to select the one that better fits the final application. For instance, a seven-phase machine with three frequency-domain subspaces could be a potential candidate to enhance the torque capability under certain constraints and the fault-tolerant properties of the system.

Chapter 6

Résumé étendu en français

6.1 Contexte scientifique

L'utilisation des entraînements électriques dans les systèmes embarqués au lieu des moteurs conventionnels a augmenté ces dernières années. C'est le cas, par exemple, de la propulsion des véhicules électriques et de la traction ferroviaire, des navires tout électrique, des avions « plus électriques » et des énergies renouvelables. Les restrictions spécifiques imposées au volume de tels systèmes et la nécessité constante d'augmenter leur puissance nominale conduisent à optimiser l'utilisation de tous les éléments de la chaîne de traction électrique. Par conséquent, les zones d'opération se rapprochent de leurs limites, laissant apparaître des situations de défaillance dans le système ou de comportement non linéaire, telles que des limitations de tension, courant ou des phénomènes de saturation magnétique. A titre d'exemple, l'utilisation de moteurs électriques pour la propulsion de véhicules électriques nécessite de contrôler le moteur sur toute sa plage de vitesse, y compris la région de défluxage (*flux-weakening* en anglais) où les limites de tension sont atteintes.

Les entraînements polyphasés, comparés à leurs homologues triphasés, permettent de réduire les tensions électriques dans la machine et dans les composants électroniques, de gérer plus de puissance avec une pulsation de couple plus faible et un contenu harmonique de courant plus faible, en plus de posséder des capacités inhérentes de tolérance aux défauts. Ces avantages en font un candidat idéal pour les applications dans lesquelles des limites peuvent être atteintes et où la fiabilité présente un intérêt particulier pour des raisons économiques et/ou de sécurité. Les recherches récentes sur les entraînements polyphasés visent à exploiter leurs caractéristiques spéciales et à les proposer comme une alternative aux systèmes triphasés, où un plus grand nombre de phases se traduit par un plus grand nombre de degrés de liberté de contrôle et de conception, qui permettent d'améliorer la fiabilité et les performances globales du système.

En conséquence, des techniques de commande ont été récemment proposées pour des entraînements polyphasés qui sont généralement une extension des structures de commande triphasées classiques, ayant pour objectif de proposer une haute performance vitesse/couple de l'entraînement. Néanmoins, il existe une certaine carence de recherche concernant les situations limites pouvant survenir dans la machine. Si le système fonctionne au-dessous de ses limites, il est possible de le décomposer en plusieurs sous-espaces commandés indépendamment (« commande moyenne »). Cependant, dans le cas d'un système fonctionnant près de ses limites, ce qui précède n'est plus possible et une « commande en mode instantané » de l'ensemble du système est

nécessaire. La principale difficulté réside dans la manière de formaliser le problème pour tenir compte des limitations imposées et des objectifs de commande à respecter.

Dans ce contexte, différentes techniques de « commande en mode instantané » sont proposées dans ce travail de thèse permettant de surmonter ces situations, où la commande directe de couple et la commande prédictive (DTC et MPC, par leurs sigles en anglais, respectivement) seront les représentants de ce type de techniques.

6.2 Objectifs

L'objectif général de cette thèse est le développement de techniques de commande en mode instantané pour contrôler de manière optimale les machines polyphasées, en étudiant la tolérance de l'entraînement dans différentes conditions de fonctionnement, telles que les limites électriques (limites de tension, de courant et de niveau maximum de magnétisation) ou la tolérance aux défauts (situation de défaut de type phase ouverte). Le sens des techniques de « commande en mode instantané » est lié à celles dont la stratégie de commande est réalisée sans intervention d'une étape de modulation de largeur d'impulsion (PWM, par ses sigles en anglais) ou d'une autre forme de modulation, fournissant des signaux de commande qui sont appliqués directement au convertisseur de puissance. Les stratégies de commande en mode instantané analysées dans cette thèse sont les plus utilisées dans la littérature, à savoir la DTC et la MPC. À cette fin, l'étude se concentre sur les entraînements polyphasés commandés avec différents sous-espaces de commande dans le domaine fréquentiel. D'une part, les machines à induction pentaphasées avec bobinages distribués, commandées avec un seul sous-espace dans le domaine fréquentiel (flux et couple dans le plan α - β). D'autre part, les machines synchrones à aimants permanents pentaphasées et les machines à induction pentaphasées avec bobinages concentrés, qui ont deux sous-espaces commandés (flux et couple dans les plans α_1 - β_1 y α_3 - β_3). L'objectif général peut être divisé plus spécifiquement par les tâches suivantes :

- Recherche sur les machines polyphasées, leurs avantages/inconvénients par rapport aux machines triphasées et leurs applications industrielles, afin d'identifier les limites et les contraintes du système. De même, l'analyse de l'état de l'art des techniques de commande en mode instantané (DTC et MPC, comme principaux représentants) appliquées aux entraînements polyphasés.
- Étude et analyse des stratégies DTC triphasées conventionnelles et leur extension au cas de tolérance aux défauts dans les machines polyphasées, en se concentrant sur un entraînement pentaphasé avec un seul sous-espace dans le domaine fréquentiel. Pour cela, il est nécessaire de mettre en place de nouvelles tables de consultation (*look-up tables* en anglais) pour les variables de contrôle, afin de prendre en compte dans la stratégie de commande les contraintes rencontrées en cas de défaut de type phase ouverte dans la machine.
- Comparaison de la capacité de tolérance à la défaillance des commandes de type DTC par rapport à d'autres techniques de commande, pour permettre une conclusion sur les forces et les faiblesses des méthodes analysées face à des fonctionnements où existent des défauts de type phase ouverte.

- Développement d'un contrôleur de courant optimal utilisant des techniques de commande MPC permettant une utilisation optimale de la capacité de couple du système en cas de limitations de tension, courant et de magnétisation. L'intérêt du contrôleur proposé est vérifié à l'aide de machines pentaphasées avec deux sous-espaces dans le domaine fréquentiel.

6.3 Positionnement de la thèse

Le travail de thèse est basé sur une convention de cotutelle internationale entre l'École Nationale Supérieure d'Arts et Métiers (appelée ci-après « Arts et Métiers ») – Campus de Lille, France, et l'Université de Séville (appelée ci-après « US »), Espagne. Les directeurs de thèse dans chaque établissement sont le Professeur Xavier Kestelyn et le Professeur Federico José Barrero García, respectivement, reconnus internationalement dans le domaine des entraînements polyphasés et ayant de nombreuses années d'expérience dans ce sujet. Par conséquent, faire la thèse sous leur direction est une excellente occasion de travailler au meilleur niveau dans ce domaine.

À Arts et Métiers, les travaux se déroulent au Laboratoire d'Electrotechnique et d'Electronique de Puissance de Lille (L2EP) au sein de l'équipe Commande, le Professeur Kestelyn étant un de ses membres. Cette équipe se focalise sur le développement de formalismes de modélisation et de commande dédiés aux systèmes de conversion d'énergie. La Représentation Energétique Macroscopique et le Formalisme Vectoriel Généralisé (EMR et GVF par leurs sigles en anglais, respectivement) sont des formalismes multi-physiques qui permettent de traiter un large champ applicatif se focalisant actuellement sur les dispositifs électriques, les entraînements polyphasés, les actionneurs piézo-électriques et les véhicules électriques. L'équipe Commande pilote également le réseau MEGEVH (Modélisation Énergétique et Gestion d'Énergie de Véhicules Hybrides), qui vise à encourager la collaboration entre les entreprises académiques et industrielles en termes de modélisation et de gestion de la puissance des véhicules hybrides.

Par ailleurs, le Professeur Barrero a dirigé le groupe de recherche Applications Cybernétiques de l'Electronique aux Technologies de l'Information (ACE-TI) à US. Les domaines de recherche de ce groupe comprennent, entre autres, les véhicules électriques, les villes intelligentes (*smart cities* en anglais) ou les réseaux de capteurs sans fil. ACE-TI se focalise actuellement sur l'adaptation d'un banc de test pour les entraînements polyphasés, qui appartient au groupe de recherche, pour son application dans la modélisation, le développement et la gestion de l'énergie des véhicules électriques. Une image du prototype de véhicule électrique est présentée à la Fig. 6.1.

Le présent travail de thèse se centre sur ce qui peut être défini comme recherche fondamentale. Par conséquent, différentes méthodes de commande en mode instantané sont analysées pour établir une technique de régulation bien formulée et définie pour les entraînements polyphasés, où les limites électriques/magnétiques et les conditions de fonctionnement critiques peuvent être gérées. Cependant, le travail nécessite une étape ultérieure de recherche orientée vers l'application, qui impliquerait l'intégration des entraînements électromagnétiques et des techniques de commande utilisés pour l'analyse dans les systèmes électriques de faible et moyenne puissance pour application industrielles.



Figure 6.1. Prototype du véhicule électrique appartenant à ACE-TI.

Différents travaux de thèse antérieurs dans les deux institutions sont liés à l'utilisation d'entraînements polyphasés et constituent les antécédents de ce travail. Côté L2EP, les thèses de Xavier Kestelyn et Paul Sandulescu doivent être soulignées [1–3], lesquelles sont axées sur la modélisation de la machine et sa commande. En outre, les études de Bassel Aslan, Hussein Zahr et Tiago José Dos Santos Moraes [4–6] ont porté sur la conception de différents types de machines polyphasées destinées à des applications industrielles. Il convient également de noter les travaux de Li Lu [7], en relation avec l'opération *flux-weakening* dans les machines polyphasées, et d'Ousmane Fall [8], en ce qui concerne l'inclusion des limites dans le système. D'autre part, les thèses de Raúl Igmarr Gregor Recalde, José Agustín Riveros Insfrán, Hugo Mauricio Guzmán Jiménez et Ignacio González Prieto, sur le développement de stratégies de commande pour les entraînements polyphasés en fonctionnement sans défauts [9, 10] et avec défauts [11, 12] représentent les travaux réalisés à ACE-TI.

6.4 Organisation du document

Ce document est organisé comme suit. Le Chapitre 1 (*Chapter 1*) présente le contexte scientifique et les objectifs de cette thèse, en montrant le positionnement et le contexte par rapport aux deux institutions dans lesquelles le travail est développé. À la fin de ce chapitre, un résumé des articles publiés dans des revues internationales et des contributions à des conférences qui ont été une conséquence de ce travail de recherche est présenté. Le Chapitre 2 décrit l'état actuel de la technique en matière de commande des entraînements électriques polyphasés. Dans ce chapitre, les recherches les plus récentes dans la littérature scientifique sont discutées pour souligner l'intérêt de ce travail. Pour sa part, le Chapitre 3 porte sur l'étude du fonctionnement avec défauts de type phase ouverte en utilisant la technique de commande DTC appliquée aux machines polyphasées avec un seul sous-espace dans le domaine fréquentiel. Une évaluation expérimentale est également effectuée pour comparer les performances des différentes stratégies de commande face à la situation limite de type défaillance. Au Chapitre 4, par contre, le cas des machines avec

deux sous-espaces dans le domaine fréquentiel est analysé. Dans ce cas, la stratégie de commande DTC semble insuffisante pour gérer la situation, car elle ne permet que de contrôler deux degrés de liberté dans le système, donc une nouvelle technique basée sur la méthode MPC est présentée pour générer des références de courant optimales en temps réel (*online*) en tenant compte des limitations électriques et magnétiques choisies, tout en régulant les courants du système pour qu'ils suivent les références optimales. Les conclusions finales et la proposition de travaux futurs figurent au Chapitre 5.

6.5 Etat de l'art des entraînements polyphasés

La littérature explorée au Chapitre 2 se concentre sur la description de l'état actuel de l'art lié à la commande des entraînements électriques polyphasés. À cette fin, les travaux de recherche les plus récents dans le domaine sont analysés pour générer un cadre théorique permettant une meilleure compréhension du travail présenté dans cette thèse. Plus précisément, la Section 2.1 présente les concepts fondamentaux et rappelle les origines des machines électriques polyphasées. Ces machines présentent une série d'avantages qui les rendent idéales comme alternative aux entraînements triphasés conventionnels dans certaines applications, où le nombre de phases représente non seulement de meilleures performances, mais également une plus grande fiabilité.

Différents types de machines polyphasées sont présentés, en accordant une attention particulière aux machines pentaphasées symétriques (synchrones à aimants permanents et à induction avec bobinages distribués/concentrés), utilisées comme exemples tout au long de ce travail et dont les modèles mathématiques sont analysés méticuleusement à la Section 2.2, tant en variables réelles (de phase) qu'en systèmes de référence fixe et rotatif. Le modèle mathématique du convertisseur de puissance est également abordé dans cette section. Ultérieurement, la Section 2.3 analyse les différentes techniques proposées pour la commande des entraînements polyphasés, en montrant l'évolution du cas triphasé à sa mise en œuvre dans le champ polyphasé. Plus précisément, les techniques étudiées dans cette section sont la commande à flux orienté (FOC, par ses sigles en anglais), la DTC et la MPC. Bien que la thèse se concentre sur les techniques DTC et MPC en tant que stratégies de commande, il semble intéressant de mettre en évidence leurs caractéristiques et leur mode de fonctionnement par rapport au schéma FOC, car c'est la stratégie de commande par excellence dans la grande majorité des entraînements électromécaniques d'application industrielle.

Afin de mettre en évidence l'intérêt de cette thèse, la Section 2.4 examine différentes situations limites pouvant être prises en compte dans l'étude des entraînements polyphasés. Cette section montre que l'état de maturité de ce type de dispositifs n'a pas encore été atteint en termes d'exploitation de leurs avantages. À cet égard, une attention particulière devrait être accordée à la tolérance aux défauts (Section 2.4.1) qui, bien qu'elle constitue l'un des avantages de l'utilisation de ce type d'entraînements par rapport aux machines triphasées, a été peu étudiée comparativement au cas sain (sans défauts). Cette thèse tente de progresser dans l'étude et la mise en œuvre de différentes stratégies de commande permettant d'améliorer la tolérance aux défauts des entraînements polyphasés dans les applications à vitesse variable. Au Chapitre 3, la technique DTC est proposée pour gérer le fonctionnement avec un défaut de type phase ouverte d'une machine polyphasée et ses performances sont comparées à différentes méthodes actuelles. Étant donné que

la méthode DTC a pour caractéristique principale la régulation de seulement deux variables de commande (flux et couple) et est considérée comme une alternative dans le cas triphasé conventionnel à la méthode FOC, il semble approprié de faire face à son étude dans les cas où le nombre des degrés de liberté du système polyphasé est similaire à celui du système triphasé.

Par ailleurs, en relation à l'obtention d'une technique optimale intégrant les limites dans la stratégie de commande, cette thèse va au-delà des propositions mentionnées à la Section 2.4.2 pour augmenter la performance de couple de la machine, où seulement des solutions sous-optimales ont été atteintes à ce jour. Classiquement, des simplifications ou des hypothèses sont faites pour obtenir les expressions analytiques des courants de référence en tenant compte des limites de tension et de courant. Dans tous les cas, ces conditions réduisent l'intérêt pour la technique DTC en tant que méthode de régulation car elles causent une augmentation du nombre de variables et des degrés de liberté à contrôler. C'est pourquoi, dans le présent travail, des techniques de commande basées sur des modèles sont appliquées pour résoudre les problèmes d'optimisation et de commande. Par conséquent, un nouveau régulateur MPC est introduit pour *i)* générer des références de courant optimales *online* en tenant compte des limites de tension, courant et niveau maximum de magnétisation, *ii)* extraire le couple maximal de la machine et *iii)* garantir les performances du système en boucle fermée (commande du courant). Ce contrôleur génère des références de courant optimales *online* grâce à une étape qui respecte les limitations électriques imposées. Ensuite, une étape de commande basée sur des modèles de prédiction pour la régulation du courant est appliquée. Cette contribution est examinée plus en détail au Chapitre 4.

Enfin, la Section 2.5 propose une analyse des différents formalismes graphiques pour les machines polyphasées, en mettant l'accent sur la structure EMR et en montrant son application à une machine pentaphasée à aimants permanents à titre d'exemple. Le chapitre conclut par les conclusions les plus importantes, qui sont rassemblées dans la Section 2.6.

6.6 Contrôleur avec un unique sous-espace à contrôler dans le domaine fréquentiel : cas de la DTC

Le Chapitre 3 se focalise sur l'utilisation de la DTC pour étudier la tolérance au fonctionnement avec défauts de type phase ouverte d'un entraînement polyphasé. La capacité de tolérance aux défauts des entraînements polyphasés est un avantage intrinsèque intéressant pour les applications de sécurité critiques, où des recherches récentes ont montré l'efficacité des stratégies FOC pour gérer les opérations après défaillance sans fluctuation. La méthode DTC a été largement utilisée comme alternative aux méthodes FOC traditionnelles pour les entraînements triphasés. Bien que cette méthode ne soit pas considérée comme un compétiteur dans le domaine polyphasé car elle est basée sur la capacité de réguler uniquement deux degrés de liberté (flux et couple dans la machine), le schéma DTC conventionnel a également été étendu aux entraînements polyphasés ces derniers temps, en utilisant des contrôleurs par hystérésis pour commander indépendamment le couple et le flux souhaités dans des machines à induction symétriques pentaphasées. En appliquant cette méthode, la commande ne peut pas se concentrer sur plus d'un sous-espace dans le domaine fréquentiel (sous-espace α - β normalement). Toute action dans le sous-espace x - y doit être une régulation de courant en boucle ouverte, afin de limiter les

harmoniques indésirables si une topologie de bobinages distribués est prise en compte. Cela se fait généralement en définissant des vecteurs virtuels de tension qui génèrent une tension nulle dans les sous-espaces qui ne peuvent pas être régulés, ce qui permet d'appliquer correctement la DTC lorsque la machine n'a pas d'asymétries dans sa conception, ce qui ne coïncide pas nécessairement avec la réalité. En tout état de cause, si la situation limite considérée est la perte d'une phase, le nombre de degrés de liberté contrôlables dans le système diminue et se rapproche de celui du cas triphasé conventionnel, où la DTC peut être considérée comme une alternative compétitive à la méthode FOC. Cela justifie de considérer la technique DTC comme une stratégie intéressante pour le cas pentaphasé et la situation limite de perte de certains degrés de liberté dans la commande.

Ce chapitre présente les premiers résultats obtenus dans la thèse, où un nouveau schéma DTC à tolérance aux défauts est présenté en utilisant une machine à induction pentaphasée avec bobinages distribués à titre d'exemple. La modélisation du système est analysée dans la Section 3.1, montrant l'effet de l'apparition du défaut de type phase ouverte dans le système physique. La méthode DTC appliquée lors de la défaillance de la machine est décrite à la Section 3.2, où les besoins du contrôleur pour gérer la nouvelle situation opérationnelle sont étudiés. La Section 3.3 présente plusieurs résultats préliminaires de simulation basés sur un environnement MATLAB[®] et Simulink[®], où la capacité de la technique DTC modifiée permettant le fonctionnement post-défaut des entraînements polyphasés est étudiée. La performance de la méthode proposée est également validée expérimentalement sur un réel banc d'essai basé sur une machine à induction pentaphasée avec bobinages distribués, dans le but de vérifier l'analyse préliminaire. La Section 3.4 fournit différents tests pour analyser les états stationnaires et transitoires, y compris l'instant où le défaut apparaît. Tous les résultats obtenus permettent de conclure que la vitesse, le couple et le flux de référence sont maintenus après la présence du défaut tant que le couple de charge appliqué est inférieur au couple maximal que le système de commande peut gérer après le défaut.

Les performances de la DTC par rapport aux autres techniques de commande FOC basées sur des contrôleurs proportionnels résonants et des techniques MPC sont effectuées dans la Section 3.5 lorsqu'un défaut de type phase ouverte se produit dans l'entraînement pentaphasé, fournissant des résultats de simulation et expérimentaux pour conclure sur les forces et les faiblesses des méthodes analysées. Les résultats obtenus montrent que la méthode DTC a la capacité de gérer un couple électrique maximal inférieur. Un contenu harmonique plus élevé est également obtenu dans le courant de phase statorique lorsque la technique DTC est appliquée, comme dans le cas triphasé. Cependant, l'utilisation d'une méthode DTC post-défaut est une option viable qui démontre une solidité accrue face aux retards dans la détection des défauts, tout en préservant une simplicité de mise en œuvre et un faible coût de calcul. Cela se traduit par une alternative intéressante aux méthodes FOC dans les applications industrielles où la fiabilité doit être augmentée et l'entraînement doit fonctionner dans des conditions de sécurité jusqu'à la maintenance corrective.

Néanmoins, lorsque la situation limite considérée implique l'inclusion de nouveaux degrés de liberté dans le système (limitations de tension, courant...), la DTC ne semble pas être une alternative de commande intéressante en raison de ses propres limitations. Par conséquent, il est conseillé de proposer des alternatives de commande en mode instantané permettant de contrôler un grand nombre de variables. Au Chapitre 4, la méthode MPC est analysée en tant que technique de commande en mode instantané permettant d'inclure un plus grand nombre de degrés de liberté dans la stratégie de commande.

6.7 Contrôleur avec deux sous-espaces indépendants à contrôler dans le domaine fréquentiel : cas de la MPC

La commande optimale des entraînements de puissance modernes nécessite de prendre en compte les contraintes électriques dans la stratégie du contrôleur, notamment les limites de tension et de courant imposées par le convertisseur de puissance et la machine électrique ou la saturation magnétique due aux parties ferromagnétiques. Ce problème a été largement analysé dans les entraînements triphasés conventionnels, mais rarement étudié dans le cas polyphasé, où les contrôleurs optimaux prenant en compte les limites électriques n'ont été que très peu pris en compte malgré l'intérêt actuel de la technologie polyphasée dans les applications de haute densité de puissance, de large plage de vitesse ou de tolérance aux défauts. Comme indiqué ci-dessus, la technique DTC perd de son intérêt dans cette situation, car elle ne peut contrôler que deux degrés de liberté. Par conséquent, une autre stratégie de commande en mode instantané est nécessaire pour gérer un plus grand nombre de degrés de liberté pour ce problème. Dans ce contexte, la méthode MPC apparaît comme un candidat à cette fin, en tant que stratégie de commande qui offre une grande flexibilité face à des systèmes avec multiples entrées et sorties soumis à des contraintes.

Au Chapitre 4, un contrôleur optimal généralisé utilisant les techniques MPC est introduit, permettant une utilisation optimale de la capacité de couple du système sous contraintes de tension, courant et magnétiques. Une description des limites électriques incluses dans la stratégie de contrôle optimal est détaillée dans la Section 4.1. La méthode de commande proposée est présentée à la Section 4.2 et est basée sur deux étapes prédictives en cascade. Premièrement, une étape MPC génère la référence de courant du stator optimale qui respecte les limites électriques de l'entraînement afin d'exploiter la caractéristique de performance maximale. Ultérieurement, un régulateur de type FCS-MPC régule le courant du stator et génère l'état de commutation dans le convertisseur de puissance. Les réussites de cette technique MPC en deux étapes par rapport aux méthodes classiques peuvent être résumées ci-dessous :

- Le contrôleur proposé permet de prendre en compte les contraintes électriques dans la stratégie du régulateur, notamment les limites de tension et courant imposées par le convertisseur de puissance et la machine électrique. Ainsi, une demande industrielle importante est satisfaite en ce qui concerne l'obtention des exigences plus élevées en termes de couple maximal et de densité de puissance des moteurs modernes, car une augmentation des niveaux de fiabilité du moteur est imposée en introduisant des contrôleurs stricts capables de gérer les mécanismes de défaillance et les limites électriques critiques.
- L'utilisation d'un contrôleur de courant basé sur la méthode FCS-MPC permet de supprimer l'étape de modulation PWM, ce qui améliore les performances du couple en boucle fermée en fournissant un transitoire plus rapide. Notons également que le réglage du contrôleur nécessite moins d'efforts par rapport aux méthodes basées sur PI-PWM.
- Bien que des contrôleurs optimaux aient déjà été étudiés dans la littérature, seules des solutions sous-optimales ont été proposées dans le domaine polyphasé. Dans ce champ particulier de recherche, certaines simplifications et/ou hypothèses ont été prises en compte dans la stratégie de commande pour considérer des limites électriques, comme indiqué ci-

dessus. Cependant, la méthode proposée permet le calcul *online* de la référence de courant optimale, garantissant ainsi la condition d'optimalité du problème.

Deux topologies différentes de machines pentaphasées sont utilisées comme exemples d'entraînements modernes de haute performance pour la validation expérimentale de la technique prédictive en deux étapes : une machine synchrone pentaphasée à aimants permanents et une machine pentaphasée à induction avec bobinages concentrés. Ce sont des entraînements polyphasés habituels qui peuvent être considérés comme des systèmes avec deux sous-espaces indépendants à réguler dans le domaine fréquentiel, où les courants fondamentaux et les harmoniques de rang 3 sont des composantes orthogonales impliquées dans la production de couple. La validation de la stratégie de commande est discutée à la Section 4.3, divisée en deux parties. L'implémentation de la technique dans un environnement de simulation en temps réel basée sur les technologies OPAL-RT est utilisée comme une étape préliminaire pour valider l'efficacité de la proposition dans des conditions de fonctionnement stationnaires et transitoires, où des courants de référence optimaux sont générés, tandis que le système est composé d'une machine à aimants permanents. Ensuite, les performances du contrôleur sont vérifiées expérimentalement en utilisant l'une des topologies de machine électrique polyphasée la plus étudiée en raison de sa perspective industrielle prometteuse : la machine pentaphasée à induction avec bobinages concentrés. Les résultats obtenus prouvent que le générateur de références de courant optimales produit la meilleure combinaison de références de courant $d-q$ pour obtenir le couple maximal tout en minimisant les pertes cuivre et en respectant les limites électriques imposées, en obtenant une amélioration significative dans la production de couple lorsque l'harmonique de rang 3 est exploitée. Le fonctionnement dynamique du système est également testé, montrant un suivi rapide et fluide du courant et de la vitesse.

Il convient de noter que, bien que dans ce travail des cas particuliers de machines polyphasées sont utilisés, la proposition peut facilement être étendue à des machines avec n phases, en considérant des fonctions de coût et des problèmes d'optimisation plus complexes.

6.8 Conclusions

L'objectif général de ce travail de thèse a été le développement de techniques de commande pour les machines polyphasées, analysant la tolérance de l'entraînement à différentes conditions de fonctionnement limites, telles que les limitations électriques/magnétiques ou les défaillances telles que le défaut de type phase ouverte. Différentes méthodes de commande en mode instantané sont proposées pour rechercher des alternatives à la méthode FOC dans le champ polyphasé qui n'ont pas encore été abordées, de la même manière que la DTC l'est pour la FOC dans le cas triphasé. Des validations expérimentales ont été effectuées pour corroborer les approches initiales, en utilisant des cas particuliers d'entraînements pentaphasés disponibles dans les laboratoires où ce travail est effectué. Cependant, toutes les techniques proposées peuvent facilement être étendues aux machines possédant n phases.

Tout d'abord, la technique DTC a été proposée pour gérer le fonctionnement en cas de défaut de type phase ouverte dans la machine polyphasée. Notons que l'utilisation de la DTC dans des entraînements polyphasés peut être limitée en fonctionnement normal en raison de l'impossibilité

de réguler plus de deux degrés de liberté (couple électrique et flux du stator). Cependant, lorsque des situations de défaillance apparaissent, le nombre de degrés de liberté dans le système est réduit et les inconvénients liés à l'utilisation de la méthode DTC peuvent également être atténués, avec des avantages similaires à ceux obtenus dans les entraînements triphasés où la DTC est devenue, il y a longtemps, une alternative bien connue et intéressante dans les applications industrielles aux méthodes FOC. La technique DTC a été étendue efficacement dans ce travail pour faire face au fonctionnement de la machine polyphasée avec un défaut de type phase ouverte. Les références de vitesse, couple et flux sont régulées avec succès après l'apparition du défaut si le couple de charge appliqué est inférieur au couple maximal que le schéma de commande après défaut peut gérer. En outre, une évaluation expérimentale a été réalisée entre la DTC et d'autres méthodes, en révélant qu'il n'existe pas de technique de commande idéale pour gérer l'apparition de défauts. Si la robustesse, la simplicité ou le coût de calcul sont les caractéristiques souhaitables, la méthode DTC offre les meilleures performances. Dans le cas contraire, si la qualité du courant du stator en termes de distorsion harmonique ou la valeur du couple électrique maximal post-défaut sont requises dans le fonctionnement après défaut, la solution la plus appropriée est l'utilisation de techniques FOC.

Lorsque le nombre de degrés de liberté augmente, la DTC semble être une méthode de commande inadéquate, capable de réguler uniquement le couple et le flux. Une alternative intéressante du point de vue de la commande en mode instantané peut être l'utilisation de la commande prédictive, qui a été récemment appliquée avec succès dans le domaine. La technique MPC s'est avérée une excellente solution pour optimiser la capacité de couple de l'entraînement sous des contraintes de limitations de tension, courant et magnétiques imposées par le convertisseur de puissance et la machine électrique. En ce sens, une nouvelle technique est introduite, consistant en deux étapes MPC en cascade, ce qui permet le calcul *online* des références optimales de courant. Les résultats expérimentaux obtenus montrent que la méthode peut générer une combinaison optimale de références de courant $d-q$ pour obtenir un couple maximal tout en minimisant les pertes cuivre et en respectant les limites imposées.

Pour conclure, il convient de souligner l'internationalisation de ce travail qui a été développé dans le cadre d'une convention internationale de cotutelle de thèse entre Arts et Métiers et l'Université de Séville, avec un financement du doctorant par Arts et Métiers. Ce travail a également été financé par deux projets de recherche soutenus par le gouvernement espagnol. Par ailleurs, les résultats obtenus ont donné lieu à un nombre important d'articles publiés dans des revues internationales indexées, des contributions à des conférences de prestige reconnu, ainsi que des chapitres de livres et des brevets enregistrés (voir Tableau 6.1).

Tableau 6.1. Résumé de l'internationalisation résultant de cette thèse

Réussite	Nombre
Articles dans des revues	10 (+ 2 en révision)
Contributions à des conférences	5
Brevets espagnols	1
Chapitres de livres	1
Participation à des projets R&D	2

Chapter 7

Resumen extenso en español

7.1 Contexto científico

El uso de accionamientos eléctricos en sistemas integrados en lugar de motores convencionales ha crecido en los últimos años. Es el caso, por ejemplo, de la propulsión de vehículos eléctricos y la tracción ferroviaria, los buques totalmente eléctricos, los aviones “más eléctricos” y las energías renovables. Las restricciones específicas impuestas al volumen de tales sistemas y la constante necesidad de aumentar su potencia nominal conducen a optimizar la utilización de todos los componentes del tren de potencia eléctrico. Por lo tanto, las zonas de funcionamiento se acercan a sus límites, apareciendo situaciones de fallo en el sistema o comportamientos no lineales, como limitaciones de tensión y corriente o fenómenos de saturación magnética. Como ejemplo, el uso de accionamientos eléctricos para la propulsión de vehículos eléctricos requiere controlar el motor en todo su rango de velocidad, incluida la región de debilitamiento de flujo (*flux-weakening* en inglés) donde se alcanzan los límites de tensión.

Comparados con los accionamientos trifásicos, los multifásicos reducen las tensiones eléctricas en la máquina y en los componentes electrónicos de potencia, ya que pueden administrar más potencia con menor pulsación de par y menor contenido de armónicos de corriente, además de tener capacidades inherentes de tolerancia a fallo. Tales ventajas los hacen un candidato ideal en aplicaciones donde se pueden alcanzar límites y donde la fiabilidad es de especial interés por razones económicas y/o de seguridad. Recientes estudios sobre estos accionamientos apuntan a explotar sus características especiales y presentarlos a la industria como una alternativa a los trifásicos, donde el mayor número de fases da como resultado un mayor número de grados de libertad de control y diseño, que pueden mejorar la fiabilidad general y el rendimiento del sistema.

Consecuentemente, se han propuesto técnicas de control en tiempos recientes para los accionamientos multifásicos que generalmente son una extensión de las estructuras de control trifásicas convencionales, teniendo como objetivo el alto rendimiento de velocidad/par del accionamiento. A pesar de todo, existe una cierta carencia de investigación referente a las situaciones límite que se pueden dar en la máquina. Si el sistema funciona por debajo de sus límites, es posible descomponerlo en varios subespacios controlados de manera independiente (“control promedio”). Sin embargo, en el caso de un sistema que funciona cerca de sus límites, ya no es posible lo anterior y es necesario un “control directo” de todo el sistema. La principal dificultad radica en la manera de formalizar el problema para poder tener en cuenta las restricciones impuestas junto con los objetivos de control que se han de respetar.

En este contexto, se proponen diferentes técnicas de “control directo” en este trabajo de Tesis Doctoral para superar estas situaciones, siendo el Control Directo de Par y el Control Predictivo basado en Modelos (DTC y MPC, por sus siglas en inglés, respectivamente) los representantes de este tipo de técnicas.

7.2 Objetivos

El objetivo general de este trabajo de Tesis Doctoral es el desarrollo de técnicas de control directo para controlar de forma óptima máquinas multifásicas, estudiando la tolerancia del accionamiento a diferentes condiciones operativas, tales como límites eléctricos (límites de tensión, de corriente y de nivel máximo de magnetización) o la tolerancia al fallo (situación de falta de fase abierta). El significado de técnicas de “control directo” se relaciona con aquellas cuya estrategia de control se realiza sin la intervención de una etapa de modulación de ancho de pulso (PWM, por sus siglas en inglés) u otra forma de modulación, proporcionando señales de control que se aplican directamente al convertidor de potencia. Las estrategias de control directo que se analizan en esta Tesis son las más utilizadas en la literatura, es decir, el DTC y el MPC. Para este propósito, el estudio se centra en accionamientos multifásicos controlados usando diferentes subespacios de control en el dominio de frecuencia. Por un lado, máquinas de inducción de 5 fases con devanados distribuidos, controlados usando un único subespacio en el dominio de frecuencia (flujo y par en el plano α - β). Por otro lado, máquinas síncronas de imanes permanentes de 5 fases y máquinas de inducción de 5 fases con devanados concentrados, las cuales poseen dos subespacios controlados (flujo y par en los planos α_1 - β_1 y α_3 - β_3). El objetivo general se puede dividir más específicamente en las siguientes tareas:

- Investigación sobre máquinas multifásicas, sus ventajas/inconvenientes con respecto a las trifásicas y sus aplicaciones industriales, con el objetivo de identificar las limitaciones y restricciones del sistema. Del mismo modo, análisis del estado de arte de las técnicas de control directo (DTC y MPC, como principales representantes) a aplicar en el accionamiento multifásico.
- Estudio y análisis de estrategias DTC trifásicas convencionales y su extensión al caso de tolerancia al fallo en máquinas multifásicas, centrándose en un dispositivo de 5 fases con un único subespacio en el dominio de frecuencia. Para ello, es necesaria la implementación de nuevas tablas de búsqueda (*look-up tables* en inglés) para las variables de control, con el objetivo de tener en cuenta en la estrategia de control las restricciones encontradas cuando ocurre una falta de fase abierta en la máquina.
- Comparación de la capacidad de tolerancia al fallo del DTC con respecto a otras técnicas de control, para concluir las fortalezas y debilidades de los métodos analizados cuando se enfrentan a la operación con fallo de fase abierta.
- Desarrollo de un controlador de corriente óptimo utilizando técnicas de control MPC que permita la utilización de forma óptima de la capacidad de par del sistema bajo limitaciones de tensión, corriente y magnetización. El interés del controlador propuesto se verifica utilizando máquinas de 5 fases con dos subespacios en el dominio de frecuencia.

7.3 Posicionamiento de la Tesis Doctoral

El trabajo de Tesis Doctoral está basado en un acuerdo internacional de cotutela de tesis entre l'École Nationale Supérieure d'Arts et Métiers (Arts et Métiers, a partir de ahora) – Campus de Lille, Francia, y la Universidad de Sevilla (US), España. Los directores de tesis en cada institución son el Profesor Xavier Kestelyn y el Profesor Federico José Barrero García, respectivamente, reconocidos internacionalmente en el campo de los accionamientos multifásicos y con muchos años de experiencia en el tema. Por lo tanto, hacer la Tesis Doctoral bajo su codirección es una gran oportunidad para trabajar al mejor nivel en este campo.

En Arts et Métiers, el trabajo tiene lugar en el Laboratoire d'Electrotechnique et d'Electronique de Puissance de Lille (L2EP) dentro del equipo Control, siendo el Profesor Kestelyn uno de sus miembros. Este equipo se centra en el desarrollo de formalismos de modelado y control dedicados a sistemas de conversión de energía. La Representación Energética Macroscópica y el Formalismo Vectorial Generalizado (EMR y GVF, por sus siglas en inglés, respectivamente) son formalismos multi-físicos que permiten manejar un amplio campo de aplicaciones, entre las que destacan en la actualidad dispositivos eléctricos, accionamientos multifásicos, actuadores piezoeléctricos y vehículos eléctricos. El equipo Control también lidera la red MEGEVH (Modelado Energético y Gestión Energética de Vehículos Híbridos), que tiene como objetivo fomentar la colaboración entre sociedades académicas e industriales en materia de modelado y gestión de potencia de vehículos híbridos.

Por otro lado, el Profesor Barrero ha liderado el grupo de investigación Aplicaciones Cibernéticas de la Electrónica a las Tecnologías de la Información (ACE-TI) en la US. Los campos de investigación de este grupo incluyen, entre otros, vehículos eléctricos, ciudades inteligentes (*smart cities* en inglés) o redes de sensores inalámbricos. En la actualidad, ACE-TI se centra en adaptar un banco de pruebas para accionamientos multifásicos, que pertenece al grupo de investigación, para su aplicación en el modelado, desarrollo y gestión de la energía en vehículos eléctricos. Una imagen del prototipo del vehículo eléctrico se presenta en la Fig. 7.1.



Figura 7.1. Prototipo del vehículo eléctrico perteneciente a ACE-TI.

El presente trabajo de Tesis Doctoral se centra en lo que se puede definir como investigación básica. En consecuencia, se analizan diferentes métodos de control directo para establecer una técnica de regulación presentada y bien definida para unidades multifásicas, donde se puedan gestionar los límites eléctricos/magnéticos y las condiciones críticas de funcionamiento. Sin embargo, el trabajo necesita de una etapa posterior de investigación orientada a la aplicación, que involucraría la integración de los accionamientos electromagnéticos usados y las técnicas de control para su análisis en sistemas eléctricos de baja y media potencia para aplicaciones industriales.

Diferentes trabajos previos de Tesis Doctoral en ambas instituciones están relacionados con el uso de accionamientos multifásicos y constituyen los antecedentes de este trabajo. Por parte del L2EP, las Tesis Doctorales de Xavier Kestelyn y Paul Sandulescu deben destacarse [1–3], las cuales están centradas en el modelado de la máquina y su control. Además, los estudios de Bassel Aslan, Hussein Zahr y Tiago José Dos Santos Moraes [4–6] estuvieron centrados en el diseño de diferentes tipos de máquinas multifásicas para aplicaciones industriales. Cabe señalar también los trabajos de Li Lu [7], en relación a la operación *flux-weakening* en máquinas multifásicas, y Ousmane Fall [8], con respecto a la inclusión de límites en el sistema. Por otro lado, las Tesis Doctorales de Raúl Igmarr Gregor Recalde, José Agustín Riveros Insfrán, Hugo Mauricio Guzmán Jiménez e Ignacio González Prieto, sobre el tema del desarrollo de estrategias de control para accionamientos multifásicos en operación sin faltas [9, 10] y con faltas [11, 12] representan los trabajos precedentes en ACE-TI.

7.4 Organización del documento

El presente documento está organizado de la siguiente manera. El Capítulo 1 (*Chapter 1*) introduce el contexto científico y los objetivos de la presente Tesis, mostrando el posicionamiento y los antecedentes en relación con las dos instituciones en las que se realiza el trabajo. Al final de dicho capítulo se presenta un resumen de los artículos de revista y las publicaciones en congresos que han sido consecuencia de este trabajo de investigación doctoral. El Capítulo 2 describe el estado de arte actual relacionado con el control de accionamientos eléctricos multifásicos. En dicho capítulo se comentan las investigaciones más recientes de la literatura científica para enfatizar el interés de este trabajo. Por su parte, el Capítulo 3 está centrado en el estudio de la operación de falta de fase abierta utilizando la técnica de control DTC en máquinas multifásicas con un único subespacio en el dominio de frecuencia. También se lleva a cabo una evaluación experimental que compara el rendimiento de diferentes estrategias de control cuando se enfrentan a la situación límite de la falta. En el Capítulo 4, por otro lado, se analiza el caso de las máquinas con dos subespacios en el dominio de frecuencia. En este caso, la estrategia de control DTC se antoja insuficiente para abordar la situación, dado que sólo permite controlar dos grados de libertad en el sistema, por lo que se presenta una nueva técnica basada en el MPC para generar referencias de corriente óptimas de forma *online* teniendo en cuenta las restricciones eléctricas y magnéticas programadas, al mismo tiempo que se regulan las corrientes del sistema de forma que sigan las referencias óptimas. Las conclusiones finales y la propuesta de trabajo futuro se recogen en el Capítulo 5.

7.5 Estado del arte de los accionamientos multifásicos

La literatura explorada en el Capítulo 2 está enfocada a describir el estado del arte actual relacionado con el control de accionamientos eléctricos multifásicos. Para tal fin, se analizan los trabajos de investigación más recientes en el área para generar un marco teórico que permita una mejor comprensión del trabajo presentado en esta Tesis. Más específicamente, la Sección 2.1 presenta los conceptos básicos y los orígenes de las máquinas eléctricas multifásicas. Dichas máquinas poseen una serie de beneficios que las hacen ideales para ser una alternativa a los variadores trifásicos convencionales en ciertas aplicaciones, donde el número de fases resulta no sólo en un mejor rendimiento, sino también en una mayor fiabilidad.

Se presentan diferentes tipos de máquinas multifásicas, prestando especial atención a las máquinas simétricas de 5 fases (síncronas de imanes permanentes y de inducción con devanados distribuidos/concentrados), empleadas como casos de ejemplo a lo largo de este trabajo y cuyos modelos matemáticos se analizan minuciosamente en la Sección 2.2, tanto en variables de fase como en marcos de referencia estacionario y rotatorio. El modelo matemático del convertidor de potencia también se analiza en esta sección. Posteriormente, la Sección 2.3 analiza diferentes técnicas propuestas para el control de accionamientos multifásicos, mostrando la evolución desde el caso de trifásico hasta su implementación en el campo multifásico. Específicamente, las técnicas estudiadas en esta sección son el Control de Campo Orientado (FOC, por sus siglas en inglés), el DTC y el MPC. Si bien la Tesis se centra en DTC y MPC como estrategias de control, parece interesante destacar sus características y modo de funcionamiento con respecto al FOC, al ser la estrategia de control que se utiliza por excelencia en la gran mayoría de accionamientos electromecánicos de aplicación industrial.

Con el objetivo de destacar el interés de esta Tesis, la Sección 2.4 examina diferentes situaciones límite que pueden ser consideradas en el estudio de los accionamientos multifásicos. Esta sección muestra que aún no se ha alcanzado el estado de madurez de este tipo de dispositivos en lo que respecta a la explotación de sus ventajas. En este sentido, se debe prestar especial atención a la tolerancia a fallos (Sección 2.4.1) que, a pesar de ser una de las ventajas que más impulsa el uso de este tipo de accionamientos sobre los trifásicos convencionales, ha sido poco estudiada si se compara con el caso sano (sin faltas). Esta Tesis trata de avanzar en el estudio y la implementación de diferentes estrategias de control que permitan mejorar la tolerancia a fallos de los accionamientos multifásicos en aplicaciones de velocidad variable. En el Capítulo 3, se propone la técnica DTC para gestionar la operación de falta de fase abierta en la máquina multifásica y se compara su rendimiento con diferentes métodos actuales. Dado que el DTC tiene como característica principal la regulación de sólo dos variables de control (flujo y par) y ha llegado a ser considerada como una alternativa en el caso trifásico convencional al FOC, parece adecuado afrontar su estudio en casos en los que el número de grados de libertad del sistema multifásico se va asemejando al del sistema trifásico.

Por otro lado, en relación con la obtención de una técnica óptima que incluya los límites en la estrategia de control, esta Tesis va más allá de las propuestas mencionadas en la Sección 2.4.2 para aumentar el rendimiento de par de la máquina, donde sólo soluciones subóptimas se habían alcanzado hasta la fecha. Normalmente, se realizan algunas simplificaciones o suposiciones para obtener las expresiones analíticas para las corrientes de referencia cuando se consideran límites de

tensión y corriente. En todo caso, estos condicionantes reducen el interés en el DTC como método de regulación ya que provocan un aumento en el número de variables y grados de libertad a controlar. Es por ello que en el presente trabajo se aplican técnicas de control basadas en modelos para resolver los problemas de optimización y control. En consecuencia, se introduce un nuevo regulador MPC para *i*) generar referencias de corriente óptimas *online* considerando los límites de tensión, corriente y nivel máximo de magnetización, *ii*) extraer el par máximo de la máquina, y *iii*) garantizar el rendimiento del sistema en bucle cerrado (control de corriente). Dicho controlador genera referencias de corriente óptimas *online* por medio de una etapa que respeta las restricciones eléctricas impuestas. Después se aplica una etapa de control basada en modelos de predicción para la regulación de corriente. Esta contribución se analiza más a fondo en el Capítulo 4.

Finalmente, en la Sección 2.5 se lleva a cabo un análisis sobre diferentes formalismos gráficos para máquinas multifásicas, poniendo especial énfasis en la estructura EMR y mostrando su aplicación a una máquina de imanes permanentes de 5 fases a modo de ejemplo. El capítulo acaba con las conclusiones más relevantes recogidas en la Sección 2.6.

7.6 Controlador con un único subespacio a controlar en el dominio de frecuencia: caso del DTC

El Capítulo 3 se centra en el uso del DTC para estudiar la tolerancia a la operación de falta de fase abierta del variador multifásico. La capacidad de tolerancia al fallo de los variadores multifásicos es una interesante ventaja intrínseca para aplicaciones de seguridad crítica, donde recientes investigaciones han demostrado la efectividad de las estrategias FOC para manejar las operaciones post-falta sin rizado. El DTC se ha utilizado ampliamente como alternativa a los métodos FOC tradicionales para accionamientos trifásicos. A pesar de que este método puede no ser visto como un competidor en el campo multifásico porque se basa en la capacidad de regular sólo dos grados de libertad (flujo y par en la máquina), el esquema DTC convencional también se ha extendido a variadores multifásicos en los últimos tiempos, utilizando reguladores de histéresis para controlar de manera independiente el par y el flujo deseados en máquinas de inducción simétricas de 5 fases. Al aplicar este método, el control no puede centrarse en más de un subespacio de dominio de frecuencia (subespacio α - β normalmente). Cualquier acción en el subespacio x - y debe ser una regulación de corriente en bucle abierto, para limitar los armónicos no deseados si se considera una topología de devanados distribuidos. Esto se hace generalmente mediante la definición de vectores virtuales de tensión que generan tensión nula en los subespacios que no se pueden regular, permitiendo que el DTC se aplique con éxito cuando la máquina no tiene asimetrías en su diseño, algo que no tiene por qué coincidir con la realidad. En cualquier caso, si la situación límite considerada es la pérdida de una fase, la cantidad de grados de libertad controlables en el sistema disminuye y se acerca a la del caso trifásico convencional, donde el DTC puede considerarse una alternativa bastante competitiva al FOC. Esto justifica considerar la técnica DTC como una estrategia interesante para el caso de 5 fases y la situación límite de pérdida de ciertos grados de libertad en el control.

Este capítulo introduce los primeros resultados obtenidos en la Tesis, donde se presenta un nuevo esquema de DTC tolerante a faltas utilizando una máquina de inducción de 5 fases de

devanados distribuidos como caso de ejemplo. El modelado del sistema se analiza en la Sección 3.1, mostrando el efecto de la aparición de la falta de fase abierta en el sistema físico. El método DTC aplicado durante el funcionamiento en fallo de la máquina se describe en la Sección 3.2, donde se estudian las necesidades del controlador para gestionar la nueva situación operativa. En la Sección 3.3 se presentan varios resultados de simulación preliminares basados en un entorno MATLAB® y Simulink®, donde se estudia la capacidad de la técnica DTC modificada para gestionar el funcionamiento posterior a la falta de los variadores multifásicos. El rendimiento del método propuesto se valida también experimentalmente en una bancada de pruebas real basada en una máquina de inducción de devanados distribuidos de 5 fases, con el objetivo de verificar el análisis preliminar. La Sección 3.4 proporciona diferentes test que analizan los estados estacionario y transitorio, incluyendo el momento en el que aparece el fallo. Los resultados de simulación y experimentales obtenidos permiten concluir que las referencias de velocidad, par y flujo se mantienen después de la presencia de la falta siempre que el par de carga aplicado sea menor al par máximo que puede gestionar el esquema de control posteriormente a la falta.

El rendimiento del DTC en comparación con otras técnicas de control FOC basadas en controladores proporcionales resonantes y técnicas MPC se lleva a cabo en la Sección 3.5 cuando aparece una falta de fase abierta en el variador de 5 fases, proporcionando resultados de simulación y experimentales para concluir las fortalezas y debilidades de los métodos analizados. Los resultados obtenidos muestran que el método DTC tiene la capacidad de administrar un par eléctrico máximo menor. También se obtiene un mayor contenido armónico en la corriente de fase del estator cuando se aplica la técnica DTC, como ocurre en el caso trifásico. Sin embargo, el uso de un DTC post-falta es una opción viable que demuestra aumentar la robustez frente a los retrasos en la detección de las faltas, mientras que se preserva la simplicidad y el bajo coste computacional. Esto resulta en una alternativa interesante a los métodos FOC en aplicaciones industriales donde se necesita aumentar la fiabilidad y el accionamiento debe operar en condiciones de seguridad hasta que se realice un mantenimiento correctivo.

Sin embargo, cuando la situación límite considerada implica la inclusión de nuevos grados de libertad en el sistema (restricciones en tensiones, corrientes...), en este caso el DTC no parece ser una alternativa de control interesante debido a sus limitaciones. Por lo tanto, es aconsejable proponer alternativas de control directo que permitan controlar un alto número de variables. En el Capítulo 4 se analiza el método MPC como una técnica de control directo donde se puede incluir un mayor número de grados de libertad en la estrategia de control.

7.7 Controlador con dos subespacios independientes a controlar en el dominio de frecuencia: caso del MPC

El control óptimo de los accionamientos de potencia modernos requiere la consideración de restricciones eléctricas en la estrategia del regulador, incluyendo los límites de tensión y corriente impuestos por el convertidor de potencia y la máquina eléctrica o la saturación magnética debida al núcleo del hierro. Este problema ha sido ampliamente analizado en variadores trifásicos convencionales, pero raramente estudiado en multifásicos, donde los controladores óptimos que tienen en cuenta los límites eléctricos apenas se han considerado a pesar del interés actual de la

tecnología multifásica en aplicaciones de alta densidad de potencia, amplio rango de velocidad o tolerantes al fallo. Como se indicó anteriormente, la técnica DTC pierde interés en esta situación, ya que es capaz de controlar únicamente dos grados de libertad. Por ello, se requiere otra estrategia de control directo que maneje un mayor número de grados de libertad para este problema. En este sentido, el método MPC aparece como un candidato para tal fin, siendo además una estrategia de control que ofrece una alta flexibilidad frente a sistemas de múltiples entradas y salidas sujetos a restricciones.

En el Capítulo 4 se introduce un controlador óptimo generalizado que usa técnicas MPC, permitiendo la utilización óptima de la capacidad de par del sistema bajo limitaciones de tensión, corriente y magnéticas. Una descripción de los límites eléctricos que se incluyen en la estrategia de control óptima se detalla en la Sección 4.1. El método de control propuesto se introduce en la Sección 4.2 y se basa en dos etapas predictivas en cascada. En primer lugar, una etapa de MPC genera la referencia de corriente del estator óptima que cumple con los límites eléctricos del variador para aprovechar la característica de rendimiento máximo. Posteriormente, un controlador de tipo FCS-MPC regula la corriente del estator y genera el estado de conmutación en el convertidor de potencia. Los logros de esta técnica MPC de dos etapas en comparación con los métodos clásicos se pueden resumir a continuación:

- El controlador planteado permite la consideración de restricciones eléctricas en la estrategia del regulador, incluidos los límites de tensión y corriente impuestos por el convertidor de potencia y la máquina eléctrica. Así, se atiende una demanda industrial importante en relación con la obtención de mayores requisitos en el par máximo y la densidad de potencia de los motores modernos, porque se fuerza un incremento en los niveles de fiabilidad del variador introduciendo controladores estrictos con la capacidad de manejar los mecanismos de fallo y límites eléctricos críticos.
- La utilización de un controlador de corriente basado en el método FCS-MPC permite suprimir la etapa de modulación PWM, lo que mejora el rendimiento del par en bucle cerrado proporcionando un transitorio más rápido. Nótese también que la sintonización del controlador requiere menos esfuerzo en comparación con los métodos basados en PI-PWM.
- Aunque los controladores óptimos se han estudiado previamente en la literatura, sólo se han planteado soluciones subóptimas en el campo multifásico. En esta área de investigación particular, se consideraron algunas simplificaciones y/o suposiciones en la estrategia de control para tener en cuenta los límites eléctricos, como se indicó anteriormente. Sin embargo, el método propuesto permite el cálculo *online* de la referencia de corriente óptima, asegurando la condición de optimalidad del problema.

Se utilizan dos topologías diferentes de máquinas de 5 fases como ejemplos de accionamientos modernos de alto rendimiento para la validación experimental de la técnica predictiva de dos etapas: una máquina síncrona de imanes permanentes de 5 fases y una máquina de inducción de 5 fases de devanados concentrados. Éstas son accionamientos multifásicos comunes que pueden considerarse como sistemas con dos subespacios independientes de dominio de frecuencia para regular, donde las corrientes fundamentales y de tercer armónico son componentes ortogonales implicadas en la producción de par. La validación de la estrategia de control se analiza en la Sección 4.3, dividida en dos partes. La implementación de la técnica en un entorno de simulación

en tiempo real basado en tecnologías OPAL-RT se usa como paso previo para validar la efectividad de la propuesta en condiciones de funcionamiento estacionario y transitorio, donde se generan corrientes de referencia óptimas, y el sistema está compuesto por una máquina de imanes permanentes. A continuación, el interés del controlador se verifica experimentalmente usando una de las topologías de máquina eléctrica multifásica más investigada debido a su prometedora perspectiva industrial, como es la máquina de inducción de 5 fases con devanados concentrados. Los resultados obtenidos prueban que el generador de referencias de corrientes óptimas produce la mejor combinación de las referencias de corrientes $d-q$ para obtener el par máximo mientras minimiza las pérdidas en el cobre y respeta los límites eléctricos impuestos, mientras que se logra una mejora importante en la producción de par cuando se explota la componente del tercer armónico. El funcionamiento dinámico del sistema también se prueba, mostrando un seguimiento rápido y suave en la corriente y la velocidad.

Cabe destacar que, aunque en este trabajo se empleen casos particulares de máquinas multifásicas, la propuesta se puede extender fácilmente a máquinas de n fases, considerando funciones de coste y problemas de optimización más complejos.

7.8 Conclusiones

El objetivo general de este trabajo de Tesis Doctoral ha sido el desarrollo de técnicas de control para máquinas multifásicas, analizando la tolerancia del variador a diferentes condiciones operativas límite, tales como restricciones eléctricas/magnéticas o situaciones de fallo como una falta de fase abierta. Se proponen diferentes métodos de control directo para buscar alternativas al método FOC en el campo multifásico que no se han abordado hasta la fecha, de la misma manera que el DTC lo es para el FOC en el caso trifásico. Se han llevado a cabo validaciones experimentales para corroborar los enfoques iniciales, usando casos particulares de accionamientos de 5 fases que están disponibles en los laboratorios donde se realiza este trabajo. Sin embargo, todas las técnicas propuestas pueden extenderse fácilmente a máquinas de n fases.

En primer lugar, se propuso la técnica DTC para gestionar la operación de fallo de fase abierta de la máquina multifásica. Téngase en cuenta que el uso del DTC en variadores multifásicos puede estar limitado en el funcionamiento normal debido a la imposibilidad de regular más de dos grados de libertad (par eléctrico y flujo del estator). Sin embargo, cuando aparecen situaciones de fallo, el número de grados de libertad en el sistema se reduce y el inconveniente de usar el método DTC también puede mitigarse, siendo los beneficios similares a los obtenidos en los accionamientos trifásicos donde el DTC se convirtió, hace mucho tiempo, en una alternativa muy conocida e interesante en aplicaciones industriales a los métodos FOC. La técnica DTC se ha extendido con eficacia en este trabajo para hacer frente al funcionamiento de la máquina multifásica con una falta de fase abierta. Las referencias de velocidad, par y flujo se regulan con éxito después de la aparición de la falta si el par de carga aplicado está por debajo del par máximo que puede gestionar el esquema de control post-falta. Además, se ha llevado a cabo una evaluación experimental entre el DTC y otros métodos, que revela que no existe una técnica de control ideal para gestionar la aparición de fallos. Si la robustez, simplicidad o el coste computacional son las características deseables, el método DTC ofrece el mejor rendimiento. De lo contrario, si la calidad de la corriente

del estator en términos de distorsión armónica o el par eléctrico máximo post-falta se exige en el funcionamiento posterior a la falta, la solución más adecuada consiste en el uso de técnicas FOC.

Cuando aumenta el número de grados de libertad, el DTC parece ser un método de control inadecuado con la capacidad de regular únicamente el par y el flujo. Una alternativa interesante desde la perspectiva del control directo puede ser el uso del control predictivo, que se ha aplicado con éxito en los últimos tiempos en el campo de estudio. El MPC se ha mostrado como una excelente solución para optimizar la capacidad de par del variador bajo las restricciones de tensión, corriente y magnéticas impuestas por el convertidor de potencia y la máquina eléctrica. En este sentido, se introduce una técnica novedosa constituida por dos etapas MPC en cascada, que permite el cálculo *online* de las referencias de corriente óptimas. Los resultados experimentales obtenidos demuestran que el método puede generar una combinación óptima de las referencias de corriente $d-q$ para obtener el par máximo mientras se minimizan las pérdidas en el cobre y se respetan los límites impuestos.

Finalmente, es de destacar la internacionalización de este trabajo que ha sido desarrollado dentro de un acuerdo de cotutela internacional de tesis entre Arts et Métiers y la Universidad de Sevilla, con financiación del doctorando por parte de Arts et Métiers. Este trabajo también ha sido financiado a partir de dos proyectos de investigación respaldados por el gobierno español. Asimismo, los resultados obtenidos han dado lugar a un importante número de artículos publicados en revistas indexadas, contribuciones en congresos de reconocido prestigio, así como capítulos de libros y patentes registradas (ver Tabla 7.1).

Tabla 7.1. Sumario de la internacionalización derivada de esta Tesis Doctoral

Logro	Cantidad
Artículos en revistas	10 (+ 2 bajo revisión)
Publicaciones en congresos	5
Patentes españolas	1
Capítulos de libros	1
Participación en proyectos R&D	2

Bibliography

- [1] X. Kestelyn, “Modélisation vectorielle multimachines pour la commande des ensembles convertisseurs-machines polyphasés,” PhD Thesis, Université Lille 1 - Sciences et Technologies, December 2003.
- [2] X. Kestelyn, “Formalisme vectoriel et representation graphique causale pour la commande des systèmes électromécaniques à entrées multiples et dynamiques couplées,” Presentation for HdR, Université Lille 1 - Sciences et Technologies, December 2012.
- [3] P. Sandulescu, “Modélisation et commande d’un système à trois phases indépendantes à double fonctionnalité : Traction Électrique et Chargeur Forte Puissance pour application automobile,” PhD Thesis, Arts et Métiers ParisTech, September 2013.
- [4] B. Aslan, “Conception de machines polyphasées à aimants et bobinage concentré à pas fractionnaire avec large plage de vitesse,” PhD Thesis, Arts et Métiers ParisTech, October 2013.
- [5] H. Zahr, “Machine pentaphasée à double polarité pour électrification du domaine de transport par effet de boîte de vitesse électromagnétique,” PhD Thesis, Arts et Métiers ParisTech, December 2016.
- [6] T.J. Dos Santos Moraes, “Conception d’entraînements multi-machines multi-convertisseurs à haut niveau de fiabilité fonctionnelle,” PhD Thesis, Arts et Métiers ParisTech, October 2017.
- [7] L. Lu, E. Semail, L. Kobylanski and X. Kestelyn, “Flux-weakening strategies for a five-phase PM synchronous machine,” *Proceedings of the 2011-14th European Conference on Power Electronics and Applications (EPE 2011)*, pp. 1-7, 2011.
- [8] O. Fall, “Contribution à l’étude de machines électriques polyphasées à aimants permanents en vue d’une meilleur gestion de la commande en modes dégradés pour des applications liées aux énergies renouvelables marines,” PhD Thesis, Arts et Métiers ParisTech, January 2017.
- [9] R.I. Gregor Recalde, “Aportaciones al control de corriente de máquinas de inducción de seis fases con doble devanado trifásico independiente y asimétrico,” PhD Thesis, University of Seville, March 2010.
- [10] J.A. Riveros Insfrán, “Aportaciones en el control de máquinas multifásicas,” PhD Thesis, University of Seville, March 2013.
- [11] H.M. Guzmán Jiménez, “Extension of Finite-Control Set Model-Based Predictive Control Techniques to Fault-Tolerant Multiphase Drives: Analysis and Contributions,” PhD Thesis, University of Málaga, July 2015.

- [12] I. González Prieto, “Estudio Comparativo de Estrategias de Control Post-Falta en Accionamientos Eléctricos Multifásicos,” PhD Thesis, University of Seville, February 2016.
- [13] E.E. Ward and H. Härer, “Preliminary investigation of an inverter-fed 5-phase induction motor,” *Proceedings of the Institution of Electrical Engineers*, vol. 116, no. 6, pp. 980-984, June 1969.
- [14] E. Levi, “Multiphase Electric Machines for Variable-Speed Applications,” *IEEE Transactions on Industrial Electronics*, vol. 55, no. 5, pp. 1893-1909, May 2008.
- [15] E. Levi, R. Bojoi, F. Profumo, H.A. Toliyat and S. Williamson, “Multiphase induction motor drives – a technology status review,” *IET Electric Power Applications*, vol. 1, no. 4, pp. 489-516, July 2007.
- [16] G.K. Singh, “Modeling and analysis of six-phase synchronous generator for stand-alone renewable energy generation,” *Energy*, vol. 36, no. 9, pp. 5621-5631, September 2011.
- [17] W. Cao, B.C. Mecrow, G.J. Atkinson, J.W. Bennett and D.J. Atkinson, “Overview of Electric Motor Technologies Used for More Electric Aircraft (MEA),” *IEEE Transactions on Industrial Electronics*, vol. 59, no. 9, pp. 3523-3531, September 2012.
- [18] E. Jung, H. Yoo, S.K. Sul, H.S. Choi and Y.Y. Choi, “A Nine-Phase Permanent-Magnet Motor Drive System for an Ultrahigh-Speed Elevator,” *IEEE Transactions on Industry Applications*, vol. 48, no. 3, pp. 987-995, May-June 2012.
- [19] J. Liu, L. Huang, H. Yu, C. Wen and W. Zhong, “Study on the Characteristics of a Novel Six-Phase Fault-Torrent Linear Permanent Magnet Machine for Linear Oil Pumping,” *IEEE Transactions on Applied Superconductivity*, vol. 24, no. 3, pp. 1-5, June 2014.
- [20] R. Bojoi, “Analysis, Design and Implementation of a Dual Three-Phase Vector Controlled Induction Motor Drive,” PhD Thesis, Politecnico di Torino, 2002.
- [21] S. Williamson and S. Smith, “Pulsating torque and losses in multiphase induction machines,” *IEEE Transactions on Industry Applications*, vol. 39, no. 4, pp. 986-993, July-August 2003.
- [22] G.K. Singh, “Multi-phase induction machine drive research – a survey,” *Electric Power Systems Research*, vol. 61, no. 2, pp. 139-147, March 2002.
- [23] M. Jones and E. Levi, “A Literature Survey of the State-of-the-Art in Multiphase AC Drives,” *Proceedings 37th International Universities Power Engineering Conference (UPEC 2002)*, pp. 505-510, 2002.
- [24] E. Levi, “Advances in Converter Control and Innovative Exploitation of Additional Degrees of Freedom for Multiphase Machines,” *IEEE Transactions on Industrial Electronics*, vol. 63, no. 1, pp. 433-448, January 2016.
- [25] F. Barrero and M.J. Duran, “Recent Advances in the Design, Modeling, and Control of Multiphase Machines – Part I,” *IEEE Transactions on Industrial Electronics*, vol. 63, no. 1, pp. 449-458, January 2016.
- [26] M.J. Duran and F. Barrero, “Recent Advances in the Design, Modeling, and Control of Multiphase Machines – Part II,” *IEEE Transactions on Industrial Electronics*, vol. 63, no. 1, pp. 459-468, Jan. 2016.

-
- [27] M.A. Abbas, R. Christen and T.M. Jahns, "Six-Phase Voltage Source Inverter Driven Induction Motor," *IEEE Transactions on Industry Applications*, vol. IA-20, no. 5, pp. 1251-1259, September 1984.
- [28] K.N. Pavithran, R. Parimelalagan and M.R. Krishnamurthy, "Studies on Inverted-Fed Five-Phase Induction Motor Drive," *IEEE Transactions on Power Electronics*, vol. 3, no. 2, pp. 224-235, April 1988.
- [29] C.C. Scharlau, L.F.A. Pereira, L.A. Pereira and S. Haffner, "Performance of a Five-Phase Induction Machine With Optimized Air Gap Field Under Open Loop V/f Control," *IEEE Transactions on Energy Conversion*, vol. 23, no. 4, pp. 1046-1056, December 2008.
- [30] G.K. Singh, K. Nam and S.K. Lim, "A simple indirect field-oriented control scheme for multiphase induction machine," *IEEE Transactions on Industrial Electronics*, vol. 52, no. 4, pp. 1177-1184, August 2005.
- [31] S.N. Vukosavic, M. Jones, E. Levi and J. Varga, "Rotor flux oriented control of a symmetrical six-phase induction machine," *Electric Power Systems Research*, vol. 75, no. 2-3, pp. 142-152, August 2005.
- [32] R. Bojoi, E. Levi, F. Farina, A. Tenconi and F. Profumo, "Dual three-phase induction motor drive with digital current control in the stationary reference frame," *IEE Proceedings - Electric Power Applications*, vol. 153, no. 1, pp. 129-139, 1 January 2006.
- [33] R. Bojoi, F. Farina, G. Griva, F. Profumo and A. Tenconi, "Direct torque control for dual three-phase induction motor drives," *IEEE Transactions on Industry Applications*, vol. 41, no. 6, pp. 1627-1636, November-December 2005.
- [34] K. Hatua and V.T. Ranganathan, "Direct torque control schemes for split-phase induction machine," *IEEE Transactions on Industry Applications*, vol. 41, no. 5, pp. 1243-1254, September-October. 2005.
- [35] F. Barrero, M.R. Arahall, R. Gregor, S. Toral and M.J. Duran, "A Proof of Concept Study of Predictive Current Control for VSI-Driven Asymmetrical Dual Three-Phase AC Machines," *IEEE Transactions on Industrial Electronics*, vol. 56, no. 6, pp. 1937-1954, June 2009.
- [36] F. Barrero, M.R. Arahall, R. Gregor, S. Toral and M.J. Duran, "One-Step Modulation Predictive Current Control Method for the Asymmetrical Dual Three-Phase Induction Machine," *IEEE Transactions on Industrial Electronics*, vol. 56, no. 6, pp. 1974-1983, June 2009.
- [37] R. Gregor, F. Barrero, S. Toral, M.J. Duran, M.R. Arahall, J. Prieto and J.L. Mora, "Predictive-space vector PWM current control method for asymmetrical dual three-phase induction motor drives," *IET Electric Power Applications*, vol. 4, no. 1, pp. 26-34, January 2010.
- [38] F. Barrero, J. Prieto, E. Levi, R. Gregor, S. Toral, M.J. Duran and M. Jones, "An Enhanced Predictive Current Control Method for Asymmetrical Six-Phase Motor Drives," *IEEE Transactions on Industrial Electronics*, vol. 58, no. 8, pp. 3242-3252, August 2011.
- [39] M.J. Duran, J. Prieto, F. Barrero and S. Toral, "Predictive Current Control of Dual Three-Phase Drives Using Restrained Search Techniques," *IEEE Transactions on Industrial Electronics*, vol. 58, no. 8, pp. 3253-3263, August 2011.

- [40] C.L. Fortescue, "Method of Symmetrical Co-Ordinates Applied to the Solution of Polyphase Networks," *Transactions of the American Institute of Electrical Engineers*, vol. XXXVII, no. 2, pp. 1027-1140, July 1918.
- [41] E. Clarke, "Circuit analysis of A-C power, Volumes 1 and 2," New York: John Wiley & Sons, 1951.
- [42] H.A. Toliyat, T.A. Lipo and J.C. White, "Analysis of a concentrated winding induction machine for adjustable speed drive applications. I. Motor analysis," *IEEE Transactions on Energy Conversion*, vol. 6, no. 4, pp. 679-683, December 1991.
- [43] H.A. Toliyat, T.A. Lipo and J.C. White, "Analysis of a concentrated winding induction machine for adjustable speed drive applications. II. Motor design and performance," *IEEE Transactions on Energy Conversion*, vol. 6, no. 4, pp. 684-692, December 1991.
- [44] L.A. Pereira, C.C. Scharlau, L.F.A. Pereira and J.F. Haffner, "General Model of a Five-Phase Induction Machine Allowing for Harmonics in the Air Gap Field," *IEEE Transactions on Energy Conversion*, vol. 21, no. 4, pp. 891-899, December 2006.
- [45] R.H. Nelson and P.C. Krause, "Induction Machine Analysis for Arbitrary Displacement Between Multiple Winding Sets," *IEEE Transactions on Power Apparatus and Systems*, vol. PAS-93, no. 3, pp. 841-848, May 1974.
- [46] T. Lipo, "A d-q model for six phase induction machines," *International Conference on Electric Machines*, pp. 860-867, September 1980.
- [47] D. Hadiouche, H. Razik and A. Rezzoug, "On the modeling and design of dual-stator windings to minimize circulating harmonic currents for VSI fed AC machines," *IEEE Transactions on Industry Applications*, vol. 40, no. 2, pp. 506-515, March-April 2004.
- [48] J. Malvar, "Analysis of time and space harmonics in symmetrical multiphase induction motor drives by means of vector space decomposition," PhD Thesis, University of Vigo, November 2015.
- [49] A.M. Trzynadlowski, "Control of Induction Motors," Elsevier, October 2000.
- [50] G. Pellegrino, R. Bojoi and P. Guglielmi, "Unified Direct-Flux Vector Control for AC Motor Drives," *IEEE Transactions on Industry Applications*, vol. 47, no. 5, pp. 2093-2102, September-October 2011.
- [51] L. Zheng, J.E. Fletcher, B.W. Williams and X. He, "A Novel Direct Torque Control Scheme for a Sensorless Five-Phase Induction Motor Drive," *IEEE Transactions on Industrial Electronics*, vol. 58, no. 2, pp. 503-513, February 2011.
- [52] L. Gao, J.E. Fletcher and L. Zheng, "Low-Speed Control Improvements for a Two-Level Five-Phase Inverter-Fed Induction Machine Using Classic Direct Torque Control," *IEEE Transactions on Industrial Electronics*, vol. 58, no. 7, pp. 2744-2754, July 2011.
- [53] T.A. Lipo and F.X. Wang, "Design and Performance of a Converter Optimized AC Machine," *IEEE Transactions on Industry Applications*, vol. IA-20, no. 4, pp. 834-844, July 1984.
- [54] L.A. Pereira, C.C. Scharlau, L.F.A. Pereira and J.F. Haffner, "Model of a five-phase induction machine allowing for harmonics in the air-gap field. Part I: Parameter determination and general equations," *30th Annual Conference of IEEE Industrial Electronics Society (IECON 2004)*, vol. 1, pp. 98-103, 2004.

- [55] L.A. Pereira, C.C. Scharlau, L.F.A. Pereira and J.F. Haffner, "Model of a five-phase induction machine allowing for harmonics in the air-gap field. Part II: Transformation of co-ordinates and d-q models," *30th Annual Conference of IEEE Industrial Electronics Society (IECON 2004)*, vol. 2, pp. 1682-1687, 2004.
- [56] T. Sebastian, G. Slemon and M. Rahman, "Modelling of permanent magnet synchronous motors," *IEEE Transactions on Magnetics*, vol. 22, no. 5, pp. 1069-1071, September 1986.
- [57] P. Pillay and R. Krishnan, "Modeling, simulation, and analysis of permanent-magnet motor drives. I. The permanent-magnet synchronous motor drive," *IEEE Transactions on Industry Applications*, vol. 25, no. 2, pp. 265-273, March-April 1989.
- [58] P. Pillay and R. Krishnan, "Modeling, simulation, and analysis of permanent-magnet motor drives. II. The brushless DC motor drive," *IEEE Transactions on Industry Applications*, vol. 25, no. 2, pp. 274-279, March-April 1989.
- [59] L. Parsa and H.A. Toliyat, "Five-phase permanent-magnet motor drives," *IEEE Transactions on Industry Applications*, vol. 41, no. 1, pp. 30-37, January-February 2005.
- [60] R. Krishnan, "Electric Motor Drives: Modeling, Analysis, and Control," Pearson Education, 2001.
- [61] O. Lopez, E. Levi, F.D. Freijedo and J. Doval-Gandoy, "Number of switching state vectors and space vectors in multilevel multiphase converters," *Electronics Letters*, vol. 45, no. 10, pp. 524-525, May 2009.
- [62] J.I. Leon, O. Lopez, L.G. Franquelo, J. Doval-Gandoy, S. Vazquez, J. Alvarez and F.D. Freijedo, "Multilevel Multiphase Feedforward Space-Vector Modulation Technique," *IEEE Transactions on Industrial Electronics*, vol. 57, no. 6, pp. 2066-2075, June 2010.
- [63] K. Hasse, "Zur Dynamik drehzahl geregelter Antriebe mit stromrichtergespeisten Asynchron-Kurzschlußläufermaschinen (On dynamic of the speed controlled static AC drive with squirrel-cage induction machine)," PhD Thesis, Technical University Darmstadt, 1969.
- [64] F. Blaschke, "The principle of field orientation as applied to the new transvector closed loop control for rotating machine," *Siemens Review*, vol. 34, no. 3, pp. 217-220, 1972.
- [65] L. Zheng, J.E. Fletcher, B.W. Williams and X. He, "Dual-Plane Vector Control of a Five-Phase Induction Machine for an Improved Flux Pattern," *IEEE Transactions on Industrial Electronics*, vol. 55, no. 5, pp. 1996-2005, May 2008.
- [66] M.R. Khan, A. Iqbal and M. Ahmad, "MRAS-based sensorless control of a vector controlled five-phase induction motor drive," *Electric Power Systems Research*, vol. 78, no. 8, pp. 1311-1321, August 2008.
- [67] M.R. Arahal and M.J. Duran, "PI tuning of five-phase drives with third harmonic injection," *Control Engineering Practice*, vol. 17, no. 7, pp. 787-797, July 2009.
- [68] M. Jones, S.N. Vukosavic, D. Dujic and E. Levi, "A Synchronous Current Control Scheme for Multiphase Induction Motor Drives," *IEEE Transactions on Energy Conversion*, vol. 24, no. 4, pp. 860-868, December 2009.
- [69] A.S. Abdel-Khalik, M.I. Masoud and B.W. Williams, "Improved Flux Pattern With Third Harmonic Injection for Multiphase Induction Machines," *IEEE Transactions on Power Electronics*, vol. 27, no. 3, pp. 1563-1578, March 2012.

- [70] A.S. Abdel-Khalik, M.I. Masoud and B.W. Williams, "Vector controlled multiphase induction machine: Harmonic injection using optimized constant gains," *Electric Power Systems Research*, vol. 89, pp. 116-128, August 2012.
- [71] H.S. Che, E. Levi, M. Jones, W.P. Hew and N.A. Rahim, "Current Control Methods for an Asymmetrical Six-Phase Induction Motor Drive," *IEEE Transactions on Power Electronics*, vol. 29, no. 1, pp. 407-417, January 2014.
- [72] A.G. Yepes, J. Malvar, A. Vidal, O. López and J. Doval-Gandoy, "Current Harmonics Compensation Based on Multiresonant Control in Synchronous Frames for Symmetrical n -Phase Machines," *IEEE Transactions on Industrial Electronics*, vol. 62, no. 5, pp. 2708-2720, May 2015.
- [73] R.N. Andriamalala, H. Razik, B. Francois and X. Guillaud, "Direct Rotor Field-Oriented Control of a Dual Three-Phase Induction Machine using a novel Kalman observer," *38th Annual Conference on IEEE Industrial Electronics Society (IECON 2012)*, pp. 2251-2256, 2012.
- [74] K. Iffouzar, S. Taraft, H. Aouzellag, K. Ghedamsi and D. Aouzellag, "DRFOC of polyphase induction motor based on fuzzy logic controller speed," *4th International Conference on Electrical Engineering (ICEE 2015)*, pp. 1-7, 2015.
- [75] J.W. Kelly, E.G. Strangas and J.M. Miller, "Multiphase space vector pulse width modulation," *IEEE Transactions on Energy Conversion*, vol. 18, no. 2, pp. 259-264, June 2003.
- [76] A. Iqbal and E. Levi, "Space Vector PWM Techniques for Sinusoidal Output Voltage Generation with a Five-Phase Voltage Source Inverter," *Electric Power Components and Systems*, vol. 34, no.2, pp. 119-140, 2006.
- [77] O. Lopez, D. Dujic, M. Jones, F.D. Freijedo, J. Doval-Gandoy and E. Levi, "Multidimensional Two-Level Multiphase Space Vector PWM Algorithm and Its Comparison With Multifrequency Space Vector PWM Method," *IEEE Transactions on Industrial Electronics*, vol. 58, no. 2, pp. 465-475, February 2011.
- [78] A. Iqbal and S. Moinuddin, "Comprehensive Relationship Between Carrier-Based PWM and Space Vector PWM in a Five-Phase VSI," *IEEE Transactions on Power Electronics*, vol. 24, no. 10, pp. 2379-2390, October 2009.
- [79] D. Dujic, M. Jones, E. Levi, J. Prieto and F. Barrero, "Switching Ripple Characteristics of Space Vector PWM Schemes for Five-Phase Two-Level Voltage Source Inverters – Part 1: Flux Harmonic Distortion Factors," *IEEE Transactions on Industrial Electronics*, vol. 58, no. 7, pp. 2789-2798, July 2011.
- [80] M. Jones, D. Dujic, E. Levi, J. Prieto and F. Barrero, "Switching Ripple Characteristics of Space Vector PWM Schemes for Five-Phase Two-Level Voltage Source Inverters – Part 2: Current Ripple," *IEEE Transactions on Industrial Electronics*, vol. 58, no. 7, pp. 2799-2808, July 2011.
- [81] J. Prieto, M. Jones, F. Barrero, E. Levi and S. Toral, "Comparative Analysis of Discontinuous and Continuous PWM Techniques in VSI-Fed Five-Phase Induction Motor," *IEEE Transactions on Industrial Electronics*, vol. 58, no. 12, pp. 5324-5335, December 2011.

- [82] D. Dujic, "Development of Pulse-Width-Modulation Techniques for Multi-Phase and Multi-Leg Voltage Source Inverters," PhD Thesis, Liverpool John Moores University, 2008.
- [83] M.J. Duran, J. Prieto and F. Barrero, "Space Vector PWM With Reduced Common-Mode Voltage for Five-Phase Induction Motor Drives Operating in Overmodulation Zone," *IEEE Transactions on Power Electronics*, vol. 28, no. 8, pp. 4030-4040, August 2013.
- [84] M.J. Duran, J. Prieto, F. Barrero, J.A. Riveros and H. Guzman, "Space-Vector PWM With Reduced Common-Mode Voltage for Five-Phase Induction Motor Drives," *IEEE Transactions on Industrial Electronics*, vol. 60, no. 10, pp. 4159-4168, October 2013.
- [85] H. Xu, H.A. Toliyat and L.J. Petersen, "Five-phase induction motor drives with DSP-based control system," *IEEE Transactions on Power Electronics*, vol. 17, no. 4, pp. 524-533, July 2002.
- [86] L. Parsa, H.A. Toliyat and A. Goodarzi, "Five-Phase Interior Permanent-Magnet Motors With Low Torque Pulsation," *IEEE Transactions on Industry Applications*, vol. 43, no. 1, pp. 40-46, January-February 2007.
- [87] A. Abdelkhalik, M. Masoud and W. Barry, "Eleven-phase induction machine: steady-state analysis and performance evaluation with harmonic injection," *IET Electric Power Applications*, vol. 4, no. 8, pp. 670-685, September 2010.
- [88] P. Zheng, Y. Sui, J. Zhao, C. Tong, T.A. Lipo and A. Wang, "Investigation of a Novel Five-Phase Modular Permanent-Magnet In-Wheel Motor," *IEEE Transactions on Magnetics*, vol. 47, no. 10, pp. 4084-4087, October 2011.
- [89] J. Karttunen, S. Kallio, P. Peltoniemi, P. Silventoinen and O. Pyrhönen, "Decoupled Vector Control Scheme for Dual Three-Phase Permanent Magnet Synchronous Machines," *IEEE Transactions on Industrial Electronics*, vol. 61, no. 5, pp. 2185-2196, May 2014.
- [90] Y. Hu, Z. Q. Zhu and K. Liu, "Current Control for Dual Three-Phase Permanent Magnet Synchronous Motors Accounting for Current Unbalance and Harmonics," *IEEE Journal of Emerging and Selected Topics in Power Electronics*, vol. 2, no. 2, pp. 272-284, June 2014.
- [91] K. Wang, Z.Q. Zhu and G. Ombach, "Torque Improvement of Five-Phase Surface-Mounted Permanent Magnet Machine Using Third-Order Harmonic," *IEEE Transactions on Energy Conversion*, vol. 29, no. 3, pp. 735-747, September 2014.
- [92] I. Takahashi and T. Noguchi, "A New Quick-Response and High-Efficiency Control Strategy of an Induction Motor," *IEEE Transactions on Industry Applications*, vol. IA-22, no. 5, pp. 820-827, September 1986.
- [93] M. Depenbrock, "Direct self-control (DSC) of inverter-fed induction machine," *IEEE Transactions on Power Electronics*, vol. 3, no. 4, pp. 420-429, October 1988.
- [94] G.S. Buja and M.P. Kazmierkowski, "Direct torque control of PWM inverter-fed AC motors - a survey," *IEEE Transactions on Industrial Electronics*, vol. 51, no. 4, pp. 744-757, August 2004.
- [95] ABB Group, "DTC: A motor control technique for all seasons," ABB White Paper, April 2015 [Online]. Available: http://library.e.abb.com/public/0e07ab6a2de30809c1257e2d0042db5e/ABB_WhitePaper_DTC_A4_20150414.pdf.

- [96] R. Kianinezhad, B. Nahid, F. Betin and G.A. Capolino, "A novel Direct Torque Control (DTC) method for dual three phase induction motors," *IEEE International Conference on Industrial Technology (ICIT 2006)*, pp. 939-943, 2006.
- [97] R. Kianinezhad, R. Alcharea, B. Nahid, F. Betin and G. Capolino, "A novel direct torque control (DTC) for six-phase induction motors with common neutrals," *International Symposium on Power Electronics, Electrical Drives, Automation and Motion (SPEEDAM 2008)*, pp. 107-112, 2008.
- [98] L. Parsa and H.A. Toliyat, "Sensorless Direct Torque Control of Five-Phase Interior Permanent-Magnet Motor Drives," *IEEE Transactions on Industry Applications*, vol. 43, no. 4, pp. 952-959, July-August 2007.
- [99] Y. Gao and L. Parsa, "Modified Direct Torque Control of Five-Phase Permanent Magnet Synchronous Motor Drives," *22nd Annual IEEE Applied Power Electronics Conference and Exposition (APEC 2007)*, pp. 1428-1433, 2007.
- [100] J.A. Riveros, M.J. Duran, F. Barrero and S. Toral, "Direct torque control for five-phase induction motor drives with reduced common-mode voltage," *38th Annual Conference on IEEE Industrial Electronics Society (IECON 2012)*, pp. 3616-3621, 2012.
- [101] Y.N. Tatte and M.V. Aware, "Direct Torque Control of Five-Phase Induction Motor With Common-Mode Voltage and Current Harmonics Reduction," *IEEE Transactions on Power Electronics*, vol. 32, no. 11, pp. 8644-8654, November 2017.
- [102] Y. Fei, Z. Xiaofeng, Q. Minzhong and D. Chengdong, "The direct torque control of multiphase permanent magnet synchronous motor based on low harmonic space vector PWM," *IEEE International Conference on Industrial Technology (ICIT 2008)*, pp. 1-5, 2008.
- [103] P. Cortes, M.P. Kazmierkowski, R.M. Kennel, D.E. Quevedo and J. Rodriguez, "Predictive Control in Power Electronics and Drives," *IEEE Transactions on Industrial Electronics*, vol. 55, no. 12, pp. 4312-4324, December 2008.
- [104] S. Kouro, P. Cortes, R. Vargas, U. Ammann and J. Rodriguez, "Model Predictive Control – A Simple and Powerful Method to Control Power Converters," *IEEE Transactions on Industrial Electronics*, vol. 56, no. 6, pp. 1826-1838, June 2009.
- [105] M.R. Arahal, F. Barrero, S. Toral, M.J. Duran and R. Gregor, "Multi-phase current control using finite-state model-predictive control," *Control Engineering Practice*, vol. 17, no. 5, pp. 579-587, May 2009.
- [106] J. Rodriguez, M.P. Kazmierkowski, J.R. Espinoza, P. Zanchetta, H. Abu-Rub, H.A. Young and C.A. Rojas, "State of the Art of Finite Control Set Model Predictive Control in Power Electronics," *IEEE Transactions on Industrial Informatics*, vol. 9, no. 2, pp. 1003-1016, May 2013.
- [107] C. S. Lim, E. Levi, M. Jones, N. A. Rahim, and W. P. Hew, "FCS-MPC-based current control of a five-phase induction motor and its comparison with PI-PWM control," *IEEE Transactions on Industrial Electronics*, vol. 61, no. 1, pp. 149-163, January 2014.
- [108] H. Miranda, P. Cortes, J.I. Yuz and J. Rodriguez, "Predictive Torque Control of Induction Machines Based on State-Space Models," *IEEE Transactions on Industrial Electronics*, vol. 56, no. 6, pp. 1916-1924, June 2009.

-
- [109] J.A. Riveros, J. Prieto, F. Barrero, S. Toral, M. Jones and E. Levi, "Predictive Torque Control for five-phase induction motor drives," *36th Annual Conference on IEEE Industrial Electronics Society (IECON 2010)*, pp. 2467-2472, 2010.
- [110] J.A. Riveros, F. Barrero, E. Levi, M.J. Durán, S. Toral and M. Jones, "Variable-Speed Five-Phase Induction Motor Drive Based on Predictive Torque Control," *IEEE Transactions on Industrial Electronics*, vol. 60, no. 8, pp. 2957-2968, August 2013.
- [111] M.J. Duran, J.A. Riveros, F. Barrero, H. Guzman and J. Prieto, "Reduction of Common-Mode Voltage in Five-Phase Induction Motor Drives Using Predictive Control Techniques," *IEEE Transactions on Industry Applications*, vol. 48, no. 6, pp. 2059-2067, November-December 2012.
- [112] O. Fall, N.K. Nguyen, J.F. Charpentier, P. Letellier, E. Semail and X. Kestelyn, "Variable speed control of a 5-phase permanent magnet synchronous generator including voltage and current limits in healthy and open-circuited modes," *Electric Power Systems Research*, vol. 140, pp. 507-516, November 2016.
- [113] A.G. Yepes, J.A. Riveros, J. Doval-Gandoy, F. Barrero, O. Lopez, B. Bogado, M. Jones and E. Levi, "Parameter Identification of Multiphase Induction Machines With Distributed Windings – Part 1: Sinusoidal Excitation Methods," *IEEE Transactions on Energy Conversion*, vol. 27, no. 4, pp. 1056-1066, December 2012.
- [114] J.A. Riveros, A.G. Yepes, F. Barrero, J. Doval-Gandoy, B. Bogado, O. Lopez, M. Jones and E. Levi, "Parameter Identification of Multiphase Induction Machines With Distributed Windings – Part 2: Time-Domain Techniques," *IEEE Transactions on Energy Conversion*, vol. 27, no. 4, pp. 1067-1077, December 2012.
- [115] M. Siami, D.A. Khaburi, A. Abbaszadeh and J. Rodríguez, "Robustness Improvement of Predictive Current Control Using Prediction Error Correction for Permanent-Magnet Synchronous Machines," *IEEE Transactions on Industrial Electronics*, vol. 63, no. 6, pp. 3458-3466, June 2016.
- [116] C. Martin, M. Bermudez, F. Barrero, M.R. Arahall, X. Kestelyn and M.J. Duran, "Sensitivity of predictive controllers to parameter variation in five-phase induction motor drives," *Control Engineering Practice*, vol. 68, pp. 23-31, November 2017.
- [117] J. Rodríguez, R.M. Kennel, J.R. Espinoza, M. Trincado, C.A. Silva and C.A. Rojas, "High-Performance Control Strategies for Electrical Drives: An Experimental Assessment," *IEEE Transactions on Industrial Electronics*, vol. 59, no. 2, pp. 812-820, February 2012.
- [118] T. Geyer, G. Papafotiou and M. Morari, "Model Predictive Direct Torque Control – Part I: Concept, Algorithm, and Analysis," *IEEE Transactions on Industrial Electronics*, vol. 56, no. 6, pp. 1894-1905, June 2009.
- [119] T. Geyer, "A Comparison of Control and Modulation Schemes for Medium-Voltage Drives: Emerging Predictive Control Concepts Versus PWM-Based Schemes," *IEEE Transactions on Industry Applications*, vol. 47, no. 3, pp. 1380-1389, May-June 2011.
- [120] J. Holtz, "The representation of AC machine dynamics by complex signal flow graphs," *IEEE Transactions on Industrial Electronics*, vol. 42, no. 3, pp. 263-271, June 1995.
- [121] A. Consoli, "Special Section on Robust Operation of Electrical Drives," *IEEE Transactions on Power Electronics*, vol. 27, no. 2, pp. 476-478, February 2012.

- [122] L. de Lillo, L. Empringham, P.W. Wheeler, S. Khwran-On, C. Gerada, M.N. Othman and X. Huang, "Multiphase Power Converter Drive for Fault-Tolerant Machine Development in Aerospace Applications," *IEEE Transactions on Industrial Electronics*, vol. 57, no. 2, pp. 575-583, February 2010.
- [123] L. Parsa and H.A. Toliyat, "Fault-Tolerant Interior-Permanent-Magnet Machines for Hybrid Electric Vehicle Applications," *IEEE Transactions on Vehicular Technology*, vol. 56, no. 4, pp. 1546-1552, July 2007.
- [124] X. Huang, A. Goodman, C. Gerada, Y. Fang and Q. Lu, "Design of a Five-Phase Brushless DC Motor for a Safety Critical Aerospace Application," *IEEE Transactions on Industrial Electronics*, vol. 59, no. 9, pp. 3532-3541, September 2012.
- [125] S.S. Gjerde, P.K. Olsen, K. Ljøkelsøy and T.M. Undeland, "Control and Fault Handling in a Modular Series-Connected Converter for a Transformerless 100 kV Low-Weight Offshore Wind Turbine," *IEEE Transactions on Industry Applications*, vol. 50, no. 2, pp. 1094-1105, March-April 2014.
- [126] M. Barcaro, N. Bianchi and F. Magnussen, "Faulty Operations of a PM Fractional-Slot Machine With a Dual Three-Phase Winding," *IEEE Transactions on Industrial Electronics*, vol. 58, no. 9, pp. 3825-3832, September 2011.
- [127] N.K. Nguyen, F. Meinguet, E. Semail and X. Kestelyn, "Fault-Tolerant Operation of an Open-End Winding Five-Phase PMSM Drive With Short-Circuit Inverter Fault," *IEEE Transactions on Industrial Electronics*, vol. 63, no. 1, pp. 595-605, January 2016.
- [128] L. Zarri, M. Mengoni, Y. Gritli, A. Tani, F. Filippetti, G. Serra and D. Casadei, "Detection and Localization of Stator Resistance Dissymmetry Based on Multiple Reference Frame Controllers in Multiphase Induction Motor Drives," *IEEE Transactions on Industrial Electronics*, vol. 60, no. 8, pp. 3506-3518, August 2013.
- [129] A.S. Abdel-Khalik, M.I. Masoud, S. Ahmed and A. Massoud, "Calculation of derating factors based on steady-state unbalanced multiphase induction machine model under open phase(s) and optimal winding currents," *Electric Power Systems Research*, vol. 106, pp. 214-225, January 2014.
- [130] H. Guzman, F. Barrero and M.J. Duran, "IGBT-Gating Failure Effect on a Fault-Tolerant Predictive Current-Controlled Five-Phase Induction Motor Drive," *IEEE Transactions on Industrial Electronics*, vol. 62, no. 1, pp. 15-20, January 2015.
- [131] S. Dwari and L. Parsa, "An Optimal Control Technique for Multiphase PM Machines Under Open-Circuit Faults," *IEEE Transactions on Industrial Electronics*, vol. 55, no. 5, pp. 1988-1995, May 2008.
- [132] D. Foito, J. Maia, V.F. Pires and J.F. Martins, "Fault diagnosis in six-phase induction motor using a current trajectory mass center," *Measurement*, vol. 51, pp. 164-173, May 2014.
- [133] M. Salehifar, R.S. Arashloo, J.M. Moreno-Equilaz, V. Sala and L. Romeral, "Fault Detection and Fault Tolerant Operation of a Five Phase PM Motor Drive Using Adaptive Model Identification Approach," *IEEE Journal of Emerging and Selected Topics in Power Electronics*, vol. 2, no. 2, pp. 212-223, June 2014.
- [134] M.J. Duran, I. Gonzalez-Prieto, N. Rios-Garcia and F. Barrero, "A Simple, Fast, and Robust Open-Phase Fault Detection Technique for Six-Phase Induction Motor Drives," *IEEE Transactions on Power Electronics*, vol. 33, no. 1, pp. 547-557, January 2018.

-
- [135] S. Dwari and L. Parsa, "Fault-Tolerant Control of Five-Phase Permanent-Magnet Motors With Trapezoidal Back EMF," *IEEE Transactions on Industrial Electronics*, vol. 58, no. 2, pp. 476-485, February 2011.
- [136] H.S. Che, M.J. Duran, E. Levi, M. Jones, W.P. Hew and N.A. Rahim, "Postfault Operation of an Asymmetrical Six-Phase Induction Machine With Single and Two Isolated Neutral Points," *IEEE Transactions on Power Electronics*, vol. 29, no. 10, pp. 5406-5416, October 2014.
- [137] N. Bianchi, E. Fornasiero and S. Bolognani, "Thermal Analysis of a Five-Phase Motor Under Faulty Operations," *IEEE Transactions on Industry Applications*, vol. 49, no. 4, pp. 1531-1538, July-August 2013.
- [138] R. Kianinezhad, B. Nahid-Mobarakeh, L. Baghli, F. Betin and G.A. Capolino, "Modeling and Control of Six-Phase Symmetrical Induction Machine Under Fault Condition Due to Open Phases," *IEEE Transactions on Industrial Electronics*, vol. 55, no. 5, pp. 1966-1977, May 2008.
- [139] F. Baudart, B. Dehez, E. Matagne, D. Telteu-Nedelcu, P. Alexandre and F. Labrique, "Torque Control Strategy of Polyphase Permanent-Magnet Synchronous Machines With Minimal Controller Reconfiguration Under Open-Circuit Fault of One Phase," *IEEE Transactions on Industrial Electronics*, vol. 59, no. 6, pp. 2632-2644, June 2012.
- [140] H. Guzman, M.J. Duran, F. Barrero, B. Bogado and S. Toral, "Speed Control of Five-Phase Induction Motors With Integrated Open-Phase Fault Operation Using Model-Based Predictive Current Control Techniques," *IEEE Transactions on Industrial Electronics*, vol. 61, no. 9, pp. 4474-4484, September 2014.
- [141] X. Kestelyn and E. Semail, "A Vectorial Approach for Generation of Optimal Current References for Multiphase Permanent-Magnet Synchronous Machines in Real Time," *IEEE Transactions on Industrial Electronics*, vol. 58, no. 11, pp. 5057-5065, November 2011.
- [142] R.S. Arashloo, J.L. Romeral Martinez, M. Salehifar and M. Moreno-Eguilaz, "Genetic algorithm-based output power optimisation of fault tolerant five-phase brushless direct current drives applicable for electrical and hybrid electrical vehicles," *IET Electric Power Applications*, vol. 8, no. 7, pp. 267-277, August 2014.
- [143] M.A. Fnaiech, F. Betin, G.A. Capolino and F. Fnaiech, "Fuzzy Logic and Sliding-Mode Controls Applied to Six-Phase Induction Machine With Open Phases," *IEEE Transactions on Industrial Electronics*, vol. 57, no. 1, pp. 354-364, January 2010.
- [144] A. Tani, M. Mengoni, L. Zarri, G. Serra and D. Casadei, "Control of Multiphase Induction Motors With an Odd Number of Phases Under Open-Circuit Phase Faults," *IEEE Transactions on Power Electronics*, vol. 27, no. 2, pp. 565-577, February 2012.
- [145] A. Mohammadpour and L. Parsa, "A Unified Fault-Tolerant Current Control Approach for Five-Phase PM Motors With Trapezoidal Back EMF Under Different Stator Winding Connections," *IEEE Transactions on Power Electronics*, vol. 28, no. 7, pp. 3517-3527, July 2013.
- [146] A. Mohammadpour, S. Sadeghi and L. Parsa, "A Generalized Fault-Tolerant Control Strategy for Five-Phase PM Motor Drives Considering Star, Pentagon, and Pentacle Connections of Stator Windings," *IEEE Transactions on Industrial Electronics*, vol. 61, no. 1, pp. 63-75, January 2014.

- [147] N. Bianchi, S. Bolognani and M.D. Pre, "Strategies for the Fault-Tolerant Current Control of a Five-Phase Permanent-Magnet Motor," *IEEE Transactions on Industry Applications*, vol. 43, no. 4, pp. 960-970, July-August 2007.
- [148] H.S. Che, E. Levi, M. Jones, M.J. Duran, W.P. Hew and N.A. Rahim, "Operation of a Six-Phase Induction Machine Using Series-Connected Machine-Side Converters," *IEEE Transactions on Industrial Electronics*, vol. 61, no. 1, pp. 164-176, January 2014.
- [149] F. Locment, E. Semail and X. Kestelyn, "Vectorial Approach-Based Control of a Seven-Phase Axial Flux Machine Designed for Fault Operation," *IEEE Transactions on Industrial Electronics*, vol. 55, no. 10, pp. 3682-3691, October 2008.
- [150] A. Mohammadpour and L. Parsa, "Global Fault-Tolerant Control Technique for Multiphase Permanent-Magnet Machines," *IEEE Transactions on Industry Applications*, vol. 51, no. 1, pp. 178-186, January-February 2015.
- [151] A. Mohammadpour, S. Mishra and L. Parsa, "Fault-Tolerant Operation of Multiphase Permanent-Magnet Machines Using Iterative Learning Control," *IEEE Journal of Emerging and Selected Topics in Power Electronics*, vol. 2, no. 2, pp. 201-211, June 2014.
- [152] F. Betin and G.A. Capolino, "Shaft Positioning for Six-Phase Induction Machines With Open Phases Using Variable Structure Control," *IEEE Transactions on Industrial Electronics*, vol. 59, no. 6, pp. 2612-2620, June 2012.
- [153] M.A. Shamsi-Nejad, B. Nahid-Mobarakeh, S. Pierfederici and F. Meibody-Tabar, "Fault Tolerant and Minimum Loss Control of Double-Star Synchronous Machines Under Open Phase Conditions," *IEEE Transactions on Industrial Electronics*, vol. 55, no. 5, pp. 1956-1965, May 2008.
- [154] A.S. Abdel-Khalik, A.S. Morsy, S. Ahmed and A.M. Massoud, "Effect of Stator Winding Connection on Performance of Five-Phase Induction Machines," *IEEE Transactions on Industrial Electronics*, vol. 61, no. 1, pp. 3-19, January 2014.
- [155] H. Guzman, M.J. Duran, F. Barrero, L. Zarri, B. Bogado, I. Gonzalez-Prieto and M.R. Arahal, "Comparative Study of Predictive and Resonant Controllers in Fault-Tolerant Five-Phase Induction Motor Drives," *IEEE Transactions on Industrial Electronics*, vol. 63, no. 1, pp. 606-617, January 2016.
- [156] S. Halász, "Optimal Control of Voltage Source Inverters Supplying Induction Motors," *Control in Power Electronics and Electrical Drives*, pp. 379-385, 1978.
- [157] M.P. Kazmierkowski, R. Krishnan and F. Blaabjerg, "Control in Power Electronics: Selected Problems," Academic Press Series in Engineering, August 2002.
- [158] A.V. Volkov and Y.S. Skal'ko, "Optimal control over a variable-frequency asynchronous electric drive with SVI-PWM from the point of view of total power losses," *Russian Electrical Engineering*, vol. 79, no. 9, pp. 486-496, September 2008.
- [159] J. Lemmens, P. Vanassche and J. Driesen, "Optimal Control of Traction Motor Drives Under Electrothermal Constraints," *IEEE Journal of Emerging and Selected Topics in Power Electronics*, vol. 2, no. 2, pp. 249-263, June 2014.
- [160] X. Xu and D.W. Novotny, "Selection of the flux reference for induction machine drives in the field weakening region," *IEEE Transactions on Industry Applications*, vol. 28, no. 6, pp. 1353-1358, November/December 1992.

- [161] S.H. Kim and S.K. Sul, "Maximum torque control of an induction machine in the field weakening region," *IEEE Transactions on Industry Applications*, vol. 31, no. 4, pp. 787-794, July/August 1995.
- [162] S.H. Kim and S.K. Sul, "Voltage control strategy for maximum torque operation of an induction machine in the field-weakening region," *IEEE Transactions on Industrial Electronics*, vol. 44, no. 4, pp. 512-518, August 1997.
- [163] L. Harnefors, K. Pietilainen and L. Gertmar, "Torque-maximizing field-weakening control: design, analysis, and parameter selection," *IEEE Transactions on Industrial Electronics*, vol. 48, no. 1, pp. 161-168, February 2001.
- [164] S. Bolognani, S. Calligaro, R. Petrella and F. Pogni, "Flux-weakening in IPM motor drives: Comparison of state-of-art algorithms and a novel proposal for controller design," *Proceedings of the 2011-14th European Conference on Power Electronics and Applications (EPE 2011)*, pp. 1-11, 2011.
- [165] J.M. Kim and S.K. Sul, "Speed control of interior permanent magnet synchronous motor drive for the flux weakening operation," *IEEE Transactions on Industry Applications*, vol. 33, no. 1, pp. 43-48, January/February 1997.
- [166] X. Cai, Z. Zhang, J. Wang and R. Kennel, "Optimal Control Solutions for PMSM Drives: A Comparison Study With Experimental Assessments," *IEEE Journal of Emerging and Selected Topics in Power Electronics*, vol. 6, no. 1, pp. 352-362, March 2018.
- [167] E. Levi, D. Dujic, M. Jones and G. Grandi, "Analytical Determination of DC-Bus Utilization Limits in Multiphase VSI Supplied AC Drives," *IEEE Transactions on Energy Conversion*, vol. 23, no. 2, pp. 433-443, June 2008.
- [168] M. Mengoni, L. Zarri, A. Tani, L. Parsa, G. Serra and D. Casadei, "High-Torque-Density Control of Multiphase Induction Motor Drives Operating Over a Wide Speed Range," *IEEE Transactions on Industrial Electronics*, vol. 62, no. 2, pp. 814-825, February 2015.
- [169] S. Kouro, M.A. Perez, J. Rodriguez, A.M. Llor and H.A. Young, "Model Predictive Control: MPC's Role in the Evolution of Power Electronics," *IEEE Industrial Electronics Magazine*, vol. 9, no. 4, pp. 8-21, December 2015.
- [170] X. Kestelyn, O. Gomofov, J. Buire, F. Colas, N.K. Nguyen and E. Semail, "Investigation on model predictive control of a five-phase permanent magnet synchronous machine under voltage and current limits," *IEEE International Conference on Industrial Technology (ICIT 2015)*, pp. 2281-2287, 2015.
- [171] Y. Iwasaki and H.A. Simon, "Causality and model abstraction," *Artificial Intelligence*, vol. 67, no. 1, pp. 143-194, May 1994.
- [172] J.P. Hautier and J. Faucher, "Le graphe informationnel causal", *Bulletin de l'Union des Physiciens*, vol. 90, pp. 167-189, June 1996.
- [173] J.P. Hautier and P.J. Barre, "The causal ordering graph – A tool for modelling and control law synthesis", *Studies in Informatics and Control Journal*, vol. 13, no. 4, pp. 265-283, December 2004.
- [174] H. Paynter, "Analysis and design of engineering systems," MIT Press, 1961.
- [175] A. Bouscayrol, B. Davat, B. de Fornel, B. François, J.P. Hautier, F. Meibody-Tabar and M. Pietrzak-David, "Multi-converter multi-machine systems: application for electromechanical drives", *EPJ Applied Physics*, vol. 10, no. 2, pp. 131-147, May 2000.

- [176] A. Bouscayrol, X. Guillaud, P. Delarue and B. Lemaire-Semail, "Energetic Macroscopic Representation and Inversion-Based Control Illustrated on a Wind-Energy-Conversion System Using Hardware-in-the-Loop Simulation," *IEEE Transactions on Industrial Electronics*, vol. 56, no. 12, pp. 4826-4835, December 2009.
- [177] L. Boulon, D. Hissel, A. Bouscayrol and M.C. Pera, "From Modeling to Control of a PEM Fuel Cell Using Energetic Macroscopic Representation," *IEEE Transactions on Industrial Electronics*, vol. 57, no. 6, pp. 1882-1891, June 2010.
- [178] K. Chen, P. Delarue, A. Bouscayrol, P.E. Vidal and M. Pietrzak-David, "Minimum Copper Loss and Power Distribution Control Strategies of Double-Inverter-Fed Wound-Rotor Induction Machines Using Energetic Macroscopic Representation," *IEEE Transactions on Energy Conversion*, vol. 25, no. 3, pp. 642-651, September 2010.
- [179] L. Horrein, A. Bouscayrol, Y. Cheng, M. El Fassi, "Dynamical and quasi-static multi-physical models of a diesel internal combustion engine using Energetic Macroscopic Representation," *Energy Conversion and Management*, vol. 91, pp. 280-291, February 2015.
- [180] C. Mayet, P. Delarue, A. Bouscayrol, E. Chattot and J.N. Verhille, "Comparison of Different EMR-Based Models of Traction Power Substations for Energetic Studies of Subway Lines," *IEEE Transactions on Vehicular Technology*, vol. 65, no. 3, pp. 1021-1029, March 2016.
- [181] X. Kestelyn, E. Semail and D. Loroil, "Direct torque control of multi-phase permanent magnet synchronous motor drive: application to a five-phase," *IEEE International Conference on Electric Machines and Drives*, pp. 137-143, 2005.
- [182] J.R. Fu and T.A. Lipo, "Disturbance-free operation of a multiphase current-regulated motor drive with an opened phase," *IEEE Transactions on Industry Applications*, vol. 30, no. 5, pp. 1267-1274, September/October 1994.
- [183] H.M. Ryu, J.W. Kim and S.K. Sul, "Synchronous-frame current control of multiphase synchronous motor under asymmetric fault condition due to open phases," *IEEE Transactions on Industry Applications*, vol. 42, no. 4, pp. 1062-1070, July-August 2006.
- [184] O. Gomozov, J.P.F. Trovão, X. Kestelyn and M.R. Dubois, "Adaptive Energy Management System Based on a Real-Time Model Predictive Control With Nonuniform Sampling Time for Multiple Energy Storage Electric Vehicle," *IEEE Transactions on Vehicular Technology*, vol. 66, no. 7, pp. 5520-5530, July 2017.
- [185] J. Bélanger, P. Venne and J.N. Paquin, "The What, Where and Why of Real-Time Simulation," *Planet RT*, vol. 1, no. 1, pp. 25-29, January 2010.
- [186] C.S. Lim, N.A. Rahim, W.P. Hew and E. Levi, "Model Predictive Control of a Two-Motor Drive With Five-Leg-Inverter Supply," *IEEE Transactions on Industrial Electronics*, vol. 60, no. 1, pp. 54-65, January 2013.
- [187] C.S. Lim, E. Levi, M. Jones, N.A. Rahim and W.P. Hew, "A Comparative Study of Synchronous Current Control Schemes Based on FCS-MPC and PI-PWM for a Two-Motor Three-Phase Drive," *IEEE Transactions on Industrial Electronics*, vol. 61, no. 8, pp. 3867-3878, August 2014.

Appendices

Appendix A

Discrete-Time State-Space Models

A.1 Five-phase induction machine with distributed windings

In this case, the stator currents and the rotor flux, in the stationary reference frame, are assumed as state variables. Then, using equations (2.91)–(2.94), the machine model can be expressed as:

$$\frac{di_{s\alpha}}{dt} = \frac{1}{\sigma \cdot L_s} \cdot v_{s\alpha} - \left(\frac{1}{\sigma \cdot \tau_s} + \frac{1-\sigma}{\sigma \cdot \tau_r} \right) \cdot i_{s\alpha} + \frac{1-\sigma}{\sigma \cdot \tau_r \cdot L_m} \cdot \lambda_{r\alpha} + \frac{1-\sigma}{\sigma \cdot L_m} \cdot \omega_r \cdot \lambda_{r\beta} \quad (\text{A.1})$$

$$\frac{di_{s\beta}}{dt} = \frac{1}{\sigma \cdot L_s} \cdot v_{s\beta} - \left(\frac{1}{\sigma \cdot \tau_s} + \frac{1-\sigma}{\sigma \cdot \tau_r} \right) \cdot i_{s\beta} - \frac{1-\sigma}{\sigma \cdot L_m} \cdot \omega_r \cdot \lambda_{r\alpha} + \frac{1-\sigma}{\sigma \cdot \tau_r \cdot L_m} \cdot \lambda_{r\beta} \quad (\text{A.2})$$

$$\frac{di_{sx}}{dt} = \frac{1}{L_{ls}} \cdot v_{sx} - \frac{1}{\tau_{ls}} \cdot i_{sx} \quad (\text{A.3})$$

$$\frac{di_{sy}}{dt} = \frac{1}{L_{ls}} \cdot v_{sy} - \frac{1}{\tau_{ls}} \cdot i_{sy} \quad (\text{A.4})$$

$$\frac{d\lambda_{r\alpha}}{dt} = \frac{L_m}{\tau_r} \cdot i_{s\alpha} - \frac{1}{\tau_r} \cdot \lambda_{r\alpha} - \omega_r \cdot \lambda_{r\beta} \quad (\text{A.5})$$

$$\frac{d\lambda_{r\beta}}{dt} = \frac{L_m}{\tau_r} \cdot i_{s\beta} + \omega_r \cdot \lambda_{r\alpha} - \frac{1}{\tau_r} \cdot \lambda_{r\beta} \quad (\text{A.6})$$

being σ , τ_s , τ_r and τ_{ls} defined as follows:

$$\sigma = 1 - \frac{L_m^2}{L_s \cdot L_r} \quad (\text{A.7})$$

$$\tau_s = \frac{L_s}{R_s} \quad (\text{A.8})$$

$$\tau_r = \frac{L_r}{R_r} \quad (\text{A.9})$$

$$\tau_{ls} = \frac{L_{ls}}{R_s} \quad (\text{A.10})$$

Rewriting (A.1)–(A.6) in matrix form, the discrete-time state-space model is detailed by:

$$\frac{d}{dt}[X] = [A] \cdot [U] + [B] \cdot [X] \quad (\text{A.11})$$

where:

$$[X] = [i_{s\alpha} \quad i_{s\beta} \quad i_{sx} \quad i_{sy} \quad \lambda_{r\alpha} \quad \lambda_{r\beta}]^T \quad (\text{A.12})$$

$$[U] = [v_{s\alpha} \quad v_{s\beta} \quad v_{sx} \quad v_{sy}]^T \quad (\text{A.13})$$

$$[A] = \begin{bmatrix} \frac{1}{\sigma \cdot L_s} & 0 & 0 & 0 \\ 0 & \frac{1}{\sigma \cdot L_s} & 0 & 0 \\ 0 & 0 & \frac{1}{L_{ls}} & 0 \\ 0 & 0 & 0 & \frac{1}{L_{ls}} \\ 0 & 0 & 0 & 0 \\ 0 & 0 & 0 & 0 \end{bmatrix} \quad (\text{A.14})$$

$$[B] = \begin{bmatrix} -\left(\frac{1}{\sigma \cdot \tau_s} + \frac{1-\sigma}{\sigma \cdot \tau_r}\right) & 0 & 0 & 0 & \frac{1-\sigma}{\sigma \cdot \tau_r \cdot L_m} & \frac{1-\sigma}{\sigma \cdot L_m} \cdot \omega_r \\ 0 & -\left(\frac{1}{\sigma \cdot \tau_s} + \frac{1-\sigma}{\sigma \cdot \tau_r}\right) & 0 & 0 & -\frac{1-\sigma}{\sigma \cdot L_m} \cdot \omega_r & \frac{1-\sigma}{\sigma \cdot \tau_r \cdot L_m} \\ 0 & 0 & -\frac{1}{\tau_{ls}} & 0 & 0 & 0 \\ 0 & 0 & 0 & -\frac{1}{\tau_{ls}} & 0 & 0 \\ \frac{L_m}{\tau_r} & 0 & 0 & 0 & -\frac{1}{\tau_r} & -\omega_r \\ 0 & \frac{L_m}{\tau_r} & 0 & 0 & \omega_r & -\frac{1}{\tau_r} \end{bmatrix} \quad (\text{A.15})$$

In (A.15), it can be noted that there are elements in matrix $[B]$ that depend on the instantaneous value of the rotor speed (ω_r). Then, it is possible to divide matrix $[B]$ into a constant matrix $[B_c]$ and a speed-dependent matrix $[B_{\omega r}]$ as presented in (A.16)–(A.18), permitting to estimate offline the first one, while only the second one is calculated online.

$$[B] = [B_c] + [B_{\omega r}] \quad (\text{A.16})$$

$$[B_c] = \begin{bmatrix} -\left(\frac{1}{\sigma \cdot \tau_s} + \frac{1-\sigma}{\sigma \cdot \tau_r}\right) & 0 & 0 & 0 & \frac{1-\sigma}{\sigma \cdot \tau_r \cdot L_m} & 0 \\ 0 & -\left(\frac{1}{\sigma \cdot \tau_s} + \frac{1-\sigma}{\sigma \cdot \tau_r}\right) & 0 & 0 & 0 & \frac{1-\sigma}{\sigma \cdot \tau_r \cdot L_m} \\ 0 & 0 & -\frac{1}{\tau_{ls}} & 0 & 0 & 0 \\ 0 & 0 & 0 & -\frac{1}{\tau_{ls}} & 0 & 0 \\ \frac{L_m}{\tau_r} & 0 & 0 & 0 & -\frac{1}{\tau_r} & 0 \\ 0 & \frac{L_m}{\tau_r} & 0 & 0 & 0 & -\frac{1}{\tau_r} \end{bmatrix} \quad (\text{A.17})$$

$$[B_{\omega r}] = \begin{bmatrix} 0 & 0 & 0 & 0 & 0 & \frac{1-\sigma}{\sigma \cdot L_m} \cdot \omega_r \\ 0 & 0 & 0 & 0 & -\frac{1-\sigma}{\sigma \cdot L_m} \cdot \omega_r & 0 \\ 0 & 0 & 0 & 0 & 0 & 0 \\ 0 & 0 & 0 & 0 & 0 & 0 \\ 0 & 0 & 0 & 0 & 0 & -\omega_r \\ 0 & 0 & 0 & 0 & \omega_r & 0 \end{bmatrix} \quad (\text{A.18})$$

Finally, equation (A.11) is discretized with a sampling period T_s , assuming constant input and constant matrices during the whole sampling period:

$$\frac{d}{dt} [X^k] = [A] \cdot [U^k] + [B] \cdot [X^k] = \frac{[X^{k+1}] - [X^k]}{T_s} \quad (\text{A.19})$$

$$[X^{k+1}] = [\Gamma] \cdot [U^k] + [\Phi] \cdot [X^k] \quad (\text{A.20})$$

$$[\Gamma] = [A] \cdot T_s \quad (\text{A.21})$$

$$[\Phi] = [I] + [B] \cdot T_s \quad (\text{A.22})$$

A.2 Five-phase induction machine with concentrated windings

Proceeding in an analogous way as in the previous case, the machine model is discretized in the state space using equations (2.107)–(2.110). In this case, the stator currents and the rotor flux, in the rotating reference frame, are assumed as state variables. Note that, in order to simplify the analysis, the model of fundamental and third harmonic components will be separately studied, since they are totally decoupled.

Model of the fundamental component

The equations for the state-space variables are presented as follows:

$$\begin{aligned} \frac{di_{sd1}}{dt} = & \frac{1}{\sigma_1 \cdot L_{s1}} \cdot v_{sd1} - \left(\frac{1}{\sigma_1 \cdot \tau_{s1}} + \frac{1-\sigma_1}{\sigma_1 \cdot \tau_{r1}} \right) \cdot i_{sd1} + \omega_{a1} \cdot i_{sq1} + \frac{1-\sigma_1}{\sigma_1 \cdot \tau_{r1} \cdot L_{m1}} \cdot \lambda_{rd1} + \\ & + \frac{1-\sigma_1}{\sigma_1 \cdot L_{m1}} \cdot \omega_r \cdot \lambda_{rq1} \end{aligned} \quad (\text{A.23})$$

$$\begin{aligned} \frac{di_{sq1}}{dt} = & \frac{1}{\sigma_1 \cdot L_{s1}} \cdot v_{sq1} + \omega_{a1} \cdot i_{sd1} - \left(\frac{1}{\sigma_1 \cdot \tau_{s1}} + \frac{1-\sigma_1}{\sigma_1 \cdot \tau_{r1}} \right) \cdot i_{sq1} - \frac{1-\sigma_1}{\sigma_1 \cdot L_{m1}} \cdot \omega_r \cdot \lambda_{rd1} + \\ & + \frac{1-\sigma_1}{\sigma_1 \cdot \tau_{r1} \cdot L_{m1}} \cdot \lambda_{rq1} \end{aligned} \quad (\text{A.24})$$

$$\frac{d\lambda_{rd1}}{dt} = \frac{L_{m1}}{\tau_{r1}} \cdot i_{sd1} - \frac{1}{\tau_{r1}} \cdot \lambda_{rd1} + (\omega_{a1} - \omega_r) \cdot \lambda_{rq1} \quad (\text{A.25})$$

$$\frac{d\lambda_{rq1}}{dt} = \frac{L_{m1}}{\tau_{r1}} \cdot i_{sq1} - \frac{1}{\tau_{r1}} \cdot \lambda_{rq1} - (\omega_{a1} - \omega_r) \cdot \lambda_{rd1} \quad (\text{A.26})$$

where the following constants have been used:

$$\sigma_1 = 1 - \frac{L_{m1}^2}{L_{s1} \cdot L_{r1}} \quad (\text{A.27})$$

$$\tau_{r1} = \frac{L_{r1}}{R_{r1}} \quad (\text{A.28})$$

$$\tau_{s1} = \frac{L_{s1}}{R_s} \quad (\text{A.29})$$

Rewriting (A.23)–(A.26) in matrix form, the discrete-time state-space model is detailed by:

$$\frac{d}{dt} [X_1] = [A_1] \cdot [U_1] + [B_1] \cdot [X_1] \quad (\text{A.30})$$

where:

$$[X_1] = [i_{sd1} \quad i_{sq1} \quad \lambda_{rd1} \quad \lambda_{rq1}]^T \quad (\text{A.31})$$

$$[U_1] = [v_{sd1} \quad v_{sq1}]^T \quad (\text{A.32})$$

$$[A_1] = \begin{bmatrix} \frac{1}{\sigma_1 \cdot L_{s1}} & 0 \\ 0 & \frac{1}{\sigma_1 \cdot L_{s1}} \\ 0 & 0 \\ 0 & 0 \end{bmatrix} \quad (\text{A.33})$$

$$[B_1] = \begin{bmatrix} -\left(\frac{1}{\sigma_1 \cdot \tau_{s1}} + \frac{1-\sigma_1}{\sigma_1 \cdot \tau_{r1}}\right) & \omega_{a1} & \frac{1-\sigma_1}{\sigma_1 \cdot \tau_{r1} \cdot L_{m1}} & \frac{1-\sigma_1}{\sigma_1 \cdot L_{m1}} \cdot \omega_r \\ -\omega_{a1} & -\left(\frac{1}{\sigma_1 \cdot \tau_{s1}} + \frac{1-\sigma_1}{\sigma_1 \cdot \tau_{r1}}\right) & -\frac{1-\sigma_1}{\sigma_1 \cdot L_{m1}} \cdot \omega_r & \frac{1-\sigma_1}{\sigma_1 \cdot \tau_{r1} \cdot L_{m1}} \\ \frac{L_{m1}}{\tau_{r1}} & 0 & -\frac{1}{\tau_{r1}} & \omega_{a1} - \omega_r \\ 0 & \frac{L_{m1}}{\tau_{r1}} & -(\omega_{a1} - \omega_r) & -\frac{1}{\tau_{r1}} \end{bmatrix} \quad (\text{A.34})$$

In (A.34), it can be noted that there are elements in matrix $[B_1]$ that depend on the instantaneous values of the rotor speed (ω_r) and the rotating speed of the plane d_1-q_1 (ω_{a1}). Then, it is possible to divide matrix $[B_1]$ into a constant matrix $[B_{1c}]$ and speed-dependent matrices, $[B_{1\omega a}]$ and $[B_{1\omega r}]$, as presented in (A.35)–(A.38), permitting to estimate offline the first one, while the other ones are calculated online.

$$[B_1] = [B_{1c}] + [B_{1\omega a}] + [B_{1\omega r}] \quad (\text{A.35})$$

$$[B_{1c}] = \begin{bmatrix} -\left(\frac{1}{\sigma_1 \cdot \tau_{s1}} + \frac{1-\sigma_1}{\sigma_1 \cdot \tau_{r1}}\right) & 0 & \frac{1-\sigma_1}{\sigma_1 \cdot \tau_{r1} \cdot L_{m1}} & 0 \\ 0 & -\left(\frac{1}{\sigma_1 \cdot \tau_{s1}} + \frac{1-\sigma_1}{\sigma_1 \cdot \tau_{r1}}\right) & 0 & \frac{1-\sigma_1}{\sigma_1 \cdot \tau_{r1} \cdot L_{m1}} \\ \frac{L_{m1}}{\tau_{r1}} & 0 & -\frac{1}{\tau_{r1}} & 0 \\ 0 & \frac{L_{m1}}{\tau_{r1}} & 0 & -\frac{1}{\tau_{r1}} \end{bmatrix} \quad (\text{A.36})$$

$$[B_{1\omega a}] = \begin{bmatrix} 0 & \omega_{a1} & 0 & 0 \\ -\omega_{a1} & 0 & 0 & 0 \\ 0 & 0 & 0 & \omega_{a1} \\ 0 & 0 & -\omega_{a1} & 0 \end{bmatrix} \quad (\text{A.37})$$

$$[B_{1\omega r}] = \begin{bmatrix} 0 & 0 & 0 & \frac{1-\sigma_1}{\sigma_1 \cdot L_{m1}} \cdot \omega_r \\ 0 & 0 & -\frac{1-\sigma_1}{\sigma_1 \cdot L_{m1}} \cdot \omega_r & 0 \\ 0 & 0 & 0 & -\omega_r \\ 0 & 0 & \omega_r & 0 \end{bmatrix} \quad (\text{A.38})$$

Finally, equation (A.30) is discretized with a sampling period T_s , assuming constant input and constant matrices during the whole sampling period:

$$\frac{d}{dt} [X_1^k] = [A_1] \cdot [U_1^k] + [B_1] \cdot [X_1^k] = \frac{[X_1^{k+1}] - [X_1^k]}{T_s} \quad (\text{A.39})$$

$$[X_1^{k+1}] = [\Gamma_1] \cdot [U_1^k] + [\Phi_1] \cdot [X_1^k] \quad (\text{A.40})$$

$$[\Gamma_1] = [A_1] \cdot T_s \quad (\text{A.41})$$

$$[\Phi_1] = [I] + [B_1] \cdot T_s \quad (\text{A.42})$$

Model of the third harmonic component

The equations for the state-space variables are presented as follows:

$$\begin{aligned} \frac{di_{sd3}}{dt} &= \frac{1}{\sigma_3 \cdot L_{s3}} \cdot v_{sd3} - \left(\frac{1}{\sigma_3 \cdot \tau_{s3}} + \frac{1-\sigma_3}{\sigma_3 \cdot \tau_{r3}} \right) \cdot i_{sd3} + 3\omega_{a3} \cdot i_{sq3} + \frac{1-\sigma_3}{\sigma_3 \cdot \tau_{r3} \cdot L_{m3}} \cdot \lambda_{rd3} + \\ &+ \frac{1-\sigma_3}{\sigma_3 \cdot L_{m3}} \cdot 3\omega_r \cdot \lambda_{rq3} \end{aligned} \quad (\text{A.43})$$

$$\begin{aligned} \frac{di_{sq3}}{dt} &= \frac{1}{\sigma_3 \cdot L_{s3}} \cdot v_{sq3} + 3\omega_{a3} \cdot i_{sd3} - \left(\frac{1}{\sigma_3 \cdot \tau_{s3}} + \frac{1-\sigma_3}{\sigma_3 \cdot \tau_{r3}} \right) \cdot i_{sq3} - \frac{1-\sigma_3}{\sigma_3 \cdot L_{m3}} \cdot 3\omega_r \cdot \lambda_{rd3} + \\ &+ \frac{1-\sigma_3}{\sigma_3 \cdot \tau_{r3} \cdot L_{m3}} \cdot \lambda_{rq3} \end{aligned} \quad (\text{A.44})$$

$$\frac{d\lambda_{rd3}}{dt} = \frac{L_{m3}}{\tau_{r3}} \cdot i_{sd3} - \frac{1}{\tau_{r3}} \cdot \lambda_{rd3} + 3(\omega_{a3} - \omega_r) \cdot \lambda_{rq3} \quad (\text{A.45})$$

$$\frac{d\lambda_{rq3}}{dt} = \frac{L_{m3}}{\tau_{r3}} \cdot i_{sq3} - \frac{1}{\tau_{r3}} \cdot \lambda_{rq3} - 3(\omega_{a3} - \omega_r) \cdot \lambda_{rd3} \quad (\text{A.46})$$

where the following constants have been used:

$$\sigma_3 = 1 - \frac{L_{m3}^2}{L_{s3} \cdot L_{r3}} \quad (\text{A.47})$$

$$\tau_{r3} = \frac{L_{r3}}{R_{r3}} \quad (\text{A.48})$$

$$\tau_{s3} = \frac{L_{s3}}{R_s} \quad (\text{A.49})$$

Rewriting (A.43)–(A.46) in matrix form, the discrete-time state-space model is detailed by:

$$\frac{d}{dt}[X_3] = [A_3] \cdot [U_3] + [B_3] \cdot [X_3] \quad (\text{A.50})$$

where:

$$[X_3] = [i_{sd3} \quad i_{sq3} \quad \lambda_{rd3} \quad \lambda_{rq3}]^T \quad (\text{A.51})$$

$$[U_3] = [v_{sd3} \quad v_{sq3}]^T \quad (\text{A.52})$$

$$[A_3] = \begin{bmatrix} \frac{1}{\sigma_3 \cdot L_{s3}} & 0 \\ 0 & \frac{1}{\sigma_3 \cdot L_{s3}} \\ 0 & 0 \\ 0 & 0 \end{bmatrix} \quad (\text{A.53})$$

$$[B_3] = \begin{bmatrix} -\left(\frac{1}{\sigma_3 \cdot \tau_{s3}} + \frac{1-\sigma_3}{\sigma_3 \cdot \tau_{r3}}\right) & 3\omega_{a3} & \frac{1-\sigma_3}{\sigma_3 \cdot \tau_{r3} \cdot L_{m3}} & \frac{1-\sigma_3}{\sigma_3 \cdot L_{m3}} \cdot 3\omega_r \\ -3\omega_{a3} & -\left(\frac{1}{\sigma_3 \cdot \tau_{s3}} + \frac{1-\sigma_3}{\sigma_3 \cdot \tau_{r3}}\right) & -\frac{1-\sigma_3}{\sigma_3 \cdot L_{m3}} \cdot 3\omega_r & \frac{1-\sigma_3}{\sigma_3 \cdot \tau_{r3} \cdot L_{m3}} \\ \frac{L_{m3}}{\tau_{r3}} & 0 & -\frac{1}{\tau_{r3}} & 3(\omega_{a3} - \omega_r) \\ 0 & \frac{L_{m3}}{\tau_{r3}} & -3(\omega_{a3} - \omega_r) & -\frac{1}{\tau_{r3}} \end{bmatrix} \quad (\text{A.54})$$

In (A.54), it can be noted that there are elements in matrix $[B_3]$ that depend on the instantaneous values of the rotor speed (ω_r) and the rotating speed of the plane d_3-q_3 (ω_{a3}). Then, it is possible to divide matrix $[B_3]$ into a constant matrix $[B_{3c}]$ and speed-dependent matrices, $[B_{3\omega a}]$ and $[B_{3\omega r}]$, as presented in (A.55)–(A.58), permitting to estimate offline the first one, while the other ones are calculated online.

$$[B_3] = [B_{3c}] + [B_{3\omega a}] + [B_{3\omega r}] \quad (\text{A.55})$$

$$[B_{3c}] = \begin{bmatrix} -\left(\frac{1}{\sigma_3 \cdot \tau_{s3}} + \frac{1-\sigma_3}{\sigma_3 \cdot \tau_{r3}}\right) & 0 & \frac{1-\sigma_3}{\sigma_3 \cdot \tau_{r3} \cdot L_{m3}} & 0 \\ 0 & -\left(\frac{1}{\sigma_3 \cdot \tau_{s3}} + \frac{1-\sigma_3}{\sigma_3 \cdot \tau_{r3}}\right) & 0 & \frac{1-\sigma_3}{\sigma_3 \cdot \tau_{r3} \cdot L_{m3}} \\ \frac{L_{m3}}{\tau_{r3}} & 0 & -\frac{1}{\tau_{r3}} & 0 \\ 0 & \frac{L_{m3}}{\tau_{r3}} & 0 & -\frac{1}{\tau_{r3}} \end{bmatrix} \quad (\text{A.56})$$

$$[B_{3\omega a}] = \begin{bmatrix} 0 & 3\omega_{a3} & 0 & 0 \\ -3\omega_{a3} & 0 & 0 & 0 \\ 0 & 0 & 0 & 3\omega_{a3} \\ 0 & 0 & -3\omega_{a3} & 0 \end{bmatrix} \quad (\text{A.57})$$

$$[B_{3\omega r}] = \begin{bmatrix} 0 & 0 & 0 & \frac{1-\sigma_3}{\sigma_3 \cdot L_{m3}} \cdot 3\omega_r \\ 0 & 0 & -\frac{1-\sigma_3}{\sigma_3 \cdot L_{m3}} \cdot 3\omega_r & 0 \\ 0 & 0 & 0 & -3\omega_r \\ 0 & 0 & 3\omega_r & 0 \end{bmatrix} \quad (\text{A.58})$$

Finally, equation (A.50) is discretized with a sampling period T_s , assuming constant input and constant matrices during the whole sampling period:

$$\frac{d}{dt} [X_3^k] = [A_3] \cdot [U_3^k] + [B_3] \cdot [X_3^k] = \frac{[X_3^{k+1}] - [X_3^k]}{T_s} \quad (\text{A.59})$$

$$[X_3^{k+1}] = [\Gamma_3] \cdot [U_3^k] + [\Phi_3] \cdot [X_3^k] \quad (\text{A.60})$$

$$[\Gamma_3] = [A_3] \cdot T_s \quad (\text{A.61})$$

$$[\Phi_3] = [I] + [B_3] \cdot T_s \quad (\text{A.62})$$

A.3 Five-phase permanent magnet synchronous machine

Proceeding analogously as in the previous case, the machine model is discretized in the state space using equations (2.124)–(2.125). In this case, the stator currents in the rotating reference frame are the state variables. Note that, in order to simplify the analysis, the model of fundamental and third harmonic components will be separately studied, since they are totally decoupled.

Model of the fundamental component

The equations for the state-space variables are presented as follows:

$$\frac{di_{sd1}}{dt} = \frac{1}{L_{sd1}} \cdot v_{sd1} - \frac{R_s}{L_{sd1}} \cdot i_{sd1} + \frac{L_{sq1}}{L_{sd1}} \cdot \omega_r \cdot i_{sq1} \quad (\text{A.63})$$

$$\frac{di_{sq1}}{dt} = \frac{1}{L_{sq1}} \cdot v_{sq1} - \frac{L_{sd1}}{L_{sq1}} \cdot \omega_r \cdot i_{sd1} - \frac{R_s}{L_{sq1}} \cdot i_{sq1} - \frac{\lambda_{m1}}{L_{sq1}} \cdot \omega_r \quad (\text{A.64})$$

Rewriting (A.63)–(A.64) in matrix form, the discrete-time state-space model is detailed by:

$$\frac{d}{dt} [X_1] = [A_1] \cdot [U_1] + [B_1] \cdot [X_1] + [D_1] \quad (\text{A.65})$$

$$[X_1] = [i_{sd1} \quad i_{sq1}]^T \quad (\text{A.66})$$

$$[U_1] = [v_{sd1} \quad v_{sq1}]^T \quad (\text{A.67})$$

$$[A_1] = \begin{bmatrix} \frac{1}{L_{sd1}} & 0 \\ 0 & \frac{1}{L_{sq1}} \end{bmatrix} \quad (\text{A.68})$$

$$[B_1] = \begin{bmatrix} -\frac{R_s}{L_{sd1}} & \frac{L_{sq1}}{L_{sd1}} \cdot \omega_r \\ -\frac{L_{sd1}}{L_{sq1}} \cdot \omega_r & -\frac{R_s}{L_{sq1}} \end{bmatrix} \quad (\text{A.69})$$

$$[D_1] = \begin{bmatrix} 0 \\ -\frac{\lambda_{m1}}{L_{sq1}} \cdot \omega_r \end{bmatrix} \quad (\text{A.70})$$

In (A.69), it can be noted that there are elements in matrix $[B_1]$ that depend on the instantaneous values of the rotor speed (ω_r). Then, it is possible to divide matrix $[B_1]$ into a

constant matrix $[B_{1c}]$ and a speed-dependent matrix $[B_{1\omega r}]$ as presented in (A.71)–(A.73), permitting to estimate offline the first one, while only the second one is calculated online.

$$[B_1] = [B_{1c}] + [B_{1\omega r}] \quad (\text{A.71})$$

$$[B_{1c}] = -R_s \cdot [A_1] \quad (\text{A.72})$$

$$[B_{1\omega r}] = \begin{bmatrix} 0 & \frac{L_{sq1}}{L_{sd1}} \cdot \omega_r \\ -\frac{L_{sd1}}{L_{sq1}} \cdot \omega_r & 0 \end{bmatrix} \quad (\text{A.73})$$

Finally, equation (A.65) is discretized with a sampling period T_s , assuming constant input and constant matrices during the whole sampling period:

$$\frac{d}{dt} [X_1^k] = [A_1] \cdot [U_1^k] + [B_1] \cdot [X_1^k] + [D_1] = \frac{[X_1^{k+1}] - [X_1^k]}{T_s} \quad (\text{A.74})$$

$$[X_1^{k+1}] = [\Gamma_1] \cdot [U_1^k] + [\Phi_1] \cdot [X_1^k] + [\Psi_1] \quad (\text{A.75})$$

$$[\Gamma_1] = [A_1] \cdot T_s \quad (\text{A.76})$$

$$[\Phi_1] = [I] + [B_1] \cdot T_s \quad (\text{A.77})$$

$$[\Psi_1] = [D_1] \cdot T_s \quad (\text{A.78})$$

Model of the third harmonic component

The equations for the state-space variables are presented as follows:

$$\frac{di_{sd3}}{dt} = \frac{1}{L_{sd3}} \cdot v_{sd3} - \frac{R_s}{L_{sd3}} \cdot i_{sd3} - \frac{L_{sq3}}{L_{sd3}} \cdot 3\omega_r \cdot i_{sq3} \quad (\text{A.79})$$

$$\frac{di_{sq3}}{dt} = \frac{1}{L_{sq3}} \cdot v_{sq3} + \frac{L_{sd3}}{L_{sq3}} \cdot 3\omega_r \cdot i_{sd3} - \frac{R_s}{L_{sq3}} \cdot i_{sq3} - \frac{\lambda_{m3}}{L_{sq3}} \cdot 3\omega_r \quad (\text{A.80})$$

Rewriting (A.79)–(A.80) in matrix form, the discrete-time state-space model is detailed by:

$$\frac{d}{dt} [X_3] = [A_3] \cdot [U_3] + [B_3] \cdot [X_3] + [D_3] \quad (\text{A.81})$$

$$[X_3] = [i_{sd3} \quad i_{sq3}]^T \quad (\text{A.82})$$

$$[U_3] = [v_{sd3} \quad v_{sq3}]^T \quad (\text{A.83})$$

$$[A_3] = \begin{bmatrix} \frac{1}{L_{sd3}} & 0 \\ 0 & \frac{1}{L_{sq3}} \end{bmatrix} \quad (\text{A.84})$$

$$[B_3] = \begin{bmatrix} -\frac{R_s}{L_{sd3}} & -\frac{L_{sq3}}{L_{sd3}} \cdot 3\omega_r \\ \frac{L_{sd3}}{L_{sq3}} \cdot 3\omega_r & -\frac{R_s}{L_{sq3}} \end{bmatrix} \quad (\text{A.85})$$

$$[D_3] = \begin{bmatrix} 0 \\ -\frac{\lambda_{m3}}{L_{sq3}} \cdot 3\omega_r \end{bmatrix} \quad (\text{A.86})$$

It is again possible to divide matrix $[B_3]$ of (A.85) into a constant matrix $[B_{3c}]$ and a speed-dependent matrix $[B_{3\omega r}]$ as presented in (A.87)–(A.89), permitting to estimate offline the first one.

$$[B_3] = [B_{3c}] + [B_{3\omega r}] \quad (\text{A.87})$$

$$[B_{3c}] = -R_s \cdot [A_3] \quad (\text{A.88})$$

$$[B_{3\omega r}] = \begin{bmatrix} 0 & -\frac{L_{sq3}}{L_{sd3}} \cdot 3\omega_r \\ \frac{L_{sd3}}{L_{sq3}} \cdot 3\omega_r & 0 \end{bmatrix} \quad (\text{A.89})$$

Finally, equation (A.81) is discretized with a sampling period T_s , assuming constant input and constant matrices during the whole sampling period:

$$\frac{d}{dt} [X_3^k] = [A_3] \cdot [U_3^k] + [B_3] \cdot [X_3^k] + [D_3] = \frac{[X_3^{k+1}] - [X_3^k]}{T_s} \quad (\text{A.90})$$

$$[X_3^{k+1}] = [\Gamma_3] \cdot [U_3^k] + [\Phi_3] \cdot [X_3^k] + [\Psi_3] \quad (\text{A.91})$$

$$[\Gamma_3] = [A_3] \cdot T_s \quad (\text{A.92})$$

$$[\Phi_3] = [I] + [B_3] \cdot T_s \quad (\text{A.93})$$

$$[\Psi_3] = [D_3] \cdot T_s \quad (\text{A.94})$$

Appendix B

Flux and Torque Estimators for DTC

B.1 Healthy operation

The flux estimator considers the same discrete-time state-space model used in Appendix A.1 to estimate the rotor fluxes in the α - β plane and subsequently calculate the stator fluxes through the following equation:

$$\begin{pmatrix} \hat{\lambda}_{s\alpha} \\ \hat{\lambda}_{s\beta} \end{pmatrix} = \begin{pmatrix} \sigma \cdot L_s & 0 & \frac{L_m}{L_r} & 0 \\ 0 & \sigma \cdot L_s & 0 & \frac{L_m}{L_r} \end{pmatrix} \cdot \begin{pmatrix} i_{s\alpha} \\ i_{s\beta} \\ \hat{\lambda}_{r\alpha} \\ \hat{\lambda}_{r\beta} \end{pmatrix} \quad (\text{B.1})$$

The modulus of the stator flux in the α - β plane is obtained in (B.2), in order to be compared with the stator flux reference (λ_s^*) in the flux hysteresis comparator to obtain the output signal $d\lambda$ (see Fig. 2.13).

$$\hat{\lambda}_s = \|\hat{\lambda}_{s\alpha\beta}\| = \sqrt{\hat{\lambda}_{s\alpha}^2 + \hat{\lambda}_{s\beta}^2} \quad (\text{B.2})$$

On the other hand, the torque estimation is made through the equation obtained in the development of the IM model in the stationary reference frame in Section 2.2.1, see (B.3). The comparison with the reference torque (T_{em}^*) provides the output signal dT .

$$\hat{T}_{em} = p \cdot \frac{5}{2} \cdot (\hat{\lambda}_{s\alpha} \cdot i_{s\beta} - \hat{\lambda}_{s\beta} \cdot i_{s\alpha}) \quad (\text{B.3})$$

The look-up table of the DTC controller selects the appropriate virtual voltage vector in each sampling time according to the outputs of the hysteresis controllers and the sector where the stator flux is currently located, which is estimated as follows:

$$\theta_a = \tan^{-1} \left(\frac{\hat{\lambda}_{s\beta}}{\hat{\lambda}_{s\alpha}} \right) \quad (\text{B.4})$$

$$\text{Sector} = \begin{cases} 1 & \text{if } -\frac{\pi}{10} \leq \theta_a \leq \frac{\pi}{10} \\ 2 & \text{if } \frac{\pi}{10} \leq \theta_a \leq \frac{3\pi}{10} \\ 3 & \text{if } \frac{3\pi}{10} \leq \theta_a \leq \frac{5\pi}{10} \\ 4 & \text{if } \frac{5\pi}{10} \leq \theta_a \leq \frac{7\pi}{10} \\ 5 & \text{if } \frac{7\pi}{10} \leq \theta_a \leq \frac{9\pi}{10} \\ 6 & \text{if } \frac{9\pi}{10} \leq \theta_a \leq \frac{11\pi}{10} \\ 7 & \text{if } \frac{11\pi}{10} \leq \theta_a \leq \frac{13\pi}{10} \\ 8 & \text{if } \frac{13\pi}{10} \leq \theta_a \leq \frac{15\pi}{10} \\ 9 & \text{if } \frac{15\pi}{10} \leq \theta_a \leq \frac{17\pi}{10} \\ 10 & \text{if } \frac{17\pi}{10} \leq \theta_a \leq \frac{19\pi}{10} \end{cases} \quad (\text{B.5})$$

B.2 Post-fault operation

In this case, the flux and torque estimators use the same equations provided in the previous section, with the only difference that the sector identification is made through the next equation:

$$\text{Sector} = \begin{cases} 1 & \text{if } -\frac{\pi}{8} \leq \theta_a \leq \frac{\pi}{8} \\ 2 & \text{if } \frac{\pi}{8} \leq \theta_a \leq \frac{3\pi}{8} \\ 3 & \text{if } \frac{3\pi}{8} \leq \theta_a \leq \frac{5\pi}{8} \\ 4 & \text{if } \frac{5\pi}{8} \leq \theta_a \leq \frac{7\pi}{8} \\ 5 & \text{if } \frac{7\pi}{8} \leq \theta_a \leq \frac{9\pi}{8} \\ 6 & \text{if } \frac{9\pi}{8} \leq \theta_a \leq \frac{11\pi}{8} \\ 7 & \text{if } \frac{11\pi}{8} \leq \theta_a \leq \frac{13\pi}{8} \\ 8 & \text{if } \frac{13\pi}{8} \leq \theta_a \leq \frac{15\pi}{8} \end{cases} \quad (\text{B.6})$$

Appendix C

Electrical and Mechanical Parameters

C.1 Five-phase IM drive with distributed windings

The main parameters used for this type of machine is shown in Table C.1.

Table C.1. Electrical and mechanical parameters of the five-phase DW-IM drive.

Parameter	Value	Unit
Stator resistance, R_s	12.85	Ω
Rotor resistance, R_r	4.80	Ω
Stator leakage inductance, L_{ls}	79.93	mH
Rotor leakage inductance, L_{lr}	79.93	mH
Mutual inductance, M	681.7	mH
Rotational inertia, J_m	0.02	kg-m ²
Number of pole pairs, p	3	-

C.2 Five-phase PMSM drive

The main parameters used for this type of machine is shown in Table C.2.

Table C.2. Parameters of the five-phase PMSM drive and considered limits.

Parameter	Value	Unit
Stator resistance, R_s	37	m Ω
Stator inductances (fundamental), L_{sd1} and L_{sq1}	0.155	mH
Stator inductances (third harmonic), L_{sd3} and L_{sq3}	0.051	mH
Magnet flux linkage (fundamental), λ_{m1}	19.4	mWb
Magnet flux linkage (third harmonic), λ_{m3}	0.675	mWb
Pole pairs, p	7	-
Voltage limit, V_{dc}	35	V
Current limit, I_{VSI}	50	A
Maximum torque, $T_{em,max}$	19.27	N-m
Maximum mechanical speed, $\omega_{m,max}$	240	rad/s

C.3 Five-phase IM drive with concentrated windings

The main parameters used for this type of machine is shown in Table C.3.

Table C.3. Parameters of the five-phase CW-IM drive and considered limits.

Parameter	Value	Unit
Stator resistance, R_s	19.45	Ω
Rotor resistances, R_{r1} and R_{r3}	13.54	Ω
Stator leakage inductance, L_{ls}	100.7	mH
Rotor leakage inductance, L_{lr}	38.6	mH
Mutual inductance (fundamental), L_{m1}	656.5	mH
Mutual inductance (third harmonic), L_{m3}	72.9	mH
Pole pairs, p	3	-
Voltage limit, V_{dc}	300	V
Current limit, I_{VSI}	2.5	A
Rated d -current, $I_{sd, rated}$	0.9	A
Maximum torque, $T_{em, max}$	8.13	N-m

NOUVELLES TECHNIQUES DE COMMANDE POUR LES ENTRAÎNEMENTS ÉLECTRIQUES POLYPHASÉS : COMMANDE EN MODE INSTANTANÉ (DTC ET MPC) DANS DES SITUATIONS LIMITES

RESUME : Les entraînements électriques polyphasés ont acquis une importance particulière ces derniers temps pour leur utilisation dans des applications où la fiabilité présente un intérêt pour des raisons économiques et de sécurité. Cette thèse se centre sur le développement de techniques de commande en mode instantané pour contrôler de manière optimale les machines polyphasées, en analysant leur tolérance dans différentes conditions de fonctionnement, telles que lors de l'atteinte de limites électriques (limites de tension, de courant et de niveau maximum de magnétisation) ou de défauts de type phase ouverte. Tout d'abord, la technique DTC est proposée pour gérer le cas de défaut de type phase ouverte dans la machine polyphasée. Une comparaison de la tolérance à la défaillance des commandes de type DTC par rapport à d'autres techniques de commande est réalisée, permettant une conclusion sur les forces et les faiblesses des méthodes analysées. Enfin, un contrôleur de courant optimal est développé utilisant des techniques MPC permettant une utilisation optimale de la capacité de couple du système en cas de limitations électriques. Des résultats de simulation et des validations expérimentales sont effectués pour corroborer les approches initiales, en utilisant des cas particuliers d'entraînements pentaphasés commandés avec différents sous-espaces de commande dans le domaine fréquentiel.

Mots clés : Machines polyphasées, commande en mode instantané, contrôle optimal en situations limites, DTC, défaut de type phase ouverte, MPC, limites électriques.

NOVEL CONTROL TECHNIQUES IN MULTIPHASE DRIVES: DIRECT CONTROL METHODS (DTC AND MPC) UNDER LIMIT SITUATIONS

ABSTRACT: Multiphase drives have gained special relevance in recent times for their use in applications where reliability is of interest for economical and safety reasons. This Thesis focuses on the development of direct control techniques to optimally control multiphase machines, analyzing their tolerance to different limit operating conditions, such as electrical constraints (voltage, current and magnetization level limits) or failure situations such as an open-phase fault. First, the DTC technique is proposed to manage the open-phase fault operation of the multiphase machine. A comparison of the fault-tolerant capability of DTC with other control techniques is carried out, to conclude the strengths and weaknesses of the analyzed methods facing this limit operation. Finally, an optimal current controller is developed using MPC techniques that allows the optimal utilization of the system's torque capability under electrical limitations. Simulation results and experimental validations are obtained to corroborate the initial approaches, through the use of particular cases of five-phase drives controlled using different frequency-domain control subspaces.

Keywords : Multiphase machines, direct control methods, optimal control in limit situations, DTC, open-phase fault operation, MPC, electrical limits.